Structural and Biochemical Studies of Polyketide Synthase and Fatty Acid Synthase Dehydratase

by

Gregory J. Dodge

A dissertation submitted in partial fulfillment
of the requirements for the degree of
Doctorate of Philosophy
(Biological Chemistry)
in the University of Michigan
2018

Doctoral Committee:

    Professor Janet L. Smith, Chair
    Assistant Professor Alison RH Narayan
    Professor David H. Sherman
    Associate Professor Raymond C. Trievel
    Associate Professor Zhaohui Xu

Gregory J. Dodge

gjdodg@umich.edu

ORCID iD: 0000-0002-6555-8350

Dedication

This dissertation is dedicated to my wife, Ashley Dodge.

Acknowledgements

I would like to thank my mentor, Janet Smith for her guidance over the last five years. None of this work would have been possible without her support and patience during my training. In particular, I'm grateful for the opportunities to start and shape my own projects beyond the scope of my initial work. The skills that I've gained during my stay in the Smith lab will remain invaluable to me in the future. I'm humbled to have had the opportunity to work alongside such amazing graduate students and other researchers in the Smith lab and will be forever grateful for their conversations and advice over the years.

I would like to thank all of my collaborators: Dr. Yang Li and Dr. Will Fiers of Dr. Robert A. Fecik's and Dr. Courtney C. Aldrich's labs, Danialle Ronnow of Dr. Richard E. Taylor's lab, and Dr. Kara Finzel and Dr. Ashay Patel of Dr. Michael D. Burkart's lab. I would also like to thank the staff of the GM/CA beamline at APS, Argonne National Lab, where all of the crystallographic data presented in this thesis were collected. Thank you to both William C. Brown and James E. DelProposto for guidance during my rotation and advice on cloning and protein expression. In addition, I would like to thank Wendy Feng for all of her advice and assistance with mass spectrometry experiments.

Thank you to my thesis committee: Dr. David Sherman, Dr. Ray Trievel, Dr. Alison Narayan, Dr. Zhaohui Xu for their guidance and support over the years. I would also like to thank Dr. John G. J. Tesmer for his support as a committee member until his relocation. Lastly, I would like to thank all the members of the Biological Chemistry Department, in particular Beth Goodwin and Amanda Howard.

Finally, I must thank my wife, Ashley Dodge, as well as the rest of my family for keeping me sane over the last five years. I could not have done any of this without you.

Table of Contents

List of Figures

List of Tables

List of Abbreviations

ACP, acyl carrier protein

AT, acyltransferase domain

CMT, *C*-methyltransferase domain

CoA, coenzyme-A

Cps, counts per second

Cur, curacin

DCM, dichloromethane

DH, dehydratase domain

DIBAL-H, diisobutylaluminum hydride

DIPEA, diisopropylethylamine

DMAP, 4-dimethylaminopyridine

DMSO, dimethyl sulfoxide

EDC-HCL, 1-Ethyl-3-(3-dimethylaminopropyl)carbodiimide hydrochloride

EIC, extracted ion chromatogram

ER, enoyl reductase domain

ESI-MS, electrospray ionization mass spectrometry

FAS, fatty acid synthase

FDA, U.S. Food and Drug Administration

GaMD , gaussian accelerated molecular dynamics

GNAT, GCN5(yeast histone)-related *N*-acetyltransferase

HPLC, high performance liquid chromatography

IPTG, isopropyl β-D-1-thiogalctopyranoside

KR, ketoreductase

KS, ketosynthase domain

LC–MS/MS, liquid chromatography-tandem mass spectrometry

LOD, limit of detection

MRM, multiple reaction monitoring

NAC, *N*-acetylcysteamine

NMR, nuclear magnetic resonance

OD, optical density

OMT, *O*-methyltransferase

PEG, polyethylene glycol

PKS, polyketide synthase

PME, particle mesh ewald

Ppant, phosphopantetheine

PPG, polypropylene glycol

PPTS, pyridinium p-toluenesulfonate

QTOF, quadrupole-time-of-flight

RMSD, root mean squared deviation

SAM, *S*-adenosylmethionine

SEC-MALS, size exclusion chromatography with multi-angle light scattering

TB, Terrific broth

TE, thioesterase domain

TES, triethylsilyl ether

THF, tetrahydrofuran

TIC, total ion count

TIPS, triisopropylsilyl ether

TLC, thin layer chromatography

TOF, time-of-flight

Abstract

Polyketides are chemically diverse bioactive natural products that often harbor desirable therapeutic characteristics. As such, the biological machinery used to synthesize these compounds are valuable targets for metabolic and protein engineering studies. A key characteristic of polyketide synthase (PKS) catalysis is the selective installation of many stereo- and regiocenters. To reach the full potential of PKS as a source of novel therapeutics and commodity chemicals, a molecular understanding of selective filters of each catalytic domain must be established. This thesis investigates the stereospecificity and regioselectivity of dehydratase (DH) domains from the pikromycin, curacin A, tylosin and gephyronic acid PKS pathways using a combination of biochemical assays and x-ray crystallography. These experiments establish new roles for PKS DH domains as stereoselective filters for substrate chiral centers distal from the site of catalysis, uncover previously unobserved dehydration consistent with vinylogous elimination, and establish the molecular basis for secondary isomerization. Results from these experiments facilitated the design of a novel DH/isomerase from an isomerase-inactive DH from the curacin A pathway, representing the first successful gain-of-function engineering of a PKS DH domain.

Fatty acid biosynthesis is a cornerstone of metabolism in cells. Fatty acids are involved in energy storage and production, membrane construction, temperature response, and biosynthesis of many secondary metabolites. An enigmatic facet of fatty acid biosynthesis in *E. coli* is the presence of two functionally distinct DHs, FabA and FabZ. FabA catalyzes a secondary isomerization reaction that is the source of all unsaturated fatty acids in *E. coli*, while FabZ

harbors only dehydratase function. This thesis establishes the molecular basis for the puzzling functional discrepancies between FabA and FabZ using functional crosslinking technology, x-ray crystallography, and molecular dynamics (MD) simulations. A high-resolution crystal structure of FabZ in complex with six AcpP subunits loaded with a C6 substrate was determined. This model facilitated MD simulations that demonstrated differential substrate preferences in agreement with published biochemical data, as well as differences in preferred substrate binding geometry such that FabZ catalyzes dehydration only whereas FabA can catalyze dehydration and subsequent isomerization.

The data presented in this thesis further our understanding of PKS and will aid in future experiments to capitalize on the promise of PKS as a biological machine for the synthesis of designer polyketides and commodity chemicals. The results the from *E. coli* fatty acid synthase experiments answer a decades old mechanistic question and may facilitate efforts to develop antibiotics specific to bacterial fatty acid synthase.

Chapter 1. Introduction

Natural products and fatty acids

Natural products represent a broad array of biologically synthesized molecules, ranging from relatively simple alkyl esters and acids to chemically complex compounds such as polyketides and non-ribosomal peptides. Fatty acids are an essential metabolite for all life[1-2, 7], and their biosynthesis is closely related to that of polyketides. The producing organisms synthesize these polyketides and fatty acids for purposes as diverse as the chemistry of the compounds themselves, including cell membrane homeostasis, signaling, and biological warfare. As 65% of FDA-approved small molecule therapeutics are in some way derived from natural products, these have significant clinical relevance. In addition to understanding the pharmacological properties of natural products, much work has been done to characterize the biosynthetic machinery that generates these compounds[8].

Natural product and fatty acid biosynthesis

A theme amongst many natural product biosynthesis pathways is the use of common cellular metabolites such as acyl-CoAs or amino acids as building blocks. By varying the order of building block addition and modification, the producing organisms achieve a staggering level of chemical diversity from otherwise simple starting materials. Even with modern methods, many natural products remain out of reach of total synthesis. In the case of polyketide natural products, the linear architecture and assembly-line logic of the biosynthetic pathways has led to

the hypothesis that pathway engineering efforts may be a viable alternative to total synthesis to access novel natural products, or to generate useful commodity chemicals[1].

PKS and FAS share many of the same chemical steps, and both covalently attach their nascent products to small carrier proteins[10-11]. However, there are considerable differences between the bacterial and metazoan FAS reactions, most specifically in the generation of unsaturated fatty acids[4]. In order to maintain membrane fluidity, organisms must adjust the ratio of saturated to unsaturated fatty acids in response to their environment. While higher eukaryotes synthesize unsaturated fatty acids via dedicated desaturases[12], bacteria such as *E. coli* create unsaturation during fatty acid biosynthesis[13]. The distinctions between these two schemes have led to the hypothesis that bacterial fatty acid biosynthesis may represent a viable antibiotic target[6, 14].

Thus, a mechanistic and molecular understanding of the machinery responsible for the biosynthesis of natural products and fatty acids represents a goal of great importance for medicinal chemistry, microbiology, and metabolic engineering.

Type II FAS mechanism

Fatty acid biosynthesis remains one or the best understood pathways in primary metabolism. Significant effort has been made in the past few decades in characterizing the molecular machines involved in the biosynthesis of fatty acids both biochemically and structurally. Fatty acids are universally generated from acetyl- and malonyl- CoA (Fig. 1.1). All intermediates are tethered to a small highly acidic acyl carrier protein (ACP) that adopts a 4-helix bundle structure. The ACP and nascent fatty acid are linked via a 4`-phosphopantetheine (Ppant) moiety that is attached via a phosphoester linkage to a conserved serine on the ACP. In *E. coli* FAS, the ACP (AcpP) is initially charged with a malonyl starter unit by malonyl-

CoA:ACP transacylase (FabD). Once charged, the ACP must interact with each of the catalytic domains of fatty acid synthase (FAS) to successfully generate a product.

The first step in the elongation of a fatty acid is catalyzed by the 3-ketoacyl-ACP synthase (KS).
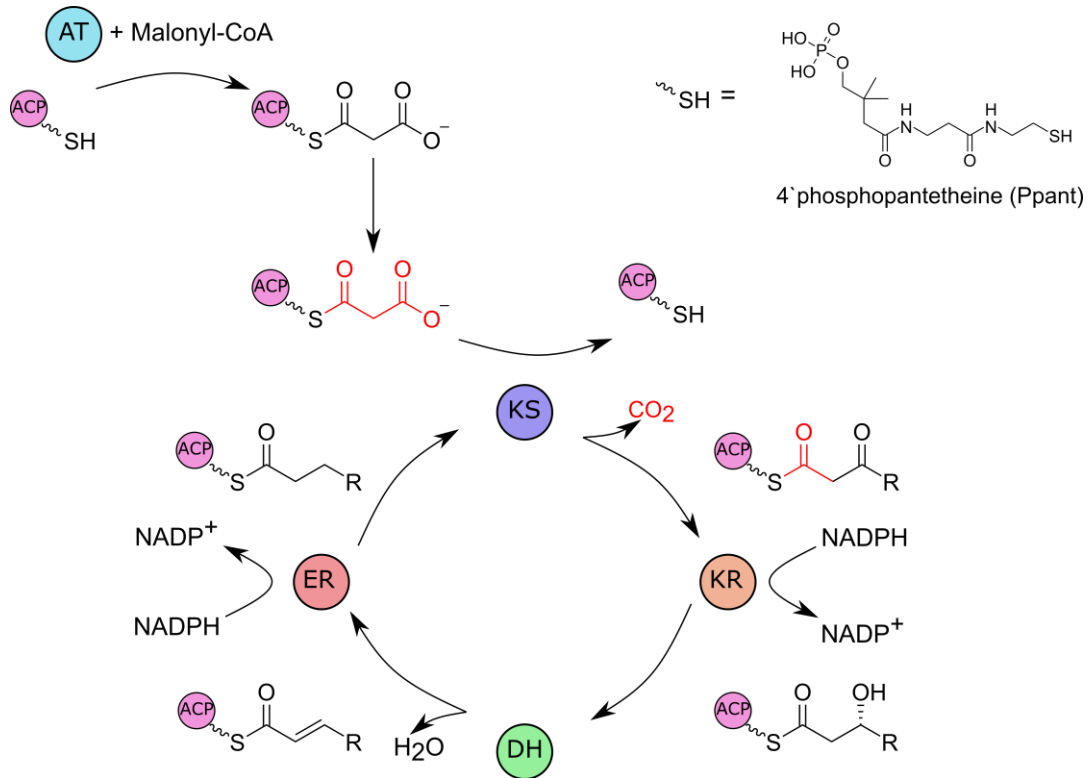
Figure 1.1 The FAS catalytic cycle

Each cycle of catalysis utilizes a malonyl extender unit to grow the nascent fatty acid by two carbons via a Claisen condensation reaction at the KS. The KR then reduces the 3-ketoacyl-ACP to a 3-hydroxyacyl-ACP, the DH eliminates the 3-hydroxyl group as water, forming a 2,3-enoyl-ACP, and finally the ER reduces the 2,3-enoyl-ACP to its fully saturated alkane form. This cycle continues until the fatty acid reaches a C16 or C18 length.

The KS extends the fatty acid via a decarboxylative Claisen condensation between the acyl moiety from ACP and an acetyl group, forming a 3-ketoacyl-ACP product, which serves as the substrate for the subsequent reactions to reduce the 3-ketoacyl-ACP to its fully saturated form. An NADPH-dependent ketoreductase (KR) converts 3-ketoacyl-ACP to 3-hydroxyacyl-ACP, a dehydratase (DH) converts 3-hydroxyacyl-ACP to *trans*-2,3-enoyl-ACP via a β-elimination of the 3-hydroxy group as water, and finally an NADPH-dependent enyolreductase (ER) reduces the *trans*-2,3-enoyl-ACP to a fully saturated acyl-ACP. This cycle continues until the fatty acid

3

reaches a C16 or C18 length, at which point a thioesterase (TE) will cleave the mature fatty acid, which will be utilized elsewhere in the cell such as for the biosynthesis of phospholipids.

Biosynthesis of unsaturated fatty acids

In *E. coli*, unsaturated fatty acids are synthesized via a branchpoint in the catalytic cycle[15]. A specific DH (FabA) harbors a secondary isomerization function, in which the typical *trans*-2,3-enyol-ACP is converted to *cis*-3,4-enoyl-ACP. Interestingly, this activity occurs only for acyl-ACPs of C10 chain length[16]. This *cis* unsaturated intermediate cannot be processed by the ER (FabI), or the normal KS (FabB) for another round of extension. Instead, a secondary KS (FabB) is used to extend the monounsaturated C10 intermediate, which can then undergo further rounds of reduction and extension until reaching a final C16 or C18 length.

Type I polyketide synthase

While the catalytic domains of FAS are conserved across all branches of life, their arrangement differs. Bacteria, such as *E. coli*, encode each enzyme in a separate gene, as well as the ACP, as a discrete soluble unit– this is referred to as a Type II system. In metazoan FAS, the entire set of elongation and reduction domains along with the ACP are domains within a single monolithic polypeptide – referred to as a Type I system. Type I FAS and Type I modular polyketide synthase (PKS) share many of the same catalytic domains, are similar in that all of their catalytic machines reside within a single polypeptide, and likely share a common ancestor (Fig. 1.2).
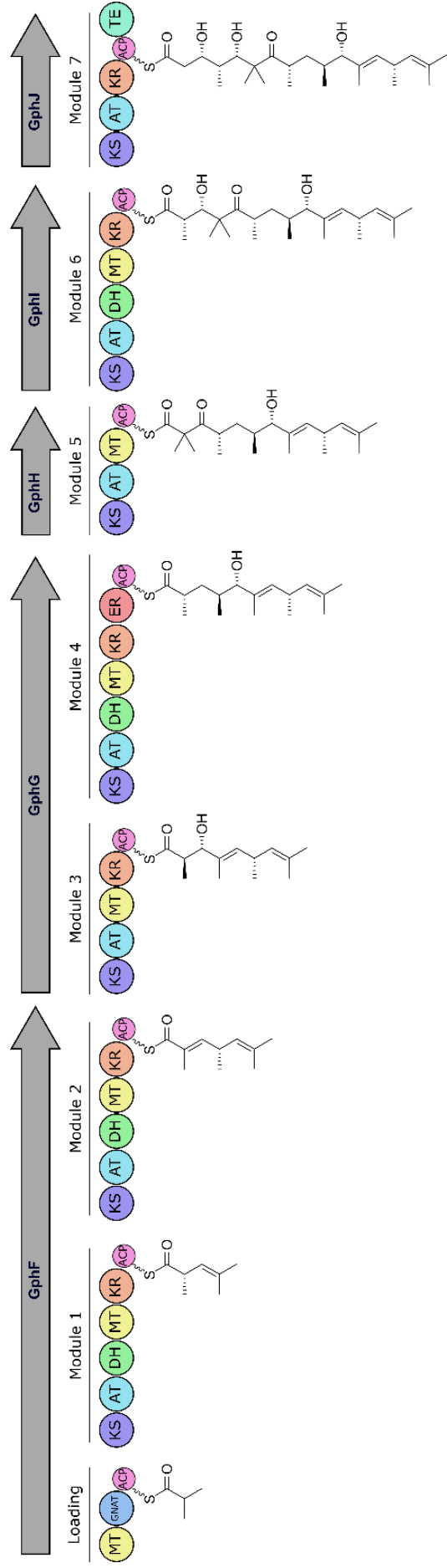
Figure 1.2 The Gephyronic acid PKS pathway, a Type I modular PKS

The starting unit for this pathway is isobutyryl-ACP, which is passed from the loading module through seven extension and modification modules. Unlike in bacterial Type II FAS, each module acts only once during catalysis. The net result is a 17C polyketide containing seven stereocenters. This product is released by the thioesterase (TE) domain, and further modified to form gephyronic acid, a potent inhibitor of eukaryotic translation.

5

Type I polyketide synthase mechanism

The strategy used by FAS is highly efficient at generating saturated and monounsaturated
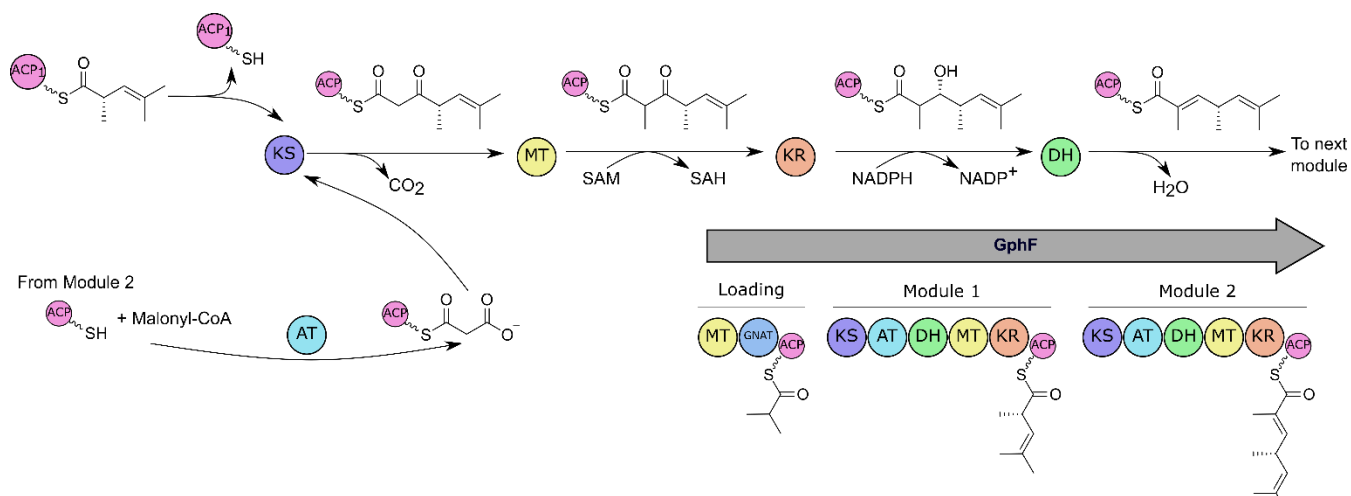
Figure 1.3 Catalytic cycle of GphF module 2

The modular AT first loads module 2 ACP with a malonyl acyl unit. The ACP then travels to the KS domain, where the polyketide intermediate from module 1 has been delivered by ACP_1. The KS then catalyzes a decarboxylative Claisen condensation, extending the polyketide chain by two carbons and eliminating CO_2. Next, the ACP travels to the C-MT, where a methyl group at the C2 position is installed using the methyl donor SAM as a cofactor. The ACP then moves to the KR domain, which reduces the C3 keto group to a hydroxyl with an NADPH cofactor. Finally, the ACP visits the DH, where the C3 hydroxyl is eliminated as water, generating an (*S*,*E*)-2,4,6-trimethylhepta-2,5-dienoyl-ACP. This intermediate is then passed on to module 4.

carbon chains around C16 in length, but the iterative biosynthetic logic, single starter acyl unit,

and limited set of reductive domains is poorly suited to attain the chemical diversity found in the

polyketide family of natural products. Type I modular PKS are able to access more diverse

chemistry than FAS by establishing slightly different catalytic rules (Figs. 1.2, 1.3). The

biosynthetic pathway is modular, with each module containing a unique set of elongation and

modification domains, which each act only once. A module ACP carries the intermediate

between domains, and hands off the product of one module to the KS of the next module in the

pathway. In addition to this assembly-line style catalysis, Type I modular PKS may contain extra

catalytic domains, such as *O*- and *C*-methyltransferases (OMT, CMT), and may be coupled with non-PKS enzymes, such as non-ribosomal peptide synthetase (NRPS) modules.

Stereochemistry in polyketides

An additional feature that differentiates polyketides from fatty acids are chiral centers. In FAS, each chiral hydroxyl is reduced to either an olefin or alkane. A PKS module may install a variety of stereocenters that will remain through biosynthesis of a natural product, depending on the composition of the module's catalytic domains. Of note are the hydroxyl modifications installed by the PKS KR domains. This step is the first in which an intermediate gains chirality, generating either a (3*R*)- or (3*S*)-hydroxyacyl-ACP from an achiral 3-ketoacyl-ACP substrate. Interestingly, sequence motifs distinguish KRs that produce (*R*)-hydroxyacyl-ACP from those that produce (*S*)-hydroxyacyl-ACP. These motifs have been used to classify A-type KRs as those which generate (*S*)-hydroxyacyl-ACP and B-type KRs as those which generate (*R*)-hydroxyacyl-ACP. Any modification domains that act after the KR are directly impacted by the stereochemistry of the hydroxyl group.

DH mechanism and structure

In general, both FAS and PKS DHs utilize a conserved His-Asp dyad to catalyze a *syn*-β-elimination reaction, at the substrate C3-hydroxyl to form an (*E*)-2,3-olefin (Fig. 1.3A). DHs are the first domains within a PKS/FAS that are presented with chiral substrate, adding an extra layer of complexity to the molecular clockwork of PKS and FAS. Not only must a DH select the
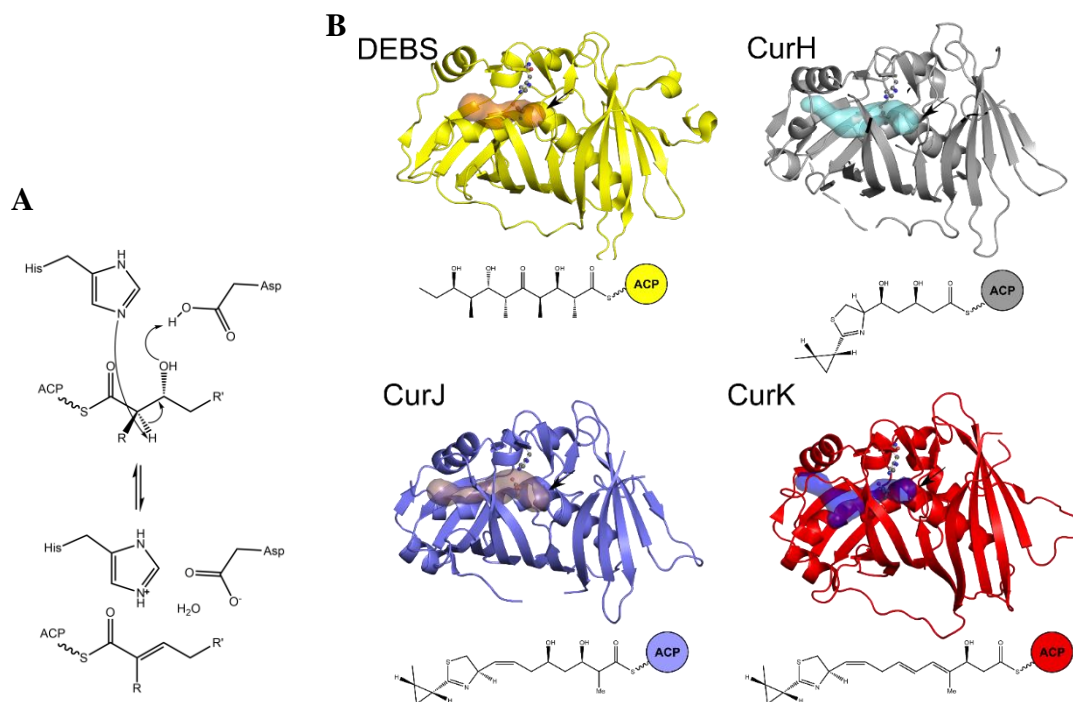
Figure 1.4 Mechanism and structure of PKS DHs

A. The catalytic mechanism of dehydration by PKS and FAS DH domains. The catalytic His deprotonates at C2, causing the Asp to act as a proton donor in the elimination of the C3 hydroxyl as water. **B**. The structures of several PKS DHs and native substrates, substrate binding pockets shown as transparent surface, binding pocket entrances indicated with arrows, catalytic residues shown in ball-and-stick. This comparison highlights the overall structural similarity of these domains, even though their substrates and binding pockets are quite different. PDBids 3EL6, 3KG7, 3KG8, 3KG9.

proper substrate stereocenter, but it also must select the proper regiochemistry of the resultant olefin. In modules lacking an ER, the olefin DH product will be retained through subsequent elongation and modification reactions, altering both the chemical characteristics and potential bioactivities of the natural product. Although the stereospecificity of PKS KR domains can be inferred from their sequences, no such motifs exist in DHs. While the structures of several PKS DHs have been solved[27, 32-33] (Fig. 1.3B), each exhibiting a canonical double-hotdog fold in which a "bun" of β-strands wraps around two central α-helical "hotdogs". The overall structures of these DHs are quite similar (RMSD ~2Å) and, taken alone, reveal little regarding substrate specificity or product selectivity. As generating authentic substrate mimics synthetically remains

challenging, the stereospecificity of DHs is a poorly explored area, leaving a critical gap in the understanding of the molecular processing of PKS.

Cis and *trans* unsaturation in polyketides

There are examples of both *cis* and *trans* unsaturated polyketides generated from modules which contain DHs. Initially, the regiochemistry of the unsaturated product of a DH was hypothesized to be correlated to the stereochemistry of the hydroxyl substrate[4]. (*R*)-hydroxy substrates (generated by a B-type KR) were associated with *trans*-unsaturated DH products, while (*S*)-hydroxy substrates (generated by an A-type KR) were associated with *cis*-unsaturated DH products. This classification has fallen out of favor as more PKS pathways have been sequenced and annotated, as many do not fit this model[40-41].

Olefin rearrangement by PKS and FAS DHs
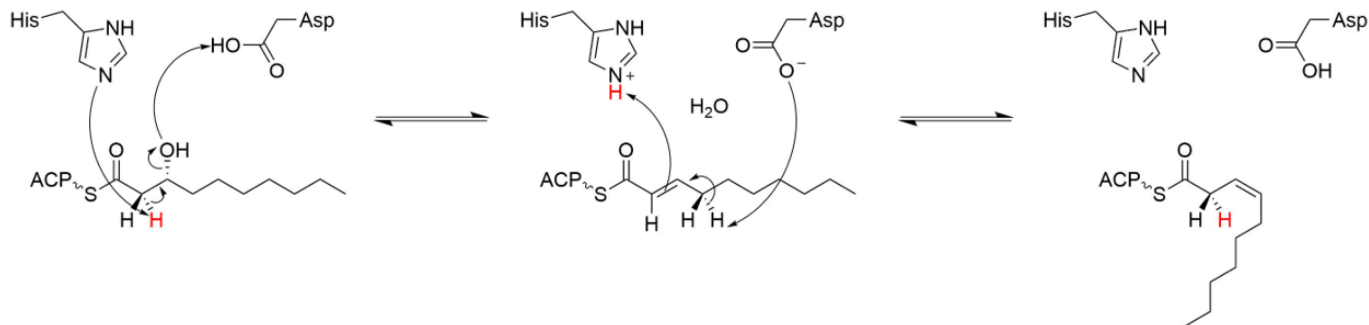
Figure 1.5 Sequential dehydration and isomerization by FabA

The His-Asp dyad are required for both reactions. The initial dehydrated intermediate contains an (E)-2,3-olefin, while the final product contains a (Z)-3,4-olefin. The molecular basis for this secondary function remains unclear.

Of the DHs characterized to date, several have been shown to catalyze secondary reactions. A recently reported DH from the ambruticin biosynthetic pathway (AmbDH4) was shown to harbor secondary isomerization functionality in addition to the standard dehydration function[43] (Fig. 1.5). Several other annotated PKS modules seem to generate 3,4-enoyl (odd-to-even) intermediates as opposed to the usual 2,3-enoyl (even-to-odd) intermediates – often in

9

modules containing a DH[40, 44-45], and many polyketides whose pathways have not been annotated

contain odd-to-even olefins. There are no reported structures of DHs harboring secondary

isomerization, and although the ambruticin DH/isomerase has been characterized biochemically,

the molecular basis for secondary function is poorly understood. In *E. coli* FAS, FabA exhibits

secondary isomerization functionality after dehydration, generating a *cis*-3,4-enoyl-ACP (Figs.

Figure 1.6 The reaction courses of characterized multifunctional DHs from PKS and FAS

1.5, 1.6). The molecular basis for the dual FabA dehydration and isomerization activity, and the

FabZ can only dehydration only activity has remained an enigma for decades.

Cyclization by PKS DHs

     Some DHs have been shown catalyze secondary reactions beyond olefin rearrangement.

Another DH from the ambruticin biosynthetic pathway (AmbDH3) was recently reported to

catalyze the formation of a tetrahydropyran moiety from the 2,3-enoyl intermediate of

dehydration[1](Fig. 1.6). In the structure of this DH, an amino acid adjacent to the catalytic His-Asp dyad was implicated (V173) in the secondary pyran cyclase function. In typical PKS DHs, this position is occupied by a well conserved Tyr. Mutagenesis experiments demonstrated that when V173 was substituted by a Tyr, cyclization activity was lost, while dehydration remained unchanged. These experiments hint that secondary functionality in PKS DHs may derive from subtle alterations to the substrate binding pocket, which are not immediately obvious at the sequence level.

Epimerization by PKS DHs

Another secondary function that has been attributed to DHs is methyl epimerization. As mentioned above, AmbDH4 has been shown to epimerize the C4 position of its substrate during catalysis (Fig 1.6). Additionally, "orphan" DHs are found in some modules with KR domains predicted to be redox-inactive[3-4]. Of these, both NanDH1 and NanDH5 from the nanchangmycin biosynthetic pathway were shown to harbor cryptic epimerase activity of C2-methyl groups on truncated substrate mimics. A more intriguing result from these studies showed the EryDH4 from the erythromycin biosynthetic pathway and NanDH2 from nanchangmycin biosynthesis, two DHs found in modules with active KRs, also exhibited C2-methyl epimerase activity. The structure of EryDH4 is known, but there are no distinguishing features in the active site that explain this unexpected C2 epimerase function.

ACP-DH interactions in PKS and FAS

In addition to understanding the stereoselectivity and regiospecificity of DHs, characterization of ACP-DH interactions is a critically underexplored area in both PKS and FAS. These experiments pose significant technical challenges due to the transient nature of the ACP –

Figure 1.7 Crystal structure of the crosslinked AcpP=FabA complex solved to 1.9-Å

FabA shown in pale and dark green, AcpP shown in magenta. Crosslinking probe and catalytic His-Asp dyad shown as sticks. PDBid 4KEH

DH interaction, along with difficulties designing minimal systems suitable for assay. While the ACP and DH must interact, the ACP is only a carrier for the real substrate – the hydroxylated nascent polyketide or fatty acid. Thus, a truly native complex will likely be dependent not only on protein-protein interactions, but also protein-substrate interactions between the DH and the hydroxyacyl-Ppant. Recent advancements in synthetic probe design have led to the development of mechanistic crosslinking compounds that can be loaded directly onto ACP, facilitating the trapping of a complex representative of that formed during fatty acid biosynthesis.

The crosslinking probes were used to trap a stable 1:1 complex of AcpP and FabA from *E. coli* FAS (AcpP=FabA), facilitating the determination of the crystal structure of the complex at atomic resolution[7-8] (Fig. 1.7). These studies gave critical insight into the binding mode of AcpP with a FAS catalytic domain, but in the absence of a complementary structure of the AcpP-FabZ complex, it remains unclear what drives the distinct mechanistic differences between these two FAS DHs.

Thesis overview

This thesis further establishes the molecular basis of catalysis, stereospecificity, regioselectivity, and non-canonical function of DH domains in PKS. DHs from the pikyromycin, tylosin, curacin, and gephryonic acid PKS pathways are studied by mass spectrometry-based assays and x-ray crystallography. Libraries of chiral substrate mimics established previously unknown sensitivity to the chirality of positions distal from the C3 site of elimination in the pikromycin and tylosin systems. Studies on DHs from the curacin A pathway uncover an unusual C5 dehydration consistent with vinylogous elimination by the CurH and CurJ DHs and facilitated the trapping of a substrate fragment in the CurJ DH, visualized in a crystal structure. Biochemical and structural studies of GphF DH1 from the gephryonic acid pathway elucidated the molecular requirements for secondary isomerization function in PKS DHs. The results from the GphF DH1 experiments facilitated the rational engineering of a dual function dehydratase-isomerase from the isomerase-inactive CurK DH – the first successful gain-of-function engineering experiment of a PKS DH.

This thesis also investigates the protein-protein interactions between the *E. coli* FAS DH FabZ and its carrier protein AcpP. A novel fusion construct was designed to generate milligram quantities of FabZ, a previously insoluble protein. In combination with an optimized crosslinking protocol, a stable 1:1 complex of AcpP=FabZ facilitated crystallization. A high-resolution crystal structure of the complex served as the foundation for molecular dynamics simulations that identified key differences in the preferred conformations of a variety of substrates in FabA and FabZ. Taken together, the results for the first time establish the molecular differences between FabA and FabZ catalysis that lead to the FabA secondary isomerization function.

Bibliography

1.   Cronan, J. J., Rock, C. O., Biosynthesis of membrane lipids. *EcoSal Plus* **2008,** *3* (1).
2.   Rock, C. O., Cronan, J. E., *Escherichia coli* as a model for the regulation of dissociable (type II) fatty acid biosynthesis. *Biochimica et Biophysica Acta (BBA)-Lipids and Lipid Metabolism* **1996,** *1302* (1), 1-16.
3.   Enoch, H. G., Catala, A., Strittmatter, P., Mechanism of rat liver microsomal stearyl-CoA desaturase. Studies of the substrate specificity, enzyme-substrate interactions, and the function of lipid. *Journal of Biological Chemistry* **1976,** *251* (16), 5095-5103.
4.   Heath, R. J., Rock, C. O., Roles of the FabA and FabZ β-hydroxyacyl-acyl carrier protein dehydratases in *Escherichia coli* fatty acid biosynthesis. *J. Biol. Chem.* **1996,** *271* (44), 27795-27801.
5.   Campbell, J. W., Cronan Jr, J. E., Bacterial fatty acid biosynthesis: targets for antibacterial drug discovery. *Annual Reviews in Microbiology* **2001,** *55* (1), 305-332.
6.   Brock, D., Kass, L., Bloch, K., β-Hydroxydecanoyl thioester dehydrase II. Mode of action. *Journal of Biological Chemistry* **1967,** *242* (19), 4432-4440.
7.   Maier, T., Leibundgut, M., Ban, N., The crystal structure of a mammalian fatty acid synthase. *Science* **2008,** *321* (5894), 1315-1322.
8.   Jenke-Kodama, H., Sandmann, A., Müller, R., Dittmann, E., Evolutionary implications of bacterial polyketide synthases. *Molecular biology and evolution* **2005,** *22* (10), 2027-2039.
9.   Buchholz, T. J., Geders, T. W., Bartley III, F. E., Reynolds, K. A., Smith, J. L., Sherman, D. H., Structural basis for binding specificity between subclasses of modular polyketide synthase docking domains. *ACS chemical biology* **2009,** *4* (1), 41-52.
10.   Caffrey, P., Conserved amino acid residues correlating with ketoreductase stereospecificity in modular polyketide synthases. *ChemBioChem* **2003,** *4* (7), 654-657.
11.   Faille, A., Gavalda, S., Slama, N., Lherbet, C., Maveyraud, L., Guillet, V., Laval, F., Quémard, A., Mourey, L., Pedelacq, J.-D., Insights into substrate modification by dehydratases from Type I Polyketide Synthases. *Journal of molecular biology* **2017,** *429* (10), 1554-1569.
12.   Gay, D., You, Y.-O., Keatinge-Clay, A., Cane, D. E., Structure and stereospecificity of the dehydratase domain from the terminal module of the rifamycin polyketide synthase. *Biochemistry* **2013,** *52* (49), 8916-8928.
13.   Akey, D. L., Razelun, J. R., Tehranisa, J., Sherman, D. H., Gerwick, W. H., Smith, J. L., Crystal structures of dehydratase domains from the curacin polyketide biosynthetic pathway. *Structure* **2010,** *18* (1), 94-105.
14.   Valenzano, C. R., You, Y.-O., Garg, A., Keatinge-Clay, A., Khosla, C., Cane, D. E., Stereospecificity of the dehydratase domain of the erythromycin polyketide synthase. *Journal of the American Chemical Society* **2010,** *132* (42), 14697-14699.
15.   He, L., Zhang, L., Liu, X., Li, X., Zheng, M., Li, H., Yu, K., Chen, K., Shen, X., Jiang, H., Discovering potent inhibitors against the β-hydroxyacyl-acyl carrier protein dehydratase (FabZ) of Helicobacter pylori: structure-based design, synthesis, bioassay, and crystal structure determination. *Journal of medicinal chemistry* **2009,** *52* (8), 2465-2481.
16.   Zhang, L., Liu, W., Hu, T., Du, L., Luo, C., Chen, K., Shen, X., Jiang, H., Structural basis for catalytic and inhibitory mechanisms of β-hydroxyacyl-acyl carrier protein dehydratase (FabZ). *Journal of Biological Chemistry* **2008,** *283* (9), 5370-5379.
17.   Kimber, M. S., Martin, F., Lu, Y., Houston, S., Vedadi, M., Dharamsi, A., Fiebig, K. M., Schmid, M., Rock, C. O., The structure of (3R)-hydroxyacyl-acyl carrier protein dehydratase

(FabZ) from Pseudomonas aeruginosa. *Journal of Biological Chemistry* **2004,** *279* (50), 52593-52602.

18.　　Keatinge-Clay, A., Crystal structure of the erythromycin polyketide synthase dehydratase. *Journal of molecular biology* **2008,** *384* (4), 941-953.

19.　　Sung, K. H., Berkhan, G., Hollmann, T., Wagner, L., Blankenfeldt, W., Hahn, F., Insights into the Dual Activity of a Bifunctional Dehydratase-Cyclase Domain. *Angewandte Chemie International Edition* **2018,** *57* (1), 343-347.

20.　　Chang, Z., Sitachitta, N., Rossi, J. V., Roberts, M. A., Flatt, P. M., Jia, J., Sherman, D. H., Gerwick, W. H., Biosynthetic Pathway and Gene Cluster Analysis of Curacin A, an Antitubulin Natural Product from the Tropical Marine Cyanobacterium Lyngbya m ajuscula. *Journal of natural products* **2004,** *67* (8), 1356-1367.

21.　　Young, J., Stevens, D. C., Carmichael, R., Tan, J., Rachid, S., Boddy, C. N., Müller, R., Taylor, R. E., Elucidation of gephyronic acid biosynthetic pathway revealed unexpected SAM-dependent methylations. *Journal of natural products* **2013,** *76* (12), 2269-2276.

22.　　Alhamadsheh, M. M., Palaniappan, N., DasChouduri, S., Reynolds, K. A., Modular polyketide synthases and cis double bond formation: establishment of activated cis-3-cyclohexylpropenoic acid as the diketide intermediate in phoslactomycin biosynthesis. *Journal of the American Chemical Society* **2007,** *129* (7), 1910-1911.

23.　　Shah, D. D., You, Y.-O., Cane, D. E., Stereospecific Formation of E-and Z-Disubstituted Double Bonds by Dehydratase Domains from Modules 1 and 2 of the Fostriecin Polyketide Synthase. *Journal of the American Chemical Society* **2017,** *139* (40), 14322-14330.

24.　　August, P. R., Tang, L., Yoon, Y. J., Ning, S., Müller, R., Yu, T.-W., Taylor, M., Hoffmann, D., Kim, C.-G., Zhang, X., Biosynthesis of the ansamycin antibiotic rifamycin: deductions from the molecular analysis of the rif biosynthetic gene cluster of Amycolatopsis mediterranei S699. *Chemistry & biology* **1998,** *5* (2), 69-79.

25.　　Bock, M., Buntin, K., Müller, R., Kirschning, A., Stereochemical determination of thuggacins A–C, highly active antibiotics from the myxobacterium Sorangium cellulosum. *Angewandte Chemie International Edition* **2008,** *47* (12), 2308-2311.

26.　　Tohyama, S., Kakinuma, K., Eguchi, T., The complete biosynthetic gene cluster of the 28-membered polyketide macrolactones, halstoctacosanolides, from Streptomyces halstedii HC34. *The Journal of antibiotics* **2006,** *59* (1), 44.

27.　　Berkhan, G., Merten, C., Holec, C., Hahn, F., The Interplay between a Multifunctional Dehydratase Domain and a C-Methyltransferase Effects Olefin Shift in Ambruticin Biosynthesis. *Angewandte Chemie International Edition* **2016,** *55* (43), 13589-13592.

28.　　Taft, F., Brünjes, M., Knobloch, T., Floss, H. G., Kirschning, A., Timing of the Δ10, 12-Δ11, 13 double bond migration during ansamitocin biosynthesis in Actinosynnema pretiosum. *Journal of the American Chemical Society* **2009,** *131* (11), 3812-3813.

29.　　Schmitz, F. J., Gunasekera, S. P., Yalamanchili, G., Hossain, M. B., Van der Helm, D., Tedanolide: a potent cytotoxic macrolide from the Caribbean sponge Tedania ignis. *Journal of the American Chemical Society* **1984,** *106* (23), 7251-7252.

30.　　Meragelman, T. L., Willis, R. H., Woldemichael, G. M., Heaton, A., Murphy, P. T., Snader, K. M., Newman, D. J., Van Soest, R., Boyd, M. R., Cardellina, J. H., Candidaspongiolides, distinctive analogues of tedanolide from sponges of the genus Candidaspongia. *Journal of natural products* **2007,** *70* (7), 1133-1138.

31.   Cheng, J.-F., Lee, J.-S., Sakai, R., Jares-Erijman, E. A., Silva, M. V., Rinehart, K. L., Myriaporones 1− 4, Cytotoxic Metabolites from the Mediterranean Bryozoan M yriapora truncata. *Journal of natural products* **2007,** *70* (3), 332-336.

32.   Berkhan, G., Hahn, F., A Dehydratase Domain in Ambruticin Biosynthesis Displays Additional Activity as a Pyran-Forming Cyclase. *Angewandte Chemie International Edition* **2014,** *53* (51), 14240-14244.

33.   Sung, K. H., Berkhan, G., Hollmann, T., Wagner, L., Blankenfeldt, W., Hahn, F., Insights into the dual activity of a bifunctional dehydratase-cyclase domain. *Angewandte Chemie, International Edition in English* **2018,** *57* (1), 343-347.

34.   Garg, A., Xie, X., Keatinge-Clay, A., Khosla, C., Cane, D. E., Elucidation of the cryptic epimerase activity of redox-inactive ketoreductase domains from modular polyketide synthases by tandem equilibrium isotope exchange. *Journal of the American Chemical Society* **2014,** *136* (29), 10190-10193.

35.   Ishikawa, F., Haushalter, R. W., Burkart, M. D., Dehydratase-specific probes for fatty acid and polyketide synthases. *Journal of the American Chemical Society* **2011,** *134* (2), 769-772.

36.   Ishikawa, F., Haushalter, R. W., Lee, D. J., Finzel, K., Burkart, M. D., Sulfonyl 3-alkynyl pantetheinamides as mechanism-based cross-linkers of acyl carrier protein dehydratase. *Journal of the American Chemical Society* **2013,** *135* (24), 8846-8849.

37.   Meier, J. L., Haushalter, R. W., Burkart, M. D., A mechanism based protein crosslinker for acyl carrier protein dehydratases. *Bioorganic & medicinal chemistry letters* **2010,** *20* (16), 4936-4939.

38.   Nguyen, C., Haushalter, R. W., Lee, D. J., Markwick, P. R., Bruegger, J., Caldara-Festin, G., Finzel, K., Jackson, D. R., Ishikawa, F., O'Dowd, B., Trapping the dynamic acyl carrier protein in fatty acid biosynthesis. *Nature* **2014,** *505* (7483), 427-431.

39.   Finzel, K., Nguyen, C., Jackson, D. R., Gupta, A., Tsai, S.-C., Burkart, M. D., Probing the substrate specificity and protein-protein interactions of the E. coli fatty acid dehydratase, FabA. *Chemistry & biology* **2015,** *22* (11), 1453-1460.

40.   Li, Y., Fiers, W. D., Bernard, S. M., Smith, J. L., Aldrich, C. C., Fecik, R. A., Polyketide intermediate mimics as probes for revealing cryptic stereochemistry of ketoreductase domains. *ACS chemical biology* **2014,** *9* (12), 2914-22.

41.   Chung-hsi, L., Yuen-hwa, Y., Yao, L., Yong-jun, L., Ai-hsueh, C., Chi-yi, H., 3-aminoacyl-tetrahydrothiazole-2-thione as an active amide for peptide synthesis (I). *Tetrahedron Letters* **1981,** *22* (36), 3467-3470.

42.   Abiko, A., Liu, J.-F., Masamune, S., The Anti-Selective Boron-Mediated Asymmetric Aldol Reaction of Carboxylic Esters. *Journal of the American Chemical Society* **1997,** *119* (10), 2586-2587.

43.   Barbier, J., Jansen, R., Irschik, H., Benson, S., Gerth, K., Bohlendorf, B., Hofle, G., Reichenbach, H., Wegner, J., Zeilinger, C., Kirschning, A., Muller, R., Isolation and total synthesis of icumazoles and noricumazoles--antifungal antibiotics and cation-channel blockers from Sorangium cellulosum. *Angew Chem Int Ed Engl* **2012,** *51* (5), 1256-60.

44.   Nagao, Y., Hagiwara, Y., Kumagai, T., Ochiai, M., Inoue, T., Hashimoto, K., Fujita, E., New C-4-chiral 1,3-thiazolidine-2-thiones: excellent chiral auxiliaries for highly diastereo-controlled aldol-type reactions of acetic acid and .alpha.,.beta.-unsaturated aldehydes. *The Journal of Organic Chemistry* **1986,** *51* (12), 2391-2393.

45.   Nagao, Y., Dai, W. M., Ochiai, M., Tsukagoshi, S., Fujita, E., Highly diastereoselective alkylation of chiral tin(II) enolates onto cyclic acyl imines. An efficient asymmetric synthesis of bicyclic alkaloids bearing a nitrogen atom ring juncture. *The Journal of Organic Chemistry* **1990,** *55* (4), 1148-1156.
46.   Smith, J. L., Sherman, D. H., An enzyme assembly line. *Science* **2008,** *321* (5894), 1304.

Chapter 2. Functional characterization of a dehydratase domain from the pikromycin polyketide synthase

Summary

Metabolic engineering of polyketide synthase (PKS) pathways represents a promising approach to natural products discovery. The dehydratase (DH) domains of PKSs, which generate an α,β-unsaturated bond through a dehydration reaction, have been poorly studied compared to other domains, likely due to the simple nature of the chemical reaction they catalyze and lack of a convenient assay to measure substrate turnover. Herein we report the first steady-state kinetic analysis of a PKS DH domain employing LC-MS/MS analysis for product quantitation. PikDH2 was selected as a model DH domain. Its substrate specificity and mechanism were interrogated with a systematic series of synthetic triketide substrates containing a nonhydrolyzable thioether linkage as well as by site-directed mutagenesis, evaluation of the pH dependence of catalytic efficiency (V_{max}/K_M), and through kinetic characterization of a mechanism-based inhibitor. These studies revealed PikDH2 converts d-alcohol substrates to *trans*-olefin products. The reaction was reversible with equilibrium constants ranging from 1.2–2. Moreover, the enzyme activity was robust and PikDH2 was used on a preparative scale for the chemoenzymatic synthesis of unsaturated triketide products. PikDH2 was shown to possess remarkably strict substrate specificity and was unable to turnover substrates epimeric at the β, γ or δ-positions. We also demonstrated PikDH2 has a key ionizable group with a pK_a of 7.0 and can be irreversibly

inactivated through covalent modification by a mechanism-based inhibitor, which provides a foundation for future structural studies to elucidate substrate–protein interactions.

Introduction

Polyketides derived from modular type I polyketide synthases (PKSs) have drawn enormous attention and interest from chemists for decades due to their intricate structures, stereochemical complexity and diverse pharmacological activities. Sharing the same evolutionary history with fatty acid synthases (FASs)[1-2], modular type I PKSs employ similar assembly-line molecular machinery wherein the chain intermediates remain covalently attached to acyl carrier protein (ACP) domains during biosynthesis. Unlike FASs, the presence of the three processing domains in PKSs: ketoreductase (KR), dehydratase (DH) and enoylreductase (ER), are varied in each module, leading to a fully reduced, partially reduced or unreduced segment on the polyketide chain. Owing to its assembly-line attribute and varying combination of processing domains, PKSs have been exploited through combinatorial biosynthesis and metabolic engineering to provide large libraries of polyketide analogs[3-5].

Many polyketides such as the archetypical macrolide antibiotic pikromycin, the antifungal polyene amphotericin B, the linear polyketide discodermolide, and the mixed nonribosomal peptide-polyketide curacin, contain one or more double bonds that serve as conformational constraints and are essential for biological activity (Figure 2.1)[6-7]. The double bonds are formed by DH domains through abstraction of the α-proton and concomitant protonation of the β-hydroxyl group of the nascent β-hydroxyacyl-ACP polyketide intermediate, resulting in loss of one water molecule. As observed in FAS DHs, the characteristic double hotdog fold is also found in PKS DHs to form the active site with two catalytic residues, aspartic acid and histidine[8-12]. The olefin geometry of DH products cannot be predicted through a signature fingerprint as in the KRs[13] since the active site residues appear quite similar in both *cis*- and *trans*-olefin generating DHs[11,14]. Initial evidence suggested the geometry of a double bond was exclusively dependent on the stereochemistry of the DH substrate, provided by the upstream KR module wherein A-type KR products (l-alcohols) lead to *cis*-double bonds while *trans*-olefins arise from B-type KR products (d-alcohols);[15] although exceptions have recently been observed[12,16-17]. Post-PKS tailoring enzymes such as enoyl reductases or isomerases can further obscure the original olefin geometry[12,16-17,18].

Steady-state kinetic analysis using simple diffusible *N*-acetylcysteamine (NAC) thioester precursors, successfully employed to interrogate the substrate specificity of other PKS domains and modules[19-24], has thus far been ineffective for studying isolated DH domains. This is likely due to the extremely low activity of the excised DH domains, which necessitates overnight incubations to generate sufficient product for detection. Moreover, the simple nature and ready reversibility of the dehydration reaction cannot be easily monitored by conventional radio-TLC or spectrophotometric assays. Cane and co-workers have also shown, at least in one example,
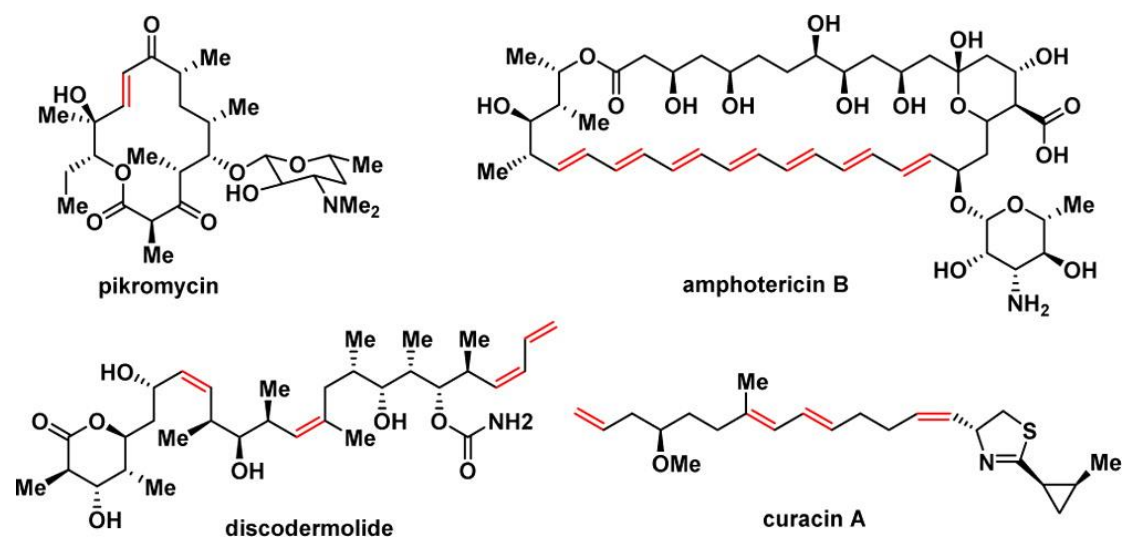
Figure 2.1 Structures of pikromycin, amphotericin B, discodermolide and curacin A

that a NAC thioester substrate was not properly delivered to a DH active site resulting in reversal of diastereospecificity[12]. This result highlights the potential importance of the ACP for chaperoning the polyketide intermediate for proper recognition and processing by DHs. Despite these aforementioned challenges, significant progress has been made in PKS functional characterization using NAC and ACP-bound substrates, which has provided useful insight into the substrate specificity and compelling evidence that (*E*)-unsaturated polyketide intermediates involve a stereospecific *syn*-elimination[12, 16-17,25-27]. To further advance our understanding of DH domains, we report herein the first detailed steady-state kinetic characterization of an individual DH domain through monitoring reaction progress by liquid chromatography-tandem mass spectrometry (LC-MS/MS). The substrate specificity was studied with a systematic series of synthetic triketide analogs to probe the impact of both vicinal and distal stereochemistry and through mutagenesis of active-site residues. The ability to monitor reaction progress also permitted the study of pH dependence on catalytic activity and kinetic characterization of a mechanism-based irreversible inhibitor designed to facilitate co-crystallization and elucidation of substrate-protein interactions.

Methods

General biology procedures.

All chemical reagents were purchased from Sigma-Aldrich and were used directly without further purification. *E. coli* BL21(DE3) cells were from New England BioLabs. IPTG was acquired through Gold Biotechnology. His60 Ni Superflow resin was purchased from Clontech Laboratories, Inc. OD_{600} was measured on an Eppendorf BioPhotometer. Sonication was carried out by Branson Sonifier 450. Gel filtration purification was performed on HiLoad 16/600 Superdex 200 pg column (GE). The protein mass spectra data was obtained by Bruker BioTOF II mass

spectrometer. LC–MS/MS was conducted with AB Sciex QTRAP 5500 mass spectrometer and Shimadzu LC system.

Cloning and mutagenesis.

The PikKR2-DH2 didomain was cloned from the cosmid pLZ51 into the expression vector pMCSG7[7] using ligation independent cloning (LIC). PikKR2-DH2 forward primer: 5'-**TACTTCCAATCCAATGCC**AGCCGCGTCGGCGGG-3'; PikKR2-DH2 reverse primer: 5'-**TTATCCACTTCCAATGCTA**CGGCCGGGCCCGG-3' (LIC-overhangs in **bold**; inserted stop codon underlined). The insert was confirmed via sequencing. Primers for the F3746L, F3750L, and F3750Y variants were designed via the QuikChange primer design tool website (Agilent) (Table 2.1). Mutagenesis was run using the standard protocol provided with the QuikChange Lightning Site Directed Mutagenesis kit (Agilent). Mutated codons are underlined below. All mutations were confirmed via sequencing.

Table 2.1 Primers of mutants F3746L, F3750L, and F3750Y.

Mutant	Primers (5' – 3')
F3746L	gaacagcggacctaaggcgaggccgtt
	aacggcctcgccttaggtccgctgttc
F3750L	cagcccctgtaacagcggaccgaagg
	ccttcggtccgctgttacaggggctg
F3750Y	gcgttcagcccctgatacagcggaccgaag
	cttcggtccgctgtatcaggggctgaacgc

Protein expression and purification.

    Competent *E. coli* BL21 (DE3) cells were transformed with pMCSG7 containing PikKR2-DH2 and grown in Terrific Broth (TB) media with 100 µg/mL ampicillin at 37 °C until OD_{600} reached to 1.2. The cultures were cooled to 20 °C and 200 µM IPTG was added to induce protein expression. After overnight expression, cells were harvested by centrifugation at 6,000*g* and 4 °C for 10 min. The resulting cell pellet was frozen at –80 °C for 10 min, resuspended in lysis buffer (50 mM HEPES, 300 mM NaCl, 10 mM imidazole, pH 8.0) and lysed by sonication. After centrifuging at 50,000*g* and 4 °C for 10 min, the cleared lysate was incubated with His-60 Ni superflow resin (2 mL) at 4 °C for 1 h and then loaded onto a gravity column. The column was washed with 14 mL of wash buffer (10 mM imidazole, 50 mM HEPES, 300 mM NaCl, pH 8.0) and eluted with 2.5 mL elution buffer (500 mM imidazole, 50 mM HEPES, 300 mM NaCl, pH 8.0). The protein was further purified via size exclusion chromatography on a Superdex 16/600 200pg gel filtration column eluting at 0.5 mL min^{-1} with 50 mM sodium phosphate (pH 7.1) and 150 mM NaCl. Purified protein was stored in storage buffer (50 mM Tris, 150 mM NaCl, 10%

(v/v) glycerol, pH 8.0) at –80 °C. Protein concentration was determined using the Bio-Rad protein assay kit with bovine serum albumin as the standard. Exact molecular weight of the purified monomeric protein was determined by ESI mass spectrometry. All the mutants were expressed and purified in an analogous way (Fig. 2.2 and Table 2.2).
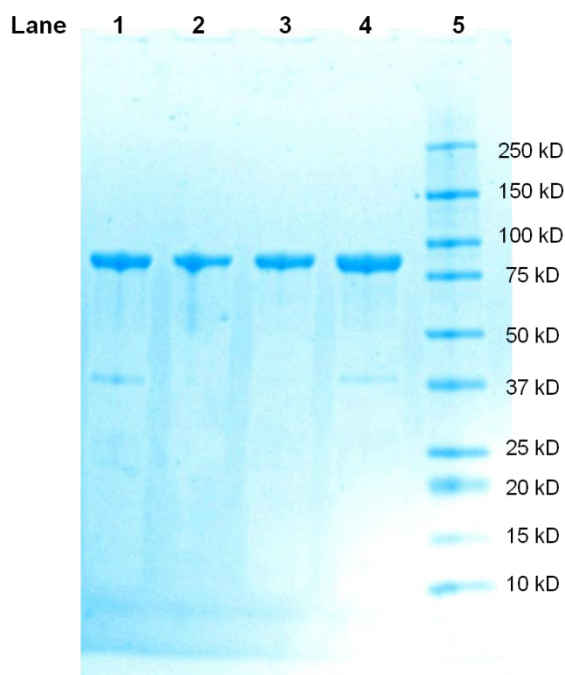
Figure 2.2 SDS-PAGE gel electrophoresis of purified PikDH2-KR2 and mutants on BIO-RAD precast gels (Mini-PROTEAN® TGX™ gels) stained by Bio-Safe™ Coomassie G-250 Stain

Lane 1 was loaded with PikDH2-KR2 wild type; Lane 2 was loaded with PikDH2-KR2 F3746L; Lane 3 was loaded with PikDH2-KR2 F3750L; Land 4 was loaded with PikDH2-KR2 F3750Y. Lane 5 was loaded with Kaleidoscope Precision Plus Protein Standards (BIO-RAD).

Table 2.2 Characterization of PikKR2-DH2 and mutants; including calculated molecular weight, monomeric molecular weight (ESI mass spectrometry), and overexpression yield.

Protein	Calculated MW (Da)	Monomeric MW (Da)	Yield (mg/L)
Wild-type	83009	83012	36
F3746L	82975	82975	66

25

F3750Y	83025	83028	29
F3750L	82975	82978	46

Determination of initial velocity conditions. (Data generated by Yang Li)

Substrate **2a** (6 mM) was incubated with PikDH2-KR2 (1.25–10 µM) and reaction buffer (50 mM Tris, 150 mM NaCl, pH 8.0) in a total volume of 50 µL at 25 °C. At 2, 5, 10, 20 and 40 min time points, 5 µL of the reaction mixture was added to 495 µL of 1:1 MeCN–reaction buffer (100-fold dilution) to quench the reaction. The resulting solution was vortexed, centrifuged. 60 µL of the diluted reaction solution was added to a HPLC vial with 10 µL of internal standard **3** (320 nM) and analyzed by LC-MS/MS (Table 2.3) employing a Kinetix reverse-phase C_{18} column (50 mm × 2.1 mm, 2.6 µm, Phenomenex) operated at 0.4 mL min^{-1} with a gradient between mobile phase A (15 mM ammonium acetate in H_2O) and mobile phase B (MeCN). The gradient program was 0 min, 5% B; 2 min, 5% B; 7 min, 55% B; 8 min, 95% B; 9 min, 95% B; 9.5 min, 5% B; 12 min, 5% B. Standard curve of enzymatic product **4** was generated by injecting the authentic standard at varying concentrations with a fixed concentration of an internal standard **3**. The amount of enzymatic product formation at each time point was calculated by plotting the area ratio (analyte/internal standard) into the standard curve. Each reaction was performed in duplicate. The progress curve at varying enzyme concentrations was generated and the initial velocity at each enzyme concentration was obtained (Figure 2.3).

26
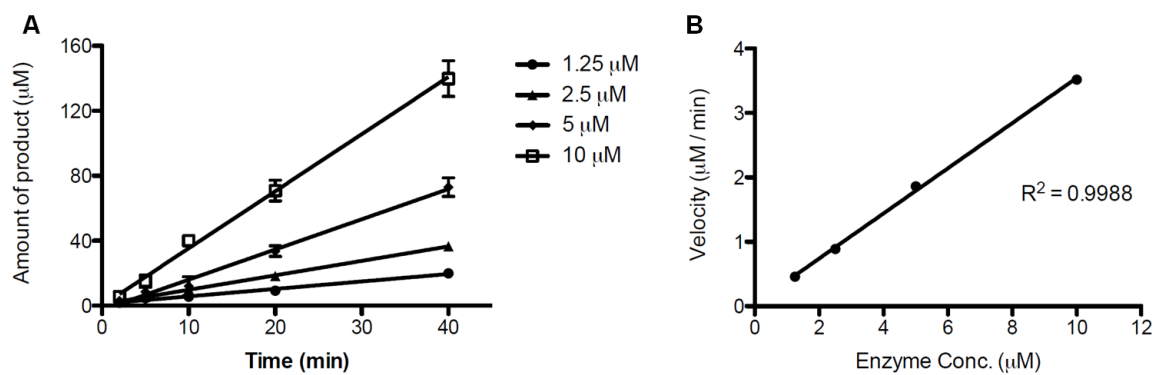
Figure 2.3 Measurement of initial velocity.

(A) Progress curve of PikDH2 dehydration reaction at varying enzyme concentrations (1.25–10 µM); **(B)** Plot of initial velocity *vs.* enzyme concentration.

Table 2.3 LC-MS/MS analysis of analytes 1a, 2a, 3 and 4.

Analyte	HPLC retention time (min)	Transition	Internal standard
1a	4.69	314→198	**2a**
2a	4.45, 4.98	328→212	**1a**
3	4.73	274→216	**4**
4	5.00	288→120	**3**

Reversibility of the dehydration reaction. (Data generated by Yang Li)

Compounds **1a**, **2a**, **3** and **4** (1 mM) were individually added to the reaction buffer (50 mM Tris, 150 mM NaCl, pH 8.0) with PikDH2-KR2 (10 µM) in a total volume of 100 µL, respectively. After 20 h incubation, 5 µL of the reaction mixture was quenched by adding to 495 µL of 1:1 MeCN–reaction buffer (100-fold dilution). 10 µL of the diluted reaction mixture was added to 90 µL of 1:1 MeCN–reaction buffer (10-fold dilution, total 1000-fold dilution). The identities of the enzymatic products were determined by co-injection of authentic standards (Figs. 2.4, 2.5) and total amount was calculated by standard curve with internal standard added in. Each reaction was performed in duplicate.

Kinetic analysis of dehydration reaction by LC-MS/MS.

The enzymatic reactions were carried out in a total volume of 50 µL under initial velocity conditions containing PikDH2-KR2 (5 µM), reaction buffer (50 mM Tris, 150 mM NaCl, pH 8.0) and substrates **1a** or **2a** at variable concentrations (0.25, 0.5, 1, 2, 3, 4, 6 mM). The final DMSO concentration was held constant at 3%. After incubation at 25 °C for 15 min, 5 µL of the reaction mixture was added to 495 µL of 1:1 MeCN–reaction buffer (100-fold dilution). The resulting

solution was vortexed, centrifuged and analyzed by LC-MS/MS as described above. Control

reactions for each concentration of substrate were performed without the addition of enzyme. Each
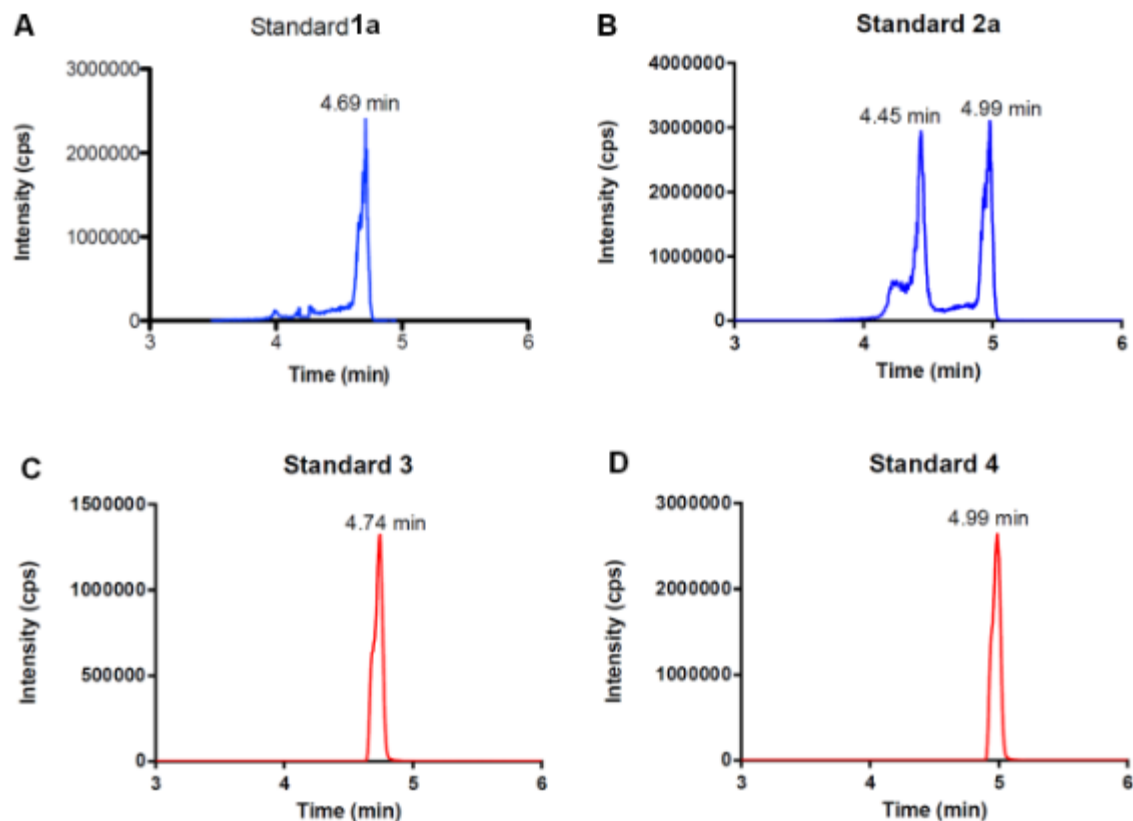
Figure 2.5 LC-MS/MS analysis of standards.

(**A**) **1a** (MRM *m/z* 314→198); (**B**) **2a** (MRM *m/z* 328→212); (**C**) **3** (MRM *m/z* 274→216); (**D**) **4** (MRM *m/z* 288→120)
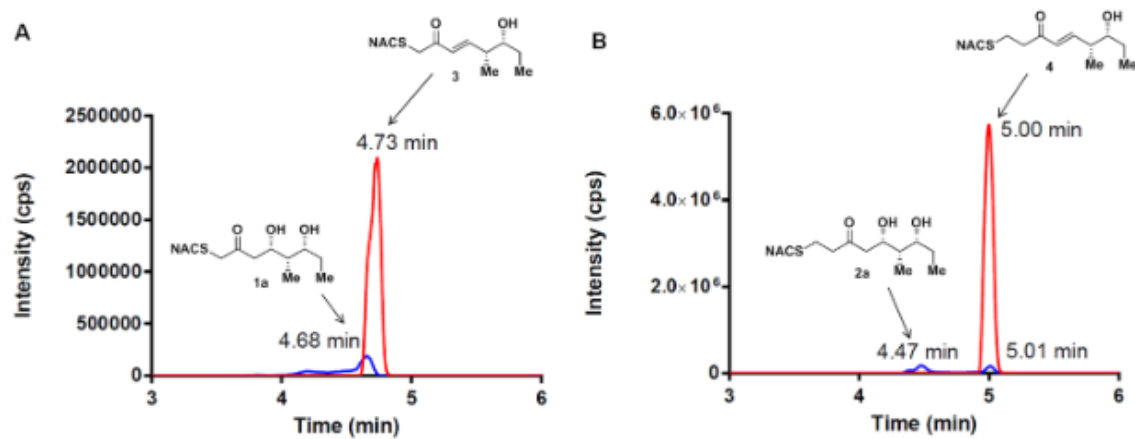
Figure 2.4 LC-MS/MS traces for hydration reactions of substrates 3 (A) and substrate 4 (B) by pikKR2-DH2

reaction was performed in duplicate. Apparent steady-state kinetic parameters were determined by fitting the normalized v_0 vs [S] plots to the Michaelis–Menten equation by nonlinear regression analysis using GraphPad Prism 5.0 (Fig. 2.6). Kinetic parameters of PikDH2-KR2 mutants were acquired in an analogous way except in some cases saturation was not achieved and the curve was fit by linear regression to provide specificity constants (Fig. 2.8).
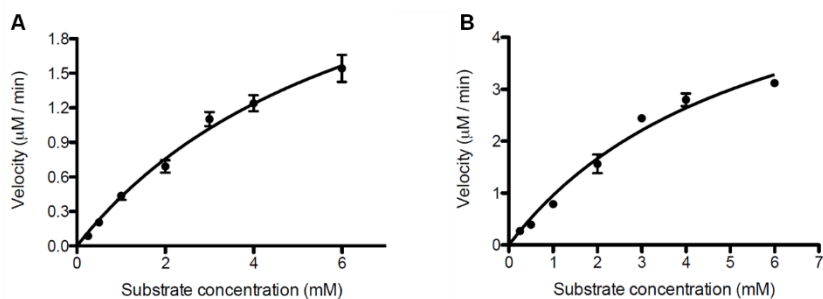
Figure 2.6 Michaelis-Menten curves of PikDH2.

(**A**) with substrates **1a**; (**B**) with substrates **2a**.
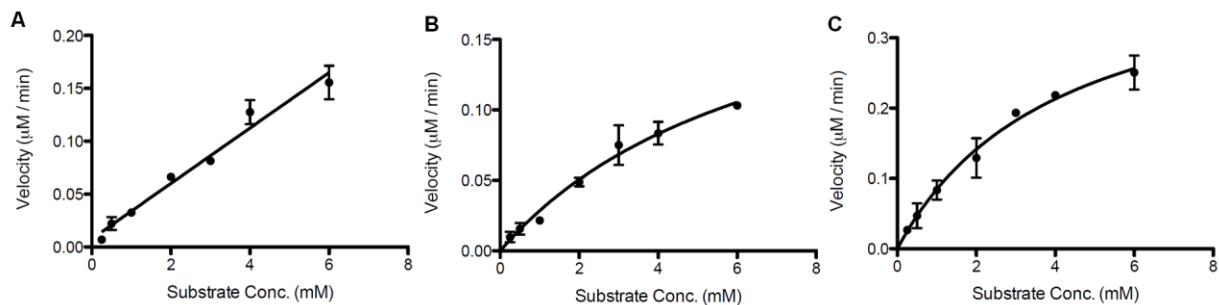
Figure 2.7 Michaelis-Menten and linear curves of PikDH2 mutants with substrate 2a

(**A**) F3746L; (**B**) F3750L; (**C**) F3750Y.

Homology model of PikDH2.

The PikDH2 homology model (residues 1-293 of the PikKR2-DH2 didomain) was built in LOMETS[8] using the CurK dehydratase from the curacin pathway as a template (PDB 3KG9) (Fig. 2.8)[9]. The PikDH2 model has an RMSD of 0.290 Å compared to the template, with a Z-score of 27.3 and 22% sequence identity.
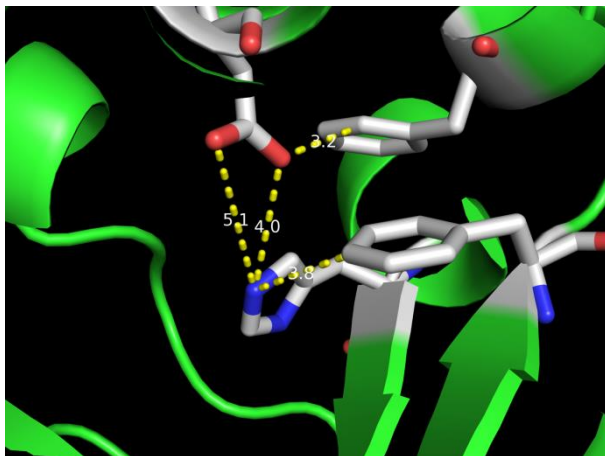
Figure 2.8 Active site of PikDH2 homology model.

Catalytic residues Asp3800 and His3611 as well as hydrophobic residues Phe3746 and Phe3750 have been depicted in detail.

pH dependency profile of PikDH2. (Data generated by Yang Li)

The effect of pH on kinetic parameters was obtained by using HEPES (pH 6.6–7.5), Tris (pH 8.0), and bicine (pH 8.5–9.0). At desired pH values, enzymatic reactions were conducted with substrate **2a** (0–3 mM) under the conditions described above. Kinetic parameters V_{max}/K_M at different pH were obtained via fitting the v_0 vs $[S]$ plots to by linear regression analysis. The pK_a value of the ionizable group was obtained through fitting V_{max}/K_M to eq 1:

$$\log \frac{V_{max}}{K_M} = \log \frac{C}{1-[H]^+/K_a} \tag{1}$$

where, C is the pH-independent plateau value, $[H]^+$ is the hydrogen ion concentration, and K_a is the dissociation constant of the acid.[10]

Inhibition assay with mechanism-based inhibitor 6. (Data generated by Yang Li)

Inhibitor **6** (10–40 µM) was incubated with substrate **2a** (5 mM), PikDH2-KR2 (5 µM), reaction buffer (50 mM Tris, 150 mM NaCl, pH 8.0) in a total volume of 50 µL at 25 °C. At 2, 4, 8, 16 min time points, 5 µL of the reaction mixture was added to 495 µL of 1:1 MeCN–reaction buffer (100-fold dilution). The resulting solution was vortexed, centrifuged and analyzed by LC-MS/MS to detect the enzymatic product formation. Each reaction was conducted in duplicate. Inhibitor **6** showed time-dependent inhibition of PikDH2. The progress curve was fit to eq 2 and eq 3 for tight binding time-dependent inhibition:

$$[P] = v_s t + \frac{(1-\gamma)(v_i - v_s)}{\gamma k_{obs}} \ln \frac{1 - \exp(-k_{obs}t)}{1-\gamma} \tag{2}$$

$$\gamma = \frac{[E]}{[I]} \left(1 - \frac{v_s}{v_i}\right)^2 \tag{3}$$

where $[P]$ is the concentration of enzymatic product, t is the reaction time, v_i is the initial velocity, v_s is the steady state velocity, and k_{obs} is the observed rate constant of inhibition. Since mechanism-based inhibition is irreversible, the v_s value is equal to 0, thus the γ value is equal to the ratio of enzyme concentration to inhibitor concentration. The secondary plot of $1/k_{obs}$ versus $1/[I]$ was fit to a Kitz and Wilson plot to provide $K_{I,app}$ and k_{inact} values. The true K_I value was deduced from eq 4:

$$K_{I,app} = \frac{K_I}{1 + [S]/K_M} \tag{4}$$

where $[S]$ is the substrate concentration, and K_M is the Michaelis-Menten constant for the substrate.

General chemistry procedures.

(All synthesis protocols run by Yang Li)

All commercial reagents were used as provided unless otherwise indicated. Substrate analogs **1a**[5], **2a**[5], intermediates **S1**[1,2], **S2**[3,4], **S9**[5] **and S14**[5,6] were prepared by the published procedures. THF and CH_2Cl_2 were purified by passage through alumina columns. All reactions were performed under an inert atmosphere of dry N_2 in oven-dried (150 ºC) glassware. Flash chromatography was conducted on silica gel (230–400 mesh) using the indicated solvent systems. TLC was performed on 250 µm, F_{254} silica gel plates, and visualized by UV and *p*-anisaldehyde stain. Optical rotations were determined on a Rudolph Autopol III polarimeter using the sodium D line (λ = 589 nm) at the temperature indicated and are reported as follows: $[\alpha]_D^{temp}$, concentration (*c* = g/100 mL), and solvent. ^1H and ^{13}C NMR spectra were recorded on a Bruker 400 spectrometer at 400 Hz for ^1H NMR and at 100 Hz for ^{13}C NMR. Chemical shifts are reported in ppm from an internal standard of residual $CHCl_3$ (7.26 ppm for ^1H NMR and 77.00 for ^{13}C NMR). Proton chemical data are reported as follows: chemical shift (ppm), multiplicity (s = singlet, d = doublet, t = triplet, q = quartet, quin = quintet, sext = sextet, m = multiplet, br = broad), coupling constant (Hz), and integration. High resolution mass spectra were obtained on a Bruker BioTOF II ESI-TOF/MS using either PEG or PPG standards as high resolution calibrants.

(3*S*,4*S*,5*R*)-5-[(*tert*-Butyldimethylsilyl)oxy]-3-hydroxy-1-[(*R*)-4-isopropyl-2-thioxothiazolidin-3-yl]-4-methylheptan-1-one (**S3**).
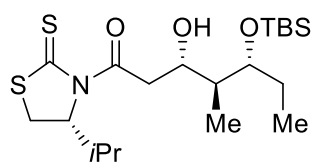
To a solution of thiazolidinethione **S2** (172 mg, 0.846 mmol, 1.60 equiv) in CH_2Cl_2 (4.2 mL) at –40 °C was added $TiCl_4$ (99 µL, 0.90 mmol, 1.7 equiv). An aliquot of *i*-Pr_2NEt (0.16 mL, 0.90 mmol, 1.7 equiv) was added after stirring at –40 °C for 30 min. The reaction mixture was stirred at –40 °C

an additional 2 h, and then cooled to –78 °C. Aldehyde **S1** (122 mg, 0.529 mmol, 1.00 equiv) was added and rinsed with CH_2Cl_2 (3 × 0.3 mL). The reaction was stirred at –78 °C for 80 min, quenched by addition of saturated aqueous NH_4Cl (20 mL) and allowed to warm to room temperature. The organics were extracted with CH_2Cl_2 (3 × 20 mL), dried (Na_2SO_4), filtered and concentrated under reduced pressure. Purification by flash chromatography (20% EtOAc/hexanes) afforded the title compound (140 mg, 61%) as a yellow oil: R_f = 0.34 (20% EtOAc/hexanes); $[\alpha]_D^{22}$ = –258 (*c* 1.00, $CHCl_3$); ^1H NMR ($CDCl_3$, 400 MHz) δ 5.16 (t, *J* = 6.8 Hz 1H), 4.19–4.11 (m, 1H), 3.75 (q, *J* = 6.0 Hz, 1H), 3.64 (dd, *J* = 17.7, 2.0 Hz, 1H), 3.51 (dd, *J* = 11.5, 8.0 Hz, 1H), 3.15 (dd, *J* = 17.7, 9.9 Hz, 1H), 3.02 (d, *J* = 11.5 Hz, 1H), 2.36 (dq, *J* = 13.5, 6.8 Hz, 1H), 1.85 (sext, *J* = 7.0 Hz, 1H), 1.58–1.40 (m, 2H), 1.06 (d, *J* = 6.8 Hz, 3H), 0.97 (d, *J* = 6.9 Hz, 3H), 0.93–0.83 (m, 15H), 0.06 (s, 3H), 0.05 (s, 3H); ^{13}C NMR ($CDCl_3$, 100 MHz) δ 203.0, 173.4, 75.1, 71.4, 69.4, 43.0, 42.5, 30.8, 30.6, 25.9, 25.6, 19.1, 18.1, 17.8, 11.4, 9.2, -4.4, -4.6; HRMS (ESI-TOF) *m/z*: [M + Na]$^+$ calcd for $C_{20}H_{39}NO_3S_2SiNa$ 456.2033, found 456.2057.

(3*S*,4*R*,5*R*)-3,5-Dihydroxy-*N*-methoxy-*N*,4-dimethylheptanamide (**S5**).
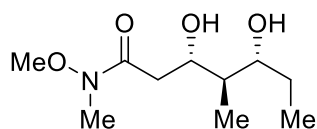
To a solution of thiazolidinethione **S3** (136 mg, 0.314 mmol, 1.00 equiv) in CH_2Cl_2 (5 mL) at room temperature was added *N,O*-dimethylhydroxylamine hydrochloride (123 mg, 1.26 mmol, 4.00 equiv) and imidazole (171 mg, 2.51 mmol, 8.00 equiv), followed by the addition of DMAP (7.7 mg, 0.063 mmol, 0.20 equiv). The reaction mixture was stirred at room temperature until the bright yellow color faded (24 h), then quenched with water. The layers were separated, and the aqueous layer was extracted with CH_2Cl_2 (3 × 10 mL). The combined organic layers were washed with saturated aqueous NaCl (20 mL), dried (Na_2SO_4), filtered and concentrated under reduced pressure

to afford the crude **S4** as a colorless oil, which was used directly in the next reaction without further purification. $R_f = 0.41$ (30% EtOAc/hexanes).

To a solution of silyl ether **S4** prepared above (105 mg, 0.314 mmol, 1.00 equiv) in THF (10 mL) at 0 °C was added TBAF (1.0 M in THF, 0.94 mL, 0.94 mmol, 3.0 equiv). The reaction mixture was stirred at 0 °C for 7 h, then quenched by addition of saturated aqueous NH_4Cl (10 mL). The reaction mixture was extracted with EtOAc (3 × 10 mL), and the combined organic layers were washed with saturated aqueous NaCl (20 mL), dried (Na_2SO_4), filtered, and concentrated under reduced pressure. Purification by flash chromatography (5% MeOH/CH_2Cl_2) afforded the title compound (60 mg, 87% over 2 steps) as a colorless oil: $R_f = 0.30$ (5% MeOH/CH_2Cl_2); $[\alpha]_D^{21} = -43.4$ (c 0.650, CHCl$_3$); ^{1}H NMR (CDCl$_3$, 400 MHz) δ 4.07–3.99 (m, 1H), 3.69 (s, 3H), 3.59 (td, $J = 7.9, 2.9$ Hz, 1H), 3.19 (s, 3H), 2.80 (d, $J = 16.5$ Hz, 1H), 2.51 (dd, $J = 16.5, 9.8$ Hz, 1H), 1.71–1.60 (m, 2H), 1.41 (dquin, $J = 14.7, 7.4$ Hz, 1H), 0.97 (t, $J = 7.4$ Hz, 3H), 0.82 (d, $J = 6.9$ Hz, 3H); ^{13}C NMR (CDCl$_3$, 100 MHz) δ 173.9, 76.3, 72.9, 61.3, 42.8, 36.0, 31.9, 27.1, 12.9, 9.3; HRMS (ESI-TOF) m/z: [M + Na]$^+$ calcd for $C_{10}H_{21}NO_4Na$ 242.1363, found 242.1368.

(3S,4R,5R)-N-Methoxy-N,4-dimethyl-3,5-bis[(triethylsilyl)oxy]heptanamide (**S6**).
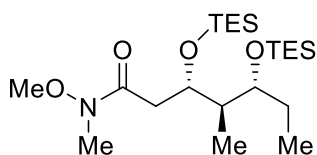
To a solution of alcohol **S5** (54 mg, 0.25 mmol, 1.0 equiv) in CH_2Cl_2 (10 mL) at 0 °C was added i-Pr$_2$NEt (0.15 mL, 0.89 mmol, 3.6 equiv) and TESOTf (0.18 mL, 0.79 mmol, 3.2 equiv). After stirring at 0 °C for 60 min, the reaction mixture was quenched by the addition of saturated aqueous NaHCO$_3$ (20 mL). The layers were separated, and the aqueous layer was extracted with CH$_2$Cl$_2$ (3 × 10 mL). The combined organic layers were washed with saturated aqueous NaCl (50 mL), dried (Na$_2$SO$_4$), filtered and concentrated under reduced pressure. Purification by flash chromatography (10%

EtOAc/hexanes) afforded the title compound (73 mg, 66%) as a colorless oil: R_f = 0.44 (10% EtOAc/hexanes); $[\alpha]_D^{22}$ = –31.0 (c 1.50, CHCl$_3$); ^{1}H NMR (CDCl$_3$, 400 MHz) δ 4.50–4.43 (m, 1H), 3.68 (s, 3H), 3.60 (q, J = 5.7 Hz, 1H), 3.16 (s, 3H), 2.76–2.65 (m, 1H), 2.36 (dd, J = 15.0, 2.9 Hz, 1H), 1.85–1.77 (m, 1H), 1.58–1.44 (m, 2H), 0.99–0.83 (m, 24H), 0.64–0.52 (m, 12H); ^{13}C NMR (CDCl$_3$, 100 MHz) δ 173.1, 74.5, 69.5, 61.2, 43.7, 35.5, 32.0, 26.4, 10.3, 8.8, 7.0, 6.9, 5.2, 5.0; HRMS (ESI-TOF) m/z: [M + Na]$^+$ calcd for C$_{22}$H$_{49}$NO$_4$Si$_2$Na 470.3092, found 470.3097.

(5S,6R,7R)-6-Methyl-5,7-bis[(triethylsilyl)oxy]non-1-en-3-one (**S7**).
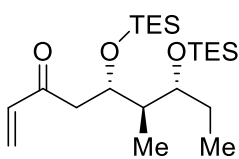
To a solution of Weinreb amide **S6** (73 mg, 0.16 mmol, 1.0 equiv) in THF (5 mL) at 0 °C was added vinyl magnesium bromide (1.0 M in THF, 0.48 mL, 0.48 mmol, 3.0 equiv). After stirring at 0 °C for 55 min, the reaction mixture was quenched by the addition of saturated aqueous NH$_4$Cl (5 mL). The layers were separated, and the aqueous layer was extracted with EtOAc (3 × 10 mL). The combined organic layers were washed with saturated aqueous NaCl (20 mL), dried (Na$_2$SO$_4$) and concentrated under reduced pressure. Purification by flash chromatography (10% EtOAc/hexanes) afforded the title compound (45 mg, 66%) as a colorless oil: R_f = 0.60 (10% EtOAc/hexanes); $[\alpha]_D^{21}$ = –34.6 (c 0.800, CHCl$_3$); ^{1}H NMR (CDCl$_3$, 400 MHz) δ 6.38 (dd, J = 17.6, 10.5 Hz, 1H), 6.20 (dd, J = 17.6, 1.0 Hz, 1H), 5.79 (dd, J = 10.5, 1.1 Hz, 1H), 4.51–4.45 (m, 1H), 3.58 (q, J = 5.3 Hz, 1H), 2.77 (q, J = 8.8 Hz, 1H), 2.59 (dd, J = 15.5, 2.9 Hz, 1H), 1.84–1.76 (m, 1H), 1.57–1.45 (m, 2H), 1.00–0.82 (m, 24H), 0.57 (app. dq, J = 19.0, 7.8 Hz, 12H); ^{13}C NMR (CDCl$_3$, 100 MHz) δ 200.0, 137.5, 127.8, 74.6, 69.1, 43.52, 43.46, 26.5, 10.3, 8.6, 7.0, 6.9, 5.2, 5.0; HRMS (ESI-TOF) m/z: [M + Na]$^+$ calcd for C$_{22}$H$_{46}$O$_3$Si$_2$Na 437.2878, found 437.2854.

(5*S*,6*R*,7*S*)-5,7-Dihydroxy-6-methyl-1-[*N*-(2-acetamidoethyl)thio]nonan-3-one (**2c**).
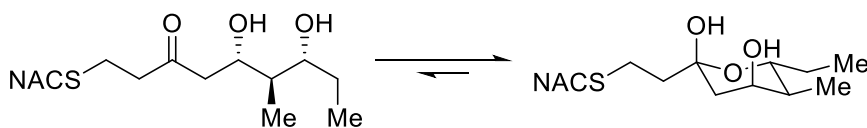
To a solution of vinyl ketone **S7** (32 mg, 0.078 mmol, 1.0 equiv) in THF (5 mL) was added *N*-acetylcysteamine (12 µL, 0.12 mmol, 1.5 equiv) and a catalytic amount of Cs_2CO_3. The reaction was stirred at room temperature for 40 min, before quenching with saturated aqueous NH_4Cl (5 mL). The layers were separated, and the aqueous layer was extracted with EtOAc (3 × 10 mL). The combined organic layers were washed with saturated aqueous NaCl (40 mL), dried (Na_2SO_4), filtered and concentrated under reduced pressure to yield crude **S8** (35 mg) as a colorless oil, which was used in the next reaction without further purification: R_f = 0.36 (5% $MeOH/CH_2Cl_2$).

To a solution of silyl ether **S8** prepared above (35 mg, 0.066 mmol, 1.0 equiv) in THF (6 mL) at 0 °C was added a solution of 70% HF-pyridine:pyridine:THF (1:2:8, 3 mL). The reaction was stirred at 0 °C for 3.5 h, then quenched with saturated aqueous $NaHCO_3$ to bring the reaction to pH 7, and extracted with EtOAc (3 × 10 mL). The combined organic layers were washed with saturated aqueous NaCl (40 mL), dried (Na_2SO_4), filtered and concentrated under reduced pressure. Purification by flash chromatography (5% $MeOH/CH_2Cl_2$) afforded the title compound (17 mg, 72% over 2 steps) as a colorless oil: R_f = 0.20 (5% $MeOH/CH_2Cl_2$); $[\alpha]_D^{21}$ = 41.1 (*c* 1.00, $CHCl_3$); ^{1}H NMR ($CDCl_3$, 400 MHz) δ 6.10 (s, 1H), 4.98 (s, 1H), 3.97–3.85 (m, 1H), 3.75–3.68 (m, 1H), 3.50–3.36 (m, 3H), 2.78–2.61 (m, 4H), 2.04–1.96 (m, 4H), 1.90–1.81 (m, 2H), 1.71–1.59 (m, 2H), 1.50–1.32 (m, 2H), 0.96–0.90 (m, 6H); ^{13}C NMR ($CDCl_3$, 100 MHz) δ 170.4, 97.1, 70.4, 70.2, 41.4, 39.9, 38.3 (overlap), 31.5, 25.4, 25.0, 23.2, 13.9, 9.3; HRMS (ESI-TOF) *m/z*: [M + Na]+ calcd for $C_{14}H_{27}NO_4SNa$ 328.1553, found 328.1551.

(3*S*,4*R*,5*S*)-5-[(*tert*-Butyldimethylsilyl)oxy]-3-hydroxy-1-[(*R*)-4-isopropyl-2-thioxothiazolidin-3-yl]-4-methylheptan-1-one (***diastereomer*-S3**).
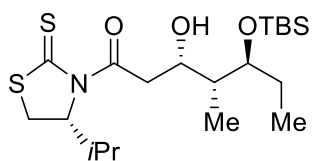
The title compound was prepared using otherwise identical conditions as described for the preparation of aldol product **S3** except for the use of aldehyde (+)–**S1** (157 mg, 0.771 mmol, 1.00 equiv). Purification by flash chromatography (20% EtOAc/hexanes) afforded the title compound (129 mg, 62%) as a yellow oil: R_f = 0.46 (20% EtOAc/hexanes); $[\alpha]_D^{21}$ = –211 (*c* 2.00, CHCl$_3$); ^{1}H NMR (CDCl$_3$, 400 MHz) δ 5.19–5.13 (m, 1H), 4.66 (d, *J* = 9.4 Hz, 1H), 3.72–3.65 (m, 2H), 3.51 (dd, *J* = 11.4, 8.0 Hz, 1H), 3.42 (dd, *J* = 17.1, 9.3 Hz, 1H), 3.27 (dd, *J* = 17.1, 2.0 Hz, 1H), 3.01 (d, *J* = 11.5 Hz, 1H), 2.40 (dq, *J* = 13.5, 6.7 Hz, 1H), 1.82–1.59 (m, 3H), 1.06 (d, *J* = 6.8 Hz, 3H), 1.01 (d, *J* = 7.1 Hz, 3H), 0.98 (d, *J* = 7.0 Hz, 3H), 0.88 (s, 9H), 0.87 (t, *J* = 7.5 Hz), 0.093 (s, 3H), 0.085 (s, 3H); ^{13}C NMR (CDCl$_3$, 100 MHz) δ 203.0, 172.2, 79.3, 71.6, 66.7, 43.8, 38.0, 30.9, 30.5, 27.5, 25.8, 19.1, 17.9, 17.7, 11.7, 9.5, -4.4, -4.9; HRMS (ESI-TOF) *m/z*: [M + Na]$^+$ calcd for C$_{20}$H$_{39}$NO$_3$S$_2$SiNa 456.2033, found 456.2052.

(3*S*,4*S*,5*S*)-3,5-Dihydroxy-*N*-methoxy-*N*,4-dimethylheptanamide (***diastereomer*-S5**).
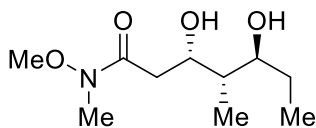
Identical reaction conditions employed for the synthesis of weinreb amide **S4** were used, except for the use of thiazolidinethione ***diastereomer*-S3** (129 mg, 0.297 mmol, 1.00 equiv). The crude product was used to carry out the next reaction without further purification: R_f = 0.34 (30% EtOAc/hexanes).

The title compound was prepared using otherwise identical conditions as described for the preparation of diol **S5**, except for the use of silyl ether ***diastereomer*-S4** prepared above (99 mg, 0.297 mmol, 1.00 equiv). Purification by flash chromatography (5% MeOH/CH$_2$Cl$_2$) afforded the

title compound (45 mg, 69% over 2 steps) as a colorless oil: $R_f = 0.29$ (5% MeOH/CH$_2$Cl$_2$); $[\alpha]_D^{22}$ = –40.4 (c 1.00, CHCl$_3$); ^{1}H NMR (CDCl$_3$, 400 MHz) δ 4.39 (dt, J = 9.8, 2.8 Hz, 1H), 3.69 (s, 4H), 3.55–3.48 (m, 1H), 3.22–3.14 (m, 4H), 2.68–2.49 (m, 2H), 1.72–1.65 (m, 1H), 1.63–1.44 (m, 2H), 1.00–0.91 (m, 6H); ^{13}C NMR (CDCl$_3$, 100 MHz) δ 173.9, 76.1, 69.4, 61.3, 40.6, 34.7, 31.9, 28.1, 11.9, 9.8; HRMS (ESI-TOF) m/z: [M + Na]$^+$ calcd for C$_{10}$H$_{21}$NO$_4$Na 242.1363, found 242.1366.

(3S,4S,5S)-N-Methoxy-N,4-dimethyl-3,5-bis[(triethylsilyl)oxy]heptanamide (***diastereomer*-S6**).
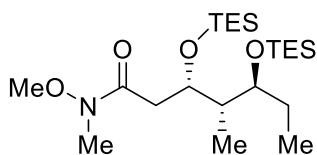
The title compound was prepared using otherwise identical conditions as described for the preparation of silylether **S6**, except for the use of alcohol ***diastereomer*-S5** (42 mg, 0.19 mmol, 1.0 equiv). Purification by flash chromatography (10% EtOAc/hexanes) afforded the title compound (57 mg, 66%) as a colorless oil: $R_f = 0.45$ (10% EtOAc/hexanes); $[\alpha]_D^{21}$ = –26.3 (c 1.00, CHCl$_3$); ^{1}H NMR (CDCl$_3$, 400 MHz) δ 4.25 (q, J = 5.6 Hz, 1H), 3.68 (s, 3H), 3.57 (dt, J = 7.9, 3.6 Hz, 1H), 3.16 (s, 3H), 2.66 (dd, J = 15.0, 6.7 Hz, 1H), 2.57 (dd, J = 15.0, 5.6 Hz, 1H), 1.73–1.65 (m, 1H), 1.55–1.44 (m, 1H), 1.43–1.35 (m, 1H), 1.00–0.85 (m, 24H), 0.60 (app. dq, J = 7.9, 3.5 Hz, 12H); ^{13}C NMR (CDCl$_3$, 100 MHz) δ 172.4, 75.9, 70.8, 61.2, 45.0, 38.8, 32.0, 25.5, 10.4, 9.6, 7.0, 5.2; HRMS (ESI-TOF) m/z: [M + Na]$^+$ calcd for C$_{22}$H$_{49}$NO$_4$Si$_2$Na 470.3092, found 470.3088.

(5*S*,6*S*,7*S*)-6-Methyl-5,7-bis[(triethylsilyl)oxy]non-1-en-3-one (***diastereomer-S7***).
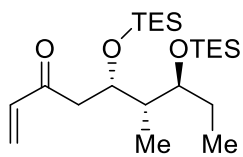
The title compound was prepared using otherwise identical conditions as described for the preparation of enone **S7**, except for the use Weinreb amide ***diastereomer-S6*** (42 mg, 0.094 mmol, 1.0 equiv). Purification by flash chromatography (5% EtOAc/hexanes) afforded the title compound (28 mg, 72%) as a colorless oil: R_f = 0.68 (10% EtOAc/hexanes); $[\alpha]_D^{21}$ = –27.0 (*c* 0.650, CHCl$_3$); ^{1}H NMR (CDCl$_3$, 400 MHz) δ 6.37 (dd, *J* = 17.6, 10.5 Hz, 1H), 6.21 (d, *J* = 17.6 Hz, 1H), 5.83 (d, *J* = 10.5 Hz, 1H), 4.28 (q, *J* = 5.7 Hz, 1H), 3.55 (dt, *J* = 7.8, 4.0 Hz, 1H), 2.84–2.70 (m, 2H), 1.69–1.61 (m, 1H), 1.53–1.34 (m, 2H), 0.99–0.84 (m, 24H), 0.58 (app. dq, *J* = 7.9, 4.0 Hz, 12H); ^{13}C NMR (CDCl$_3$, 100 MHz) δ 199.1, 137.1, 128.3, 75.6, 70.2, 46.5, 44.9, 25.6, 10.1, 9.7, 7.00, 5.2; HRMS (ESI-TOF) *m/z*: [M + Na]$^+$ calcd for C$_{22}$H$_{46}$O$_3$Si$_2$Na 437.2878, found 437.2847.

(5*S*,6*S*,7*S*)-5,7-Dihydroxy-6-methyl-1-[*N*-(2-acetamidoethyl)thio]nonan-3-one (**2d**).
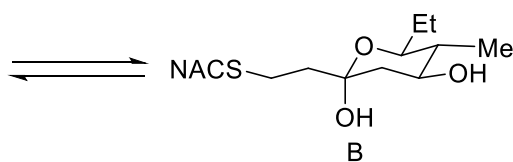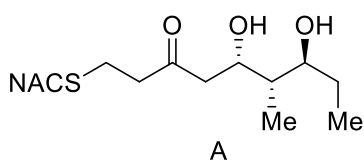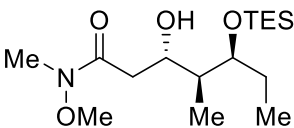
Identical reaction conditions as reported for the synthesis of thioether **S8** were employed, except for the use of vinyl ketone ***diastereomer-S7*** (14 mg, 0.034 mmol, 1.0 equiv). The crude product ***diastereomer-S8*** was used to carry out the next reaction without further purification: R_f = 0.45 (5% MeOH/CH$_2$Cl$_2$).

The title compound was prepared using otherwise identical conditions as described for the preparation of thioether **2c**, except for the use of silyl ether ***diastereomer-S8*** prepared above (18 mg, 0.034 mmol, 1.0 equiv). Purification by flash chromatography (5% MeOH/CH$_2$Cl$_2$) afforded the title compound (5.8 mg, 56% over 2 steps) as a colorless oil: R_f = 0.27 (5% MeOH/CH$_2$Cl$_2$);

Due to the instability of the compound the optical rotation could not be obtained; ^{1}H NMR (CDCl$_3$, 400 MHz, approximately 3:17 mixture of A:B where the integrations have been normalized) δ 6.03 (s, 0.15H), 5.89 (s, 0.85H), 4.45 (dt, J = 10.1, 2.4 Hz, 0.15H), 3.69 (dt, J = 10.7, 4.8 Hz, 0.85H), 3.54–3.36 (m, 3.15H), 3.20 (s, 0.85H), 2.83–2.62 (m, 4.45H), 2.46 (dd, J = 16.4, 2.7 Hz, 0.15H), 2.11 (dd, J = 12.3, 4.8 Hz, 0.85H), 1.99 (s, 3H), 1.95–1.89 (m, 1.7H), 1.76–1.68 (m, 1H), 1.46–1.30 (m, 1.85H), 1.28–1.21 (m, 1H), 1.01–0.87 (m, 6H); ^{13}C NMR (CDCl$_3$, 100 MHz, major isomer B) δ 170.2, 97.3, 74.6, 70.0, 43.2, 43.0, 41.1, 38.2, 31.4, 25.3, 25.2, 23.3, 12.6, 9.6; HRMS (ESI-TOF) m/z: [M + Na]$^+$ calcd for C$_{14}$H$_{27}$NO$_4$SNa 328.1553, found 328.1560.

(3S,4S,5S)-3-Hydroxy-N-methoxy-N,4-dimethyl-5-[(triethylsilyl)oxy]heptanamide (**S10**).

To a solution of freshly distilled i-Pr$_2$NH (0.21 mL, 1.5 mmol, 1.5 equiv) in THF (30 mL) at –78 °C was added n-BuLi (1.2 M in THF, 1.2 mL, 1.4 mmol, 1.4 equiv). After stirring at –78 °C for 30 min, N-methoxy-N-methylacetamide (0.15 mL, 1.4 mmol, 1.4 equiv) was added. The reaction mixture was stirred at –78 °C for an additional 30 min, followed by the dropwise addition of a solution of aldehyde **S9** (233 mg, 1.01 mmol, 1.00 equiv) in THF (0.5 mL). The reaction mixture was stirred at –78 °C for an additional 1 h, then quenched by the addition of saturated aqueous NH$_4$Cl (20 mL). The layers were separated and the aqueous layer was extracted with EtOAc (3 × 20 mL). The combined organic layers were dried (Na$_2$SO$_4$), filtered and concentrated under reduced pressure. Purification by flash chromatography (40% EtOAc/hexanes) afforded the title compound **S10** (169 mg, 50%) as a colorless oil (total yield = 75%, dr = 2: 1): [α]$_D^{22}$ = –32.2 (c 1.00, CHCl$_3$); ^{1}H NMR (CDCl$_3$, 400 MHz) δ 4.16 (d, J = 2.9 Hz, 1H), 4.01 (tt, J = 9.0, 3.0 Hz, 1H), 3.95 (dt, J = 6.8, 2.2 Hz, 1H), 3.70 (s, 3H), 3.20 (s, 3H), 2.66 (d, J = 14.3 Hz, 1H), 2.52 (dd, J = 15.7, 9.2 Hz, 1H), 1.74–1.63 (m, 1H), 1.60–1.46 (m, 2H), 0.96 (t, J = 7.9 Hz, 9H), 0.87 (t, J = 7.5 Hz, 3H), 0.81 (d, J = 7.0 Hz, 3H), 0.62

(q, J = 7.9 Hz, 6H); ^{13}C NMR (CDCl$_3$, 100 MHz) δ 173.7, 75.1, 70.0, 61.2, 41.8, 36.9, 31.9, 26.6, 10.7, 10.6, 6.9, 5.2; HRMS (ESI-TOF) *m/z*: [M + Na]$^+$ calcd for C$_{16}$H$_{35}$NO$_4$SiNa 356.2228, found 356.2226.

(3*S*,4*R*,5*S*)-*N*-Methoxy-*N*,4-dimethyl-3,5-bis[(triethylsilyl)oxy]heptanamide (**S11**).
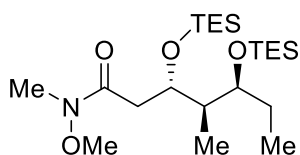
To a solution of alcohol **S10** (122 mg, 0.366 mmol, 1.00 equiv) in CH$_2$Cl$_2$ (10 mL) at 0 °C was added *i*-Pr$_2$NEt (0.11 mL, 0.66 mmol, 1.8 equiv) and TESOTf (0.13 mL, 0.59 mmol, 1.6 equiv). After stirring at 0 °C for 1 h, the reaction mixture was quenched by the addition of saturated aqueous NaHCO$_3$ (10 mL). The layers were separated, and the aqueous layer was extracted with CH$_2$Cl$_2$ (3 × 10 mL). The combined organic layers were washed with saturated aqueous NaCl (20 mL), dried (Na$_2$SO$_4$), filtered and concentrated under reduced pressure. Purification by flash chromatography (20% EtOAc/hexanes) afforded the title compound (155 mg, 95%) as a colorless oil: R_f = 0.65 (20% EtOAc/hexanes); $[\alpha]_D^{22}$ = –28.2 (*c* 1.00, CHCl$_3$); ^{1}H NMR (CDCl$_3$, 400 MHz) δ 4.30 (dt, *J* = 9.7, 3.0 Hz, 1H), 3.70 (s, 3H), 3.52 (q, *J* = 5.6 Hz, 1H), 3.17 (s, 3H), 2.87–2.72 (m, 1H), 2.20 (dd, *J* = 14.9, 2.0 Hz, 1H), 1.86–1.74 (m, 1H), 1.61–1.49 (m, 2H), 0.98–0.85 (m, 24H), 0.63–0.54 (m, 12H); ^{13}C NMR (CDCl$_3$, 100 MHz) δ 173.1, 75.2, 71.1, 61.2, 42.9, 34.8, 32.0, 27.7, 8.9, 8.8, 7.0, 6.8, 5.4, 4.9; HRMS (ESI-TOF) *m/z*: [M + Na]$^+$ calcd for C$_{22}$H$_{49}$NO$_4$Si$_2$Na 470.3092, found 470.3093.

(5*S*,6*R*,7*S*)-6-Methyl-5,7-bis[(triethylsilyl)oxy]non-1-en-3-one (**S12**).
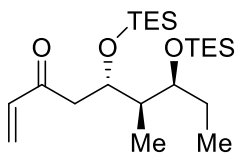
To a solution of Weinreb amide **S11** (155 mg, 0.346 mmol, 1.00 equiv) in THF (15 mL) at 0 °C was added vinyl magnesium bromide (1.0 M in THF, 1.04 mL, 1.04 mmol, 3.00 equiv). The reaction mixture was stirred at 0 °C for 70 min, quenched by the addition of saturated aqueous NH_4Cl (10 mL), and allowed to warm up to room temperature. The layers were separated, and the aqueous layer was extracted with EtOAc (3 × 20 mL). The combined organic layers were washed with saturated aqueous NaCl (30 mL), dried (Na_2SO_4), and concentrated under reduced pressure. Purification by flash chromatography (10% EtOAc/hexanes) afforded the title compound (77 mg, 53%) as a colorless oil: $R_f = 0.64$ (10% EtOAc/hexanes); $[\alpha]_D^{23} = -34.8$ (*c* 1.00, CHCl$_3$); ^{1}H NMR (CDCl$_3$, 400 MHz) δ 6.36 (dd, *J* = 17.6, 10.5 Hz, 1H), 6.20 (dd, *J* = 17.6, 1.1 Hz, 1H), 5.81 (dd, *J* = 10.5, 1.1 Hz, 1H), 4.30 (ddd, *J* = 9.2, 3.5, 2.3 Hz, 1H), 3.58–3.50 (m, 1H), 2.86 (dd, *J* = 15.6, 9.3 Hz, 1H), 2.49 (dd, *J* = 15.6, 2.3 Hz, 1H), 1.83–1.73 (m, 1H), 1.57–1.47 (m, 2H), 0.99–0.84 (m, 24H), 0.57 (q, *J* = 7.8 Hz, 6H), 0.54 (q, *J* = 7.8 Hz, 6H); ^{13}C NMR (CDCl$_3$, 100 MHz) δ 200.2, 137.6, 128.1, 75.3, 71.1, 42.82, 42.77, 27.8, 9.2, 8.3, 7.0, 6.9, 5.4, 5.0; HRMS (ESI-TOF) *m/z*: [M + Na]$^+$ calcd for $C_{22}H_{46}O_3Si_2Na$ 437.2878, found 437.2868.

(5*S*,6*R*,7*S*)-6-Methyl-1-[*N*-(2-acetamidoethyl)thio]-5,7-bis[(triethylsilyl)oxy]nonan-3-one (**S13**).
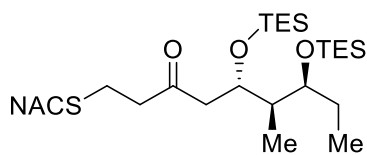
To a solution of vinyl ketone **S12** (42 mg, 0.10 mmol, 1.0 equiv) in THF (8 mL) was added *N*-acetylcysteamine (16 µL, 0.15 mmol, 1.5 equiv) and a catalytic amount of Cs_2CO_3. The reaction was stirred at room temperature for 1.5 h, then quenched by the addition of saturated aqueous NH_4Cl (10 mL). The layers were separated and the aqueous layer was extracted with EtOAc (3 × 10 mL). The combined organic layers were washed with saturated aqueous NaCl (40 mL), dried (Na_2SO_4),

filtered and concentrated under reduced pressure. Purification by flash chromatography (5% MeOH/CH$_2$Cl$_2$) afforded the title compound (38 mg, 70%) as a colorless oil: R_f = 0.37 (5% MeOH/CH$_2$Cl$_2$); $[\alpha]_D^{23}$ = –28.4 (*c* 1.00, CHCl$_3$); ^{1}H NMR (CDCl$_3$, 400 MHz) δ 6.07 (s, 1H), 4.31–4.20 (m, 1H), 3.54–3.43 (m, 3H), 2.83–2.58 (m, 7H), 2.40 (dd, *J* = 15.5, 1.9 Hz, 1H), 2.01 (s, 3H), 1.78–1.70 (m, 1H), 1.57–1.42 (m, 2H), 1.01–0.81 (m, 24H), 0.56 (app. quin, *J* = 8.0 Hz, 12H); ^{13}C NMR (CDCl$_3$, 100 MHz) δ 208.3, 170.1, 75.2, 71.3, 46.1, 44.4, 42.5, 38.4, 32.3, 27.7, 25.0, 23.2, 9.2, 8.0, 7.0, 6.9, 5.4, 5.0; HRMS (ESI-TOF) *m/z*: [M + Na]$^+$ calcd for C$_{26}$H$_{55}$NO$_3$SSi$_2$Na 556.3283, found 556.3291.

(5*S*,6*R*,7*S*)-5,7-Dihydroxy-6-methyl-1-[*N*-(2-acetamidoethyl)thio]nonan-3-one (**2e**).
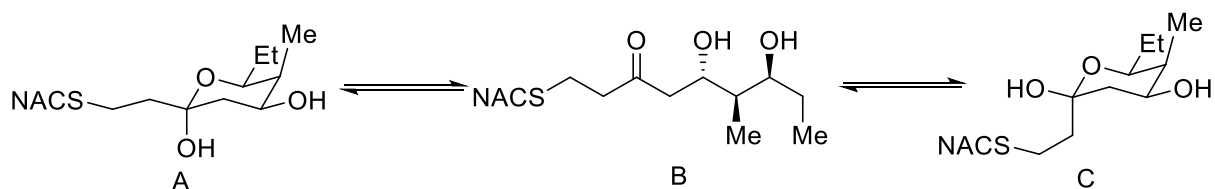
To a solution of silyl ether **S13** (44 mg, 0.082 mmol, 1.0 equiv) in THF (6 mL) at 0 °C was added a solution of 70% HF-pyridine:pyridine:THF (1:2:8, 3 mL). The reaction was stirred at 0 °C for 4.5 h, then quenched by the addition of saturated aqueous NaHCO$_3$ to bring the reaction to pH 7, and extracted with *n*-butanol (5 × 20 mL). The combined organic layers were washed with saturated aqueous NaCl (40 mL), dried (Na$_2$SO$_4$), filtered, and concentrated under reduced pressure. Purification by flash chromatography (10% MeOH/EtOAc) afforded the title compound (16 mg, 64%) as a colorless oil: R_f = 0.36 (10% MeOH/EtOAc); $[\alpha]_D^{22}$ = –35.5 (*c* 0.52, CHCl$_3$); ^{1}H NMR (CDCl$_3$, 400 MHz, approximately 6:6:1 mixture of A:B:C where the integrations have been normalized) δ 6.61 (s, 0.08H), 6.08 (s, 0.46H), 5.98 (s, 0.46H), 4.20 (dt, *J* = 11.9, 4.8 Hz, 0.46H), 4.17–4.08 (m, 0.46H), 4.07–4.03 (m, 0.08H), 3.85–3.77 (m, 1H), 3.75–3.69 (m, 0.16H), 3.53–3.34 (m, 1.84H), 3.22–3.13 (m, 0.32H), 2.86–2.58 (m, 5.52H), 2.00–1.98 (m, 3H), 1.95–1.84 (m,

1.38H), 1.81 (dd, J = 4.8, 12.5 Hz, 0.46H), 1.65–1.34 (m, 3H), 1.09 (d, J = 7.2 Hz, 0.24H), 1.05 (t, J = 7.3 Hz, 0.24H), 0.98–0.87 (m, 4.14H), 0.80 (d, J = 6.9 Hz, 1.38H); ^{13}C NMR (CDCl$_3$, 100 MHz, major isomers A and B) δ 209.9, 170.4, 170.3, 97.5, 73.8, 72.9, 71.6, 67.5, 48.1, 43.4, 41.5, 41.3, 38.6, 38.3, 37.3, 37.1, 31.9, 31.4, 26.7, 25.2, 25.1, 25.0, 23.23, 23.21, 10.9, 10.8, 10.3, 3.6; HRMS (ESI-TOF) m/z: [M + Na]$^+$ calcd for C$_{14}$H$_{27}$NO$_4$SNa 328.1553, found 328.1560.

(±)-3-Hydroxy-1-(2-thioxothiazolidin-3-yl)pentan-1-one [(±)-**S15**].
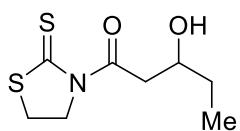
To a solution of thiazolidinethione **S14** (1.06 g, 6.55 mmol, 1.00 equiv) in CH$_2$Cl$_2$ (30 mL) at –40 °C was added TiCl$_4$ (0.79 mL, 7.2 mmol, 1.1 equiv). Hünig's base (*i*-Pr$_2$Net) (1.37 mL, 7.86 mmol, 1.20 equiv) was added after stirring at –40 °C for 30 min. The reaction mixture was stirred at –40 °C for another 2 h, and then cooled to –78 °C. Freshly distilled propionaldehyde (0.851 mL, 11.8 mmol, 1.80 equiv) was added. The reaction was stirred at –78 °C for 3 h, quenched by addition of saturated aqueous NH$_4$Cl (40 mL) and allowed to warm up to room temperature. The organics were extracted with CH$_2$Cl$_2$ (3 × 40 mL), dried (Na$_2$SO$_4$), filtered, and concentrated under reduced pressure. Purification by flash chromatography (40% EtOAc/hexanes) afforded the title compound (825 mg, 57%) as a yellow oil: R_f = 0.14 (30% EtOAc/hexanes); ^{1}H NMR (CDCl$_3$, 400 MHz) δ 4.66–4.55 (m, 2H), 4.08–3.95 (m, 1H), 3.53 (dd, J = 17.6, 2.3 Hz, 1H), 3.35–3.24 (m, 3H), 2.87 (d, J = 3.9 Hz, 1H), 1.66–1.49 (m, 2H), 0.98 (t, J = 7.4 Hz, 3H); ^{13}C NMR (CDCl$_3$, 100 MHz) δ 201.9, 174.3, 69.5, 55.7, 45.4, 29.4, 28.3, 9.9; HRMS (ESI-TOF) m/z: [M + Na]$^+$ calcd for C$_8$H$_{13}$NO$_2$S$_2$Na 242.0280, found 242.0281.

(±)-*S*-(2-Acetamidoethyl)-3-hydroxypentanethioate [(±)-**5**].
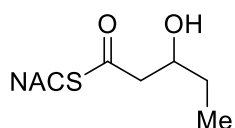
To a solution of thiazolidinethione (±)-**S15** (821 mg, 3.74 mmol, 1.00 equiv) in CH_2Cl_2 (30 mL) at room temperature was added imidazole (763 mg, 11.2 mmol, 3.00 equiv) and *N*-acetylcysteamine (0.44 mL, 4.1 mmol, 1.1 equiv). The reaction was stirred at room temperature for 12 h, then quenched by the addition of saturated aqueous NH_4Cl (30 mL), and extracted with CH_2Cl_2 (3 × 20 mL). The combined organic layers were washed with saturated aqueous NaCl (40 mL), dried (Na_2SO_4), filtered, and concentrated under reduced pressure. Purification by flash chromatography (5% $MeOH/CH_2Cl_2$) afforded the title compound (566 mg, 69%) as a colorless oil: R_f = 0.24 (5% $MeOH/CH_2Cl_2$); ^{1}H NMR (CDCl$_3$, 400 MHz) δ 5.79 (s, 1H), 4.04–3.96 (m, 1H), 3.53–3.40 (m, 2H), 3.11–2.98 (m, 2H), 2.77 (dd, *J* = 15.4, 3.3 Hz, 1H), 2.68 (dd, *J* = 15.4, 8.7 Hz, 1H), 2.61 (s, 1H), 1.97 (s, 3H), 1.61–1.45 (m, 2H), 0.97 (t, *J* = 7.4 Hz, 3H); ^{13}C NMR (CDCl$_3$, 100 MHz) δ 199.6, 170.4, 70.1, 50.6, 39.3, 29.6, 28.9, 23.2, 9.8; HRMS (ESI-TOF) *m/z*: [M + Na]$^+$ calcd for $C_9H_{17}NO_3SNa$ 242.0821, found 242.0827.

(5*R*,6*R*,*E*)-6-Hydroxy-5-methyl-1-[*N*-(2-acetamidoethyl)thio]oct-3-en-2-one (**3**).
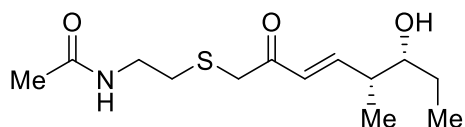
The enzymatic reaction was carried out with 4 mM diol **1a** (5.8 mg, 0.020 mmol, 1.0 equiv, dissolved in 200 μL 1: 1 DMSO: H_2O) in 10% glycerol, 1.5 M NaCl, 0.5 M Tris (pH 8.0) and 40 μM PikKR2-DH2 (16.6 mg, 0.2 μmol, 1 mol%) in a volume of 5 mL. The reaction mixture was shaken at room temperature at a speed of 150 rpm for 24 h and then extracted with EtOAc (5 × 10 mL). The organic layers were combined, washed with saturated aqueous NaCl (20 mL), dried (Na_2SO_4), filtered, and concentrated under reduced pressure. Since the enzymatic product and starting material had the same R_f values, separation of enzymatic product was accomplished by converting the starting material to its acetonide. The enzymatic reaction residue was dissolved in CH_2Cl_2 (2 mL) and *O,O*-

dimethoxypropane (25 µL) and PPTS (cat.) were added. After stirring at room temperature for 3 h, the reaction was quenched by the addition of saturated aqueous NH_4Cl (2 mL). The layers were separated, and the aqueous layer was extracted with CH_2Cl_2 (3 × 5 mL). The combined organic layers were washed with saturated aqueous NaCl (10 mL), dried (Na_2SO_4), filtered and concentrated under reduced pressure. Purification by flash chromatography (5% MeOH/CH_2Cl_2) afforded the title compound (2.8 mg, 51%) as colorless oil: R_f = 0.23 (5% MeOH/CH_2Cl_2); $[\alpha]_D^{22}$ = 20.0 (c 0.0900, $CHCl_3$); ^{1}H NMR ($CDCl_3$, 400 MHz) δ 6.97 (dd, J = 15.9, 7.6 Hz, 1H), 6.28 (dd, J = 15.9, 1.3 Hz, 1H), 6.04 (s, 1H), 3.58–3.51 (m, 1H), 3.48–3.36 (m, 4H), 2.66 (t, J = 6.3 Hz, 2H), 2.55–2.42 (m, 1H), 1.99 (s, 3H), 1.73 (s, 1H), 1.57–1.49 (m, 1H), 1.48–1.38 (m, 1H), 1.11 (d, J = 6.8 Hz, 3H), 0.98 (t, J = 7.4 Hz, 3H); ^{13}C NMR ($CDCl_3$, 100 MHz) δ 194.8, 170.2, 151.7, 127.9, 75.8, 42.4, 39.0, 38.4, 32.2, 27.4, 23.3, 13.6, 10.4; HRMS (ESI-TOF) m/z: [M + Na]$^+$ calcd for $C_{13}H_{23}NO_3SNa$ 296.1291, found 296.1292.

(6R,7R,E)-7-Hydroxy-6-methyl-1-[N-(2-acetamidoethyl)thio]non-4-en-3-one (**4**).
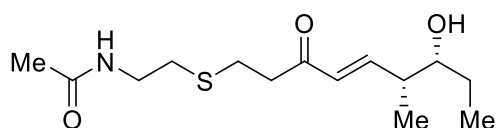
The enzymatic reaction was carried out with 4 mM diol **2a** (6.1 mg, 0.020 mmol, 1.0 equiv, dissolved in 200 µL 1: 1 DMSO: H_2O) in 10% glycerol, 1.5 M NaCl, 0.5 M Tris (pH 8.0) and 40 µM PikKR2-DH2 (16.6 mg, 0.2 µmol, 1 mol%) in a volume of 5 mL. The reaction mixture was shaken at room temperature at a speed of 150 rpm for 24 h. The enzymatic product was extracted with EtOAc (5 × 10 mL) and the combined organic layers were washed with saturated aqueous NaCl (20 mL), dried (Na_2SO_4), filtered, and concentrated under reduced pressure. Purification by flash chromatography (5% MeOH/CH_2Cl_2) afforded the title compound (3.3 mg, 58%) as colorless oil: R_f = 0.21 (5% MeOH/CH_2Cl_2); $[\alpha]_D^{22}$ = 22.0 (c 0.100, $CHCl_3$); ^{1}H NMR ($CDCl_3$, 400 MHz) δ 6.94 (dd, J = 16.1, 7.6 Hz, 1H), 6.13 (dd, J = 16.1, 1.2 Hz, 1H), 6.02 (s, 1H), 3.58–3.50 (m, 1H), 3.45 (q, J = 6.3 Hz,

2H), 2.93–2.87 (m, 2H), 2.84–2.78 (m, 2H), 2.67 (t, J = 6.5 Hz, 2H), 2.47 (sext, J = 6.9 Hz, 1H), 2.02–1.97 (m, 4H), 1.59–1.47 (m, 1H), 1.46–1.35 (m, 1H), 1.09 (d, J = 6.8 Hz, 3H), 0.98 (t, J = 7.4 Hz, 3H); ^{13}C NMR (CDCl$_3$, 100 MHz) δ 198.5, 170.4, 150.7, 129.8, 75.8, 42.3, 39.7, 38.7, 31.9, 27.3, 25.8, 23.3, 13.5, 10.4; HRMS (ESI-TOF) m/z: [M + Na]$^+$ calcd for C$_{14}$H$_{25}$NO$_3$SNa 310.1447, found 310.1438.

Results

The pikromycin biosynthetic pathway is one of the most well-explored type I PKSs and has served as a model system for fundamental investigations of PKS catalysis[22-24, 28-31]. We selected the DH domain from pikromycin PKS module 2 (PikDH2) for our studies since it is responsible for the *trans*-olefin in pikromycin (Fig. 2.1) and Cane *et al*. revealed that the cryptic β-hydroxy stereochemistry of the triketide substrate possesses the d-configuration[24,32]. We predicted a larger, multi-domain portion of the PKS would create a more native context for *in vitro* analysis[32]. The region of *pikAI* encoding the PikKR2-DH2 didomain comprising residues
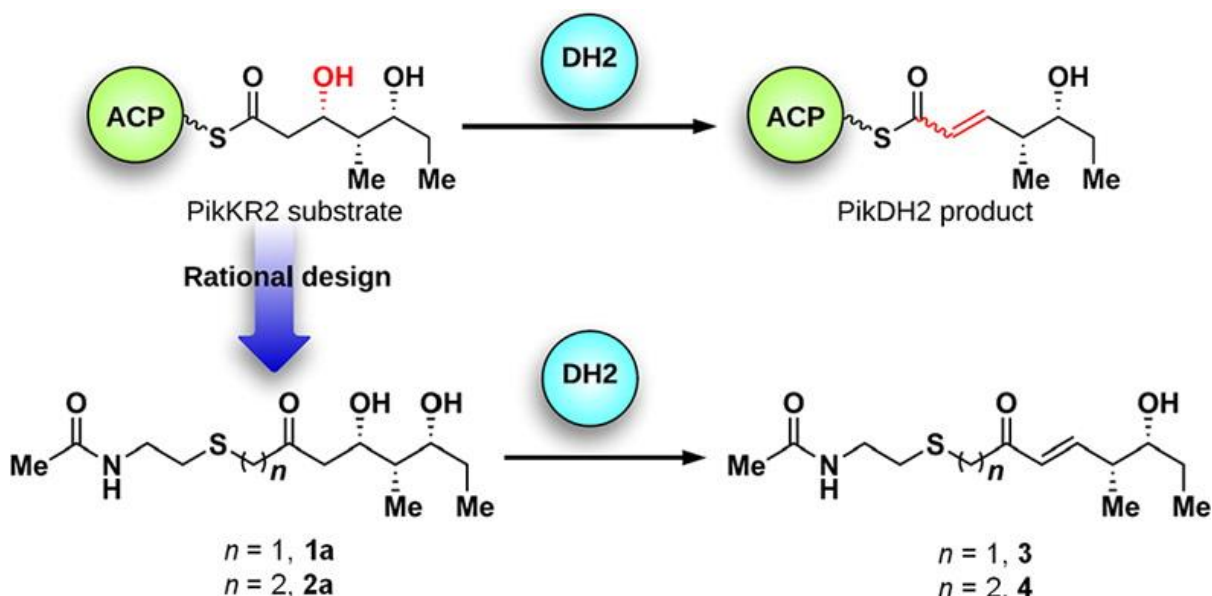
Figure 2.9 Rational design of PikDH2 substrate mimics 1a and 2a and the corresponding enzymatic products 3 and 4

3579–4365 was cloned into a pMCSG7 expression vector and the resulting protein was overexpressed and purified using standard methods. Substrate mimics **1a** and **2a** for PikDH2 are based on its natural substrate (Fig. 2.9)[32]. While maintaining the same stereochemistry on the triketide moiety, they possess two major modifications compared to the natural substrate including replacement of the ACP-phosphopantetheinyl arm with *N*-acetylcysteamine (NAC)

and insertion of one or two methylene spacers between the carbonyl and sulfur atom to avoid undesired, intramolecular lactonization while not significantly perturbing the pK_a of the α-protons[33]. These two modifications were tolerated by PikKR2, instilling confidence the downstream DH would accept these substrates[32]. Overnight incubation of substrates **1a** and **2a** with PikKR2-DH2 didomain in relatively large scale generated the corresponding enzymatic products **3** and **4**, respectively, in slightly more than 50 isolated yield (Scheme 2.1). The structures of **3** and **4** were unambiguously confirmed by NMR spectroscopy and exhibited diagnostic ^{13}C chemical shifts at 150 and 130 ppm and a $^3J_{HH}$ coupling of 16 Hz for the vinyl protons. These results are consistent with the empirical rule that d-alcohols provide *trans*-olefins.
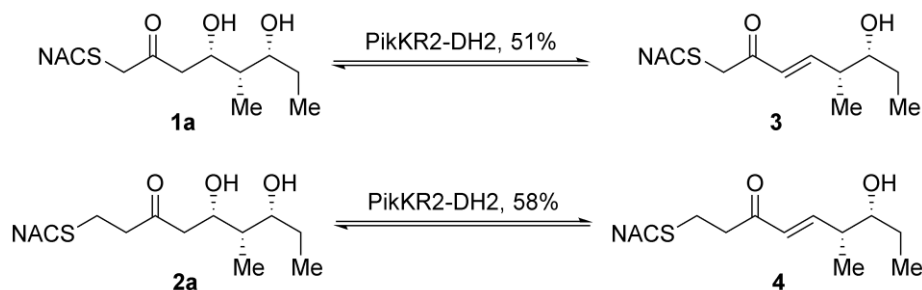
Scheme 2.1 Chemoenzymatic synthesis of enones 3 and 4 in Tris buffer (pH 8.0) at 25 °C.

Additionally, we investigated the reason for incomplete reaction. Since most FAS DHs conduct the reverse hydration reactions, enones **3** and **4** were incubated with PikKR2-DH2 to test the reversibility of the enzymatic reaction. We observed PikKR2-DH2 stereoselectively converted **3** and **4** exclusively to their hydrated products **1a** and **2a**, respectively, whose identities were confirmed by LC-MS/MS with authentic synthetic standards (Figs. 2.4, 2.5). When equilibrium was reached, the ratio of **1a** to **3** was 1:1.2 and the ratio of **2a** to **4** was 1:2, slightly favoring the dehydration products in both cases. In the biosynthetic pathway, this equilibrium is pushed towards dehydration, driven by downstream module activities.

To interrogate the stereospecificity of PikDH2, we altered the β-stereocenter of substrates **1a** and **2a** as well as every stereogenic center in **2a** through chemical synthesis (Schemes 2.2 – 2.4) resulting in substrate stereoisomers **1b** and **2b**–**e** (Table 2.4)[32]. As LC-MS/MS showed high sensitivity and selectivity for detection of KR products[32], we continued using this technique to examine the formation of DH products by their unique fragmentation patterns and/or retention times. Initial velocity was linear up to 40 min with 10 μM PikKR2-DH2 didomain (Fig. 2.3), thus we chose an end-point quench after 15 min incubation for our kinetic studies. The kinetic parameters of all substrates were obtained by fitting the saturation curves to the Michaelis-Menten equation (Table 2.4). Substrates **1a** and **2a**, maintaining the native stereochemistry, were accepted and processed rapidly by the enzyme. The K_M (6.9 ± 1.7 mM and 5.7 ± 1.4 mM) and k_{cat} values (0.67 ± 0.11 min^{-1} and 1.28 ± 0.19 min^{-1}) were comparable, suggesting the methylene spacer does not adversely impact active site binding and catalysis. Substrate **1b** and **2b**, epimeric at the β-position were not processed. This strict substrate specificity has been similarly observed with other DHs[12, 16, 26].
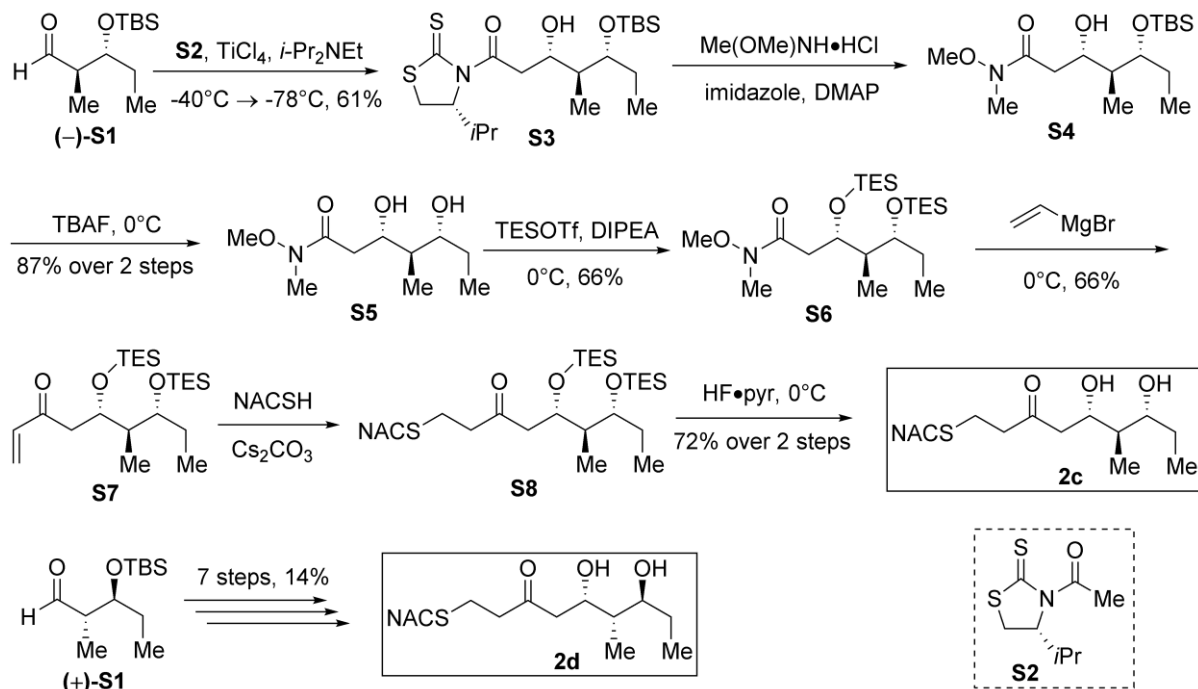
Scheme 2.2 Synthesis of substrate analogs 2c and 2d.

Anti-aldol product (–)-**S1**, synthesized using Masamune's chiral auxiliary,[1,2] was submitted to an acetate aldol reaction with thiazolidinethione **S2**[3,4] to yield alcohol **S3** as the major diastereomer. The thiazolidinethione was displaced with *N,O*-dimethylhydroxylamine to afford Weinreb amide **S4**. The TBS protecting group stable in the previous aldol reaction was ultimately problematic in the final deprotection and was therefore replaced with a TES protecting group to facilitate its later removal. This was accomplished by treatment of **S4** with TBAF to furnish **S5** and subsequent silylation with TESOTf provided **S6**. Grinard reaction and Michael addition furnished the NAC-analog **S8**. A final deprotection under mild conditions furnished the substrate analog **2c**. Substrate analog **2d** was also synthesized in an analogous way by using aldehyde (+)-**S1**

53
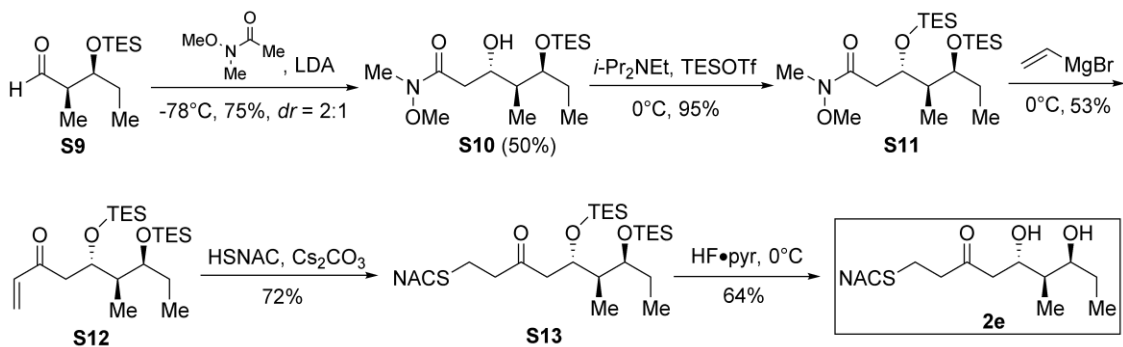
Scheme 2.3 Synthesis of substrate analog 2e

The synthetic route commenced with the acetate aldol reaction of aldehyde **S9**[5] and *N*-methoxy-*N*-methylacetamide to give Weinreb amide **S10** as the major diastereomer (dr = 2:1, separated by chromatography). TES protection provided **S11** that was converted to vinyl ketone **S12** through Grignard addition of vinylmagnesium bromide. Sequential Michael addition of *N*-acetylcysteamine and silyl deprotection provided substrate analog **2e.**
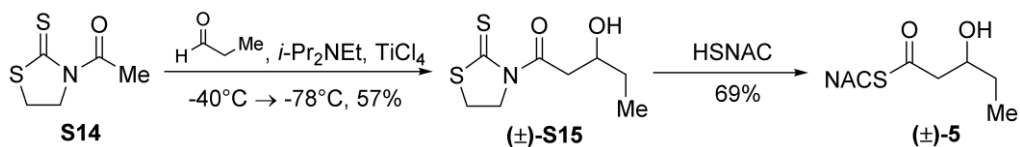
Scheme 2.4 Synthesis of substrate analog (±)-5.

Thiazolidinethione **S14**[5,6] was subjected to an acetate aldol reaction with propionaldehyde to provide a

racemic mixture of **S15**, followed by displacement with *N*-acetylcysteamine to afford NAC thioester

(±)–**5**.

Table 2.4 Structures of Substrate Analogues 1a, 1b, 2a-e, and 5 and Their Steady-State Kinetic Parameters

No.	Substrate Structure	K_M (mM)	k_{cat} (min^{-1})	k_{cat}/K_M, min^{-1} M^{-1}
1a		6.9 ± 1.7	0.67 ± 0.11	98 ± 39
1b		> 8	<0.01	<1
2a		5.7 ± 1.4	1.28 ± 0.19	225 ± 88
2b		> 8	<0.01	<1
2c		> 8	<0.01	<1
2d		> 8	<0.01	<1
2e		> 8	<0.01	<1
(±)-5		> 8	<0.01	<1

To inspect the sensitivity of PikDH2 to changes in distal stereochemistry, we next investigated substrates **2c** and **2d**, epimeric at the γ- and δ-position as well as **2e** wherein both the γ- and δ-positions are inverted. Enzymatic products of **2c**–**e** were not detected by LC-MS/MS, indicating an unprecedented degree of discrimination of these distal stereocenters. Moreover, racemic diketide **5**, similar to widely used diketide substrates to study other DHs[12, 16], was unexpectedly not converted to the corresponding dehydration product.

To study the chemical mechanism of PikDH2, the pH dependence of catalytic efficiency (V_{max}/K_M) with substrate **2a** was obtained from pH 6.6 to 9.0 (Table 2.5). The hyperbolic curve implicates at least one key ionizable group responsible for binding and catalysis (from either the free enzyme or the free substrate)[34] with a pK_a value of 7.0 ± 0.1 (Fig. 2.10A). The protonation of this ionizable group at low pH values abolished the enzyme activity. The pK_a values for the two hydroxyl groups of substrate **2a** are expected to be ~14–16. Thus we expect the observed ionizable group is a general base in the enzyme, presumably the conserved histidine residue
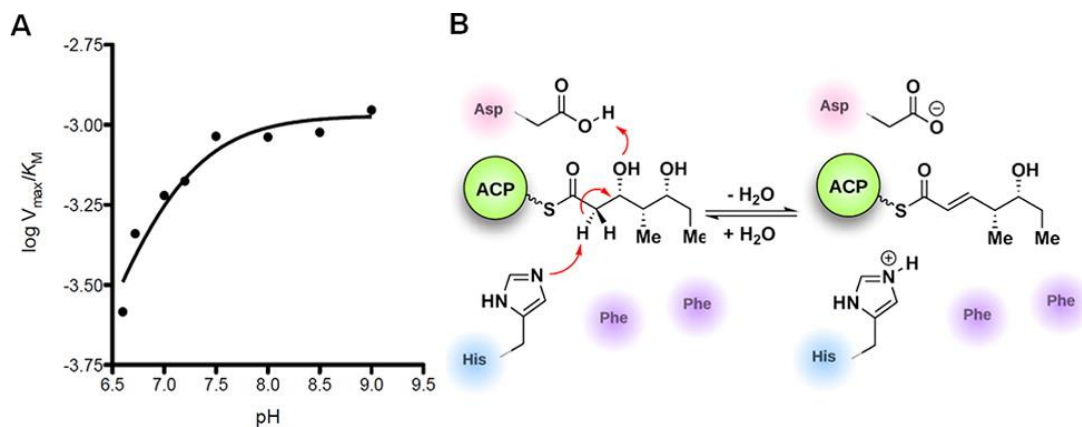
Figure 2.10 (A) pH dependence of log(V_{max}/K_M). **(B)** Mechanism and key residues involved in dehydration reaction

Table 2.5 V_{max}/K_M values at varying hydrogen ion concentrations.

pH	V_{max}/K_M ($\times 10^{-3}$min^{-1})
6.6	0.2606 ± 0.0157
6.7	0.4571 ± 0.0276
7.0	0.6014 ± 0.0147
7.2	0.6675 ± 0.0504
7.5	0.9206 ± 0.0345
8.0	0.9154 ± 0.0376
8.5	0.9479 ± 0.0413
9.0	1.112 ± 0.0428

(His3611), which abstracts the α-proton. An aspartic acid residue protonates the β-hydroxyl group to facilitate the loss of a water molecule (Fig. 2.10B)[8-12]. The slightly perturbed pK_a of 7.0 for the catalytic histidine, compared to pK_a of 6.0 for the free amino acid, indicates the influence of adjacent residues to form a slightly negatively charged cavity[35].

In order to understand the basis for the remarkable selectivity of PikDH2 we next aligned the amino acid sequence of PikDH2 with other DHs of known 3D structure[10-12]. Two catalytic residues, the histidine (His3611) in an **HXXGXXXP** motif and the aspartic acid (Asp3800) in an **HPALLD** motif, are also found in PikDH2. However, the tyrosine in a **Y**GP motif (observed in most DHs), whose role was proposed to assist the protonation of the β-hydroxyl group[14], is absent in this DH. Instead, a phenylalanine (Phe3746, **F**GP motif) is located only 3.8 Å from the catalytic histidine in a PikDH2 homology model (Fig. 2.8), suggesting that this residue could impact substrate binding at the active site. The F3746L point mutant was generated and tested with substrate surrogate **2a** to verify this possibility. The specificity constant dropped to 1/40 of the wild type, indicating the important role this phenylalanine plays for substrate binding (Table 2.6). Another phenylalanine, residue 3750, conserved in most DHs, is also near the catalytic residues (3.2 Å from the aspartic acid) in the homology model. Mutants F3750Y and F3750L

Table 2.6 Kinetic Parameters of PikDH2 Mutants

Mutant	K_M (mM)	k_{cat} (min^{-1})	k_{cat}/K_M, min^{-1} M^{-1}
WT	5.7 ± 1.4	1.28 ± 0.19	225 ± 88
F3746L	>40	N/A	5.2 ± 0.3
F3750Y	4.14 ± 1.4	0.086 ± 0.013	21 ± 9
F3750L	7.1 ± 2.6	0.046 ± 0.011	6.5 ± 3.9

had similar K_M values to the wild type, but 15–30-fold decreased k_{cat} values, demonstrating that change of Phe3750 hampers the catalytic activity of PikDH2. We hypothesize that the two

phenylalanine residues (F3746 and F3750) may shape a hydrophobic pocket at the active site to position the substrate as well as maintain the catalytically active state.

Co-crystallography of PKSs is particularly challenging since substrate affinity is often low due to the intramolecular nature of substrate presentation. With the hope of aiding structural studies and potentially allowing visualization of protein interfaces between ACP and DH domains[36-37], we set out to screen for a suitable PikDH2 suicide substrate that would covalently react within the enzyme active site. 3-Decynoyl-*N*-acetylcysteamine (**6**) developed by Bloch was the first described mechanism-based inhibitor for any enzyme, which coincidentally inactivates FAS DHs[38]. Burkart and co-workers recently developed second-generation DH probes with improved chemical stability and demonstrated these could inactivate functionally and structurally related PKS DHs[36-37]. Therefore, we evaluated the ability of **6** to irreversibly inhibit PikDH2 using our discontinuous assay monitoring the dehydration of substrate **2a** by LC-MS/MS. Compound **6** was shown to exhibit time-dependent inhibition and the kinetic constants for inactivation were determined using the Kitz–Wilson method[39]. The kinetic parameters K_I and k_{inact} were 156 ± 34 µM and 0.36 ± 0.06 min^{-1} (Figs. 2.11A-C). Enzyme activity could not be recovered by dialysis and substrate protected PikDH2 from inactivation. Consequently, we expect **6** covalently labels PikDH2 in analogy to FAS DHs through abstraction of an α-proton by the catalytic histidine residue of the enzyme to form a reactive allene via propargylic rearrangement, which subsequently undergoes nucleophilic attack by the catalytic histidine (Fig. 2.11A)[40-41].
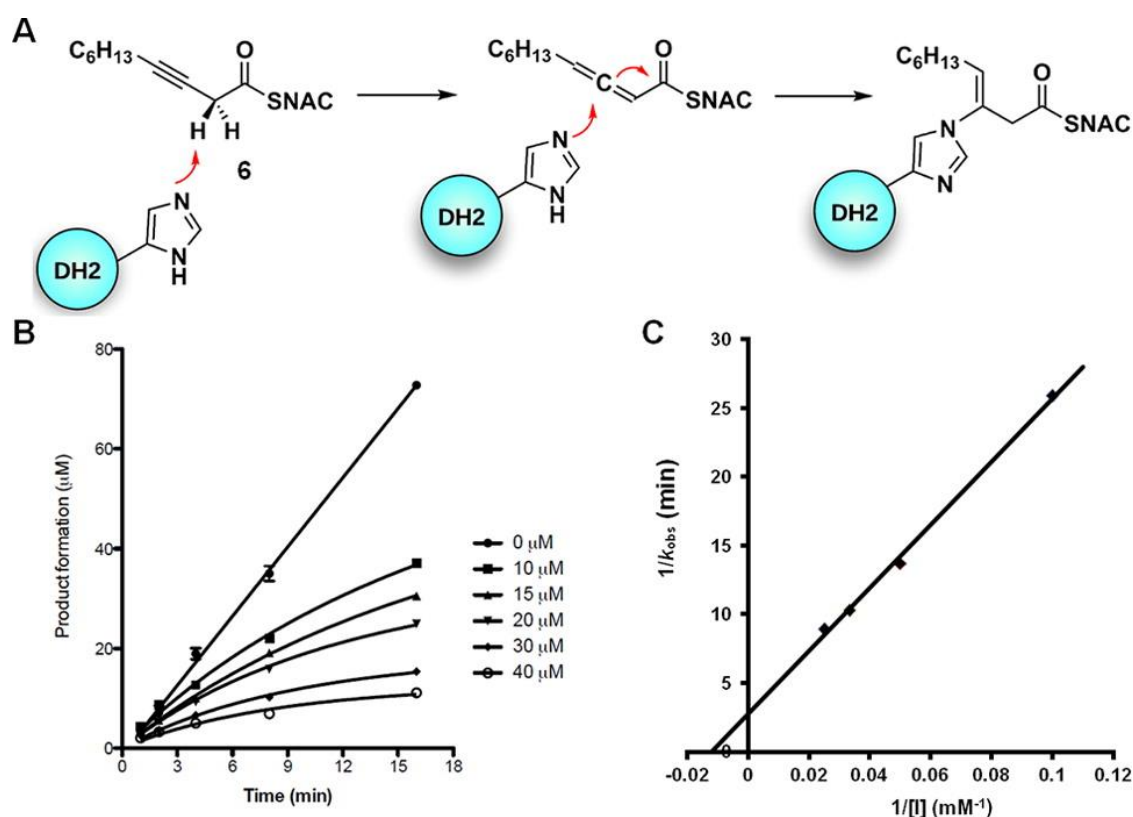
Figure 2.11 (A) Mechanism of DH domain inactivation by 3-decynoyl-N-acetylcysteamine (6). (B) Time course of the inactivation of PikDH2 with 10–40 μM 6.

Symbols represent the mean ± SD from duplicate experiments. (C) Kitz–Wilson plot[19] of the inhibition data ($1/k_{obs}$ vs $1/[I]$).

Discussion

In summary, we have performed the first steady-state kinetic analysis of a PKS DH domain by using LC-MS/MS analysis for product quantitation. PikDH2 was found to process only d-alcohols to furnish *trans*-olefin products. The enzyme showed an unforeseen extremely high stereospecificity at the β-, γ- and δ-positions of the substrate, potentially revealing a challenge for future metabolic engineering efforts. The pH dependence of k_{cat}/K_M identified a general base with a pK_a of 7.0 critical for substrate binding and catalysis, which we assign to

histidine (His3611). Mutagenesis and kinetic studies uncovered a critical hydrophobic region shaped by two phenylalanine residues that is essential for substrate binding as well as catalytic activity and suggest the tyrosine in a YGP motif (observed in most DHs) implicated in DH catalysis is not required for activity. In the search for a co-crystallography candidate for PikDH2, we demonstrated that an alkyne-based probe irreversibly modified this non-iterative type I PKS DH. These studies provide a foundation for future efforts aimed to uncover the protein-substrate interactions that govern binding and catalysis. Our findings further reinforce the utility of diffusible NAC substrate mimics containing a ketone isostere in place of the labile thioester for studying intrinsically unstable PKS chain intermediates.

Bibliography

1.   Smith, S., Tsai, S.-C., The type I fatty acid and polyketide synthases: a tale of two megasynthases. *Natural product reports* **2007,** *24* (5), 1041-1072.
2.   Smith, J. L., Sherman, D. H., An enzyme assembly line. *Science* **2008,** *321* (5894), 1304.
3.   McDaniel, R., Thamchaipenet, A., Gustafsson, C., Fu, H., Betlach, M., Betlach, M., Ashley, G., Multiple genetic modifications of the erythromycin polyketide synthase to produce a library of novel "unnatural" natural products. *Proceedings of the National Academy of Sciences* **1999,** *96* (5), 1846-1851.
4.   Tang, L., Shah, S., Chung, L., Carney, J., Katz, L., Khosla, C., Julien, B., Cloning and heterologous expression of the epothilone gene cluster. *Science* **2000,** *287* (5453), 640-642.
5.   Werneburg, M., Busch, B., He, J., Richter, M. E., Xiang, L., Moore, B. S., Roth, M., Dahse, H.-M., Hertweck, C., Exploiting enzymatic promiscuity to engineer a focused library of highly selective antifungal and antiproliferative aureothin analogues. *Journal of the American Chemical Society* **2010,** *132* (30), 10407-10413.
6.   Verdier-Pinard, P., Lai, J.-Y., Yoo, H.-D., Yu, J., Marquez, B., Nagle, D. G., Nambu, M., White, J. D., Falck, J., Gerwick, W. H., Structure-activity analysis of the interaction of curacin A, the potent colchicine site antimitotic agent, with tubulin and effects of analogs on the growth of MCF-7 breast cancer cells. *Molecular pharmacology* **1998,** *53* (1), 62-76.
7.   Martello, L. A., LaMarche, M. J., He, L., Beauchamp, T. J., Smith III, A. B., Horwitz, S. B., The relationship between Taxol and (+)-discodermolide: synthetic analogs and modeling studies. *Chemistry & biology* **2001,** *8* (9), 843-855.
8.   Leesong, M., Henderson, B. S., Gillig, J. R., Schwab, J. M., Smith, J. L., Structure of a dehydratase–isomerase from the bacterial pathway for biosynthesis of unsaturated fatty acids: two catalytic activities in one active site. *Structure* **1996,** *4* (3), 253-264.
9.   Kimber, M. S., Martin, F., Lu, Y., Houston, S., Vedadi, M., Dharamsi, A., Fiebig, K. M., Schmid, M., Rock, C. O., The structure of (3R)-hydroxyacyl-acyl carrier protein dehydratase (FabZ) from Pseudomonas aeruginosa. *Journal of Biological Chemistry* **2004,** *279* (50), 52593-52602.
10.   Keatinge-Clay, A., Crystal structure of the erythromycin polyketide synthase dehydratase. *Journal of molecular biology* **2008,** *384* (4), 941-953.
11.   Akey, D. L., Razelun, J. R., Tehranisa, J., Sherman, D. H., Gerwick, W. H., Smith, J. L., Crystal structures of dehydratase domains from the curacin polyketide biosynthetic pathway. *Structure* **2010,** *18* (1), 94-105.
12.   Gay, D., You, Y.-O., Keatinge-Clay, A., Cane, D. E., Structure and stereospecificity of the dehydratase domain from the terminal module of the rifamycin polyketide synthase. *Biochemistry* **2013,** *52* (49), 8916-8928.
13.   Caffrey, P., Conserved amino acid residues correlating with ketoreductase stereospecificity in modular polyketide synthases. *ChemBioChem* **2003,** *4* (7), 654-657.
14.   Keatinge-Clay, A. T., The structures of type I polyketide synthases. *Natural product reports* **2012,** *29* (10), 1050-1073.
15.   Reid, R., Piagentini, M., Rodriguez, E., Ashley, G., Viswanathan, N., Carney, J., Santi, D. V., Hutchinson, C. R., McDaniel, R., A model of structure and catalysis for ketoreductase domains in modular polyketide synthases. *Biochemistry* **2003,** *42* (1), 72-79.

16.   Vergnolle, O., Hahn, F., Baerga-Ortiz, A., Leadlay, P. F., Andexer, J. N., Stereoselectivity of isolated dehydratase domains of the borrelidin polyketide synthase: implications for cis double bond formation. *ChemBioChem* **2011,** *12* (7), 1011-1014.

17.   Kandziora, N., Andexer, J. N., Moss, S. J., Wilkinson, B., Leadlay, P. F., Hahn, F., Uncovering the origin of Z-configured double bonds in polyketides: intermediate E-double bond formation during borrelidin biosynthesis. *Chemical Science* **2014,** *5* (9), 3563-3567.

18.   Kusebauch, B., Busch, B., Scherlach, K., Roth, M., Hertweck, C., Functionally Distinct Modules Operate Two Consecutive α, β→ β, γ Double-Bond Shifts in the Rhizoxin Polyketide Assembly Line. *Angewandte Chemie* **2010,** *122* (8), 1502-1506.

19.   Holzbaur, I. E., Harris, R. C., Bycroft, M., Cortes, J., Bisang, C., Staunton, J., Rudd, B. A., Leadlay, P. F., Molecular basis of Celmer's rules: the role of two ketoreductase domains in the control of chirality by the erythromycin modular polyketide synthase. *Chemistry & biology* **1999,** *6* (4), 189-195.

20.   Wu, N., Kudo, F., Cane, D. E., Khosla, C., Analysis of the molecular recognition features of individual modules derived from the erythromycin polyketide synthase. *Journal of the American Chemical Society* **2000,** *122* (20), 4847-4852.

21.   Cane, D. E., Kudo, F., Kinoshita, K., Khosla, C., Precursor-directed biosynthesis: biochemical basis of the remarkable selectivity of the erythromycin polyketide synthase toward unsaturated triketides. *Chemistry & biology* **2002,** *9* (1), 131-142.

22.   Lu, H., Tsai, S.-C., Khosla, C., Cane, D. E., Expression, site-directed mutagenesis, and steady state kinetic analysis of the terminal thioesterase domain of the methymycin/picromycin polyketide synthase. *Biochemistry* **2002,** *41* (42), 12590-12597.

23.   Yin, Y., Lu, H., Khosla, C., Cane, D. E., Expression and kinetic analysis of the substrate specificity of modules 5 and 6 of the picromycin/methymycin polyketide synthase. *Journal of the American Chemical Society* **2003,** *125* (19), 5671-5676.

24.   Wu, J., Zaleski, T. J., Valenzano, C., Khosla, C., Cane, D. E., Polyketide double bond biosynthesis. Mechanistic analysis of the dehydratase-containing module 2 of the picromycin/methymycin polyketide synthase. *Journal of the American Chemical Society* **2005,** *127* (49), 17393-17404.

25.   Guo, X., Liu, T., Valenzano, C. R., Deng, Z., Cane, D. E., Mechanism and stereospecificity of a fully saturating polyketide synthase module: nanchangmycin synthase module 2 and its dehydratase domain. *Journal of the American Chemical Society* **2010,** *132* (42), 14694-14696.

26.   Valenzano, C. R., You, Y.-O., Garg, A., Keatinge-Clay, A., Khosla, C., Cane, D. E., Stereospecificity of the dehydratase domain of the erythromycin polyketide synthase. *Journal of the American Chemical Society* **2010,** *132* (42), 14697-14699.

27.   Berkhan, G., Hahn, F., A Dehydratase Domain in Ambruticin Biosynthesis Displays Additional Activity as a Pyran-Forming Cyclase. *Angewandte Chemie International Edition* **2014,** *53* (51), 14240-14244.

28.   Xue, Y., Zhao, L., Liu, H.-w., Sherman, D. H., A gene cluster for macrolide antibiotic biosynthesis in Streptomyces venezuelae: architecture of metabolic diversity. *Proceedings of the National Academy of Sciences* **1998,** *95* (21), 12111-12116.

29.   Beck, B. J., Aldrich, C. C., Fecik, R. A., Reynolds, K. A., Sherman, D. H., Substrate recognition and channeling of monomodules from the pikromycin polyketide synthase. *Journal of the American Chemical Society* **2003,** *125* (41), 12551-12557.

30.   Kittendorf, J. D., Sherman, D. H., The methymycin/pikromycin pathway: a model for metabolic diversity in natural product biosynthesis. *Bioorganic & medicinal chemistry* **2009,** *17* (6), 2137-2146.

31.   Dutta, S., Whicher, J. R., Hansen, D. A., Hale, W. A., Chemler, J. A., Congdon, G. R., Narayan, A. R., Håkansson, K., Sherman, D. H., Smith, J. L., Structure of a modular polyketide synthase. *Nature* **2014,** *510* (7506), 512.

32.   Li, Y., Fiers, W. D., Bernard, S. M., Smith, J. L., Aldrich, C. C., Fecik, R. A., Polyketide intermediate mimics as probes for revealing cryptic stereochemistry of ketoreductase domains. *ACS chemical biology* **2014,** *9* (12), 2914-2922.

33.   Amyes, T. L., Richard, J. P., Generation and stability of a simple thiol ester enolate in aqueous solution. *Journal of the American Chemical Society* **1992,** *114* (26), 10297-10302.

34.   Fersht, A., *Structure and mechanism in protein science: a guide to enzyme catalysis and protein folding*. Macmillan: 1999.

35.   Purich, D. L., Allison, R. D., *Handbook of biochemical kinetics: a guide to dynamic processes in the molecular life sciences*. Elsevier: 1999.

36.   Ishikawa, F., Haushalter, R. W., Burkart, M. D., Dehydratase-specific probes for fatty acid and polyketide synthases. *Journal of the American Chemical Society* **2011,** *134* (2), 769-772.

37.   Ishikawa, F., Haushalter, R. W., Lee, D. J., Finzel, K., Burkart, M. D., Sulfonyl 3-alkynyl pantetheinamides as mechanism-based cross-linkers of acyl carrier protein dehydratase. *Journal of the American Chemical Society* **2013,** *135* (24), 8846-8849.

38.   Brock, D., Kass, L., Bloch, K., β-Hydroxydecanoyl thioester dehydrase II. Mode of action. *Journal of Biological Chemistry* **1967,** *242* (19), 4432-4440.

39.   Kitz, R., Wilson, I. B., Esters of methanesulfonic acid as irreversible inhibitors of acetylcholinesterase. *Journal of Biological Chemistry* **1962,** *237* (10), 3245-3249.

40.   Endo, K., Helmkamp, G. M., Jr., Bloch, K., Mode of inhibition of beta-hydroxydecanoyl thioester dehydrase by 3-decynoyl-N-acetylcysteamine. *Journal of Biological Chemistry* **1970,** *245* (17), 4293-6.

41.   Schwab, J. M., Ho, C. K., Li, W. B., Townsend, C. A., Salituro, G. M., β-Hydroxydecanoyl thioester dehydrase. Complete characterization of the fate of the" suicide" substrate 3-decynoyl-NAC. *Journal of the American Chemical Society* **1986,** *108* (17), 5309-5316.

Chapter 3. Tylosin polyketide synthase module 3: stereospecificity, stereoselectivity and steady-state kinetic analysis of β-processing domains *via* diffusible, synthetic substrates

Summary

Polyketide synthase (PKS) β-processing domains are responsible for much of the stereochemical complexity of polyketide natural products. Although the importance of β-processing domains has been well noted and significantly explored, key stereochemical details pertaining to cryptic stereochemistry and the impact of remote stereogenic centers have yet to be fully discerned. To uncover the inner workings of ketoreductases (KR) and dehydratases (DH) from the tylosin pathway a didomain composed of TylDH3-KR3 was recombinantly expressed and interrogated with full-length tetraketide substrates to probe the impact of vicinal and distal stereochemistry. *In vitro* product isolation analysis revealed the products of the cryptic KR as d-alcohols and of the DH as *trans*-olefins. Steady-state kinetic analysis of the dehydration reaction demonstrated a strict stereochemical tolerance at the β-position as d-configured substrates were processed more than 100 times more efficiently than l-alcohols. Unexpectedly, the k_{cat}/K_M values were diminished 14- to 45-fold upon inversion of remote ε- and ζ-stereocenters. This stereochemical discrimination is predicted to be driven by a combination of allylic $A^{1,3}$ strain that likely disfavors binding of the ε-epimer and a loss of electrostatic interactions with the ζ-epimer. Our results strongly suggest that dehydratases may play a role in refining the stereochemical

outcomes of preceding modules through their substrate stereospecificity, honing the configurational purity of the final PKS product.

Introduction

Polyketides, polyoxygenated secondary metabolites isolated from fungal, plant and bacterial producing organisms, represent an incredibly diverse natural product family with manifold bioactivites[1-3]. Constituents of this natural product class are thought to serve as defensive and cell–cell signaling agents arising from billions of years of evolution. The complex and varied structural characteristics of polyketides are derived from their highly tunable, assembly line-like biosynthesis. Modular type I polyketide synthases (PKSs) are characterized by multi-functional proteins equipped with numerous catalytic domains, each responsible for a unique enzymatic reaction in the biosynthetic pathway[4]. A minimal module consists of acyl carrier protein (ACP), ketosynthase (KS) and acyl transferase (AT) domains. Additionally, polyketide modules often carry out varying degrees of β-carbon processing by successive action of ketoreductase (KR), dehydratase (DH), and enoyl reductase (ER) domains. These catalytic domains transform the β-keto moiety produced from the ACP, KS, and AT domains into hydroxyl, olefin, and saturated alkane products depending on their presence in the biosynthetic pathway. The β-processing domains create stereogenic centers and set the olefin geometry present in the final natural product with extremely stringent fidelity[5-8].

The stereochemical and/or geometric outcome of β-processing domains is often concealed or obscured through subsequent, downstream catalytic events. These instances of hidden domain action can fall into two broad categories: cryptic ketoreductase stereochemistry and cryptic dehydratase geometry. Cryptic KR reductions arise from presence of a subsequent DH domain, catalytically eliminating water and, in so doing, removing both α- and β-stereogenic

65

centers. *trans*-Olefin configuration arises from the elimination of d-alcohols while *cis*-olefins emanate from enzyme-mediated isomerization events.[9-10] Despite recent, compelling evidence suggesting that, in phoslactomycin biosynthesis, PKS DH domain-catalyzed generation of *Z*-olefins occurs from l-alcohols, *in vitro* validation has yet to be obtained.[11-12] Olefin geometry may be rendered cryptic through successive reduction by an ER domain, potentially yielding a new α-stereogenic center in the process. Cryptic reductions have received a significant amount of attention over the last decade resulting in several novel approaches to their study.[13-14] Bioinformatic analysis has shown promise in predicting stereogenic centers based on amino acid sequence of the KR domain in question[9, 15-16].

Tylosin (**1**), a 16-membered macrolactone product of *Streptomyces fradiae*, was chosen as a model system for our initial cryptic domain studies. The tylosin polyketide synthase includes one loading module and seven extension modules terminating in a thioesterase (TE) domain affording the aglycone tylactone (**2**) (Fig. 3.1)[17]. By virtue of their DH domains, modules 2, 3, and 5 have cryptic KR stereochemistry. Additionally, module 5 housing an ER domain constitutes a complete reductive sequence further obscuring the geometry of the precursor olefin. Prior methods to study cryptic KRs and DHs using synthetic substrates have generally been limited to diketides. Truncated substrates, while synthetically more accessible, are often poorly tolerated resulting in low conversion and exhibit loose stereochemical discrimination[8, 18]. As a result, the inferred substrate specificity obtained using truncated substrates remains dubious given their significant deviation from the native chain intermediates. Cane *et al.* overcame this limitation through the *in situ* chemoenzymatic synthesis of a triketide from a diketide substrate using a KS-AT didomain and excised ACP domain from the DEBS pathway[19]. However, we

anticipated this strategy would be difficult to implement for tetraketides as this would require the

use of two complete modules in tandem.
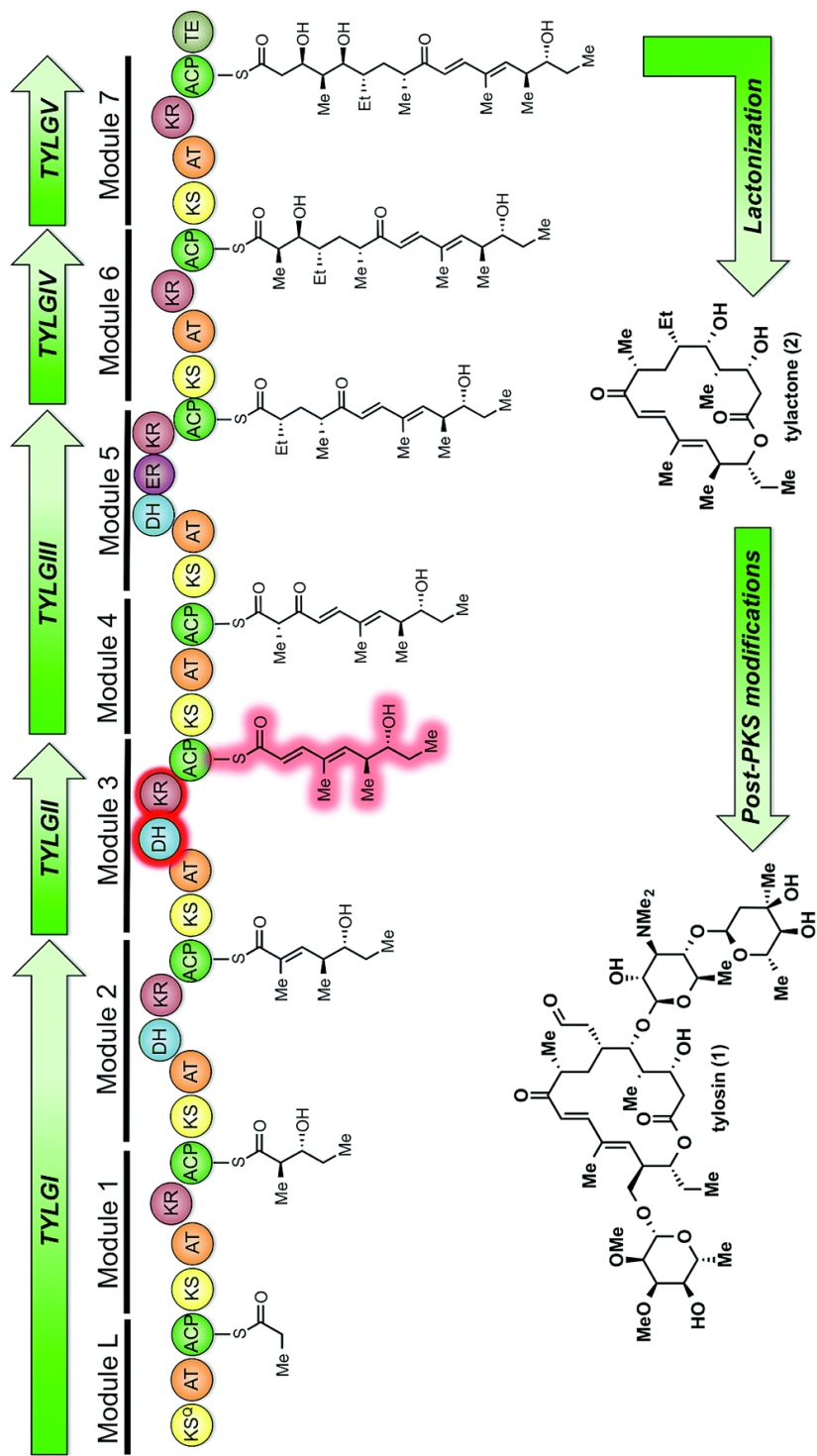
Figure 3.1 The modular PKS of tylactone (1).

The 3 β-processing domains and their postulated product are highlighted in red.
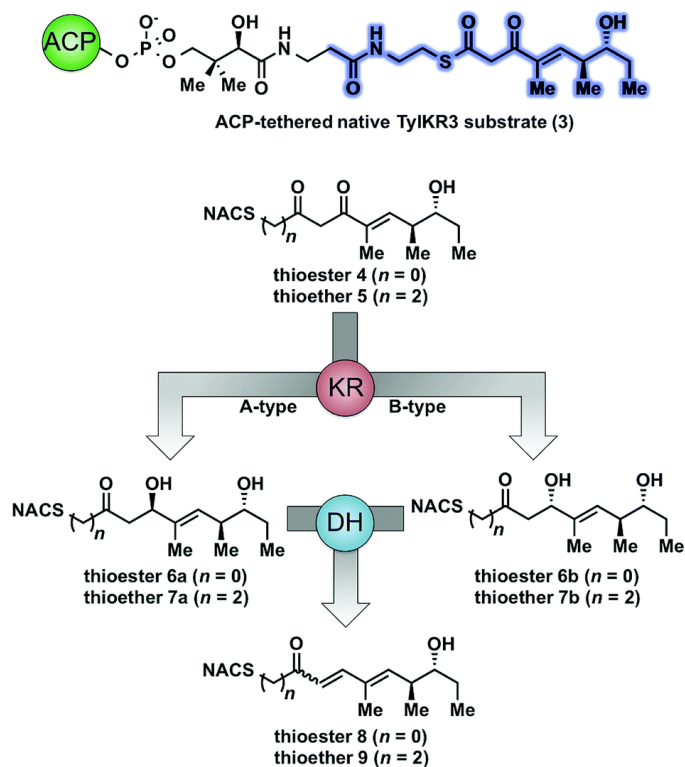
Figure 3.2 Native and synthetic TylKR3 substrates and their possible β-processing products.

The truncated region of the native substrate serving as the basis for substrates **4** and **5** is highlighted in blue.

As part of ongoing studies in our laboratories, we are interested in the development and use of small molecule tools for exploring innate reactivity within polyketide synthase modules. In the present study we sought to probe the enzyme catalyzed turnover of full-length tetraketide substrates **4**, **6a** and **6b** by TylKR3 and TylDH3 *via* LC-MS/MS detection (Fig. 3.2). One virtue of our chosen tetraketides is that they uniformly lack a δ-hydroxyl moiety which has been shown to spontaneously lactonize onto the thioester.[18-20] Our previous strategy utilized stable full-length polyketide intermediate mimics that are resistant to spontaneous intramolecular lactonization through replacement of the labile thioester linkage with a stable thioether moiety[14, 21]. In light of these results, we sought to validate the use of thioether analogs **5**, **7a** and **7b** for direct comparison with the aforementioned thioester substrates. This would constitute the first steady-state analysis of a polyketide dehydratase domain using native substrates, uncover the cryptic stereochemistry of TylKR3, and would offer a unique, more native context to discover innate substrate biases. The use of a natural full-length tetraketide chain intermediates and epimers at each stereogenic center would also allow us to evaluate the impact of vicinal and distal stereochemistry on KR and DH substrate processing.

Methods

General chemistry procedures.

(All synthesis protocols were run by Will Fiers)

All chemical reagents were used as provided unless explicitly indicated otherwise. Tetrahydrofuran (THF) and dichloromethane (CH_2Cl_2) were purified via passage through alumina columns. All reactions were performed under anhydrous argon atmosphere using oven-dried (150 °C) glassware. Reaction mixtures were stirred magnetically using oven-dried magnetic stir bars. Compound purification via flash chromatography utilized silica gel (300–400 mesh) in the

indicated solvent system. TLC was performed using 250 μm, F_{254} silica gel plates and visualized UV and *para*-anisaldehyde stain. A Rudolph Autopol III polarimeter at the indicated temperature using the sodium D line ($\lambda = 589$ nm) unless otherwise specified and reported as follows: $[\alpha]_D^{temp}=$ rotation (*c* g/100 mL, solvent). ^{1}H and ^{13}C NMR spectra were recorded on a Bruker 400 spectrometer at 400 Hz for ^{1}H NMR and at 100 Hz for ^{13}C NMR. Chemical shifts are reported in ppm based on an internal standard of residual $CHCl_3$ (7.26 ppm in ^{1}H NMR and 77.16 in ^{13}C NMR). Proton chemical data are reported in the following format: chemical shift (ppm) (multiplicity (s = singlet, d= doublet, t = triplet, q = quartet, quin = quintet, sextet = sextet, sept = septet, m = multiplet, br = broad peak), *J* = coupling constant (Hz), integration). High-resolution mass spectra (HRMS) were obtained on a Bruker BioTOF II ESI-TOF/MS using either PEG or PPG standards as high resolution calibrants.

(S)-3-((4S,5R,E)-5-hydroxy-2,4-dimethylhept-2-enoyl)-4-isopropyloxazolidin-2-one (12).
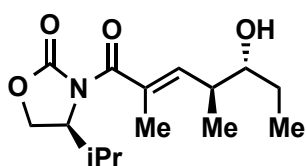
An oven-dried round bottom flask (250 mL) equipped with magnetic stir bar charged with freshly distilled propionaldehyde[22] (4.93 mL, 68.3 mmol, 2 equiv.) in anhydrous dichloromethane (120 mL) was placed in dry ice-acetone bath (-78 °C) and allowed to equilibrate. To the cooled solution was added titanium(IV) chloride (3.77 mL, 34.2 mmol, 1 equiv.). To the resulting yellow reaction mixture was slowly added the vinylketene silyl *N,O*-acetal **11**[23] (11.60 g, 34.2 mmol, 1 equiv.) as a solution in CH_2Cl_2 (45 mL, anhydrous). The reaction quickly adopted a dark red hue. Following completion of addition the reaction mixture was transferred to dry ice-acetonitrile bath (-40 °C) and stirred for 21 hours. The reaction mixture was quenched upon treatment with saturated Rochelle's salt (aq.) followed by saturated sodium bicarbonate (aq.) solutions at -40

°C. The cloudy, white solution was allowed to warm to room temperature and stirred for 1 hour. The resulting biphasic solution was separated, and the aqueous layer was extracted with dichloromethane (3 x 75 mL) and ethyl acetate (3 x 75 mL). The combined organic solutions were dried over anhydrous Na_2SO_4, filtered, and concentrated under vacuum. The resulting crude oil was dry-loaded onto silica column and purified via flash chromatography (30% EtOAc/hexanes) yielding the title compound (**12**) (8.76 g, 30.9 mmol, 90%) as a viscous, slightly yellow oil. R_f = 0.20 (20% EtOAc/hexanes); $[\alpha]_D^{23}$ = 28.3 (*c* 1.00, CHCl$_3$); ^{1}H NMR (CDCl$_3$, 400 MHz) δ 5.82 (d, *J* = 10.4 Hz, 1H), 4.58 (dt, *J* = 8.8, 4.8 Hz, 1H), 4.34 (t, *J* = 8.8 Hz, 1H), 4.18 (dd, *J* = 7.2, 7.6 Hz, 1H), 3.32–3.25 (m, 1H), 3.08 (br, 1H), 2.63–2.52 (m, 1H), 2.38–2.28 (m, 1H), 1.94 (s, 3H), 1.76–1.64 (m, 1H), 1.44 (app sept, *J* = 7.6 Hz, 1H), 1.01 (t, *J* = 7.2 Hz, 3H), 0.98 (d, *J* = 7.2 Hz, 3H), 0.95–0.89 (m, 6H); ^{13}C NMR (CDCl$_3$, 100 MHz) δ 171.7, 154.7, 142.5, 131.2, 76.7, 63.6, 58.3, 39.9, 28.6, 26.8, 18.0, 16.3, 15.4, 14.1, 10.1; HRMS (ESI-TOF) *m/z*: [M + Na]$^+$ Calcd for C$_{15}$H$_{24}$NO$_4$Na 306.1676; Found 306.1673.

(*S*)-3-((4*S*,5*R*,*E*)-2,4-dimethyl-5-((triisopropylsilyl)oxy)-hept-2-enoyl)-4-isopropyloxazolidin-2-one (**13**).
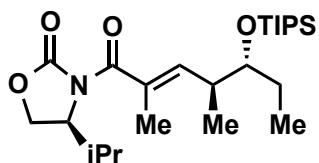
A solution containing the aldol adduct **12** (889 mg, 3.14 mmol, 1 equiv.) in dichloromethane (24 mL, anhydrous) was cooled via ice-water bath. To the chilled, colorless solution was added diisopropylethylamine (0.655 mL, 3.76 mmol, 1.2 equiv.) followed by triisopropylsilyl trifluoromethylsulfonate (1.01 mL, 3.76 mmol, 1.2 equiv.). The resulting solution was stirred at 0° C (1 h) and transferred to refrigerator (3-5° C, 24 h). The yellow, clear reaction solution was

quenched upon addition of saturated sodium bicarbonate (aq.) solution at 0° C and allowed to warm to room temperature (20 min). The biphasic mixture was separated, and the aqueous layer was extracted with dichloromethane (4 x 20 mL). The combined organic layers were dried over Na_2SO_4, filtered, and concentrated under vacuum. The product residue was purified by flash chromatography (10% EtOAc/hexanes) affording the silyl ether **13** (1.3805 g, 3.14 mmol, quant.) as a transparent, colorless oil. R_f = 0.68 (20% EtOAc/hexanes); $[\alpha]_D^{21}$ = 29.5 (c 1.00, CHCl₃); ¹H NMR (CDCl₃, 400 MHz) δ 6.19 (dd, J = 9.6, 1.2 Hz, 1H), 4.50 (ddd, J = 9.2, 5.6, 4.4, 1H), 4.29 (t, J = 8.8), 4.14 (dd, J = 6.0, 9.2 Hz, 1H), 3.73(ddd, J = 5.2, 2.4, 7.6, 1H), 2.72 (ddq, 9.6, 6.8, 2.4 Hz, 1H), 2.42-2.30 (m, 1H), 1.92 (d, J = 1.2 Hz, 3H), 1.63-1.48 (m, 2H), 1.10-1.04 (m, 24H), 0.90 (t, J = 7.2 Hz, 6H), 0.86 (t, J = 7.6 Hz, 3H); ¹³C NMR (CDCl₃, 100 MHz) δ 172.4, 153.8, 141.1, 130.6, 77.8, 63.4, 58.4, 37.0, 28.3, 18.5, 18.4, 18.0, 16.7, 15.1, 13.7, 13.2, 10.5; HRMS (ESI-TOF) m/z: [M + Na]⁺ Calcd for $C_{24}H_{45}NO_4Na$ 462.3010; Found 462.3019.

(4S,5R,E)-2,4-dimethyl-5-((triisopropylsilyl)oxy)hept-2-enal (**14**).
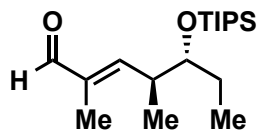
A solution of imide **13** (3.185 g, 7.24 mmol, 1 equiv.) in anhydrous dichloromethane (229 mL) was equilibrated in dry ice-acetone bath (-78 °C) under argon atmosphere. To the stirred solution was added diisobutylaluminum hydride (1.49 M in toluene, 9.73 mL, 14.5 mmol, 2 equiv.) in a dropwise fashion over two minutes. The reaction mixture was allowed to stir at -78 °C for 14 minutes then quenched upon successive addition of methanol (15 mL) and saturated, aqueous sodium potassium tartrate (15 mL). The resulting mixture was allowed to warm to room temperature and stirred vigorously overnight (14 h). The biphasic solution was separated, and the aqueous layer was extracted with dichloromethane (3 x 100 mL). Combined organic extracts were dried over

sodium sulfate, filtered and concentrated under vacuum. The resulting toluene solution was directly loaded onto flash silica column and purified (10% EtOAc/hexanes) furnishing enal **14** (1.983 g, 6.34 mmol, 88%) as a clear, colorless oil. $R_f = 0.52$ (10% EtOAc/hexanes); $[\alpha]_D^{22} = -4.3$ (*c* 1.00, CHCl$_3$); ^{1}H NMR (CDCl$_3$, 400 MHz) δ 9.40 (s, 1H), 6.59 (d, *J* = 10.0 Hz, 1H), 3.78 (app. quin, *J* = 4 Hz, 1H), 2.89 (ddq, *J* = 10.0, 6.8, 3.2 Hz, 1H), 1.76 (s, 3H), 1.65-1.54 (m, 1H), 1.41 (app. sept, *J* = 7.6, 1H), 1.12 (d, *J* = 7.2 Hz, 3H), 1.08 (s, 21H), 0.86 (t, *J* = 7.6 Hz, 3H); ^{13}C NMR (CDCl$_3$, 100 MHz) δ 195.8, 156.8, 139.1, 77.4, 37.7, 28.6, 18.4, 16.9, 13.1, 9.9, 9.6; HRMS (ESI-TOF) *m/z*: [M + Na]$^+$ Calcd for C$_{18}$H$_{36}$O$_2$SiNa 335.2377; Found 335.2372.

(3*S*,6*S*,7*R*,*E*)-3-hydroxy-1-((*R*)-4-isopropyl-2-thioxo-thiazolidin-3-yl)-4,6-dimethyl-7-((triisopropylsilyl)-oxy)non-4-en-1-one (**16**).
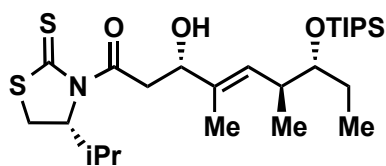
A dichloromethane (anhydrous, 19.56 mL) solution of acetyl thiazolidinone **15** (1.07 g, 5.26 mmol, 1.7 equiv.) was cooled to -40 °C (dry ice-acetonitrile bath) under inert, argon atmosphere. To the chilled, yellow solution was added titanium (IV) chloride (0.611 mL, 5.57 mmol, 1.8 equiv.) resulting in a sudden color change to bright orange. The reaction mixture was stirred for 30 minutes. Slow addition of freshly distilled diisopropylethylamine[22] (0.970 mL, 5.57 mmol, 1.8 equiv.) over three minutes caused a dramatic color change to blood red. The enolate solution was stirred for 2h 12 m while maintaining an external temperature of -40 °C. The reaction was cooled to -78 °C and aldehyde **14** (0.967 g, 3.09 mmol, 1 equiv.) was slowly added over the course of one minute as a solution in dichloromethane (anhydrous, 3.87 mL) and stirred for 5 h. The resulting red-orange mixture was quenched via addition of saturated, aqueous ammonium chloride (10 mL) at -78 °C. The biphasic solution was allowed to warm to room temperature and

the layers were separated. The aqueous layer was extracted with dichloromethane (3 x 15 mL) and the combined organic layers were dried over sodium sulfate, filtered and concentrated under vacuum. The resulting clear, golden oil was wet-loaded onto silica column and purified via flash chromatography (20% EtOAc/hexanes) affording the title compound **16** as a bright yellow, viscous oil (1.29 g, 2.50 mmol, 81%). $R_f = 0.29$ (20% EtOAc/hexanes); $[\alpha]_D^{22} = -219.0$ (c 1.00, CHCl$_3$); ^{1}H NMR (400 MHz, CDCl$_3$) δ 5.51 (d, $J = 9.6$ Hz, 1H), 5.15 (app. t, $J = 6.8$ Hz, 1H), 4.58 (dd, $J = 8.8, 3.2$ Hz, 1H), 3.66 (td, $J = 6.4, 3.2$ Hz, 1H), 3.56–3.44 (m, 3H), 3.03 (d, $J = 11.6$ Hz, 1H), 2.63–2.55 (m, 1H), 2.38 (app. sextet, $J = 7.2$ Hz, 1H), 1.68 (s, 3H), 1.52–1.40 (m, 2H), 1.07 (s, 24H), 0.99 (d, $J = 2.4$ Hz, 3H), 0.98 (d, $J = 2.4$ Hz, 3H), 0.85 (t, $J = 7.2$ Hz, 3H); ^{13}C NMR (CDCl$_3$, 100 MHz) δ 203.1, 173.0, 135.2, 129.1, 77.7, 73.4, 71.7, 44.3, 36.6, 31.0, 30.8, 27.6, 19.3, 18.5, 17.9, 16.9, 13.2, 12.6, 10.5; HRMS (ESI-TOF) m/z: [M + Na]$^+$ Calcd for C$_{26}$H$_{49}$NO$_3$S$_2$SiNa 538.2815; Found 538.2815.

(3S,6S,7R,E)-3-hydroxy-N-methoxy-N,4,6-trimethyl-7-((triisopropylsilyl)oxy)non-4-enamide (**17**).
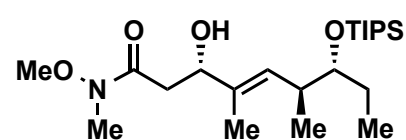
To a bright yellow dichloromethane (anhydrous, 2 mL) solution of acyl thiazolidinone 16 (203 mg, 0.39 mmol, 1 equiv.) was added imidazole (133 mg, 1.95 mmol, 5 equiv.) followed by methylmethoxyamine hydrochloride (95.0 mg, 0.98 mmol, 2.50 equiv). A catalytic amount of 4-dimethylaminopyridine (one crystal) was added to the final mixture. The reaction was stirred 20 h at room temperature and quenched via addition of saturated aqueous ammonium chloride (2 mL). The biphasic mixture was separated, and the aqueous layer was extracted with dichloromethane (4 x 10 mL). The combined organic layers were dried over sodium sulfate, filtered and concentrated under vacuum. The

crude residue was purified by flash chromatography (30% EtOAc/hexanes) providing a slightly yellow, clear, viscous oil (155 mg, 0.372 mmol, 96%). Rf = 0.34 (40% EtOAc/hexanes); $[\alpha]_D^{21}$ = -35.1 (c 1.00, CHCl3); 1H NMR (400 MHz, CDCl3) δ 5.49 (d, J = 9.6 Hz, 1H), 4.45 (dd, J = 8.0, 4.4 Hz, 1H), 3.69 (s, 3H), 3.68–3.63 (m, 1H), 3.20 (s, 3H), 2.68 – 2.56 (m, 3H), 1.69 (s, 1H), 1.47 (dq, J = 7.6, 6.8 Hz, 2H), 1.07 (s, 21H), 0.99 (d, J = 6.8 Hz, 3H), 0.85 (t, J = 7.6 Hz, 3H); 13C NMR (CDCl3, 100 MHz) δ 173.9, 135.4, 128.5, 77.8, 73.4, 61.4, 37.2, 36.6, 32.0, 27.4, 18.4, 16.8, 13.1, 12.6, 10.5; HRMS (ESI-TOF) m/z: [M + Na]+ Calcd for C22H45NO4SiNa 438.3010; Found 438.3009.

(3S,6S,7R,E)-N-methoxy-N,4,6-trimethyl-3-((tri-ethylsilyl)oxy)-7-((triisopropylsilyl)oxy)non-4-enamide (**18**).
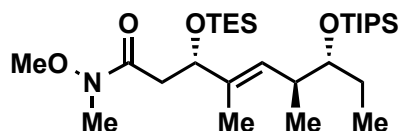
To a reaction flask containing β-hydroxy amide 17 (345 mg, 0.829 mmol, 1.00 equiv.) dissolved in anhydrous dichloromethane (15 mL) in ice-water bath (0 °C) was added 2,6-lutidine (0.387 mL, 3.32 mmol, 4.00 equiv.). The resulting basic solution was supplemented with triethylsilyl trifluoromethanesulfonate (0.375 mL, 1.66 mmol, 2.00 equiv.) and stirred for 1.5 h. The reaction was terminated via the sequential addition of methanol (3 mL) followed by saturated aqueous sodium bicarbonate (5 mL) at 0 °C. The biphasic mixture was warmed to room temperature, separated, and the aqueous fractions were extracted with dichloromethane (4 x 10 mL). The combined organic fractions were dried over anhydrous sodium sulfate, filtered and concentrated under vacuum. The resulting crude oil was wet-loaded onto silica column and purified via flash chromatography (10% EtOAc/hexanes) affording a clear, slightly yellow oil (410.6 mg, 0.776

mmol, 94%). Rf = 0.61 (20% EtOAc/hexanes); $[\alpha]_D^{23}$ = -20.6 (c 1.00, CHCl3); 1H NMR (400

MHz) δ 5.45 (d, J = 9.6 Hz, 1H), 4.58 (dd, J = 8.8, 4.4 Hz, 1H), 3.70 (s, 3H), 3.65 (td, J = 6.8, 2.8

Hz, 1H), 3.17 (s, 3H), 2.94–2.80 (m, 1H), 2.56 (dqd, J = 9.6, 6.8, 2.8 Hz, 1H), 2.31 (dd, J = 14.0,

4.4 Hz, 1H), 1.64 (s, 3H), 1.52 – 1.39 (m, 2H), 1.08 (s, 21H), 0.96 (d, J = 6.8 Hz, 3H), 0.91 (t, J

= 8.0 Hz, 9H), 0.85 (t, J = 7.6 Hz, 3H), 0.56 (q, J = 8.0 Hz, 6H); 13C NMR (CDCl3, 100 MHz) δ

172.3, 136.8, 128.0, 78.0, 75.5, 61.5, 39.7, 36.6, 32.1, 27.6, 18.4, 16.7, 13.1, 11.7, 10.8, 7.0, 4.9;

HRMS (ESI-TOF) m/z: [M + Na]+ Calcd for C28H59NO4Si2Na 552.3875; Found 552.3882.

(5S,8S,9R,E)-6,8-dimethyl-5-((triethylsilyl)oxy)-9-((triiso-propylsilyl)oxy)undeca-1,6-dien-3-

one (19).
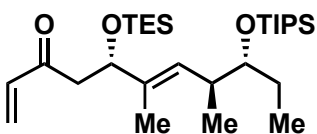
A reaction vessel containing weinreb amide **18** (237 mg, 0.448

mmol, 1 equiv.) in anhydrous tetrahydrofuran (32 mL) was placed in

ice-water bath (0 °C) and allowed to equilibrate. To the chilled, clear solution was added solution

of vinylmagnesium bromide (1.0 M in THF, 1.44 mL, 1.44 mmol, 3.20 equiv.). The reaction

mixture was stirred at 0 °C for 4 h. An additional aliquot of vinylmagnesium bromide (0.450 mL,

0.450 mmol, 1.00 equiv.) was added and the reaction mixture was stirred for 1 h prior to

quenching with saturated, aqueous ammonium chloride (10 mL). The biphasic mixture was

allowed to warm to room temperature, separated and the aqueous layer was extracted with

dichloromethane (3 x 15 mL). The combined organic layers were dried over sodium sulfate,

filtered and concentrated under vacuum. The resulting crude oil was wet-loaded onto silica

column and purified via flash chromatography (5% EtOAc/hexanes) yielding the desired enone

as a clear, colorless oil (192 mg, 0.387 mmol, 86%). R_f = 0.38 (5% EtOAc/hexanes); $[\alpha]_D^{22}$ = -

20.7 (c 0.978, CHCl3); 1H NMR (400 MHz) δ 6.36 (dd, J = 17.6, 10.8 Hz, 1H), 6.20 (d, J = 17.6

Hz, 1H), 5.82 (d, *J* = 10.8 Hz, 1H), 5.43 (d, *J* = 9.2 Hz, 1H), 4.54 (dd, *J* = 8.4, 4.4 Hz, 1H), 3.64

(td, *J* = 6.9, 2.6 Hz, 1H), 2.94 (dd, *J* = 14.0, 8.5 Hz, 1H), 2.63–2.42 (m, 2H), 1.63 (s, 3H), 1.52–

1.35 (m, 2H), 1.08 (s, 21H), 0.95 (d, *J* = 6.8, 3H), 0.89 (t, *J* = 8.0 Hz, 9H), 0.85, (t, *J* = 7.4 Hz,

3H), 0.54 (q, *J* = 8.0 Hz, 6H); ^{13}C NMR (CDCl$_3$, 100 MHz) δ 199.6, 137.6, 136.5, 128.5, 128.1,

77.9, 75.6, 47.0, 36.6, 27.6, 18.4, 13.1, 11.6, 10.8, 7.0, 6.0, 4.9; HRMS (ESI-TOF) *m/z*: [M +

Na]$^+$ Calcd for C$_{28}$H$_{56}$O$_3$Si$_2$Na 519.3660; Found 519.3647.

(5*S*,8*S*,9*R*,*E*)-5,9-dihydroxy-6,8-dimethylundeca-1,6-dien-3-one (**20**).
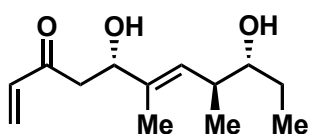
To a polypropylene tube (15 mL, BD Falcon^{TM}) containing silylether **19** (29.8 mg, 0.0600 mmol, 1 equiv.) was added acetonitrile (3.0 mL) and magnetic stir bar. The mixture was stirred in ice-water bath (0 °C) until a homogenous

solution was obtained. A solution of 48% aqueous hydrofluoric acid and acetonitrile (11:89, 8.36

mL) was slowly added to the reaction vessel. The resulting clear solution was stirred vigorously

for 1 h and placed in a refrigerator (4 °C) for 15 h. The reaction was quenched at 0 °C via

dropwise addition of a saturated aqueous sodium bicarbonate solution until the pH was 7. The

neutralized solution was extracted with ethyl acetate (4 x 15 mL). All organic fractions were

combined, dried over sodium sulfate, filtered and concentrated under vacuum. The crude residue

was wet-loaded onto silica column and purified via flash column chromatography (5%

MeOH/dichloromethane) affording the diol as a clear, colorless oil (13.3 mg, 0.586 mmol, 98%).

R$_f$ = 0.30 (5% MeOH/dichloromethane); $[\alpha]_D^{21}$ = -37.2 (*c* 0.26, CHCl$_3$); ^{1}H NMR (400 MHz) δ

6.37 (dd, *J* = 17.6, 10.3 Hz, 1H), 6.26 (dd, *J* = 17.7, 1.0 Hz, 1H), 5.90 (dd, *J* = 11.4, 1.0 Hz, 1H),

5.38 (d, *J* = 9.9 Hz, 1H), 4.52 (dd, *J* = 7.3, 4.7 Hz, 1H), 3.32 (ddd, *J* = 8.4, 6.4, 3.6 Hz, 1H), 2.99

(br, 1H), 2.86–2.80 (m, 2H), 2.53– 2.41(m, 1H), 1.69 (d, *J* = 1.2 Hz, 3H), 1.62–1.53 (m, 2H),

1.45–1.33 (m, 1H), 0.97 (t, J = 7.4 Hz, 3H), 0.96 (d, J = 6.8 Hz, 3H); ^{13}C NMR (CDCl$_3$, 100 MHz) δ 201.0, 137.6, 136.9, 129.5, 128.4, 77.0, 73.0, 44.6, 38.1, 27.1, 17.2, 13.0, 10.2; HRMS (ESI-TOF) *m/z*: [M + Na]$^+$ Calcd for C$_{13}$H$_{22}$O$_3$Na 249.1461; Found 249.1466.

N-(2-(((5S,8S,9R,E)-5,9-dihydroxy-6,8-dimethyl-3-oxoundec-6-en-1-yl)thio)ethyl)acetamide (**7b**).
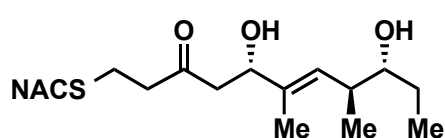
A reaction flask containing vinyl ketone **20** (3.9 mg) in anhydrous tetrahydrofuran (5 mL) was supplemented with *N*-acetylcysteamine (2.0 µL, 0.019 mmol, 1.1 equiv.). To the resulting clear solution was added a catalytic amount of cesium carbonate and the resulting reaction mixture was stirred for 5 hr at ambient temperature under argon atmosphere and quenched upon addition of a saturated, aqueous ammonium chloride solution (5 mL). The biphasic mixture was separated, and the aqueous layer was extracted with ethyl acetate (8 x 10 mL). The combined organic fractions were dried over sodium sulfate, filtered and concentrated under vacuum. The crude residue was wet-loaded onto silica flash column with a small copper(II) sulfate-impregnated silica gel plug (2 cm thick) and purified (eluent = 10% MeOH/dichloromethane) furnishing the desired thioether as a colorless, translucent oil (5.9 mg, 0.017 mmol, quant.). R_f = 0.13 (5% MeOH/dichloromethane); $[\alpha]_D^{22}$ = -24.9 (*c* 0.38, CHCl$_3$); ^{1}H NMR (400 MHz) δ 6.11 (s, 1H), 5.36 (d, J = 9.9 Hz, 1H), 4.48 (dd, J = 8.5, 3.4 Hz, 1H), 3.43 (app. q, J = 6.1 Hz, 2H), 3.37–3.24 (m, 1H), 2.86–2.58 (m, 8H), 2.49–2.39 (m, 1H), 1.99 (s, 3H), 1.66 (d, J = 1.0 Hz, 3H), 1.61–1.52 (m, 1H), 1.44–1.32 (m, 1H), 0.99–0.93 (m, 6H); ^{13}C NMR (CDCl$_3$, 100 MHz) δ 209.4, 170.5, 137.5, 128.4, 77.1, 73.1, 48.2, 43.8, 38.7, 38.0, 32.2, 27.2, 25.2, 23.4, 17.2, 13.0, 10.2; HRMS (ESI-TOF) *m/z*: [M + Na]$^+$ Calcd for C$_{17}$H$_{31}$NO$_4$SNa 368.1866; Found 368.1872.

(5*S*,8*S*,9*R*,*E*)-5-hydroxy-6,8-dimethyl-9-((triisopropylsilyl)-oxy)undeca-1,6-dien-3-one (**21**).
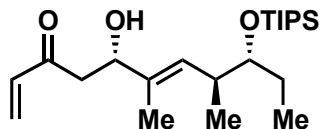
To a reaction vessel containing disilylether **19** (39.3 mg, 0.0792 mmol) in a mixture of tetrahydrofuran (1.98 mL) and deionized water (0.296 mL) was added trifluoroacetic acid (15.6 µL, 0.210 mmol, 2.65 equiv.). The acidic solution was stirred for 2.5 hr at ambient temperature and carefully neutralized upon addition of a saturated, aqueous sodium bicarbonate solution. The biphasic solution was separated, and the aqueous layer repeatedly extracted with ethyl acetate (4 x 7 mL). The combined organic layers were dried over sodium sulfate, filtered and concentrated under vacuum. The crude product was wet-loaded onto silica column and purified via flash column chromatography (10% EtOAc/hexanes) producing a light yellow, clear oil (29.5 mg, 0.0771 mmol, 97%). $R_f = 0.25$ (10% EtOAc/hexanes); $[\alpha]_D^{24} = -23.0$ (*c* 1.00, CHCl$_3$); ^{1}H NMR (400 MHz) δ 6.37 (dd, *J* = 17.7, 10.4 Hz, 1H), 6.25 (d, *J* = 16.6 Hz, 1H), 5.89 (d, *J* = 10.4 Hz, 1H), 5.48 (d, *J* = 9.6 Hz, 1H), 4.52 (dd, *J* = 9.1, 2.8 Hz, 1H), 3.65 (td, *J* = 6.2, 3.3 Hz, 1H), 2.87 (dd, *J* = 16.8, 9.2 Hz, 1H), 2.75 (dd, *J* = 16.8, 3.1 Hz, 1H), 2.62–2.54 (m, 1H), 1.68 (d, *J* = 1.3 Hz, 3H), 1.54 – 1.40 (m, 2H), 1.07 (s, 21H), 0.97 (d, *J* = 6.9 Hz, 3H), 0.85 (t, *J* = 7.5 Hz, 3H); ^{13}C NMR (CDCl$_3$, 100 MHz) δ 201.1, 136.9, 135.3, 129.2, 128.9, 77.8, 73.3, 44.8, 36.6, 27.6, 18.5, 16.9, 13.2, 12.5, 10.5; HRMS (ESI-TOF) *m/z*: [M + Na]$^+$ Calcd for C$_{22}$H$_{42}$O$_3$SiNa 405.2795, Found 405.2795.

(8*S*,9*R*,*E*)-6,8-dimethyl-9-((triisopropylsilyl)oxy)undeca-1,6-diene-3,5-dione (**22**).
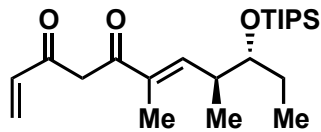
O O   OTIPS To a small flask containing *β*-hydroxy ketone **21** (80.0 mg, 0.209
Me Me Me mmol) in ethyl acetate (10 mL) was added 2-iodoxybenzoic acid (390

mg, 0.627 mmol, 3.00 equiv., 45% wt/wt). The white, cloudy solution was rapidly stirred and

heated at reflux for 2 h. The slightly yellow solution was cooled to ambient temperature and

concentrated under vacuum. The resulting concentrated solution was directly loaded onto silica

flash column and purified (5% EtOAc/hexanes) yielding a red-orange oil (72.4 mg, 0.190 mmol,

92%). R_f = 0.36 (5% EtOAc/hexanes); $[\alpha]_D^{21}$ = -47.2 (*c* 1.00, CHCl$_3$); ^{1}H NMR (400 MHz) δ

15.46 (s, 1H), 6.71 (dd, *J* = 9.9, 1.0 Hz, 1H), 6.25 (dd, *J* = 17.2, 2.0 Hz, 1H), 6.17 (dd, *J* = 9.9,

17.2 Hz, 1H), 5.89 (s, 1H), 5.64 (dd, *J* = 9.9, 2.0 Hz, 1H), 3.75 (ddd, *J* = 7.8, 4.6, 3.6 Hz, 1H),

2.81–2.72 (m, 1H), 1.87 (d, *J* = 1.1 Hz, 3H), 1.63–1.52 (m, 1H), 1.49–1.37 (m, *J* = 14.9, 7.4 Hz,

1H), 1.09–1.07 (m, 24H), 0.86 (t, *J* = 7.5 Hz, 3H); ^{13}C NMR (CDCl$_3$, 100 MHz) δ 193.1, 176.5,

143.0, 134.4, 133.3, 124.5, 96.6, 77.6, 37.8, 28.4, 18.4, 16.9, 13.2, 11.9, 10.0; HRMS (ESI-TOF)

m/z: [M + Na]$^+$ Calcd for C$_{22}$H$_{40}$O$_3$SiNa 403.2639, Found 403.2646.

(8*S*,9*R*,*E*)-9-hydroxy-6,8-dimethylundeca-1,6-diene-3,5-dione (**23**).
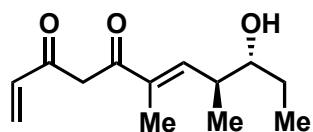
O O   OH To a polypropylene tube (15 mL, BD Falcon^{TM}) containing silylether
Me Me Me **22** (72.4 mg, 0.140 mmol) was added acetonitrile (1.23 mL). The clear

solution was equilibrated in ice-water bath (0 °C) for 10 minutes. A pre-chilled solution of 48%

aqueous hydrogen fluoride and acetonitrile (11:89, 9.84 mL) was slowly added to the rapidly

stirred solution. The resulting slightly yellow solution was placed in refrigerator (4 °C) for 40 h.

The reaction mixture was quenched via slow neutralization with aqueous, saturated sodium

bicarbonate solution at 0 °C. The aqueous layer was extracted with ethyl acetate (5 x 20 mL) and

the combined organic layers were concentrated under vacuum. The product was placed under

high vacuum for 2 h furnishing the desired alcohol **23** as a viscous, yellow oil (42.6 mg, 0.190

mmol, quant.). $R_f = 0.20$ (20% EtOAc/hexanes); $[\alpha]_D^{22} = -51.2$ (c 1.00, CHCl₃); (Compound **23**

was found to exist entirely in the enol form (not drawn)) ¹H NMR (400 MHz) δ 15.54 (br, 1H),

6.59 (dd, $J = 10.0, 0.96$ Hz, 1H), 6.28 (dd, $J = 17.2, 2.4$ Hz, 1H), 6.21 (dd, $J = 17.2, 9.5$ Hz, 1H)

5.90 (s, 1H), 5.66 (dd, $J = 9.5, 2.4$ Hz, 1H), 3.49 (dt, $J = 8.8, 4.6$ Hz, 1H), 2.73–2.60 (m, 1H),

1.89 (d, $J = 1.0$ Hz, 3H), 1.60–1.49 (m, 1H), 1.43 (dq, $J = 14.2, 7.5$ Hz, 1H), 1.08 (d, $J = 6.7$ Hz,

3H), 0.97 (t, $J = 7.4$ Hz, 3H); ¹³C NMR (CDCl₃, 100 MHz) δ 192.1, 177.7, 141.6, 135.1, 133.3,

125.0, 96.9, 76.9, 39.2, 27.9, 16.8, 12.2, 10.2; HRMS (ESI-TOF) m/z: [M + Na]⁺ Calcd for

C₁₃H₂₀O₃Na 247.1305, Found 247.1310.
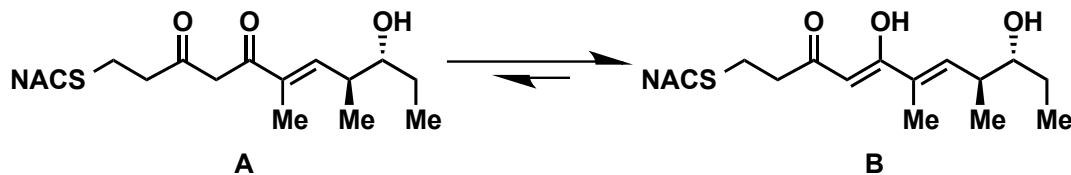
N-(2-((((8S,9R,E)-9-hydroxy-6,8-dimethyl-3,5-dioxoundec-6-en-1-yl)thio)ethyl)acet-amide (**5**).

To a round bottom flask containing vinyl ketone (12.3 mg, 0.055 mmol) in anhydrous

tetrahydrofuran (10 mL) was added N-acetylcysteamine (6.4 μL, 0.060 mmol, 1.1 equiv.) as a

solution in anhydrous THF (64 μL). The reaction mixture was supplemented with a catalytic

amount of cesium carbonate and stirred at ambient temperature for 4.5 h. The bright yellow,

transparent solution was quenched via addition of aqueous, saturated ammonium chloride

solution (5 mL) and the resulting biphasic solution was separated. The aqueous layer was

repeatedly extracted with ethyl acetate (5 x 10 mL). Combined organic fractions were dried over

anhydrous sodium sulfate, filtered and concentrated under vacuum. The crude residue was

purified by via flash column chromatography (5% MeOH/dichloromethane) providing the

desired thioether **5** as a viscous, bright orange oil (7.2 mg, 0.021 mmol, 38%). R_f = 0.30 (5%

MeOH/dichloromethane); $[\alpha]_D^{21}$ = -30.0 (*c* 0.46, CHCl$_3$); (Compound **5** existed in a ~3:1 mixture

of enol (**B**) and keto (**A**) tautomers, respectively) ^{1}H NMR (400 MHz) δ 15.58 (s, 0.75H), 6.66–

6.56 (m, 1H), 6.09 (br, 0.25H), 5.96 br, 0.75H), 5.80 (br, 0.75H), 3.96 (d, *J* = 14.7 Hz, 0.25H),

3.79 (d, *J* = 14.7 Hz, 0.25H), 3.61–3.36 (m, 3H), 2.87–2.80 (m, 2H), 2.80 – 2.74 (m, 0.50H),

2.72–2.62 (m, 4.5H), 1.98–2.02 (m, 3H), 1.85 (d, *J* = 1.2 Hz, 2.25H), 1.81 (d, *J* = 1.2 Hz, 0.75H),

1.60–1.48 (m, 1H), 1.47–1.37 (m, 1H), 1.09 (d, *J* = 6.9 Hz, 0.75H), 1.06 (dd, *J* = 6.8 Hz, 2.25H),

1.00–0.93 (m, 3H); (Only the major (enol) tautomer **B** carbon shifts are recorded) ^{13}C NMR

(CDCl$_3$, 100 MHz) δ 194.8, 183.7, 170.4, 141.2, 132.2, 96.6, 76.9, 39.7, 39.1, 38.6, 32.2, 27.9,

27.2, 23.4, 16.8, 12.4, 10.2; HRMS (ESI-TOF) *m/z*: [M + Na]$^+$ Calcd for C$_{17}$H$_{29}$NO$_4$SSi

366.1710, Found 366.1716.

S-(2-acetamidoethyl) (3*S*,6*S*,7*R*,*E*)-3-hydroxy-4,6-di-methyl-7-((triisopropylsilyl)oxy)non-4-

enethioate (**24**).
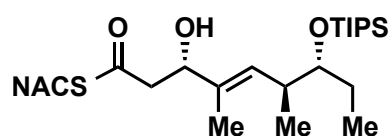
A reaction vessel containing thiazoldinethione **16** (0.142 g,
0.276 mmol) in anhydrous dichloromethane (2 mL) under argon

atmosphere was added imidazole (56.4 mg, 0.828 mmol, 3.00 equiv.). To the clear, yellow

solution was added *N*-acetylcysteamine (32.3 μL, 0.304 mmol, 1.10 equiv.) and the resulting

reaction mixture was stirred for 14 hr at ambient temperature. The crude reaction mixture was

wet-loaded onto silica column and purified by flash chromatography (5%

MeOH/dichloromethane) affording the desired thioester **24** as a transparent, slightly yellow oil

(0.119 g, 0.251 mmol, 91%). R_f = 0.32 (5% MeOH/dichloromethane); $[\alpha]_D^{22}$ = -15.0 (*c* 1.00,

CHCl$_3$); ^{1}H NMR (400 MHz) δ 5.82 (s, 1H), 5.49 (d, J = 9.7 Hz, 1H), 4.49 (d, J = 8.4 Hz, 1H),

3.65 (br, 1H), 3.45 (q, J = 5.9 Hz, 2H), 3.05 (t, J = 6.2 Hz, 2H), 2.85 (dd, J = 15.0, 9.2 Hz, 1H),

2.79 – 2.64 (m, 1H), 2.63–2.51 (m, 1H), 2.34 (br, 1H), 1.97 (s, 3H), 1.65 (s, 3H), 1.54–1.36 (m,

2H), 1.07 (s, 21H), 0.96 (d, J = 6.9 Hz, 3H), 0.84 (t, J = 7.3 Hz, 3H); ^{13}C NMR (CDCl$_3$, 100

MHz) δ 199.1, 170.5, 134.9, 129.6, 77.7, 74.4, 49.8, 39.6, 36.6, 29.0, 27.6, 23.4, 18.5, 17.0, 13.2,

12.2, 10.4; HRMS (ESI-TOF) m/z: [M + Na]$^+$ Calcd for C$_{24}$H$_{47}$NO$_4$SSiNa 496.2887, Found

494.2896.

S-(2-acetamidoethyl) (3*S*,6*S*,7*R*,*E*)-3,7-dihydroxy-4,6-dimethylnon-4-enethioate (**6b**).
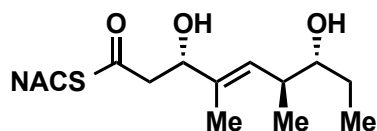
A solution of silylether **25** (33.4 mg, 0.0706 mmol) in acetonitrile (3.55 mL) in a polypropylene tube (15 mL, BD Falcon^{TM}) was cooled in ice-water bath (0 °C). To the reaction mixture was

added a chilled solution of 48% hydrofluoric acid in acetonitrile (11:89, 10.6 mL) and the

resulting combined solution was transferred to the refrigerator overnight (15 h). The reaction

mixture was neutralized via slow addition of a saturated, aqueous sodium bicarbonate solution at

0 °C. The clear solution was extracted with ethyl acetate (3 x 25 mL). The combined organic

layers were dried over anhydrous sodium sulfate, filtered and concentrated under vacuum. Flash

column chromatography (10% MeOH/dichloromethane) of the crude residue furnished the title

diol as a colorless, clear oil (14.1 mg, 0.0445 mmol, 63%). R_f = 0.44 (10%

MeOH/dichloromethane); $[\alpha]_{365}^{22}$ = -6.0 (*c* 0.51, CHCl$_3$); ^{1}H NMR (400 MHz) δ 6.16 (br, 1H),

5.38 (d, J = 9.9 Hz, 1H), 4.46 (br, 1H), 3.52–3.35 (m, 2H), 3.33–3.22 (m, 1H), 3.11–2.96 (m,

3H), 2.87 (dd, J = 14.7, 7.5 Hz 1H), 2.79 (dd, J = 14.5, 4.0 Hz 1H), 2.49–2.39 (m, 1H), 1.96 (s,

3H), 1.67 (s, 3H), 1.62–1.53 (m, 1H), 1.45–1.31 (m, 1H), 1.01–0.88 (m, 6H); ^{13}C NMR (CDCl$_3$,

100 MHz) δ 199.0, 170.7, 137.2, 128.9, 77.1, 74.0, 49.3, 39.3, 38.1, 29.3, 27.2, 23.3, 17.2, 13.1, 10.1; HRMS (ESI-TOF) m/z: $[M + Na]^+$ Calcd for $C_{15}H_{27}NO_4SNa$ 340.1553, Found 340.1565.

S-(2-acetamidoethyl) (6*S*,7*R*,*E*)-4,6-dimethyl-3-oxo-7-((triisopropylsilyl)oxy)non-4-enethioate (**25**).

To a small round bottom flask was added β-hydroxythioester **24** (20.7 mmol, 0.0437 mmol) as an ethyl acetate solution (2 mL). The colorless solution was diluted with additional ethyl acetate (3 mL) and a superstoichiometric amount of 2-iodoxybenzoic acid (81.8 mg, 0.131 mmol, 3.00 equiv., 45% wt/wt) was added. The white suspension was refluxed for 1 h. After cooling to ambient temperature the reaction mixture was filtered through celite pad (3 cm thick) and concentrated under vacuum affording the crude β-ketothioester **25** as a yellow oil which was taken to the next step without further purification. $R_f = 0.45$ (5% MeOH/dichloromethane).
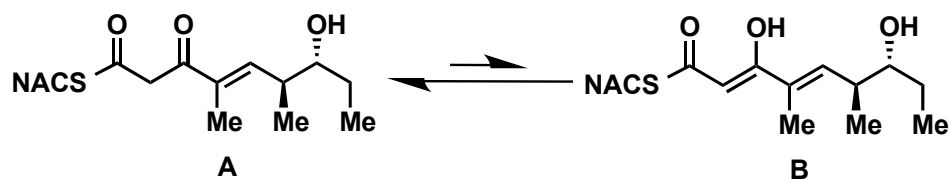
S-(2-acetamidoethyl) (6*S*,7*R*,*E*)-7-hydroxy-4,6-dimethyl-3-oxonon-4-enethioate (**4**).

The crude silylether **25** (20.6 mg, 0.0437 mmol) was transferred as an acetonitrile solution (0.200 mL) to a polypropylene tube (15 mL, BD Falcon^{TM}) and cooled via ice-water bath (0 °C). To the pre-chilled solution was added a 48% hydrofluoric acid solution diluted in acetonitrile (11:89, 2.50 mL). The reaction mixture was placed in refrigerator (4 °C) for 24 h. TLC analysis of the reaction mixture indicated incomplete conversion and an addition portion of hydrofluoric acid

solution (freshly prepared and identical to above, 1 mL) was added to the reaction mixture at 0 °C. After an additional 12 h at 4 °C, the reaction mixture was neutralized at 0 °C via addition of aqueous, saturated sodium bicarbonate solution. The reaction mixture was extracted with ethyl acetate (4 x 25 mL). The combined organic fractions were dried over anhydrous sodium sulfate, filtered and concentrated under vacuum. Crude product was purified by flash column chromatography (5% MeOH/dichloromethane) yielding a slightly yellow oil (11.8 mg, 0.0374 mmol, 86% from **24**). R_f = 0.25 (5% MeOH/dichloromethane); $[\alpha]_D^{21}$ = -35.8 (*c* 0.79, CHCl$_3$); (Compound **26** exists as in equilibrium of **A** and **B** (~3:1)) ^{1}H NMR (400 MHz) δ 12.71 (br, 0.25H), 6.65 (d, *J* = 9.8 Hz, 0.75H), 6.58 (d, *J* = 10.1 Hz, 0.25H), 6.24 (s, 0.75H), 6.05 (s, 0.25H), 5.66 (s, 0.25H), 4.08 (d, *J* = 15.0 Hz, 0.75H), 3.90 (d, *J* = 15.0 Hz, 0.75H), 3.59–3.33 (m, 3H), 3.13–3.00 (m, 2H), 2.74–2.59 (m, 1H), 2.02–1.91 (m, 3H), 1.85–1.78 (s, 3H), 1.58–1.34 (m, 2H), 1.09 (d, *J* = 6.8 Hz, 2.25H), 1.04 (d, *J* = 6.8 Hz, 0.75H), 1.00–0.90 (m, 3H); (Carbon shifts only given for major tautomer) ^{13}C NMR (CDCl$_3$, 100 MHz) δ 193.8, 193.5, 170.9, 147.7, 137.3, 76.9, 53.2, 39.5, 39.2, 29.5, 28.3, 23.2, 16.8, 11.7, 10.3; HRMS (ESI-TOF) *m/z*: [M + Na]$^+$ Calcd for C$_{15}$H$_{25}$NO$_4$SSi 338.1397, Found 338.1398.

(3*R*,6*S*,7*R*,*E*)-3-hydroxy-1-((*S*)-4-isopropyl-2-thioxo-thiazolidin-3-yl)-4,6-dimethyl-7-((triisopropylsilyl)-oxy)non-4-en-1-one (**S1**).
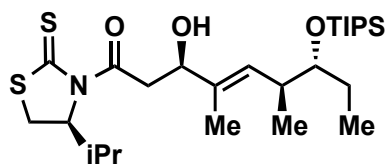
A reaction vessel containing thiazolidinethione *ent*-**15** (91.9 mg, 0.452 mmol, 1.50 equiv.) in anhydrous dichloromethane (3.00 mL) was cooled in ice-water bath (0 °C). To the chilled, bright yellow solution was added titanium(IV) chloride (55.0 μL, 0.503 mmol, 1.67 equiv.) resulting in a color change to red orange. The reaction was stirred for 5 min, then placed in dry ice-acetone

bath (-78 °C) and allowed to equilibrate. To the chilled reaction mixture was added freshly

distilled diisopropylethylamine[22] (87.6 µL, 0.503 mmol, 1.67 equiv.) dropwise over 4 min

causing a sudden color change to blood red. The solution was stirred at -78 °C for 2 h. To the

enolate solution was added aldehyde **14** (94 mg, 0.301 mmol, 1.00 equiv.) as a solution in

anhydrous dichloromethane (1 mL) over the course of 6 min. The reaction mixture was stirred at

-78 °C for an additional 6 hours and quenched upon addition of saturated, aqueous ammonium

chloride solution (5 mL). The biphasic solution was warmed to ambient temperature, separated

and the aqueous layer extracted with dichloromethane (4 x 10 mL). The combined, organic

fractions were dried over anhydrous sodium sulfate, filtered and concentrated under vacuum.

Purification by silica gel chromatography (20% EtOAc/hexanes) provided the desired aldol

adduct as a yellow, viscous oil (0.106 mg, 0.205 mmol, 68%). R_f = 0.31 (20% EtOAc/hexanes);

$[\alpha]_D^{22}$ = 217.2 (c 1.00, CHCl$_3$); ^{1}H NMR (400 MHz) δ 5.51 (d, J = 9.5 Hz, 1H), 5.15 (t, J = 6.5

Hz, 1H), 4.58 (d, J = 9.3 Hz, 1H), 3.65 (br, 1H), 3.56 – 3.38 (m, 3H), 3.03 (d, J = 11.5 Hz, 1H),

2.58 (br, 1H), 2.45 – 2.32 (m, 1H), 1.67 (s, 3H), 1.54–1.35 (m, 2H), 1.07 (app. s, 24H), 0.97 (t, J

= 6.0 Hz, 6H), 0.84 (t, J = 7.0 Hz, 3H); ^{13}C NMR (CDCl$_3$, 100 MHz) δ 203.1, 173.0, 135.1,

129.3, 77.7, 77.4, 73.5, 71.7, 44.2, 36.6, 31.0, 27.7, 19.3, 18.5, 18.0, 17.0, 13.2, 12.4, 10.4;

HRMS (ESI-TOF) m/z: [M + Na]$^+$ Calcd for C$_{26}$H$_{49}$NO$_3$S$_2$SiNa 538.2815, Found 538.2821.


S-(2-acetamidoethyl) (3*R*,6*S*,7*R*,*E*)-3-hydroxy-4,6-di-methyl-7-((triisopropylsilyl)oxy)non-4-

enethioate (**S2**).
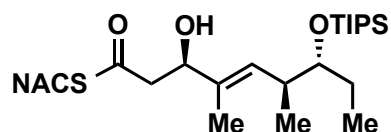
To a reaction vessel containing acyl thiazolidinethione **S1** (66.0

mg, 0.128 mmol) in anhydrous dichloromethane (2 mL) was

sequentially added imidazole (26.0 mg, 0.384 mmol, 3.00 equiv.) and *N*-acetylcysteamine (16.0

μL, 0.154 mmol, 1.20 equiv.). The transparent, yellow solution was vigorously stirred under argon atmosphere for 15 hr at ambient temperature. The reaction was quenched upon addition of an aqueous, saturated ammonium chloride solution (3 mL) and the biphasic solution was separated. The aqueous layer was extracted with dichloromethane (3 x 10 mL). The combined organic layers were dried over anhydrous sodium sulfate, filtered, concentrated under vacuum and purified via silica column flash chromatography (5% MeOH/dichloromethane) using a small plug of copper(II) sulfate impregnated silica gel (1 cm on top) furnished the title compound as a colorless oil (59.0 mg, 0.125 mmol, 97%). $R_f = 0.35$ (5% MeOH/dichloromethane); $[\alpha]_D^{22} = -7.4$ (c 1.00, CHCl$_3$); ^{1}H NMR (400 MHz) δ 5.94 (br, 1H), 5.48 (d, $J = 9.7$ Hz, 1H), 4.49 (dd, $J = 9.2$, 3.4 Hz, 1H), 3.71–3.56 (m, 1H), 3.44 (q, $J = 6.1$ Hz, 2H), 3.13–2.94 (m, 2H), 2.85 (dd, $J = 15.0$, 9.2 Hz, 1H), 2.71 (dd, $J = 14.9$, 3.6 Hz, 1H), 2.55 (ddd, $J = 9.9$, 6.8, 3.2 Hz, 1H), 2.47 (br, 1H), 1.96 (s, 3H), 1.64 (d, $J = 1.1$ Hz, 3H), 1.52–1.30 (m, 2H), 1.06 (s, 21H), 0.98 (d, $J = 6.9$ Hz, 3H), 0.82 (t, $J = 7.4$ Hz, 3H); ^{13}C NMR (CDCl$_3$, 100 MHz) δ 199.0, 170.6, 134.9, 129.7, 77.7, 74.5, 49.8, 39.5, 36.5, 28.9, 27.7, 23.3, 18.4, 17.0, 13.1, 12.0, 10.4; HRMS (ESI-TOF) m/z: [M + Na]$^+$ Calcd for C$_{24}$H$_{47}$NO$_4$SSiNa 496.2887, Found 496.2881.

S-(2-acetamidoethyl) (3*R*,6*S*,7*R*,*E*)-3,7-dihydroxy-4,6-dimethylnon-4-enethioate (**6a**).

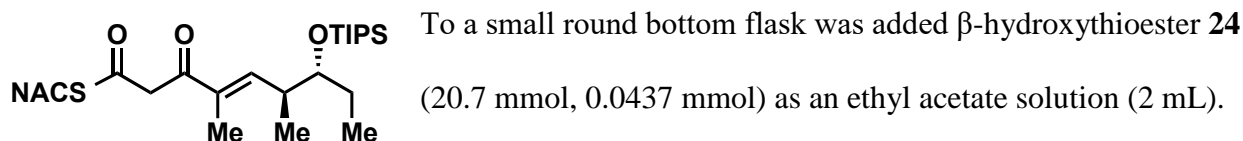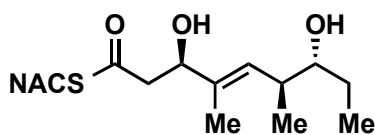The silylether **S2** (40.0 mg, 0.0845 mmol) was deprotected in a manner analogous to the production of diol **6b** affording the desired product as a clear, colorless oil (21.5 mg, 0.678 mmol, 80%). $R_f = 0.43$ (10% MeOH/dichloromethane); $[\alpha]_D^{22} = 18.2$ (c 1.00, CHCl$_3$); ^{1}H NMR (400 MHz) δ 6.19 (br, 1H), 5.34 (d, $J = 10.0$ Hz, 1H), 4.50 (t, $J = 6.6$ Hz, 1H), 3.48 (app. dq, $J = 12.4$, 6.2 Hz, 1H), 3.42–3.31 (m, 1H), 3.30–3.24 (m, 1H), 3.04 (t, $J = 6.2$ Hz, 2H), 2.83 (dd, $J = 6.6$,

3.1 Hz, 2H), 2.62 (br, 1H), 2.49–2.39 (m, 1H), 1.96 (s, 3H), 1.69 (d, J = 1.1 Hz 3H), 1.63–1.52

(m, 1H), 1.43–1.31 (m, 1H), 0.96 (t, J = 7.3 Hz, 3H), 0.96 (d, J = 6.7 Hz, 3H); ^{13}C NMR (CDCl$_3$,

100 MHz) δ 198.6, 170.7, 137.2, 129.9, 77.1, 74.5, 49.7, 39.4, 38.2, 29.3, 27.2, 23.3, 17.2, 12.2,

10.1; HRMS (ESI-TOF) *m/z*: [M + Na]$^+$ Calcd for C$_{15}$H$_{27}$NO$_4$SiNa 340.1553, Found 340.1554.

(3R,6S,7R,E)-3-hydroxy-N-methoxy-N,4,6-tri-methyl-7-((triisopropylsilyl)oxy)non-4-enamide

(S3).
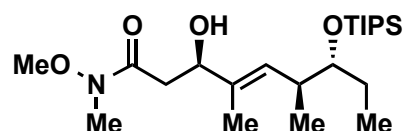
To a reaction vessel containing acyl thiazolidinethione **S1** (0.298 g, 0.578 mmol) in anhydrous dichloromethane (3 mL) was sequentially added imidazole (0.197 g, 2.89 mmol, 5.00 equiv.) and *N,O*-

dimethylhydroxylamine hydrochloride (0.141 g, 1.45 mmol, 2.50 equiv.). The reaction mixture

was stirred at ambient temperature under argon atmosphere for 16 h and quenched upon addition

of a saturated, aqueous ammonium chloride solution (4 mL). The biphasic solution was

separated, and the aqueous layer was extracted with dichloromethane. Combined organic

fractions were dried over anhydrous sodium sulfate, filtered, concentrated under vacuum and

purified via silica flash column chromatography (40% EtOAc/hexanes) yielding the desired

amide as a slightly yellow, clear oil (0.208 g, 0.501 mmol, 87%). R_f = 0.37 (40%

EtOAc/hexanes); $[\alpha]_D^{23}$ = 26.3 (*c* 1.00, CHCl$_3$); ^{1}H NMR (400 MHz) δ 5.48 (d, J = 9.6 Hz, 1H),

4.47–4.41 (m, 1H), 3.67 (s, 3H), 3.66–3.60 (m, 2H), 3.19 (s, 3H), 2.69–2.51 (m, 3H), 1.67 (s,

3H), 1.52–1.36 (m, 2H), 1.06 (s, 21H), 0.99 (d, J = 6.9 Hz, 3H), 0.84 (t, J = 7.4 Hz, 3H); ^{13}C

NMR (CDCl$_3$, 100 MHz) δ 173.9, 135.4, 129.8, 77.8, 73.6, 61.4, 37.3, 36.6, 32.0, 27.6, 18.4,

17.0, 13.1, 12.3, 10.4; HRMS (ESI-TOF) *m/z*: [M + Na]$^+$ Calcd for C$_{22}$H$_{45}$NO$_4$SiNa 438.3010,

Found 438.3010.

(3*R*,6*S*,7*R*,*E*)-*N*-methoxy-*N*,4,6-trimethyl-3-((tri-ethylsilyl)oxy)-7-((triisopropylsilyl)oxy)non-4-en-amide (**S4**).
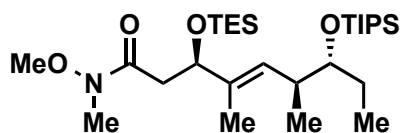
To a small, round bottom flask containing β-hydroxy amide **S3** (79.0 mg, 0.190 mmol) under argon atmosphere in an ice-water bath (0 °C) was added anhydrous dichloromethane (3.5 mL). The resulting clear solution was supplemented with 2,6-lutidine (89.0 µL, 0.761 mmol, 4.00 equiv.) and triethylsilyl trifluoromethanesulfonate (86.0 µL, 0.380 mmol, 2.00 equiv.). The reaction mixture was stirred at 0 °C for 2.5 h and quenched upon sequential addition of methanol (2 mL) and saturated, aqueous sodium bicarbonate solution (2 mL). The biphasic solution was warmed to ambient temperature and the layers were separated. The aqueous layer was extracted with dichloromethane (3 x 10 mL) and the combined organic fractions were dried over anhydrous sodium sulfate, filtered and concentrated under vacuum. The crude residue was purified by silica flash column chromatography (10-20% EtOAc/hexanes) producing the disilylether **S4** as a transparent, clear oil (89.3 mg, 0.169 mmol, 89%). R_f = 0.58 (20% EtOAc/hexanes); $[\alpha]_D^{22}$ = 9.7 (*c* 1.00, CHCl$_3$); ^{1}H NMR (400 MHz) δ 5.45 (d, *J* = 9.5 Hz, 1H), 4.59 (dd, *J* = 8.8, 4.5 Hz, 1H), 3.70 (s, 3H), 3.61 (td, *J* = 6.5, 2.8 Hz, 1H), 3.16 (s, 3H), 2.99 – 2.80 (m, 1H), 2.60–2.50 (m, 1H), 2.31 (dd, *J* = 13.9, 4.3 Hz, 1H), 1.64 (d, *J* = 1.1 Hz, 3H), 1.49–1.34 (m, 2H), 1.07 (s, 21H), 1.00 (d, *J* = 6.9 Hz, 3H), 0.91 (t, *J* = 7.9 Hz, 9H), 0.82 (t, *J* = 7.4 Hz, 3H), 0.56 (q, *J* = 7.9 Hz, 6H); ^{13}C NMR (CDCl$_3$, 100 MHz) δ 136.7, 128.2, 77.8, 75.6, 61.4, 39.5, 36.7, 32.1, 27.5, 18.5, 16.5, 13.1. 11.4, 10.7, 6.9, 4.9 (missing amide carbonyl carbon); HRMS (ESI-TOF) *m/z*: [M + Na]$^+$ Calcd for C$_{28}$H$_{59}$NO$_4$Si$_2$Na 552.3875, Found 552.3905.

(5R,8S,9R,E)-6,8-dimethyl-5-((triethylsilyl)oxy)-9-((triiso-propylsilyl)oxy)undeca-1,6-dien-3-one (**S5**).
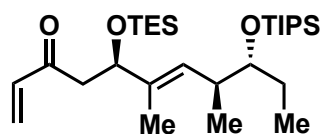
To a reaction vessel containing Weinreb amide **S4** (37.6 mg, 0.0710 mmol) under argon atmosphere was added anhydrous tetrahydrofuran (5 mL). The resulting clear solution was cooled with ice-water bath (0 °C). A solution of vinylmagnesium bromide (1.00 M) (0.224 mL, 0.224 mmol, 3.16 equiv.) was added to the stirred solution of starting material. After 3 h the reaction was quenched at 0 °C via addition of saturated, aqueous ammonium chloride solution (5 mL) and allowed to warm to ambient temperature. The biphasic solution was separated, and the aqueous layer was repeatedly extracted with ethyl acetate (3x 10 mL). The combined organic layers were dried over anhydrous sodium sulfate, filtered and concentrated under vacuum. Purification of the crude residue by silica flash column chromatography (5% EtOAc/hexanes) furnished the vinyl ketone as a clear, light yellow oil (32.7 mg, 0.658 mmol, 93%). $R_f = 0.45$ (5% EtOAc/hexanes); $[\alpha]_D^{22} = 7.6$ (c 1.00, CHCl$_3$); ^{1}H NMR (400 MHz) δ 6.35 (dd, J = 17.6, 10.5 Hz, 1H), 6.19 (d, J = 17.6 Hz, 1H), 5.81 (d, J = 10.5 Hz, 1H), 5.42 (d, J = 9.6 Hz, 1H), 4.55 (dd, J = 8.3, 4.7 Hz, 1H), 3.69 – 3.52 (m, 1H), 2.94 (dd, J = 14.0, 8.4 Hz, 1H), 2.58–2.47 (m, 2H), 1.62 (s, 3H), 1.50–1.30 (m, 2H), 1.07 (s, 21H), 0.99 (d, J = 6.9 Hz, 3H), 0.89 (t, J = 7.9 Hz, 9H), 0.81 (t, J = 7.4 Hz, 3H), 0.54 (q, J = 7.9 Hz, 6H); ^{13}C NMR (CDCl$_3$, 100 MHz) δ 199.4, 137.6, 136.4, 128.4 (2), 77.8, 75.8, 46.9, 36.6, 27.6, 18.4, 16.6, 13.2, 11.3, 10.6, 7.0, 4.9; HRMS (ESI-TOF) m/z: [M + Na]$^+$ Calcd for C$_{28}$H$_{56}$NO$_3$Si$_2$Na 519.3660, Found 519.3674.

(5*R*,8*S*,9*R*,*E*)-5,9-dihydroxy-6,8-dimethylundeca-1,6-dien-3-one (**S6**).
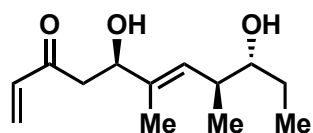
Disilylether **S5** (10.9 mg, 0.220 mmol) was transferred to a small polypropylene tube (15 mL, BD Falcon™) and cooled via ice-water bath (0 °C). The diol was dissolved in acetonitrile (1 mL) and to the resulting clear solution was added a solution of 48% hydrofluoric acid in acetonitrile (11:89, 3.2 mL). The reaction mixture was placed in a refrigerator (4 °C) for 19 h and quenched via addition of an aqueous, saturated sodium bicarbonate solution until the mixture was neutralized (pH = 7). Extraction of the reaction mixture with ethyl acetate (4 x 15 mL), drying over anhydrous sodium sulfate, filtration and concentration under vacuum gave a crude product residue. Purification via flash column chromatography (50% EtoAc/hexanes) provided the desired diol as a cloudy, colorless oil (4.97 mg, 0.220 mmol, quant.). R_f = 0.33 (50% EtOAc/hexanes); $[\alpha]_D^{21}$ = 25.6 (*c* 0.87, CHCl₃); ¹H NMR (400 MHz) δ 6.37 (dd, *J* = 17.6, 10.4 Hz, 1H), 6.26 (d, *J* = 17.6 Hz, 1H), 5.90 (d, *J* = 10.4 Hz, 1H), 5.37 (d, *J* = 10.0 Hz, 1H), 4.53 (dd, *J* = 8.4, 4.0 Hz, 1H), 3.34–3.27 (m, 1H), 2.88 (dd, *J* = 8.4, 16.8 Hz, 1H), 2.80 (dd, *J* = 16.8, 4.4 Hz, 1H) 2.52 – 2.38 (m, 1H), 1.69 (s, 3H), 1.61–1.51 (m, 1H), 1.43– 1.31(m, 1H), 0.97 (d, *J* = 6.8 Hz, 3H), 0.97 (t, *J* = 7.6 Hz, 3H); ¹³C NMR (CDCl₃, 100 MHz) δ 200.8, 137.4, 136.8, 129.5, 129.0, 77.1, 73.2, 44.7, 38.1, 27.2, 17.2, 12.6, 10.2; HRMS (ESI-TOF) *m/z*: [M + Na]⁺ Calcd for $C_{13}H_{22}O_3Na$ 249.1461, Found 249.1463.

N-(2-(((5*R*,8*S*,9*R*,*E*)-5,9-dihydroxy-6,8-dimethyl-3-oxoundec-6-en-1-yl)thio)ethyl)acetamide (**7a**).
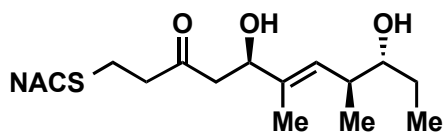
To a small round bottom flask containing vinyl ketone **S6** (26.0 mg, 0.115 mmol) in anhydrous tetrahydrofuran (9 mL) under argon atmosphere was added *N*-acetylcysteamine

(14.6 μL, 0.138 mmol, 1.20 equiv.). A catalytic amount of cesium carbonate was added to the reaction mixture and the solution was stirred at ambient temperature for 11 h. The reaction was concentrated under vacuum and purified via silica flash column chromatography (10% MeOH/dichloromethane, 1 cm plug of Cu(II)SO$_4$-silica on top) yielding the title compound as a colorless, cloudy oil (21.4 mg, 0.0620 mmol, 54%). R_f = 0.46 (10% MeOH/dichloromethane); $[\alpha]_D^{22}$ = 5.9 (c 0.59, CHCl$_3$); ^{1}H NMR (400 MHz) δ 6.17 (s, 1H), 5.36 (d, J = 10.0 Hz, 1H), 4.48 (dd, J = 8.1, 3.5 Hz, 1H), 3.43 (q, J = 6.3 Hz, 2H), 3.33–3.26 (m, 1H), 2.87 (br, 1H), 2.80 – 2.74 (m, 4H), 2.74 – 2.58 (m, 4H), 2.49 – 2.38 (m, 1H), 1.99 (s, 3H), 1.81 (s, 1H), 1.65 (s, 3H), 1.61– 1.50 (m, 1H), 1.36 (dq, J = 14.1, 7.4 Hz, 1H), 0.96 (d, J = 7.4 Hz, 3H), 0.95 (t, J = 7.7 Hz, 3H); ^{13}C NMR (CDCl$_3$, 100 MHz) δ 209.1, 170.5, 137.4, 128.9, 77.4, 73.2, 48.4, 43.6, 38.7, 38.0, 32.2, 27.3, 25.2, 23.4, 17.3, 12.6, 10.2; HRMS (ESI-TOF) m/z: [M + Na]$^+$ Calcd for C$_{17}$H$_{31}$NO$_4$SNa 368.1866, Found 368.1873.

(R)-3-((4R,5R,E)-5-hydroxy-2,4-dimethylhept-2-enoyl)-4-isopropyloxazolidin-2-one (**S7**).
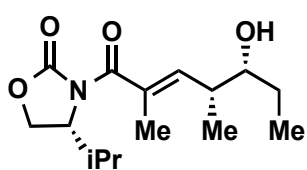
This procedure is adapted from that of Hosokawa and coworkers.[24] To a reaction vessel containing ent-**11**[25] (0.720 g, 2.12 mmol, 1.50 equiv.) in anhydrous dichloromethane (42 mL) under argon atmosphere was added freshly distilled propionaldehyde[22] (0.102 mL, 1.41 mmol, 1.00 equiv.). The resulting solution was cooled to -78 °C (acetone-dry ice). Titanium(IV) chloride (0.621 mL, 5.65 mmol, 4.00 equiv.) was added, in one portion, to the chilled solution. The reaction mixture immediately developed a dark blue hue. The reaction was stirred at -78 °C for 17 h and quenched via addition saturated aqueous sodium bicarbonate solution (10 mL) and saturated aqueous potassium sodium tartrate (10 mL). The biphasic solution was warmed to ambient temperature, separated and the aqueous layer was extracted with dichloromethane (3 x 20 mL). The combined organic layers

were dried over anhydrous sodium sulfate, filtered and concentrated under vacuum. Purification

via flash column chromatography (30% EtOAc/hexanes) furnished aldol adduct **S7** as a

colorless, clear oil (0.344 g, 1.21 mmol, 86%). R_f = 0.26 (30% EtOAc/hexanes); $[\alpha]_D^{22}$ = -65.2 (*c*

1.00, CHCl$_3$); ^{1}H NMR (400 MHz) δ 5.92 (d, *J* = 10.8 Hz, 1H), 4.56 (dt, *J* = 9.6, 5.0 Hz, 1H),

4.33 (t, *J* = 9.0 Hz, 1H), 4.18 (dd, *J* = 8.9, 5.6 Hz, 1H), 3.55 (dt, *J* = 8.8, 4.2 Hz, 1H), 2.76 – 2.64

(m, 1H), 2.40 – 2.27 (m, 1H), 1.94 (d, *J* = 1.3 Hz, 3H), 1.63–1.51 (m, 1H), 1.45 – 1.31 (m, 1H),

1.03 (d, *J* = 6.8 Hz, 3H), 0.98 (t, *J* = 7.3 Hz, 3H), 0.93 (d, 5.5 Hz, 3H), 0.91 (d, 5.7 Hz, 3H); ^{13}C

NMR (CDCl$_3$, 100 MHz) δ 171.9, 154.3, 142.5, 130.6, 77.4, 63.6, 58.3, 38.6, 28.5, 26.5, 18.0,

15.3, 14.3, 13.9, 10.8; HRMS (ESI-TOF) *m/z*: [M + Na]$^+$ Calcd for C$_{15}$H$_{25}$NO$_4$Na 306.1678,

Found 306.1680.

(S)-3-((4S,5S,E)-5-hydroxy-2,4-dimethylhept-2-enoyl)-4-isopropyloxazolidin-2-one (**ent-S7**).

The title compound was synthesized in an analogous matter to its enantiomer and was identical

with respect to ^{1}H-NMR and ^{13}C-NMR spectra. $[\alpha]_D^{22}$ = 66.0 (*c* 1.00, CHCl$_3$); HRMS (ESI-TOF)

m/z: [M + Na]$^+$ Calcd for C$_{15}$H$_{25}$NO$_4$Na 306.1678, Found 306.1682.

(*R*)-3-((4*R*,5*R*,E)-2,4-dimethyl-5-((triisopropylsilyl)oxy)-hept-2-enoyl)-4-isopropyloxazolidin-2-

one (**S8**).
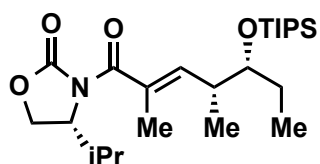
To a reaction flask containing aldol adduct **S7** (0.260 g, 0.918 mmol)

in anhydrous dichloromethane (10 mL) under argon atmosphere in

ice-water bath (0 °C) was added diisopropylethylamine (0.192 mL,

1.10 mmol, 1.20 equiv.) followed by triisopropylsilyl trifluoromethanesulfonate (0.296 mL, 1.10

mmol, 1.20 equiv.). The reaction was stirred at 0 °C for 19 h and quenched upon addition of an

aqueous, saturated sodium bicarbonate solution (5 mL). The biphasic mixture was allowed to warm to ambient temperature and separated. The aqueous layer was extracted with dichloromethane (3x 20 mL) and the combined organic fractions were dried over anhydrous sodium sulfate, filtered and concentrated under vacuum. The crude residue was purified by flash column chromatography on silica gel (10% EtOAc/hexanes) affording the desired silyl ether as a colorless oil (0.373 mg, 0.848 mmol, 92%). R_f = 0.32 (10% EtOAc/hexanes); $[\alpha]_D^{22}$ = -42.6 (c 1.00, CHCl$_3$); ^{1}H NMR (400 MHz) δ 6.04 (dd, J = 10.0, 1.4 Hz, 1H), 4.53 – 4.43 (m, 1H), 4.30 (t, J = 8.8 Hz, 1H), 4.17 (dd, J = 8.9, 5.4 Hz, 1H), 3.75 (q, J = 5.2 Hz, 1H), 2.72 – 2.59 (m, 1H), 2.46–2.34 (m, 1H), 1.92 (d, J = 1.4 Hz, 3H), 1.66 – 1.54 (m, 2H), 1.07 (s, 21H), 1.01 (d, J = 6.8 Hz, 3H), 0.92 (d, J = 7.2 Hz, 3H), 0.90 (d, J = 7.0 Hz, 3H), 0.88 (t, 7.5 Hz, 3H); ^{13}C NMR (CDCl$_3$, 100 MHz) δ 172.2, 153.7, 142.3, 129.7, 76.2, 63.5, 58.6, 36.7, 28.3, 28.0, 18.4, 18.1, 15.1, 14.1, 13.8, 13.1, 9.1; HRMS (ESI-TOF) m/z: [M + Na]$^+$ Calcd for C$_{24}$H$_{45}$NO$_4$SiNa 462.3010, Found 462.2986.

(S)-3-((4S,5S,E)-2,4-dimethyl-5-((triisopropylsilyl)oxy)hept-2-enoyl)-4-isopropyloxa-zolidin-2-one (**ent-S8**).

The title compound was synthesized in an analogous matter to its enantiomer and was identical with respect to ^{1}H-NMR and ^{13}C-NMR spectra. $[\alpha]_D^{22}$ = 45.1 (c 1.00, CHCl$_3$); HRMS (ESI-TOF) m/z: [M + Na]$^+$ Calcd for C$_{24}$H$_{45}$NO$_4$SiNa 462.3010, Found 462.3017.

(4*R*,5*R*,*E*)-2,4-dimethyl-5-((triisopropylsilyl)oxy)hept-2-enal (**S9**).
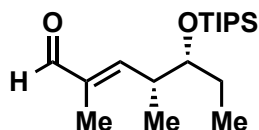
A round bottom flask containing acyl oxazolidinone **S8** (0.373 g, 0.848 mmol) dissolved in anhydrous dichloromethane (27 mL) under argon atmosphere was cooled to – 78 °C (dry ice-acetone). To the chilled reaction mixture was added a toluene solution of diisobutylaluminum hydride (1.49 M, 1.14 mL, 1.70 mmol, 2 equiv.) dropwise over two minutes. The reaction mixture was stirred at – 78 °C for 13 min and quenched upon sequential addition of methanol (10 mL) and saturated, aqueous potassium sodium tartrate solution (10 mL). The biphasic solution was allowed to warm to ambient temperature and separated. The aqueous layer was extracted with dichloromethane (3 x 15 mL) and the combined organic fractions were dried over anhydrous sodium sulfate, filtered and concentrated under vacuum. The crude product was purified via flash column chromatography (10% EtOAc/hexanes) to provide the aldehyde **S9** as a clear and colorless oil (0.229 g, 0.733 mmol, 86%). R_f = 0.56 (10% EtOAc/hexanes); $[\alpha]_D^{22}$ = -17.7 (*c* 1.00, CHCl$_3$); ^{1}H NMR (400 MHz) δ 9.39 (s, 1H), 6.55 (d, *J* = 9.8 Hz, 1H), 3.79 (dt, *J* = 8.1, 4.4 Hz, 1H), 2.93 – 2.78 (m, 1H), 1.76 (s, 3H), 1.72 – 1.49 (m, 2H), 1.10–1.04 (s, 24H), 0.89 (t, *J* = 7.5 Hz, 3H); ^{13}C NMR (CDCl$_3$, 100 MHz) δ 195.8, 158.7, 137.9, 76.4, 37.3, 27.9, 18.4, 13.6, 13.1, 9.52, 9.46; HRMS (ESI-TOF) *m/z*: [M + Na]$^+$ Calcd for C$_{18}$H$_{36}$O$_2$SiNa 335.2377, Found 335.2396.

(4*S*,5*S*,*E*)-2,4-dimethyl-5-((triisopropylsilyl)oxy)hept-2-enal (***ent*-S9**).

The title compound was synthesized in an analogous matter to its enantiomer and was identical with respect to ^{1}H-NMR and ^{13}C-NMR spectra. $[\alpha]_D^{23}$ = 18.5 (*c* 1.00, CHCl$_3$); HRMS (ESI-TOF) *m/z*: [M + Na]$^+$ Calcd for C$_{18}$H$_{36}$O$_2$SiNa 335.2377, Found 335.2375.

(3*S*,6*R*,7*R*,*E*)-3-hydroxy-1-((*R*)-4-isopropyl-2-thioxo-thiazolidin-3-yl)-4,6-dimethyl-7-((triisopropylsilyl)-oxy)non-4-en-1-one (**S10**).
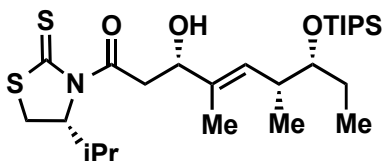
A reaction vessel containing acyl thiazolidinethione **16** (0.126 g, 0.620 mmol, 1.70 equiv.) in anhydrous dichloromethane (2.3 mL) under argon atmosphere was cooled to -40 °C (dry ice-acetonitrile bath). The equilibrated solution was supplemented by titanium(IV) chloride (72.0 μL, 0.657 mmol, 1.80 equiv.) and stirred for 30 min. To the reaction was slowly added freshly distilled diisopropylethylamine[22] (0.114 mL, 0.657 mmol, 1.80 equiv.). The blood red reaction mixture was stirred for 2 h and transferred to dry ice-acetone bath (-78 °C). A dichloromethane (1.3 mL) solution of aldehyde **S9** (0.114 g, 0.365 mmol, 1.00 equiv.) was slowly added to the cooled solution over 12 min. After stirring for 4 h at -78 °C the reaction was quenched via addition of ammonium chloride (5 mL). The biphasic mixture was warmed to ambient temperature and separated. The aqueous layer was extracted with dichloromethane (3 x 10 mL). Combined organic layers were dried over anhydrous sodium sulfate, filtered and concentrated under vacuum. The resulting crude oil was purified via flash chromatography (20% EtOAc/hexanes) to give both the aldol adduct **S10** as a thick, bright yellow oil (99.3 mg, 0.192 mmol, 53%) and the dehydration product **S11** as a viscous, yellow oil (44.4 mg, 0.0893 mmol, 24%). For **S10**: $R_f =$ 0.25 (20% EtOAc/hexanes); $[\alpha]_D^{22} = -189.2$ (*c* 1.00, CHCl₃); ¹H NMR (400 MHz) δ 5.49 (d, *J* = 9.6 Hz, 1H), 5.16 (t, *J* = 7.0 Hz, 1H), 4.56 (d, *J* = 9.3 Hz, 1H), 3.65 (dt, *J* = 6.6, 4.7 Hz, 1H), 3.53 (dd, *J* = 7.7, 3.7 Hz, 1H), 3.51–3.47 (m, 1H), 3.40 (dd, *J* = 17.4, 9.6 Hz, 1H), 3.03 (d, *J* = 11.5 Hz, 1H), 2.60–2.48 (m, 2H), 2.38 (app. sextet, *J* = 6.7 Hz, 1H), 1.67 (s, 3H), 1.61 – 1.46 (m, 2H), 1.09–1.03 (m, 24H), 0.99 (d, *J* = 7.0 Hz, 3H), 0.96 (d, *J* = 0.68 Hz, 3H), 0.86 (t, *J* = 7.4 Hz, 3H);

^{13}C NMR (CDCl$_3$, 100 MHz) δ 203.1, 173.1, 134.0, 131.4, 77.3, 73.6, 71.6, 44.2, 36.0, 31.0, 30.8, 27.8, 19.2, 18.5, 18.0, 15.2, 13.2, 12.2, 9.4; HRMS (ESI-TOF) *m/z*: [M + Na]$^+$ Calcd for C$_{26}$H$_{49}$NO$_3$S$_2$SiNa 538.2815, Found 538.2841.

(2*E*,4*E*,6*R*,7*R*)-1-((*R*)-4-isopropyl-2-thioxothiazolidin-3-yl)-4,6-dimethyl-7-((triisopropylsilyl)oxy)nona-2,4-dien-1-one (**S11**).
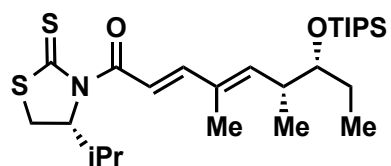
For **S11**: R_f = 0.70 (20% EtOAc/hexanes); $[\alpha]_D^{22}$ = -207.8 (*c* 0.23, CHCl$_3$); ^{1}H NMR (400 MHz) δ 7.37 (d, *J* = 15.2 Hz, 1H), 7.32 (d, *J* = 15.3 Hz, 1H), 5.97 (d, *J* = 9.9 Hz, 1H), 5.07 (ddd, *J* = 8.2, 5.6, 2.6 Hz, 1H), 3.72 (dt, *J* = 6.9, 4.6 Hz, 1H), 3.50 (dd, *J* = 11.4, 8.1 Hz, 1H), 3.09 (dd, *J* = 11.4, 2.6 Hz, 1H), 2.74 – 2.64 (m, 1H), 2.54 – 2.41 (m, 1H), 1.82 (d, *J* = 1.1 Hz, 3H), 1.64 – 1.47 (m, 2H), 1.09–1.03 (m, 24H), 1.00 (d, *J* = 6.9 Hz, 6H), 0.86 (t, *J* = 7.5 Hz, 3H); ^{13}C NMR (CDCl$_3$, 100 MHz) δ 202.6, 167.5, 150.4, 147.3, 132.5, 118.1, 72.4, 37.4, 30.9, 30.7, 28.0, 19.2, 18.5, 18.4, 17.4, 14.8, 13.2, 12.7, 9.3; HRMS (ESI-TOF) *m/z*: [M + Na]$^+$ Calcd for C$_{26}$H$_{47}$NO$_2$S$_2$SiNa 520.2710, Found 520.2713.

S-(2-acetamidoethyl) (3*S*,6*R*,7*R*,*E*)-3-hydroxy-4,6-di-methyl-7-((triisopropylsilyl)oxy)non-4-enethioate (**S12**).
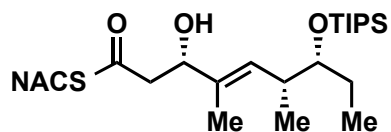
To a small round bottom flask containing acyl thiazolidinethione **S10** (50.5 mg, 0.0979 mmol) under argon atmosphere was added anhydrous dichloromethane (3 mL). A super-stoichiometric amount of imidazole (20.0 mg, 0.294 mmol, 3.00 equiv.) was added to the rapidly stirred, yellow mixture at ambient temperature. A slight excess of *N*-acetylcysteamine (11.5 μL, 0.108 mmol, 1.10 equiv.) was added to the reaction solution. After stirring for 13.5 hr at ambient temperature, the mixture was concentrated under vacuum and purified by flash column chromatography (5% MeOH/dichloromethane, 1 cm thick CuSO$_4$-SiO$_2$) affording the desired thioester as a clear, colorless wax (32.3 mg, 0.682 mmol, 70%). R_f = 0.30 (5% MeOH/dichloromethane); $[\alpha]_D^{23}$ = -2.5 (*c* 1.00, CHCl$_3$); ^{1}H NMR (400 MHz) δ 5.80 (br, 1H), 5.48 (d, *J* = 9.6 Hz, 1H), 4.48 (dd, *J* = 9.4, 3.0 Hz, 1H), 3.64 (dt, *J* = 6.8, 4.7 Hz, 1H), 3.46 (app. dq, *J* = 6.6, 1.8 Hz, 1H), 3.06 (q, *J* = 6.3 Hz, 1H), 2.84 (dd, *J* = 15.0, 9.5 Hz, 1H), 2.70 (dd, *J* = 15.0, 3.2 Hz, 1H), 2.56–2.46 (m, 1H), 1.97 (s, 3H), 1.65 (d, *J* = 1.2 Hz, 3H), 1.62–1.41 (m, 2H), 1.06 (s, 21H), 0.95 (d, *J* = 6.8 Hz, 3H), 0.85 (t, *J* = 7.4 Hz, 3H); ^{13}C NMR (CDCl$_3$, 100 MHz) δ 199.2, 170.5, 133.8, 131.7, 77.4, 74.5, 49.7, 39.6, 36.0, 29.0, 27.8, 23.4, 18.5, 15.2, 13.2, 12.0, 9.3; HRMS (ESI-TOF) *m/z*: [M + Na]$^+$ Calcd for C$_{24}$H$_{47}$NO$_4$SSiNa 496.2887, Found 496.2887.

S-(2-acetamidoethyl) (3*S*,6*R*,7*R*,*E*)-3,7-dihydroxy-4,6-dimethylnon-4-enethioate (**6c**).
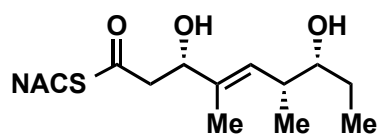
A polypropylene tube (15.0 mL, BD Falcon^{TM}) containing silylether **S12** (32.3 mg, 0.682 mmol) dissolved in acetonitrile (3.40 mL) was placed in ice-water bath (0 °C) and allowed to

equilibrate. To the chilled reaction vessel was added a solution of 48% hydrofluoric acid in acetonitrile (11:89, 8.9 mL). The reaction mixture was transferred to a refrigerator (4 °C) for 48 h and quenched at 0 °C via neutralization by saturated aqueous sodium bicarbonate solution. The resulting mixture was extracted with ethyl acetate (4 x 25 mL). The combined organic layers were dried over anhydrous sodium sulfate, filtered and concentrated under vacuum. The crude product residue was purified via silica flash column chromatography (10% MeOH/dichloromethane) furnishing the title compound as a clear, colorless oil (20.2 mg, 0.0630 mmol, 93%). R_f = 0.26 (10% MeOH/dichloromethane); $[\alpha]_{365}^{22}$ = 5.0 (c 1.47, CHCl$_3$); ^{1}H NMR (400 MHz) δ 6.23 (br, 1H), 5.35 (d, J = 9.7 Hz, 1H), 4.45 (dd, J = 7.8, 4.8 Hz, 1H), 3.41 (app. hept, J = 7.5 Hz, 2H), 3.34–3.28 (m, 1H), 3.08–2.95 (m, 2H), 2.82 (d, J = 8.2 Hz, 1H), 2.75 (d, J = 4.7 Hz, 1H), (dq, J = 12.8, 6.4 Hz, 1H), 1.95 (s, 3H), 1.65 (s, 3H), 1.56–1.43 (m, 1H), 1.35–1.22 (m, 1H), 0.96 (d, J = 6.8 Hz, 3H), 0.92 (t, 7.4 Hz, 3H); ^{13}C NMR (CDCl$_3$, 100 MHz) δ 198.7, 170.8, 135.7, 129.8, 77.2, 74.1, 49.8, 39.4, 37.8, 29.0, 27.1, 23.3, 15.7, 12.4, 10.6; HRMS (ESI-TOF) m/z: [M + Na]$^+$ Calcd for C$_{15}$H$_{27}$NO$_4$SNa 340.1553, Found 340.1547.

S-(2-acetamidoethyl) (2*E*,4*E*,6*R*,7*R*)-4,6-dimethyl-7-((triisopropylsilyl)oxy)nona-2,4-dienethioate (**S13**).
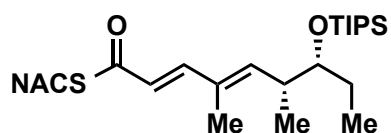
To a round bottom flask containing acyl thiazolidinethione **S11** (44.2 mg, 0.0889 mmol) under argon atmosphere was added anhydrous dichloromethane (3 mL). To the resulting clear solution was added 4-(dimethylamino)pyridine (32.6 mg, 0.267 mmol, 3.00 equiv.) followed by *N*-acetylcysteamine (10.4 µL, 0.098 mmol, 1.10 equiv.). The resulting mixture was stirred for 10 hr at ambient temperature and concentrated under vacuum. Purification of the crude residue via flash column chromatography (5% MeOH/dichloromethane) yielded the desired dienethiolate as a colorless

wax (23.1 mg, 0.0507 mmol, 57%). R_f = 0.38 (5% MeOH/dichloromethane); $[\alpha]_D^{23}$= 7.6 (c 1.00, CHCl$_3$); ^{1}H NMR (400 MHz) δ 7.25 (d, J = 15.3 Hz, 1H), 6.10 (d, J = 15.4 Hz, 1H), 6.01 (d, J = 9.8 Hz, 1H), 5.94 (br, 1H), 3.72 (dt, J = 7.0, 4.6 Hz, 1H), 3.48 (app. q, J = 5.9 Hz, 2H), 3.12 (t, J = 6.3 Hz, 2H), 2.76–2.65 (m, 1H), 1.96 (s, 3H), 1.79 (s, 3H), 1.66 –1.46 (m, 2H), 1.08–1.04 (m, 21H), 1.01 (d, J = 6.8 Hz, 3H), 0.87 (t, J = 7.5 Hz, 3H); ^{13}C NMR (CDCl$_3$, 100 MHz) δ 190.7, 170.4, 148.9, 146.9, 131.4, 122.6, 40.2, 37.5, 28.5, 27.9, 23.4, 18.42, 18.37, 14.7, 13.1, 12.4, 9.3; HRMS (ESI-TOF) m/z: [M + Na]$^+$ Calcd for C$_{24}$H$_{45}$NO$_3$SSiNa 478.2781, Found 478.2780.

S-(2-acetamidoethyl) (2*E*,4*E*,6*R*,7*R*)-7-hydroxy-4,6-dimethylnona-2,4-dienethioate (**S14**).
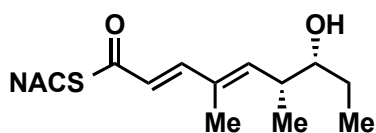
A polypropylene tube (15.0 mL, BD Falcon^{TM}) containing silylether **S13** (18.0 mg, 0.0395) dissolved in acetonitrile (4.15 mL) was equilibrated in ice-water bath (0 °C). To the chilled starting material was added a solution 48% hydrofluoric acid in acetonitrile (11:89, 5.0 mL). The resulting acidified solution was stored at 4 °C for 48 h and quenched via addition of sodium sulfate at 0 °C. The reaction mixture was extracted with ethyl acetate (4 x 15 mL) and the combined organics were dried over anhydrous sodium sulfate. Filtration and concentration under vacuum gave the crude product residue that was purified by flash column chromatography (5% MeOH/dichloromethane) providing the desired alcohol as a cloudy, colorless oil (Scheme 3.1) (8.1 mg, 0.0271 mmol, 69%). R_f = 0.28 (5% MeOH/dichloromethane); $[\alpha]_D^{22}$= 37.5 (c 0.52, CHCl$_3$); ^{1}H NMR (400 MHz) δ 7.26 (d, J = 15.5 Hz, 1H), 6.12 (d, J = 15.5 Hz, 1H), 5.94 (s, 1H), 5.87 (d, J = 10.1 Hz, 1H), 3.47 (q, J = 6.0 Hz, 2H), 3.39 (ddd, J = 9.2, 6.5, 3.4 Hz, 1H), 3.11 (t, J = 6.3 Hz, 2H), 2.63 (dt, J = 10.1, 6.6 Hz, 1H), 1.96 (s, 3H), 1.81 (d, J = 0.9 Hz, 3H), 1.61–1.49 (m, 1H), 1.41–1.27 (m,

1H), 1.06 (d, J = 6.7 Hz, 3H), 0.95 (t, J = 7.4 Hz, 3H); ^{13}C NMR (CDCl$_3$, 100 MHz) δ 190.7, 170.4, 146.8, 146.6, 132.6, 123.1, 77.0, 40.1, 39.6, 28.5, 27.9, 23.4, 15.8, 12.6, 10.4; HRMS (ESI-TOF) m/z: [M + Na]$^+$ Calcd for C$_{15}$H$_{25}$NO$_3$SSiNa 332.1447, Found 322.1447. Upon literature analysis we discovered that this compound had been synthesized through a different route by Cane, DE and co-workers.[26] Our analytical data match that of the original report in all respects.
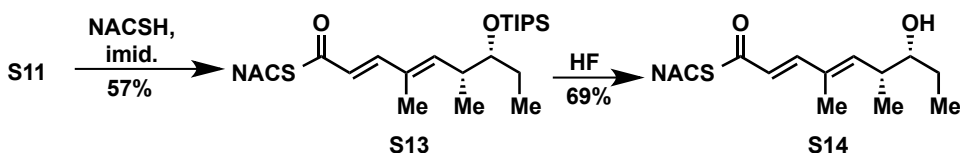
Scheme 3.1 Synthesis of dehydration product S14.

By utilizing the serendipitous byproduct **S11**, the result of dehydration during an aldol reaction, we were able to quickly produce the dehydration product **S14**. This dienethioate served as the product standard in LC-MS/MS for the enzymatic dehydration reaction of **27**. Additionally, the same compound was used as the product standard for TylDH3-catalyzed dehydration of **6d**, as it is the enantiomer of the presumed product.

(3S,6S,7S,E)-3-hydroxy-1-((R)-4-isopropyl-2-thioxo-thiazolidin-3-yl)-4,6-dimethyl-7-((triisopropylsilyl)-oxy)non-4-en-1-one (**S15**).
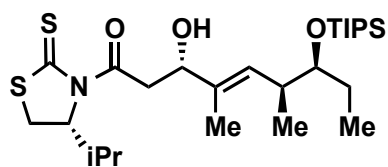
To a reaction flask containing acyl thiazolidinethione **15** (88.8 mg, 0.437 mmol, 1.70 equiv.) under argon atmosphere was added anhydrous dichloromethane (2.50 mL). The yellow solution was placed in dry ice-acetonitrile bath (- 40 °C) and allowed to equilibrate. To the chilled solution was added titanium(IV) chloride (50.7 μL, 0.463 mmol, 1.80 equiv.) and the resulting orange solution was stirred for 30 min. An aliquot of freshly distilled diisopropylethylamine[22] (80.6 μL, 0.463 mmol, 1.80 equiv.) was slowly added to the reaction mixture and the blood red solution was stirred for an additional 2 hr at - 40 °C. The reaction was transferred to a dry ice-acetone bath (-78 °C) and supplemented with a dichloromethane solution

(0.400 mL) of aldehyde *ent*-**S9** (80.3 mg, 0.257 mmol, 1.00 equiv.) in a dropwise fashion. The

resulting reaction mixture was stirred at -78 °C for 1 h 45 min and quenched upon addition of

aqueous saturated ammonium chloride (7.00 mL). The biphasic mixture was warmed to ambient

temperature and separated. The aqueous layer was extracted with dichloromethane (3 x 15 mL)

and the combined organic layers were dried over anhydrous sodium sulfate, filtered and

concentrated under vacuum. The crude product residue was purified by flash column

chromatography (20% EtOAc/hexanes) affording the aldol adduct **S15** (0.102 g, 0.198 mmol,

77%) as a bright yellow oil. $R_f = 0.38$ (20% EtOAc/hexanes); $[\alpha]_D^{22} = -199.5$ (*c* 1.00, CHCl$_3$); ^{1}H

NMR (400 MHz) δ 5.50 (d, *J* = 9.6 Hz, 1H), 5.15 (d, *J* = 6.8 Hz, 1H), 4.55 (dd, *J* = 9.4, 2.2 Hz,

1H), 3.68 (q, *J* = 4.8 Hz, 1H), 3.57–3.51 (m, 1H), 3.51–3.47 (m, 1H), 3.41 (dd, *J* = 17.4, 9.5 Hz,

1H), 3.03 (d, *J* = 11.5 Hz, 1H), 2.58–2.48 (m, 1H), 2.39 (app. sextet, *J* = 6.8 Hz, 1H), 1.67 (s,

3H), 1.61–1.49 (m, 2H), 1.10–1.03 (m, 24H), 0.99 (d, *J* = 6.9 Hz, 3H), 0.94 (d, *J* = 6.8 Hz, 3H),

0.86 (t, *J* = 7.4 Hz, 3H); ^{13}C NMR (CDCl$_3$, 100 MHz) δ 203.1, 173.0, 134.1, 131.1, 77.3, 73.2,

71.7, 44.3, 35.9, 31.0, 30.8, 27.9, 19.3, 18.4, 17.9, 15.1, 13.2, 12.7, 9.4; HRMS (ESI-TOF) *m/z*:

[M + Na]$^+$ Calcd for C$_{26}$H$_{49}$NO$_3$S$_2$SiNa 538.2815, Found 538.2830.

S-(2-acetamidoethyl) (3*S*,6*S*,7*S*,*E*)-3-hydroxy-4,6-dimethyl-7-((triisopropylsilyl)oxy)non-4-

enethioate (**S16**).
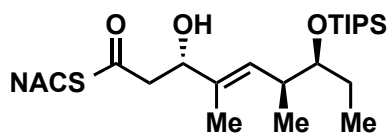
To a round bottom flask containing aldol adduct **S15** (42.0 mg,

0.0814 mmol) dissolved in anhydrous dichloromethane (3 mL)

under argon atmosphere was added imidazole (17.0 mg, 0.250,

3.07 equiv.). To the stirred reaction mixture was added *N*-acetylcysteamine (9.50 μL, 0.0893

mmol, 1.10 equiv.) and the resulting solution was stirred at ambient temperature for 7 h. The

reaction mixture was quenched upon addition of a saturated, aqueous ammonium chloride solution (5 mL) and the biphasic solution was separated. The aqueous layer was extracted with dichloromethane (4 x 15 mL) and the combined organic layers were dried over anhydrous sodium sulfate, filtered and concentrated under vacuum. Crude product residues were purified by flash column chromatography (5% MeOH/dichloromethane) providing the title compound as a clear, colorless oil (35.3 mg, 0.746 mmol, 92%). R_f = 0.23 (5% MeOH/dichloromethane); $[\alpha]_D^{22}$= -9.4 (*c* 1.00, CHCl$_3$); ^{1}H NMR (400 MHz) δ 5.85 (br, 1H), 5.48 (d, *J* = 9.6 Hz, 1H), 4.47 (dd, *J* = 9.0, 3.5 Hz, 1H), 3.76–3.60 (m, 1H), 3.45 (q, *J* = 6.2 Hz, 2H), 3.05 (dt, *J* = 5.3, 3.0 Hz, 2H), 2.82 (dd, *J* = 15.0, 9.0 Hz, 1H), 2.73 (dd, *J* = 15.0, 3.7 Hz, 1H), 2.58–2.44 (m, 1H), 1.97 (s, 3H), 1.65 (s, 3H), 1.60–1.46 (m, 2H), 1.06 (s, 21H), 0.92 (d, *J* = 6.8 Hz, 3H), 0.85 (t, *J* = 7.4 Hz, 3H); ^{13}C NMR (CDCl$_3$, 100 MHz) δ 199.1, 170.5, 133.9, 131.4, 77.4, 74.3, 49.8, 39.6, 35.9, 29.0, 27.8, 23.4, 18.4, 15.1, 13.2, 12.2, 9.3; HRMS (ESI-TOF) *m/z*: [M + Na]$^+$ Calcd for C$_{24}$H$_{47}$NO$_4$SSiNa 496.2887, Found 496.2881.

S-(2-acetamidoethyl) (3*S*,6*S*,7*S*,*E*)-3,7-dihydroxy-4,6-dimethylnon-4-enethioate (**6d**).
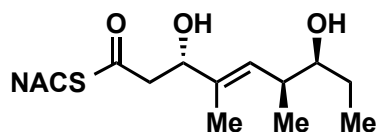
A large conical polypropylene tube (50 mL, BD Falcon^{TM}) containing silylether **S16** (35.3 mg, 0.0746 mmol) dissolved in acetonitrile (3.75 mL) was placed in ice-water (0 °C) bath and allowed to equilibrate. To the chilled reaction vessel was added a solution of 48% hydrofluoric acid diluted in acetonitrile (11:89, 5.52 mL). The resulting clear solution was stored at 4 °C for 23 h and neutralized via addition of an aqueous saturated sodium bicarbonate solution at 0 °C. The reaction mixture was extracted with ethyl acetate (4 x 15 mL) and the combined organic fractions were dried over anhydrous sodium sulfate, filtered and concentrated under vacuum. The

crude residue was purified via flash column chromatography (10% MeOH/dichloromethane) yielding the alcohol as a colorless oil (18.5 mg, 0.0583 mmol, 78%). $R_f = 0.38$ (10% MeOH/dichloromethane); $[\alpha]_D^{23} = -25.0$ (c 0.62, CHCl$_3$); ^{1}H NMR (400 MHz) δ 6.19 (br, 1H), 5.36 (d, $J = 9.7$ Hz, 1H), 4.46 (dd, $J = 8.2, 3.5$ Hz, 1H), 3.42 (q, $J = 6.1$ Hz, 2H), 3.38–3.29 (m, 1H), 3.09–2.95 (m, 2H), 2.83 (dd, $J = 14.8, 8.6$ Hz, 1H), 2.73 (dd, $J = 14.8, 3.8$ Hz, 1H), 2.48 (dq, $J = 13.3, 6.6$ Hz, 1H), 1.95 (s, 3H), 1.65 (s, 3H), 1.58–1.47 (m, 1H), 1.32 (dq, $J = 15.1, 7.8$ Hz, 1H), 0.94 (d, $J = 6.9$ Hz, 3H), 0.93 (t, $J = 7.2$ Hz, 3H); ^{13}C NMR (CDCl$_3$, 100 MHz) δ 198.8, 170.8, 135.8, 129.7, 77.3, 74.2, 49.6, 39.4, 37.8, 29.0, 26.9, 23.3, 15.8, 12.5, 10.7; HRMS (ESI-TOF) m/z: [M + Na]$^+$ Calcd for C$_{15}$H$_{27}$NO$_4$SNa 340.1553, Found 340.1556.

(±)-S-(2-acetamidoethyl) 3-hydroxypentanethioate ((±)-26).
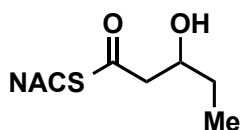
The details for the synthesis of racemic diketide substrate **26** are currently pending publication in a separate manuscript[21].

S-(2-acetamidoethyl) (2E,4E,6S,7R)-7-hydroxy-4,6-di-methylnona-2,4-dienethioate (8).
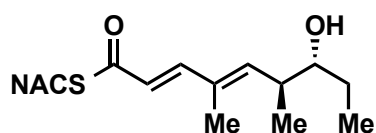
To a small polypropylene conical tube (15 mL) containing sterile deionized water (0.630 mL) was added a concentrated Tris buffer solution (0.500 M Tris-HCl, 1.50 M NaCl, pH 8.0, 0.500 mL). The clear solution was vortexed to mix and β-hydroxy thioester **6b** (3.17 mg, 0.0100 mmol) was added as a 50:50 DMSO-water stock solution (100 mM, 100 µL) and mixed by inversion. Heterologously expressed TylDH3KR3 (2.53 mg/mL stock solution, 1.52 mL, 3.85 mg, 50.3 nmol). The reaction mixture was capped and incubated at ambient temperature with shaking (250 rpm) for 26 h. The

aqueous solution was extracted with ethyl acetate (3 x 10 mL) followed by drying over anhydrous sodium sulfate, filtration and concentration under vacuum. The crude product residue was purified via flash column chromatography (5% MeOH/dichloromethane) affording a cloudy, colorless oil (2.00 mg, 0.00667 mmol, 67%). R_f = 0.32 (5% MeOH/dichloromethane); Due to stability issues, an optical rotation was not obtained; ^{1}H NMR (400 MHz, CDCl$_3$) δ 7.29 (d, J = 15.6 Hz, 1H), 6.12 (d, J = 15.5 Hz, 1H), 5.96 (d, J = 10.1 Hz, 1H), 5.91 (br, 1H), 3.52–3.39 (m, 3H), 3.12 (t, J = 6.3 Hz, 2H), 2.72–2.60 (m, 1H), 1.96 (s, 3H), 1.82 (s, 3H), 1.54–1.49 (m, 1H), 1.45–1.34 (m, 1H), 1.05 (d, J = 6.8 Hz, 3H), 0.96 (t, J = 7.4 Hz, 3H); ^{13}C NMR (CDCl$_3$, 100 MHz) δ 190.7, 170.4, 146.6, 146.0, 133.5, 123.1, 77.0, 40.2, 39.2, 28.5, 27.8, 23.4, 17.0, 12.7, 10.2; HRMS (ESI-TOF) m/z: [M + Na]$^+$ Calcd for C$_{15}$H$_{25}$NO$_3$SNa 322.1447, Found 322.1451.

N-(2-((((4E,6E,8S,9R)-9-hydroxy-6,8-dimethyl-3-oxoundeca-4,6-dien-1-yl)thio)ethyl)acetamide (**9**).
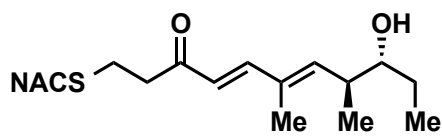
β-Hydroxy ketone **7b** (3.45 mg, 0.0100 mmol) was dehydrated in an analogous matter as the generation of dienethioate **8** resulting in dienone **9** (3.17 mg, 0.00969 mmol, 97%). R_f = 0.30 (5% MeOH/dichloromethane); Due to stability issues, an optical rotation was not obtained; ^{1}H NMR (400 MHz) δ 7.17 (d, J = 16.7 Hz, 1H), 6.05 (d, J = 15.9 Hz, 1H), 5.89 (d, J = 10.0 Hz, 1H), 3.43–3.35 (m, 3H), 2.87–2.80 (m, 2H), 2.80–2.74 (m, 3H), 2.66 – 2.54 (m, 3H), 1.94 (s, 3H), 1.76 (s, 3H), 1.52–1.42 (m, 1H), 1.40–1.28 (m, 1H), 0.99 (d, J = 6.8 Hz, 3H), 0.90 (t, J = 7.4 Hz, 3H); ^{13}C NMR (CDCl$_3$, 100 MHz) δ 198.8, 170.4, 148.7, 145.5, 133.9, 124.6, 77.0, 40.2, 39.2, 38.7, 32.3, 27.8, 26.1, 23.4, 17.1, 12.7, 10.2; HRMS (ESI-TOF) m/z: [M + Na]$^+$ Calcd for C$_{17}$H$_{29}$NO$_3$SNa 350.1760, Found 350.1762.

General biology procedures.

All chemical reagents were purchased from Sigma-Aldrich and were used directly without further purification. *E. coli* BL21–AI cells were from Life Technologies. IPTG was acquired through Gold Biotechnology. L-(+)-Arabinose (≥99%) was purchased through Sigma Aldrich. His60 Ni Superflow resin was purchased from Clontech Laboratories, Inc. OD_{600} was measured on an Eppendorf BioPhotometer. Sonication was carried out by Branson Sonifier 450. Gel filtration purification was performed on HiLoad 16/600 Superdex 200 pg column (GE). Protein mass spectrometry was carried out using an Agilent 6250 QTOF LC/MS. Kinetic LC–MS/MS was conducted with AB Sciex QTRAP 5500 mass spectrometer and Shimadzu LC system.

The TylKR3-DH3 didomain was ordered as codon-optimized synthetic DNA from Life Technologies. The synthetic DNA encoded the region 957-1682 from the tylactone synthase module 3 polypeptide. The insert was cloned into pMCSG7 using ligation independent cloning (LIC). TylKr3-DH3 synthetic forward primer: 5'-**TACTTCCAAT-CCAATGCCC**ATCCGCTGCTGAGCG-3'; TylKr3-DH3 synthetic reverse primer: 5'-**TTATCCACTTCCAATG<u>TTA</u>**GTTGGTATCTTCCGGTGTACCAGGCG-3' (LIC-overhangs in **bold**; inserted stop codon <u>underlined</u>). The insert was confirmed via sequencing.

Cloning and Expression of TylDH3-KR3 Construct

Initial efforts to recombinantly express the mono-domain TylKR3 were hampered by with poor expression levels and protein aggregation. Strategies to alleviate these issues included an increase of rare tRNA codons (Rosetta cell line), optimization of codon selection (synthetic TylKR3 gene), toxic protein-compatible expression hosts (pLysS cell line), appending a fusion protein (attempted with SUMO, mOCR, and GST), chaperone coexpression (GroEL-GroES) and

107

truncations of both N- and C-termini. Disappointingly, these techniques failed to improve expression of soluble non-aggregated TylKR3 and forced us to abandon the expression of the mono-domain construct.

The *tylGII* region encoding TylDH3-KR3 didomain comprising residues 957-1682 was cloned into a pMCSG7 vector and transformed into *E. coli* BL21-AI cells containing the pRARE plasmid. A large TB media culture (0.5 L in 2.8 L Fernbach flask) was inoculated with as small amount of overnight culture (5 mL) and incubated at 37 °C, shaking at 250 RPM until OD600 = 1.00–1.20. The culture was cooled to 20 °C and incubated with shaking (250 RPM) for 1 h. Cells were induced upon addition of IPTG (0.100 mM) and L-arabinose (1.00 g) and allowed to shake (250 RPM) at 20 °C for 19 h. The cell pellet was collected after centrifugation (4 °C, 5,000 x G, 30 min) and resuspended in lysis buffer (50 mM tricine, 50 mM ammonium sulfate, 100 mM urea, pH 8.5, 4 mL/g of pellet). The cells were lysed (3 x 2 min, 50% duty cycle, 40 % power, 4 °C) and centrifuged (4 °C, 28,600 x G, 45 min). The soluble protein was purified by sequential metal-immobilized affinity chromatography and size exclusion chromatography to afford approximately 9 mg of purified protein (18 mg / L) that was greater than 90% pure as judged by SDS-PAGE (Fig. 3.3) and to be near the predicted calculated mass by mass spectrometry (Fig. 3.4).
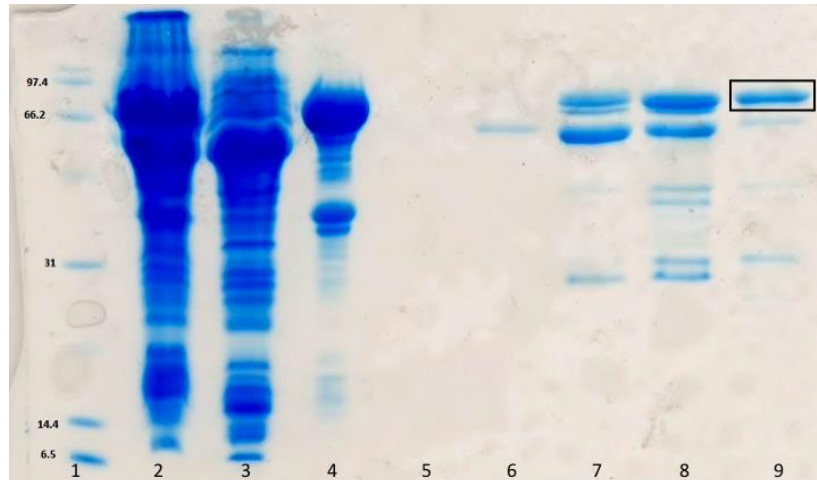
Figure 3.3 SDS-PAGE image of TylDH3-KR3 purification.

The ladder, cell lysate, insoluble pellet, soluble protein and serial nickel elution fractions are shown in lanes 1-9, respectively. The band corresponding to TylDH3-KR3 is boxed.
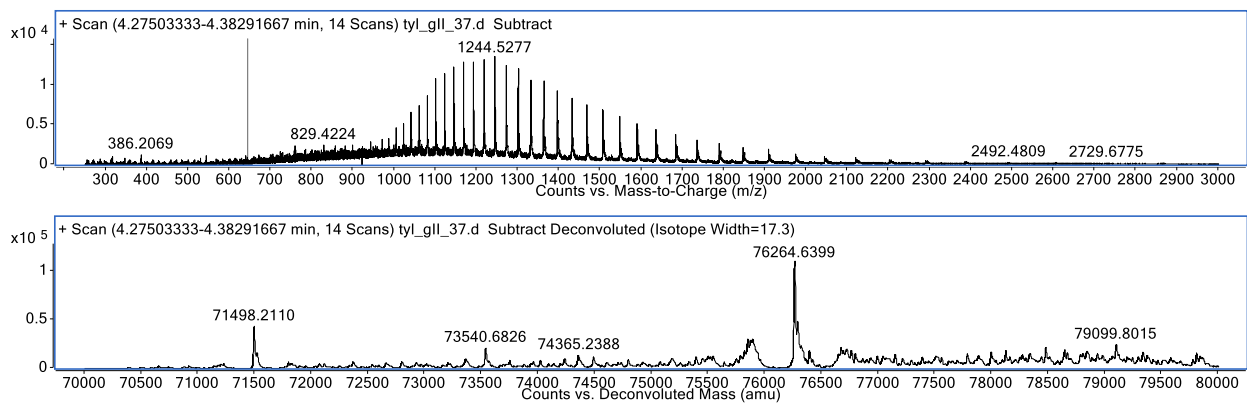
Figure 3.4 Mass spectrometry analysis of TylDH3-KR3.

The convoluted (raw) spectrum and deconvoluted are both displayed. TylDH3-KR3 was found to have a mass of 76,264 Da. The spectrum was obtained using 0.5 mg/mL of recombinant TylDH3-KR3 in 25% formic acid.

109

Determination of TylDH3-KR3 Ketoreductase Activity (Data generated by Will Fiers)

A small eppendorf tube (1.5 mL, 100 μL total volume) containing substrate **4** or **5** (1

mM), heterologously expressed TylDH3-KR3 (5 μM), NADPH (2 mM), Tris (50 mM), NaCl

(150 mM) at pH 8.0 was incubated at ambient temperature for 15 h. 60 μL of the diluted reaction

solution was added to a HPLC vial and analyzed by LC-MS/MS (Table 3.1) employing a Kinetix

reverse-phase C_{18} column (50 mm × 2.1 mm, 2.6 μm, Phenomenex) operated at 0.4 mL min^{-1}

with a gradient between mobile phase A (H_2O) and mobile phase B (MeCN). The gradient

program was 0 min, 5% B; 2 min, 5% B; 7 min, 55% B; 8 min, 70% B; 9 min, 70% B; 10.5 min,

5% B; 12 min, 5% B. Co-injection of standards **6a**, **6b**, and **8** for substrate **4** confirmed the

identity of product traces. The standards **7a**, **7b**, and **9** were used for the analysis of the

incubation of substrate **5**.

Table 3.1 LC-MS/MS analysis of analytes 6a, 6b, 8, 7a, 7b, and 9.

Analyte	HPLC retention time (min)	Transition
6a	5.19	340→184
6b	5.27	340→184
8	6.17	300→181
7a	5.24	368→212
7b	5.30	368→212
9	6.00	328→151

Analysis of TylDH3-KR3 Dehydratase Activity (Data generated by Will Fiers)

Steady-State Analysis.

The enzymatic reactions were carried out in a total volume of 50 µL under initial velocity conditions containing TylDH3-KR3 (1 µM), reaction buffer (50 mM Tris, 150 mM NaCl, pH 8.0) and substrates **6b** or **7b** at variable concentrations (0.5, 1, 2, 3, 4, 6, 8 mM). The final DMSO concentration was held constant at 4%. After incubation at 25 °C for 8 min (the reaction found to be linear up to 10 min), 5 µL of the reaction mixture was added to 495 µL of 1:1 MeCN–reaction buffer (100-fold dilution). The resulting solution was vortexed, centrifuged and analyzed by 60 µL of the diluted reaction solution was added to a HPLC vial with 10 µL of internal standard **3** (320 nM) and analyzed by LC-MS/MS (Table 3.1) employing a Kinetix reverse-phase C_{18} column (50 mm × 2.1 mm, 2.6 µm, Phenomenex) operated at 0.4 mL min^{-1} with a gradient between mobile phase A (H_2O) and mobile phase B (MeCN). The gradient program was 0 min, 5% B; 2 min, 5% B; 7 min, 55% B; 8 min, 70% B; 9 min, 70% B; 10.5 min, 5% B; 12 min, 5% B. Standard curves of enzymatic products **8** and **9** were generated by injecting the authentic standard at varying concentrations with a fixed concentration of an internal standard (**8** for the standard curve of **9** and **9** for the standard curve of **8**). The amount of enzymatic product formation at each time point was calculated by plotting the area ratio (analyte/internal standard) into the standard curve. Control reactions for each concentration of substrate were performed without the addition of enzyme. Each reaction was performed in duplicate. The specificity constants (K_M/k_{cat}) were determined by fitting the normalized v_0 vs [S] plots to linear equations (Fig. 3.5A, B).

Substrates **6c** and **6d** were analyzed in an analogous way using synthetic **S14** as the product

standard (Fig. 3.5C, D). The LC-MS/MS trace of **S14** is provided in Fig 3.6.
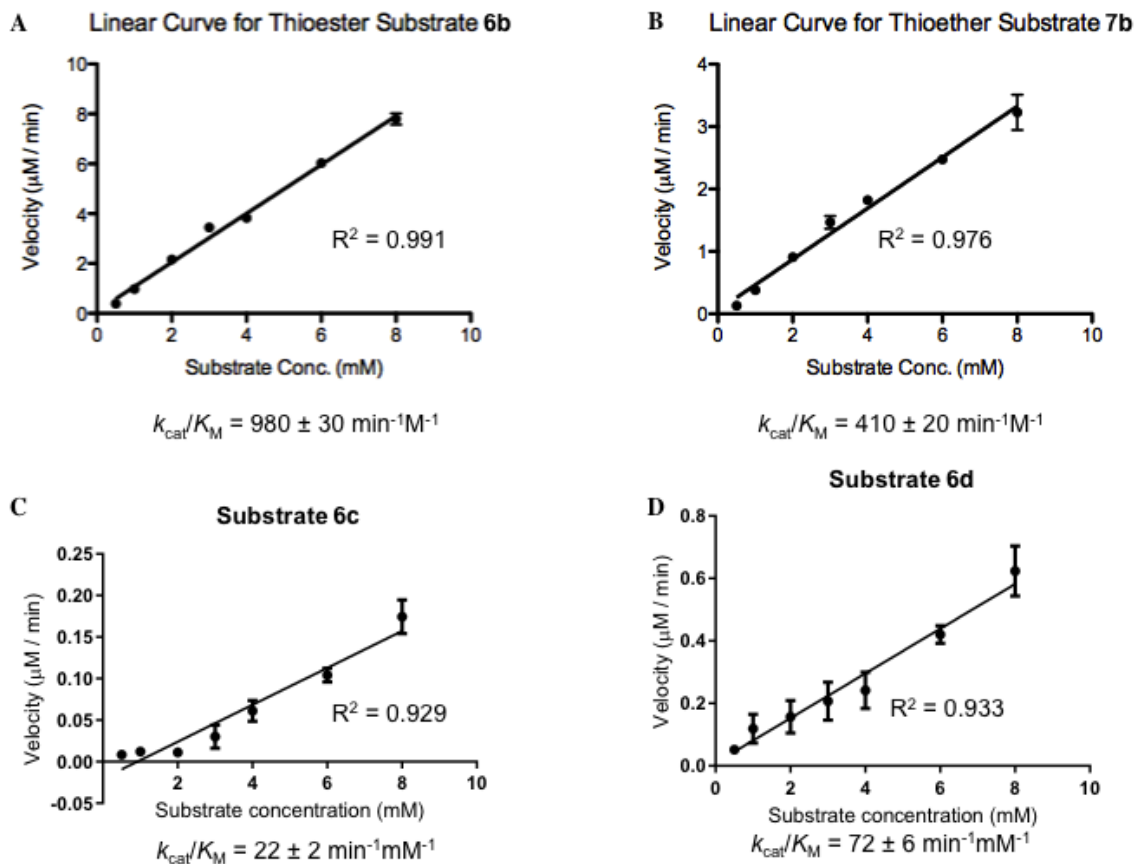
Figure 3.5 Linear regression analysis of TylDH3KR3 kinetic data with substrates 6b, 7b, 6c, and 6d.

The kinetic plots of thioester **6b**, thioether **7b**, thioester **6c** and thioester **6d** are shown in panels **A**, **B**, **C** and **D**, respectively. Represented data is the result of duplicate LC-MS/MS data normalized with controls lacking enzyme. Specificity constants (k_{cat}/K_M) for each substrate are displayed below the corresponding plot.
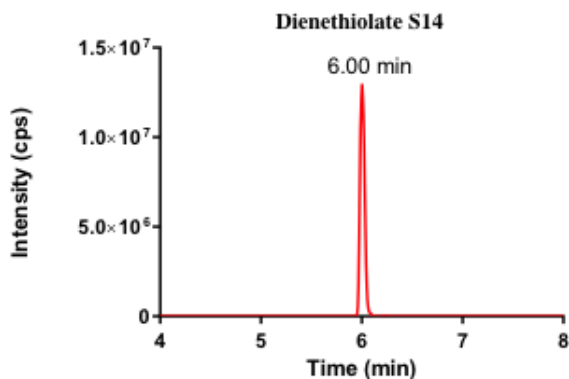
Figure 3.6 LC-MS/MS trace of dienethiolate S14.

The synthetic compound **S14** was used to confirm the identity of the dehydration products arising from thioesters **6c** and **6d**. A standard curve for quantitative determination of specificity constants was generated from the synthetic compound.

Results and discussion

Thioether substrate syntheses

The synthesis of tetraketide substrate mimic **7b** for TylDH3 began with known vinylketene silyl *N,O*-acetal **11**, obtained in two steps from commercially available *trans*-2-methyl-2-pentenoic acid **10** (Scheme 3.2). The vinylogous Mukaiyama aldol reaction of **11** with propionaldehyde set the two distal stereogenic centers with excellent yield and diastereoselectivity (92%, >98 : 2 dr), illustrating the power of Kobayashi's methodology for synthesis of this triketide building block[27]. The relative and absolute stereochemistry was confirmed by comparison of its NMR spectral data and optical rotation value to the reported enantiomer[23]. The vinylogous aldol adduct **12** was subsequently protected as the triisopropylsilyl (TIPS) ether **13** in quantitative yield and reductive removal of the oxazolidinone auxiliary with diisobutylaluminum hydride (DIBAL-H) provided aldehyde **14**.
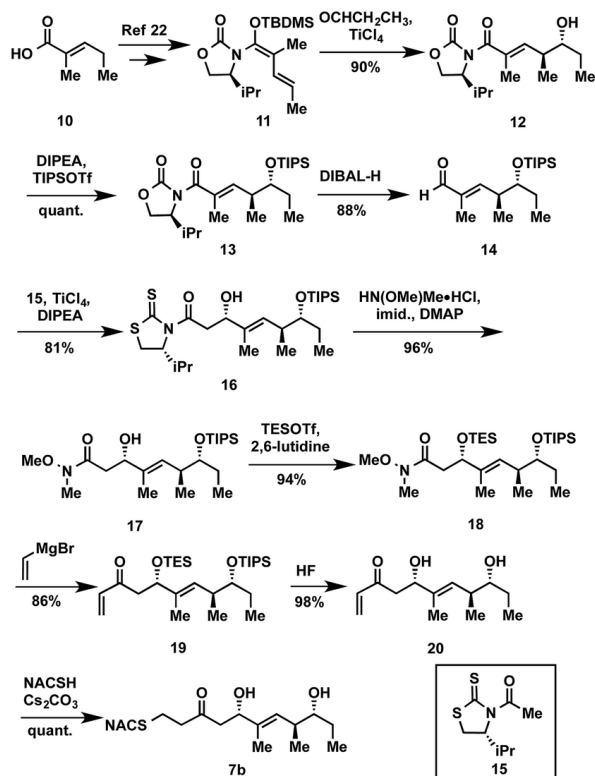
Scheme 3.2 Exemplary synthesis of thioether 7b.

With the enal **14** in hand, we were poised to set the unknown stereochemistry of the TylKR3 reduction product. Utilization of Nagao's *N*-acetylthiazolidinethione **15** under titanium-catalyzed conditions developed by Vilarrassa, Urpí and coworkers furnished the d-alcohol as the only detectable diastereomer in 81% yield[28-29]. The thiazolidinethione chiral auxiliary of **16** was displaced with methyl(methoxy)amine to afford the corresponding Weinreb amide **17**[30]. The newly formed β-hydroxyl group was protected as triethylsilyl (TES) ether **18**. Due to susceptibility to α,β-elimination, the strength of base was crucial, as tertiary amines (TEA, DIPEA) yielded exclusively the conjugated dienamide, whereas 2,6-lutidine afforded the desired TES ether. The precise order of this two-step sequence (**16 → 18**) was critical as reversal led to a sterically encumbered, hydroxyl-protected thiazolidine resistant to displacement. Grignard addition of vinylmagnesium bromide to Weinreb amide **18** provided **19** that was globally deprotected with HF to afford **20**. Regioselective Michael addition of *N*-acetylcysteamine (NAC) to the terminal enone of **20** produced TylDH3 substrate mimic **7b** containing a two-carbon spacer. The l-alcohol diastereomer **7a** was prepared in an analogous fashion from **14** employing the antipode of **15** (Schemes 3.3, 3.4).
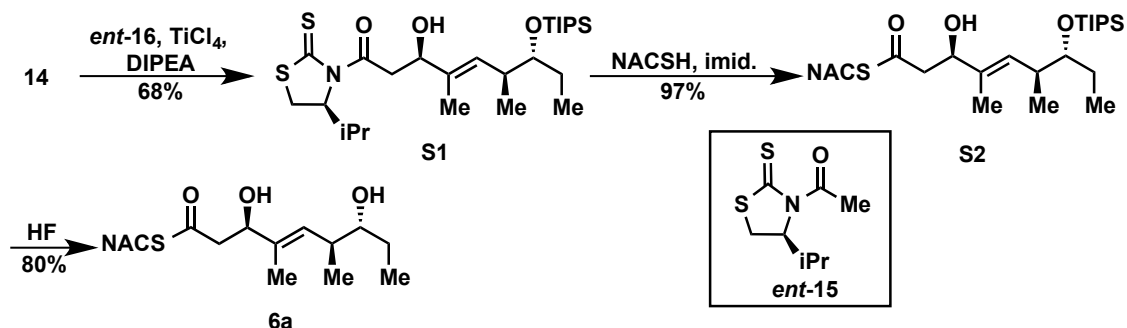
Scheme 3.3 Synthetic route towards L-alcohol substrate 6a.

An asymmetric aldol reaction between key aldehyde 14 and Nagao's chiral auxiliary *ent*-15 and displacement of the thiazoldinone with *N*-acetylcysteamine furnished thioester S2. Final deprotection with hydrogen fluoride afforded the desired diol substrate 6a.
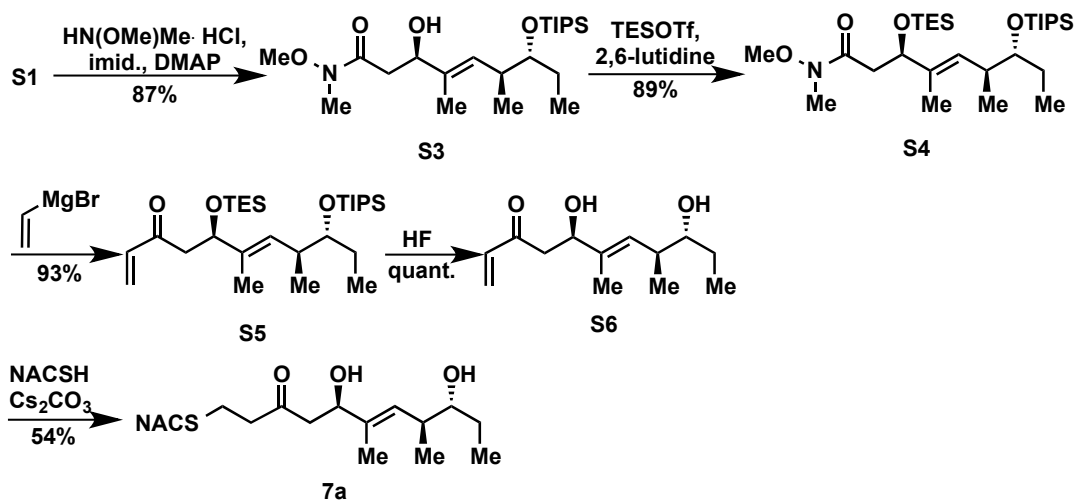
Scheme 3.4 Chemical synthesis of thioether substrate 7a.

Aldol adduct **S1** was sequentially converted to the corresponding weinreb amide (**S3**) followed by protection with triethylsilyl trifluoromethanesulfonate providing disilylether **S4**. Grignard addition and deprotection followed by Michael addition afforded thioether **7a**.

At the onset of the project we had planned to prepare the TylKR3 substrate mimic **5** from the corresponding TylDH3 substrate **7b** through regioselective oxidation of the allylic alcohol over the distal secondary alcohol. Unfortunately, **7b** and its precursor **20** proved recalcitrant to a variety of oxidants (MnO$_2$, BaMnO$_4$, Pd(OAc)$_2$/O$_2$, *etc.*), returning starting material or dehydration products under more forcing conditions[31-33]. In light of these results, we decided to chemoselectively remove the TES protecting group in **19** to provide **21** (Scheme 3.5A). A variety of common oxidants were then screened to affect the transformation of alcohol **21** to the desired β-diketone **22** including the Dess–Martin periodinane, TPAP/NMO, and SO$_3$•pyr. Surprisingly, most common reagents led to quick decomposition of the starting material or unwanted hetero-Michael additions to afford a tetrahydropyranone. A recently described β-hydroxyketone oxidation using iodoxybenzoic acid (IBX) as the oxidant was employed as a mild, neutral method[34]. This procedure afforded β-diketone **22** in near quantitative yields after simple filtration of the sparingly soluble oxidant from the products. Facile TIPS deprotection with aqueous HF provided **23**, which was reacted with NAC to afford TylKR3 substrate **5**.

Thioester product and substrate syntheses
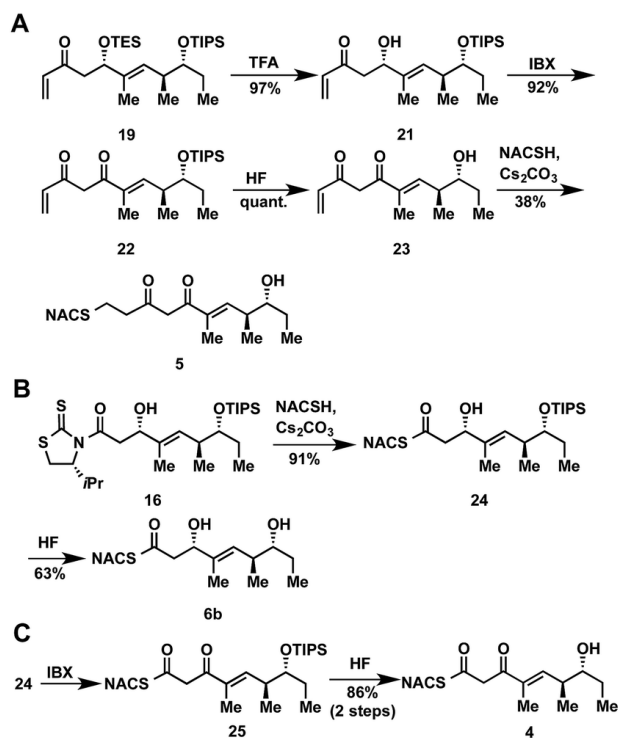
Scheme 3.5 Synthetic route to ketoreductase and thioester substrates 4, 5, and 6b.

The NAC thioester TylKR3 and TylDH3 substrates **4** and **6b** were synthesized in a straightforward approach from intermediates **16** and **24**, respectively, prepared in Scheme 3.2. The thiazolidinethione in **16** was directly displaced with NAC yielding the β-hydroxythioester **24** (Scheme 3.5B). TIPS deprotection with aqueous HF furnished the TylDH3 NAC thioester substrate mimic **6b**. As anticipated, this compound displayed reasonable stability at room temperature and was stable for several months at 4 °C. The C-2 epimeric compound **6a** could be synthesized in a similar manner (Scheme 3.4). Oxidation of β-hydroxythioester **24** would provide the required β-ketothioester. Several reaction conditions were studied to effect this transformation and it was found, once again, that IBX afforded near quantitative yield of **25** (Scheme 3.5C). TIPS deprotection promoted by aqueous HF yielded TylKR3 NAC thioester substrate mimic **4**.

Expression of tylosin module 3 β-processing domains

With TylKR3 substrate mimics **4** and **5** in hand, we sought to purify the KR and DH domains. By sequence alignment to structurally characterized domains[16, 35-37], the sequence boundaries of the KR and DH were determined. The TylKR3 was recalcitrant to purification, so we constructed a plasmid encoding the TylDH3-KR3 didomain including a portion of linker between the KR and

117

ACP domains (residues 957-1682 of tylosin PKS module 3). The didomain was stable upon purification, and used in further analysis. The molecular weight of the recombinant proteins determined by SDS-PAGE was 76 kDa and found to be 76,265 Da by mass spectrometry, both consistent with the calculated value (76,511 Da).

Enzymatic analysis of TylDH3-KR3

We initially attempted to characterize the activity of the TylKR3 domain with substrates **4** and **5** in the presence of NADPH using LC-MS/MS analysis with an internal standard for rigorous quantitation and synthetic standards for product identification. Overnight incubation of the TylDH3-KR3 didomain with **4** and **5** afforded the d-configured reduction products **6b** and **7b** in relatively minor amounts, consistent with the B-type KR domain, along with the dehydration products **8** and **9** as the major species (Scheme 3.6). NAC thioester **4** provided **6b** : **8** in ratio of 1 : 22 while NAC thioether **5** furnished **7b** : **9** in a ratio of 1 : 102 (Figs. 3.7A, B). However, the KR acted very slowly, as the total conversion in each case was less than 2% of input substrate. The combination of slow KR conversion and low KR : DH product ratio suggests that the ketoreductase product can shuttle to the dehydratase in absence of ACP tethering. It further suggests that the chemically reversible dehydration reaction is unidirectional in the TylDH3
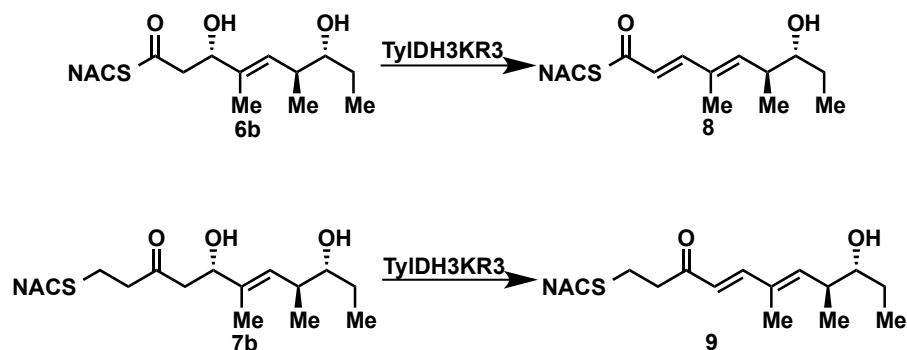
Scheme 3.6 The chemoenzymatic synthesis of dienes 8 and 9 via TylDH3KR3-catalyzed dehydration.
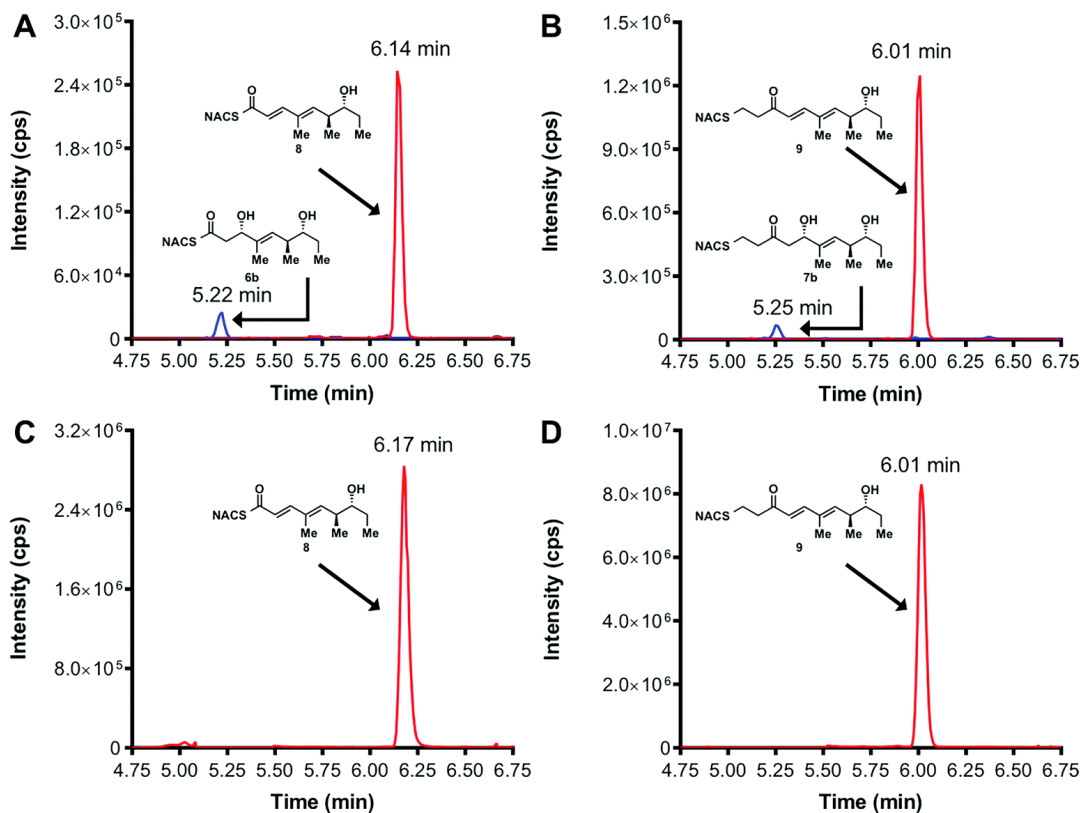
Figure 3.7 LC-MS/MS traces of in vitro ketoreduction and dehydration reactions.

Overnight incubation conducted with KR substrates **4** (panel A) and **5** (panel B) and TylDH3-KR3 in the presence of NADPH. The identity of the β-hydroxy products (shown in blue) was confirmed by co-injection with authentic standards. Incubation with synthetic **7** (panel C) and **9** (panel D) resulted in sole formation of dehydration products **10** and **11** (trace shown in red), respectively. Panels A and C blue trace represents MRM (m/z 368 → 212) red trace represents MRM (m/z 328 → 151).
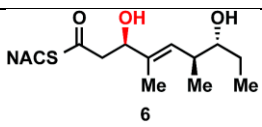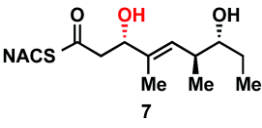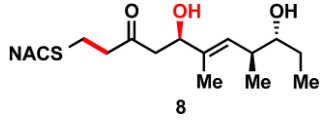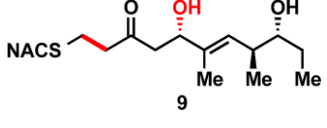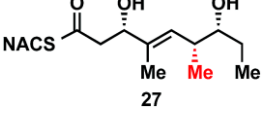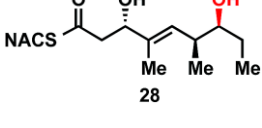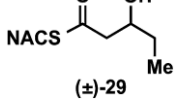
since an unexpectedly high amount of dehydration product was formed from a freely diffusible reduction product. Unfortunately, we were unable to kinetically characterize TylKR3 due to the slow substrate turnover.

We next examined the ability of TylDH3-KR3 to process DH substrates **6a**, **6b**, **7a**, and **7b**. Each substrate (1 mM) was individually incubated overnight with 10 μM TylDH3-KR3 and the reactions were analyzed by LC-MS/MS as before. The d-alcohols **6b** and **7b** led to nearly quantitative formation of *trans*-olefin products **8** and **9**, respectively (Figs. 3.7C, D) whereas l-alcohols **6a** and **7a** were not turned over by the enzyme. This further corroborates the bioinformatic prediction that the preceding B-type TylKR3 should produce d-alcohols and is consistent with empirical observations that d-alcohols yield *trans*-olefins.[7, 38] Based on the enhanced activity of TylDH3 relative to TylKR3 we performed a large-scale incubation of **6b** and **7b** and isolated **8** and **9** in 67 and 98% yield, respectively after flash chromatography. The product identities were unequivocally confirmed by NMR spectroscopy and exhibited nearly identical diagnostic ^{13}C chemical shifts of ~147 and ~133 ppm and a $^{3}J_{HH}$ coupling constant of ~16 Hz.

The enhanced activity of TylDH3 domain enabled characterization by steady-state kinetic analysis. The velocity remained linear up to 10 minutes reaction time and was also linear with respect to TylDH3-KR3 concentration from 0.25 to 1 μM. The initial rates, v_0 at a given [S] were thus determined by single-time point stopped-time incubations at 8 minutes with 0.5 μM TylDH3-KR3. Due to the limited solubility of substrates **6b** and **7b** we were unable to reach saturation, consequently the plots of initial velocity *versus* [S] were fit by linear regression analysis to determine the specificity constants (k_{cat}/K_M). Thioester **6b** and thioether **7b** displayed specificity constants of 980 ± 30 and 410 ± 20 min^{-1} M^{-1}, respectively (Fig. 3.5, Table 3.2).

The modest 2.5-fold difference in k_{cat}/K_M indicates thioethers are well tolerated, validating their use as stabilized forms of substrates otherwise prone to nonproductive, intramolecular cyclization.

Table 3.2 Steady-state kinetic analysis of TylDH3 substrates

Cmpd#	DH substrate	k_{cat}/K_M, min^{-1} M^{-1}
6a	6	$<10^a$
6b	7	980 ± 30
7a	8	$<10^a$
7b	9	410 ± 20
6c	27	22 ± 2
6d	28	72 ± 6
(±)-26	(±)-29	$<10^a$

^{a}Below the limit of detection (LOD) of products in LC-MS/MS

To explore the impact of remote stereocenters on processing by TylDH3 we synthesized full-length tetraketide NAC thioesters **6c** and **6d**, epimeric at the ε- and ζ-stereocenters, respectively (Schemes 3.7, 3.8). The specificity constant for **6c** was 22 ± 2 min^{-1} M^{-1}, which is 45-fold less than **6b** (Table 3.2). Although **6c** only differs from **6b** *via* inversion of the ε-methyl group, we expect the trisubstituted olefin may enhance the 1,3-allylic (A^{1,3}) strain and more severely impact the side chain conformation, potentially contributing to the drastic attenuation in k_{cat}/K_M.

Boddy and co-workers also invoked A^{1,3} strain to rationalize substrate tolerance in their work on PKS thioesterases[39]. We next evaluated the ζ-epimer **6d**, whose specificity constant was 72 ± 6 min^{-1} M^{-1}, approximately 14-fold less than **6b**. Since inversion of the ζ-stereocenter is not expected to significantly alter the substrate conformation, we speculate that the ζ-hydroxyl group may be important for substrate recognition that is otherwise dominated by hydrophobic

121

Figure 3.7 Synthesis of TylDH3 substrate 6c.

The outlined route closely parallels that of thioester **6b** (**Schemes 3.2** and **3.3** in manuscript). Notable differences include the use of the enantiomer of **11** (ent-**11**), the *syn*-selective vinylogous aldol promoted by excess titanium(IV) chloride, and the production of dehydration product **S12** due to an increased sensitivity of diastereomer **S11** to prolonged aldol conditions.
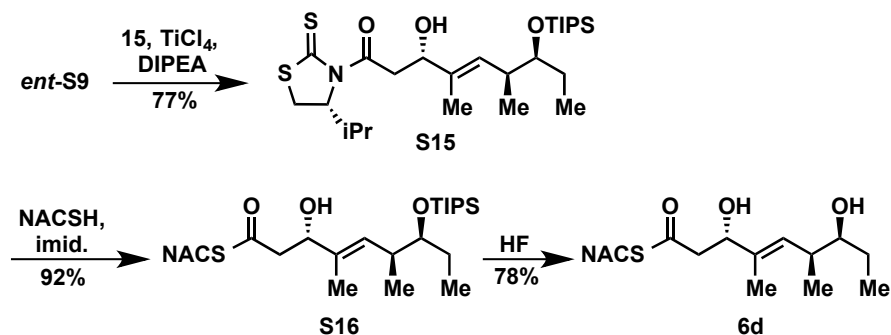
Scheme 3.8 Chemical preparation of substrate 6d.

The enantiomer of aldehyde **S9** (*ent*-**S9**) was submitted to an aldol reaction with Nagao's acyl chiral auxiliary **15** to afford aldol adduct **S15** as the only product. Interestingly, by decreasing the reaction time from 4 h to 1 h 45 min, we avoided the formation of elimination product with this diastereomer. Thiazolidinethione displacement followed by deprotection furnished the TylDH3 substrate **6d**.

interactions of this nonpolar substrate. To complete our substrate specificity studies, we also evaluated diketide (±)-26, but it was not processed, highlighting the significance of using full-length substrates.

Conclusion

The use of full-length, diffusible tetraketide probes allowed for systematic analysis of the module 3 processing domains of tylosin: TylKR3 and TylDH3. The TylKR3 domain was weakly active and produced d-alcohols stereoselectively, further confirming the accuracy of existing bioinformatic approaches[9, 15]. In contrast, the TylDH3 domain proved robust in its production of *trans*-olefins allowing for the chemoenzymatic synthesis of dehydration products. Dehydratase substrate specificity in relation to each stereocenter was independently determined through steady-state kinetic analysis *via* LC-MS/MS detection revealing unpredicted biases for the native substrate. TylDH3 did not tolerate β-stereochemistry inversion, and epimerization of distal stereocenters attenuated the activity by 14–45 fold when compared to the native substrate. This finding was rationalized through recognition of allylic $A^{1,3}$ strain within the molecule and the potential electrostatic and/or hydrogen bonding interactions of the distal hydroxyl moiety. The distant elements of the substrate were necessary for activity as truncated substrate (±)-26 was not dehydrated by TylDH3. Additionally, thioethers proved to be stable thioester surrogates.

This work highlights the *in vitro* use of didomains in the study of cryptic processes as potential solutions for insoluble and/or unreactive domains. The ACP domain has been largely assumed to control the flow of intermediates throughout the reductive progression of domains towards the ultimate module product[40-42]. Unexpectedly, we discovered that tylosin module 3 funnels diffusible substrates from ketoreductase to dehydratase independent of ACP tethering. The exact mechanism of this observed phenomenon remains to be determined and could involve

the proximity of the KR product exit and DH substrate entrance, thereby increasing the local concentration of DH substrate. Alternatively, a conformational change prior to or upon substrate release from the ketoreductase may draw the two catalytic sites together, leading to the observed shuttling process. Our results are consistent with structures of the pikromycin module 5 in which the ACP localization was determined by the tethered acyl group[43-44].

The finding that the distal stereochemical fidelity of preceding modules can be closely regulated by dehydratase activity *via* a stringently stereospecific process may have far-reaching implications in the fields of natural product isolation and synthetic biology. Specifically, this research directly supports the hypothesis that tightly controlled relative and absolute polyketide stereochemistry may not necessitate the action of exquisitely stereoselective domains but, instead, be the consequence of iterative, stereospecific checkpoints or gatekeeper domains. Stalled chain intermediates have been shown previously to be hydrolyzed by downstream TE domains, freeing a non-productive, immature polyketide acid and phosphopantetheine-ACP arm for productive product formation[45-47]. Interestingly, our work suggests that the dehydratase domain, which eliminates stereochemical information, can additionally enrich the final product optical purity. As the dehydratase-catalyzed syn-elimination of water is the only β-processing domain to require a specific, two-centered tetrahedral substrate conformation, it may be naturally sensitive to the local stereochemical features of the substrate.

Bibliography

1.   Fischbach, M. A., Walsh, C. T., Assembly-line enzymology for polyketide and nonribosomal peptide antibiotics: logic, machinery, and mechanisms. *Chemical reviews* **2006,** *106* (8), 3468-3496.

2.   Smith, S., Tsai, S.-C., The type I fatty acid and polyketide synthases: a tale of two megasynthases. *Natural product reports* **2007,** *24* (5), 1041-1072.

3.   Staunton, J., Weissman, K. J., Polyketide biosynthesis: a millennium review. *Natural product reports* **2001,** *18* (4), 380-416.

4.   Fischbach, M. A., Walsh, C. T., Antibiotics for emerging pathogens. *Science* **2009,** *325* (5944), 1089-1093.

5.   Siskos, A. P., Baerga-Ortiz, A., Bali, S., Stein, V., Mamdani, H., Spiteller, D., Popovic, B., Spencer, J. B., Staunton, J., Weissman, K. J., Molecular basis of Celmer's rules: stereochemistry of catalysis by isolated ketoreductase domains from modular polyketide synthases. *Chemistry & biology* **2005,** *12* (10), 1145-1153.

6.   Holzbaur, I. E., Harris, R. C., Bycroft, M., Cortes, J., Bisang, C., Staunton, J., Rudd, B. A., Leadlay, P. F., Molecular basis of Celmer's rules: the role of two ketoreductase domains in the control of chirality by the erythromycin modular polyketide synthase. *Chemistry & biology* **1999,** *6* (4), 189-195.

7.   Valenzano, C. R., You, Y.-O., Garg, A., Keatinge-Clay, A., Khosla, C., Cane, D. E., Stereospecificity of the dehydratase domain of the erythromycin polyketide synthase. *Journal of the American Chemical Society* **2010,** *132* (42), 14697-14699.

8.   Vergnolle, O., Hahn, F., Baerga-Ortiz, A., Leadlay, P. F., Andexer, J. N., Stereoselectivity of isolated dehydratase domains of the borrelidin polyketide synthase: implications for cis double bond formation. *ChemBioChem* **2011,** *12* (7), 1011-1014.

9.   Reid, R., Piagentini, M., Rodriguez, E., Ashley, G., Viswanathan, N., Carney, J., Santi, D. V., Hutchinson, C. R., McDaniel, R., A model of structure and catalysis for ketoreductase domains in modular polyketide synthases. *Biochemistry* **2003,** *42* (1), 72-79.

10.   Kandziora, N., Andexer, J. N., Moss, S. J., Wilkinson, B., Leadlay, P. F., Hahn, F., Uncovering the origin of Z-configured double bonds in polyketides: intermediate E-double bond formation during borrelidin biosynthesis. *Chemical Science* **2014,** *5* (9), 3563-3567.

11.   Bonnett, S. A., Whicher, J. R., Papireddy, K., Florova, G., Smith, J. L., Reynolds, K. A., Structural and stereochemical analysis of a modular polyketide synthase ketoreductase domain required for the generation of a *cis*-alkene. *Chemistry & biology* **2013,** *20* (6), 772-783.

12.   Alhamadsheh, M. M., Palaniappan, N., DasChouduri, S., Reynolds, K. A., Modular polyketide synthases and cis double bond formation: establishment of activated cis-3-cyclohexylpropenoic acid as the diketide intermediate in phoslactomycin biosynthesis. *Journal of the American Chemical Society* **2007,** *129* (7), 1910-1911.

13.   Wu, J., Zaleski, T. J., Valenzano, C., Khosla, C., Cane, D. E., Polyketide double bond biosynthesis. Mechanistic analysis of the dehydratase-containing module 2 of the picromycin/methymycin polyketide synthase. *Journal of the American Chemical Society* **2005,** *127* (49), 17393-17404.

14.   Li, Y., Fiers, W. D., Bernard, S. M., Smith, J. L., Aldrich, C. C., Fecik, R. A., Polyketide intermediate mimics as probes for revealing cryptic stereochemistry of ketoreductase domains. *ACS chemical biology* **2014,** *9* (12), 2914-2922.

15.   Caffrey, P., Conserved amino acid residues correlating with ketoreductase stereospecificity in modular polyketide synthases. *ChemBioChem* **2003,** *4* (7), 654-657.

16.   Keatinge-Clay, A. T., A tylosin ketoreductase reveals how chirality is determined in polyketides. *Chemistry & biology* **2007,** *14* (8), 898-908.

17.   Cundliffe, E., Bate, N., Butler, A., Fish, S., Gandecha, A., Merson-Davies, L., The tylosin-biosynthetic genes of *Streptomyces fradiae*. *Antonie Van Leeuwenhoek* **2001,** *79* (3-4), 229-234.

18.   Piasecki, S. K., Taylor, C. A., Detelich, J. F., Liu, J., Zheng, J., Komsoukaniants, A., Siegel, D. R., Keatinge-Clay, A. T., Employing modular polyketide synthase ketoreductases as biocatalysts in the preparative chemoenzymatic syntheses of diketide chiral building blocks. *Chemistry & biology* **2011,** *18* (10), 1331-1340.

19.   Castonguay, R., Valenzano, C. R., Chen, A. Y., Keatinge-Clay, A., Khosla, C., Cane, D. E., Stereospecificity of ketoreductase domains 1 and 2 of the tylactone modular polyketide synthase. *Journal of the American Chemical Society* **2008,** *130* (35), 11598-11599.

20.   Liu, Y., Li, Z., Vederas, J. C., Biosynthetic incorporation of advanced precursors into dehydrocurvularin, a polyketide phytotoxin from *Alternaria cinerariae*. *Tetrahedron* **1998,** *54* (52), 15937-15958.

21.   Li, Y., Dodge, G. J., Fiers, W. D., Fecik, R. A., Smith, J. L., Aldrich, C. C., Functional characterization of a dehydratase domain from the pikromycin polyketide synthase. *Journal of the American Chemical Society* **2015,** *137* (22), 7003-7006.

22.   Armarego, W. L. F., Perrin, D. D., *Purification of laboratory chemicals*. 4th ed.; Butterworth Heinemann: Oxford ; Boston, 1996; p xi, 529 p.

23.   Shirokawa, S., Shinoyama, M., Ooi, I., Hosokawa, S., Nakazaki, A., Kobayashi, S., Total synthesis of khafrefungin using highly stereoselective vinylogous Mukaiyama aldol reaction. *Organic letters* **2007,** *9* (5), 849-52.

24.   Mukaeda, Y., Kato, T., Hosokawa, S., Syn-Selective Kobayashi Aldol Reaction Using the E,E-Vinylketene Silyl N,O-Acetal. *Organic letters* **2012,** *14* (20), 5298-5301.

25.   Schmauder, A., Muller, S., Maier, M. E., Concise route to defined stereoisomers of the hydroxy acid of the chondramides. *Tetrahedron* **2008,** *64* (27), 6263-6269.

26.   Cane, D. E., Tan, W., Ott, W. R., Nargenicin biosynthesis. Incorporation of polyketide chain elongation intermediates and support for a proposed intramolecular Diels-Alder cyclization. *Journal of the American Chemical Society* **1993,** *115* (2), 527-535.

27.   Shirokawa, S.-i., Kamiyama, M., Nakamura, T., Okada, M., Nakazaki, A., Hosokawa, S., Kobayashi, S., Remote asymmetric induction with vinylketene silyl N, O-acetal. *Journal of the American Chemical Society* **2004,** *126* (42), 13604-13605.

28.   Nagao, Y., Kumagai, T., Tamai, S., Abe, T., Kuramoto, Y., Taga, T., Aoyagi, S., Nagase, Y., Ochiai, M., Highly diastereoselective alkylation onto 4-acetoxy-2-azetidinones employing tin (II) enolates of 3-acyl C-4-chiral 1, 3-thiazolidine-2-thiones. *Journal of the American Chemical Society* **1986,** *108* (15), 4673-4675.

29.   González, Á., Aiguadé, J., Urpí, F., Vilarrasa, J., Asymmetric acetate aldol reactions in connection with an enantioselective total synthesis of macrolactin A. *Tetrahedron letters* **1996,** *37* (49), 8949-8952.

30.   Nahm, S., Weinreb, S. M., N-Methoxy-N-methylamides as effective acylating agents. *Tetrahedron Letters* **1981,** *22* (39), 3815-3818.

31.   Batt, F., Bourcet, E., Kassab, Y., Fache, F., Selective Aerobic Oxidation of Allylic Alcohols to Carbonyl Compounds Using Catalytic Pd (OAc) 2: High Intramolecular Selectivity. *Synlett* **2007,** *2007* (12), 1869-1872.

32.   Firouzabadi, H., Ghaderi, E., Barium manganate. An efficient oxidizing reagent for oxidation of primary and secondary alcohols to carbonyl compounds. *Tetrahedron letters* **1978,** *19* (9), 839-840.

33.   Ball, S., Goodwin, T., Morton, R., Studies on vitamin A: 5. The preparation of retinene1—vitamin A aldehyde. *Biochemical Journal* **1948,** *42* (4), 516.

34.   Bartlett, S. L., Beaudry, C. M., High-yielding oxidation of β-hydroxyketones to β-diketones using o-iodoxybenzoic acid. *The Journal of organic chemistry* **2011,** *76* (23), 9852-9855.

35.   Keatinge-Clay, A. T., Stroud, R. M., The structure of a ketoreductase determines the organization of the β-carbon processing enzymes of modular polyketide synthases. *Structure* **2006,** *14* (4), 737-748.

36.   Zheng, J., Gay, D. C., Demeler, B., White, M. A., Keatinge-Clay, A. T., Divergence of multimodular polyketide synthases revealed by a didomain structure. *Nature chemical biology* **2012,** *8* (7), 615.

37.   Keatinge-Clay, A., Crystal structure of the erythromycin polyketide synthase dehydratase. *Journal of molecular biology* **2008,** *384* (4), 941-953.

38.   Gay, D., You, Y.-O., Keatinge-Clay, A., Cane, D. E., Structure and stereospecificity of the dehydratase domain from the terminal module of the rifamycin polyketide synthase. *Biochemistry* **2013,** *52* (49), 8916-8928.

39.   Hari, T., Labana, P., Boileau, M., Boddy, C. N., An evolutionary model encompassing substrate specificity and reactivity of type I polyketide synthase thioesterases. *ChemBioChem* **2014,** *15* (18), 2656-2661.

40.   Kapur, S., Lowry, B., Yuzawa, S., Kenthirapalan, S., Chen, A. Y., Cane, D. E., Khosla, C., Reprogramming a module of the 6-deoxyerythronolide B synthase for iterative chain elongation. *Proceedings of the National Academy of Sciences* **2012,** *109* (11), 4110-4115.

41.   Kapur, S., Chen, A. Y., Cane, D. E., Khosla, C., Molecular recognition between ketosynthase and acyl carrier protein domains of the 6-deoxyerythronolide B synthase. *Proceedings of the National Academy of Sciences* **2010,** *107* (51), 22066-22071.

42.   Haines, A. S., Dong, X., Song, Z., Farmer, R., Williams, C., Hothersall, J., Płoskoń, E., Wattana-amorn, P., Stephens, E. R., Yamada, E., A conserved motif flags acyl carrier proteins for β-branching in polyketide synthesis. *Nature chemical biology* **2013,** *9* (11), 685.

43.   Whicher, J. R., Dutta, S., Hansen, D. A., Hale, W. A., Chemler, J. A., Dosey, A. M., Narayan, A. R., Håkansson, K., Sherman, D. H., Smith, J. L., Structural rearrangements of a polyketide synthase module during its catalytic cycle. *Nature* **2014,** *510* (7506), 560.

44.   Dutta, S., Whicher, J. R., Hansen, D. A., Hale, W. A., Chemler, J. A., Congdon, G. R., Narayan, A. R., Håkansson, K., Sherman, D. H., Smith, J. L., Structure of a modular polyketide synthase. *Nature* **2014,** *510* (7506), 512.

45.   Heathcote, M. L., Staunton, J., Leadlay, P. F., Role of type II thioesterases: evidence for removal of short acyl chains produced by aberrant decarboxylation of chain extender units. *Chemistry & biology* **2001,** *8* (2), 207-220.

46.   Butler, A. R., Bate, N., Cundliffe, E., Impact of thioesterase activity on tylosin biosynthesis in *Streptomyces fradiae*. *Chemistry & biology* **1999,** *6* (5), 287-292.

47.   Claxton, H. B., Akey, D. L., Silver, M. K., Admiraal, S. J., Smith, J. L., Structure and functional analysis of RifR, the type II thioesterase from the rifamycin biosynthetic pathway. *Journal of Biological Chemistry* **2009,** *284* (8), 5021-5029.

Chapter 4. Vinylogous dehydration by a polyketide dehydratase domain in curacin biosynthesis

Summary

Polyketide synthase (PKS) enzymes continue to hold great promise as synthetic biology platforms for the production of novel therapeutic agents, biofuels and commodity chemicals. Dehydratase (DH) catalytic domains play an important role during polyketide biosynthesis through the dehydration of the nascent polyketide intermediate to provide olefins. Our understanding of the detailed mechanistic and structural underpinning of DH domains that control substrate specificity and selectivity remains limited, thus hindering our efforts to rationally re-engineer PKSs. The curacin pathway houses a rare plurality of possible double bond permutations containing conjugated olefins as well as both *cis-* and *trans*-olefins, providing an unrivaled model system for polyketide dehydration. All four DH domains implicated in curacin biosynthesis were characterized *in vitro* using synthetic substrates and activity was measured by LC-MS/MS analysis. These studies resulted in complete kinetic characterization of the all *trans* trienoate-forming CurK dehydratase, whose k_{cat} of 72 s^{-1} is more than three-orders of magnitude greater than any previously reported PKS DH domain. A novel stereospecific mechanism for diene formation involving a vinylogous enolate intermediate is proposed for the CurJ and CurH dehydratases based on incubation studies with truncated substrates. A synthetic substrate was co-crystallized with a catalytically inactive Phe substitution in the His-Asp catalytic dyad of CurJ

DH to elucidate substrate-enzyme interactions. The resulting complex suggested the structural basis for dienoate formation and provided the first glimpse into the enzyme-substrate interactions essential for the formation of olefins in polyketide natural products. This examination of both canonical and non-canonical dehydration mechanisms reveals hidden catalytic activity inherent in some DH domains that may be leveraged for future applications in synthetic biology.

Introduction

Polyketide secondary metabolites are an exquisite example of Nature's rich diversity, both in terms of molecular complexity and functionality. Small molecules from this natural product family cover a wide range of marketed medicinal agents, providing utility as hypolipodemic (lovastatin), antimicrobial (erythromycin), antineoplastic (ixabepilone), antifungal (amphotericin B), and immunosuppressive (FK-506) therapeutics. The variety in polyketide biological activity is largely attributed to their structural diversity arising from their assembly-line construction by polyketide synthases (PKSs). Type I PKSs consist of modular cassettes of megaenzymes with catalytic domains for extending, editing and transferring polyketide chains. The minimal components necessary for elongation of a polyketide intermediate include an acyl carrier protein (ACP), acyltransferase (AT), and ketosynthase (KS) domains. Each module may additionally house processing domains that alter the substituents and oxidation states at the α- and β-centers. These include *C*-methyltransferase (CMT), ketoreductase (KR), *O*-methyltransferase (OMT), dehydratase (DH), and enoyl reductase (ER) domains affording α-alkylated, β-hydroxy, β-methoxy, α,β-unsaturated or α,β-saturated products. Many of these transformations result in stereoselective formation of an optically enriched product. Subsequent elongation and processing steps by the downstream modules lead to the mature polyketide chain. Chain termination by a thioesterase (TE) domain results in lactonization or

130

hydrolysis to a macrolactone or carboxylic acid, respectively. The released polyketide is often subjected to tailoring events catalyzed by post-PKS tailoring enzymes that further diversify the natural product scaffold.

Curacin A, a mixed polyketide-nonribosomal peptide natural product isolated from the cyanobacteria *Moorea producens* (formerly *Lyngbya majuscula*) is a potent antiproliferative agent that arrests mitosis through the inhibition of tubulin polymerization[1]. Curacin A is biosynthesized via a mixed nonribosomal peptide synthase-polyketide synthase pathway incorporating three malonyl-CoA units in a cyclopropyl moiety, one L-cysteine in a thiazolidine-forming cyclization reaction, and seven units of malonyl-CoA through KS-catalyzed Claisen condensations. Both *C*-methyl and *O*-methyl substituents arise from two equivalents of *S*-adenosylmethionine (SAM) during PKS processing steps. The curacin (Cur) biosynthetic pathway has provided a wealth of information about non-canonical enzymatic processes in polyketide biosynthesis including a GCN5-related *N*-acetyltransferase (GNAT)-like strategy for polyketide chain initiation, cyclopropane synthesis through β-branching and cryptic halogenation, as well as polyketide release via off-loading of a terminal alkene[2-4]. Moreover, the Cur pathway has yielded tremendous structural insight into this unprecedented PKS chemistry and three-dimensional structures of fourteen proteins in the Cur pathway have been published[5-13].

We selected the curacin biosynthesis as a platform for studying dehydratase activity in PKSs. The pathway uniquely produces nearly every possible type of olefin substitution pattern (mono-, di-, and trisubstituted) as well as both *cis* and *trans* geometric isomers (Fig. 4.1). Additionally, curacin B and C constitute geometric isomers of curacin A and suggest a degree of pathway flexibility in regards to olefin formation (Fig. 4.2)[14]. Bioinformatic analysis of the curacin gene cluster shows that PKS modules CurG and CurI are missing DH domains while

CurF contains an extraneous DH domain[10, 15]. Neighboring curacin modules could potentially

accommodate for the missing DHs. This process, termed 'domain stuttering', involves direct

transfer of an ACP-bound intermediate to the ACP of the next domain[16]. This product could be

β-processed (dehydrated by a DH, in this case) then transferred back to the KS domain of the

same module for a typical round of extension and β-processing. We hypothesized these non-

canonical dehydration events may occur through a simpler and more efficient process by an

alternative mechanism. The Smith lab previously disclosed the structural characterization of all

four excised DH domains from CurF, CurH, CurJ and CurK providing a solid structural

foundation and a unique opportunity to capture a bound substrate[10]. The conserved, catalytic His-

Asp dyad residues necessary for syn-dehydration and the active site channels are surprisingly

quite similar giving few clues on the identity of their native substrates[17-18]. This set the stage for

our present study using synthetic substrates to probe the substrate specificity and dehydration

mechanism.
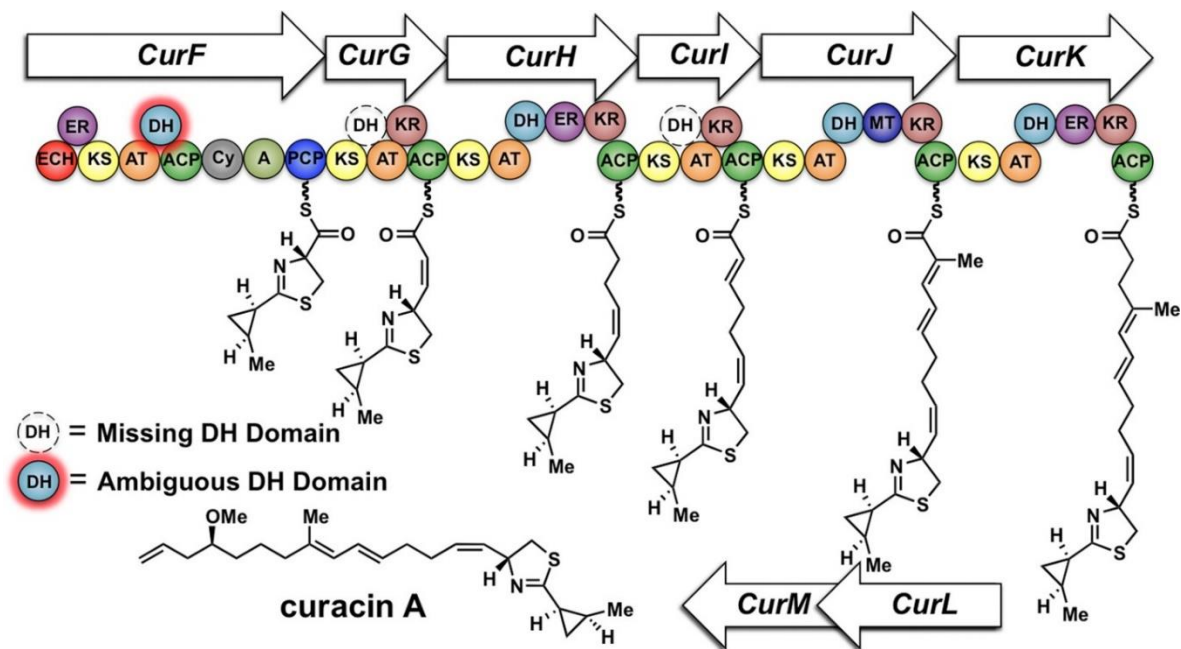
Figure 4.2 Curacin A mixed NRPS-PKS biosynthetic pathway.

The extraneous CurF dehydratase (DH) with no predicted function is highlighted in red. The absent DHs in CurG and CurI are shown with dashed lines in black and white.
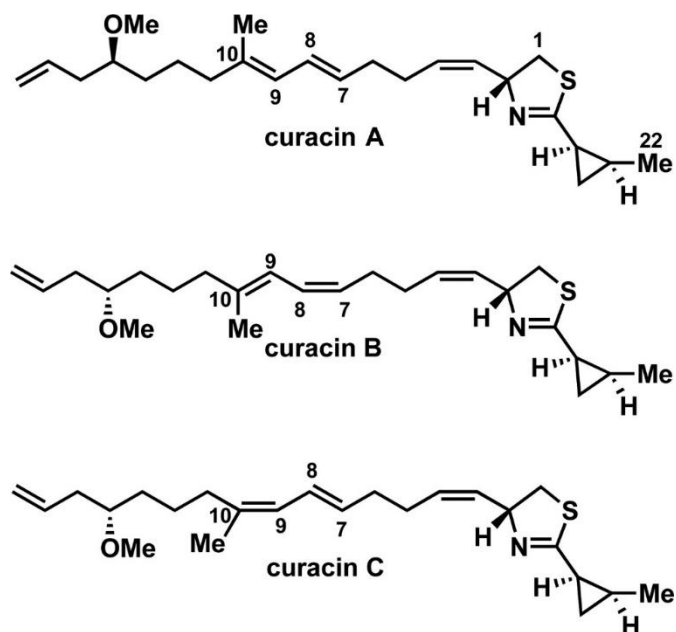
Figure 4.1 Natural geometric isomers of curacin.

Both the Δ7,8 and Δ9,10 cis-isomers of curacin A have been isolated from Moorea producens. The biosynthetic origin of these isomerizations remains unknown.

133

Methods

General chemistry procedures.

All Chemical synthesis were performed by Will Fiers (U. Minnesota)

All chemical reagents were used as provided unless indicated otherwise. Freshly distilled reagents were purified as reported[19]. Tetrahydrofuran (THF) and dichloromethane (CH_2Cl_2) were purified via passage through neutral alumina columns. All reactions were performed under an argon atmosphere using oven-dried (150 °C) glassware. Compounds were purified by flash chromatography using silica gel (300–400 mesh) in the indicated solvent system. TLC was performed using 250 µm, F254 silica gel plates and visualized by UV or through staining with *para*-anisaldehyde. Optical rotations were acquired on a polarimeter at the indicated temperature using the sodium D line ($\lambda = 589$ nm) unless otherwise specified and reported as follows: $[\alpha]_{/}^{Temp}$ $_{D}^{temp}$ = rotation (*c* g/100 mL, solvent). ^1H and ^{13}C NMR spectra were recorded on a 400 MHz NMR spectrometer. Chemical shifts are reported in ppm based on an internal standard of residual $CHCl_3$ (7.26 ppm in ^1H NMR and 77.16 in ^{13}C NMR). Proton chemical data are reported in the following format: chemical shift (ppm), multiplicity (s = singlet, d = doublet, t = triplet, q = quartet, quint = quintet, sext = sextet, sept = septet, m = multiplet, br = broad peak), coupling constant(s), and integration. High-resolution mass spectra (HRMS) were obtained on a time-of-flight (TOF) mass spectrometer using either PEG or PPG standards to calibrate the instrument.

Ethyl (2*E*,4*E*)-2-methylhepta-2,4-dienoate (**11**)

To a solution of triethyl 2-phosphonopropionate (2.81 mL, 13.1 mmol, 1.10 equiv) in THF (36 mL) at 0 °C was added sodium hydride (60% in oil, 0.595 g, 14.9 mmol, 1.25 equiv)

and the reaction stirred for 2 h. Freshly distilled 2-pentenaldehyde **9**[20] (1.16 mL, 11.9 mmol, 1.00 equiv) was then added dropwise over 20 min. After stirring at 0 °C for 5.5 h, the reaction was quenched with H_2O (20 mL). The biphasic solution was separated, and the aqueous layer was extracted with Et_2O (4 × 20 mL). The combined organic layers were dried (Na_2SO_4), filtered, and concentrated under reduced pressure. Purification by silica gel flash chromatography (95:5 pentane–Et_2O) afforded the title compound (2.00 g, quant.) as a transparent light yellow oil: R_f = 0.22 (98:2 pentane–Et_2O); ^1H NMR (CDCl_3, 400 MHz) δ 7.16 (d, J = 11.2 Hz, 1H), 6.33 (dd, J = 14.8, 11.2 Hz, 1H), 6.11 (dt, J = 15.2, 6.4 Hz, 1H), 4.20 (q, J = 7.2 Hz, 2H), 2.21 (quint, J = 7.2 Hz, 2H), 1.93 (s, 3H), 1.30 (t, J = 7.2 Hz, 3H), 1.05 (t, J = 7.6 Hz, 3H); ^{13}C NMR (CDCl_3, 100 MHz) δ 168.8, 144.6, 138.7, 125.3, 125.2, 60.6, 26.5, 14.5, 13.3, 12.7; HRMS (ESI+) m/z calcd for $C_{10}H_{16}O_2Na^+$ [M + Na]$^+$ 191.1043, found 191.1039 (error 2.1 ppm).

(2*E*,4*E*)-2-Methylhepta-2,4-dienal (**13**)

To a solution of **11** (486 mg, 2.89 mmol, 1.00 equiv) in CH_2Cl_2 (13.0 mL) at 0 °C was slowly added diisobutylaluminum hydride (1.0 M in hexanes, 6.93 mL, 6.93 mmol, 2.40 equiv). After 40 min the reaction was quenched via successive addition of MeOH (3.5 mL) and saturated aqueous sodium potassium tartrate (10.0 mL). The resulting biphasic mixture was stirred vigorously at 23 °C for 14 h. The reaction mixture was partitioned between H_2O (10.0 mL) and CH_2Cl_2 (10 mL). The biphasic mixture was separated, and the aqueous layer was extracted with CH_2Cl_2 (3 × 12 mL). The combined organic layers were dried (Na_2SO_4), filtered, and concentrated under reduced pressure to afford the allylic alcohol **12**, which was carried onto the next reaction without further purification: R_f = 0.58 (8:2 hexanes–EtOAc).

To a solution of the crude alcohol **12** prepared above in CH_2Cl_2 (15.0 mL) were sequentially added anhydrous $MgSO_4$ (1.04 g, 8.67 mmol, 3.00 equiv) and MnO_2 (88%

activated, 1.76 g, 20.2 mmol, 7.00 equiv). The resulting gray solution was vigorously stirred at 23 °C for 24 h. The reaction mixture was filtered through a pad of Celite (2.00 cm) and the filtrate concentrated under reduced pressure. Purification by silica gel flash chromatography (98:2 pentane–Et$_2$O) afforded the title compound (0.345 g, 96% over 2 steps) as a colorless oil: R_f = 0.43 (9:1 pentane–Et$_2$O); ^{1}H NMR (CDCl$_3$, 400 MHz) δ 9.42 (s, 1H), 6.83 (d, J = 11.2 Hz, 1H), 6.52 (ddt, J = 14.8, 11.2, 1.6 Hz, 1H), 6.28 (dt, J = 14.8, 6.4 Hz, 1H), 2.32–2.23 (m, 2H), 1.84 (t, J = 0.8 Hz, 3H), 1.10 (t, J = 7.6 Hz, 3H); ^{13}C NMR (CDCl$_3$, 100 MHz) δ 195.3, 149.5, 147.3, 136.2, 125.1, 26.7, 13.1, 9.5; HRMS (ESI+) m/z calcd for C$_8$H$_{12}$ONa$^+$ [M + Na]$^+$ 147.0780, found 147.0794 (error 9.5 ppm).

(4R)-3-[(3S,4E,6E)-3-Hydroxy-4-methylnona-4,6-dienoyl]-4-isopropylthiazolidine-2-thione (**15**)

To a solution of **14** (0.484 g, 2.38 mmol, 1.60 equiv) in CH$_2$Cl$_2$ (12.0 mL) at −40 °C was added TiCl$_4$ (0.277 mL, 2.53 mmol, 1.70 equiv) whereupon the solution changed from bright yellow to orange-red. The solution was stirred for 30 min at −40 °C, then freshly distilled iPr$_2$NEt (0.441 mL, 2.53 mmol, 1.70 equiv) was added dropwise. After 2.25 h the blood-red solution was cooled to −78 °C and aldehyde **13** (185.0 mg, 1.49 mmol, 1.00 equiv, dried overnight over 3 Å molecular sieves) was added over one min. The aldol reaction was stirred at −78 °C for 3.5 h and quenched with saturated aqueous NH$_4$Cl (6.0 mL). The biphasic solution was separated, and the aqueous layer was extracted with CH$_2$Cl$_2$ (4 × 10 mL). The combined organics were dried (Na$_2$SO$_4$), filtered, and concentrated under reduced pressure. Purification by silica gel flash chromatography (7:3 hexane–EtOAc) afforded the title compound (0.230 g, 47%) as a viscous bright yellow oil: R_f = 0.41 (7:3 hexane–EtOAc); [α]24D = −246 (c 1.00, CHCl$_3$); ^{1}H NMR (CDCl$_3$, 400 MHz) δ 6.24 (dd, J = 14.8, 10.8 Hz, 1H), 6.09 (d, J = 10.8 Hz, 1H), 5.76 (dt, J = 14.8, 6.8 Hz, 1H), 5.14 (t, J = 6.8 Hz, 1H), 4.61 (dd, J = 8.8, 0.8 Hz, 1H), 3.59–3.48 (m,

2H), 3.42 (dd, J = 17.2, 9.2 Hz, 1H), 3.03 (d, J = 11.6 Hz, 1H), 2.65 (br s, 1H), 2.37 (sext, J = 6.4

Hz, 1H), 2.13 (pent, J = 7.2 Hz, 2H), 1.77 (s, 3H), 1.06 (d, J = 6.8, 3H), 1.02 (d, J = 7.4, 3H),

0.99 (t, J = 8.8 Hz, 3H); ^{13}C NMR (CDCl$_3$, 100 MHz) δ 203.2, 172.9, 137.5, 135.2, 125.9, 124.9,

73.0, 71.7, 44.1, 31.0, 30.8, 26.2, 19.2, 18.0, 13.8, 13.0; HRMS (ESI+) m/z calcd for

$C_{16}H_{25}NO_2S_2Na^+$ [M + Na]$^+$ 350.1219, found 350.1207 (error 3.4 ppm).

S-(2-Acetamidoethyl) (S,4E,6E)-3-hydroxy-4-methylnona-4,6-dienethioate (**1**)

A solution of aldol adduct **15** (15.0 mg, 0.0458 mmol, 1.00 equiv) in CH$_2$Cl$_2$ (3.00 mL)

was treated with *N*-acetylcysteamine (5.0 μL, 0.050 mmol, 1.1 equiv) and imidazole (9.4 mg,

0.14 mmol, 3.0 equiv) and stirred at 23 °C for 22 h. The reaction mixture was partitioned

between H$_2$O (5 mL) and EtOAc (5 mL) and the layers were separated. The aqueous layer was

extracted with EtOAc (4 × 10 mL) and the combined organic fractions were dried (Na$_2$SO$_4$),

filtered and concentrated under reduced pressure. The crude residue was purified by flash

chromatography (95:5 CH$_2$Cl$_2$–MeOH) to afford the title compound (7.2 mg, 55%) as a colorless

oil: R_f = 0.39 (95:5 CH$_2$Cl$_2$–MeOH); [α]24D = −21 (c 0.52, CHCl$_3$); ^{1}H NMR (CDCl$_3$, 400

MHz) δ 6.22 (dd, J = 15.2, 10.4 Hz, 1H), 6.07 (d, J = 10.8 Hz, 1H), 5.83 (br s, 1H), 5.76 (dt, J =

15.2, 6.4 Hz, 1H), 4.53 (dd, J = 9.2, 3.6 Hz, 1H), 3.48–3.40 (m, 2H), 3.05 (app. sext, J = 8.0 Hz,

2H), 2.84 (dd, J = 15.2, 8.8 Hz, 1H), 2.76 (dd, J = 14.8, 4.0 Hz, 1H), 2.48 (br s, 1H), 2.13 (app.

quint, J = 7.2 Hz, 2H), 1.96 (s, 3H), 1.75 (s, 3H), 1.01 (t, J = 7.2 Hz, 3H); ^{13}C NMR (CDCl$_3$, 100

MHz) δ 199.0, 170.6, 138.0, 134.9, 126.3, 124.7, 74.0, 49.6, 39.5, 29.0, 26.1, 23.4, 13.8, 12.6;

HRMS (ESI+) m/z calcd for $C_{14}H_{23}NO_3SNa^+$ [M + Na]$^+$ 308.1291, found 308.1275 (error 5.2

ppm).

(4R)-4-Benzyl-3-[(2S,3R,4E)-3-hydroxy-2-methylhept-4-enoyl]thiazolidine-2-thione (**18**)

To a solution of thiazolidinethione **17** (0.250 g, 0.940 mmol, 1.00 equiv) in CH_2Cl_2 (4.00 mL) at 0 °C was added $TiCl_4$ (0.110 mL, 0.990 mmol, 1.05 equiv). The resulting bright orange, opaque solution was stirred for 9 min. Next, freshly distilled iPr$_2$EtN (0.183 mL, 1.05 mmol, 1.12 equiv) was added and the reaction was further stirred for 40 min at 0 °C. To the dark red mixture was slowly added freshly distilled 2-pentenaldehyde (0.138 mL, 1.41 mmol, 1.50 equiv) causing a color change to dark brown. After 2 h, the reaction was quenched with saturated aqueous NH_4Cl (5 mL). The biphasic mixture was warmed to 23 °C and the layers separated. The aqueous layer was extracted with CH_2Cl_2 (3 × 10 mL) and the combined organic layers were dried (Na_2SO_4), filtered, and concentrated under reduced pressure. Purification by flash chromatography (8:2 hexanes–EtOAc) afforded the title compound (0.252 g, 72 %) as a viscous, yellow oil: R_f = 0.20 (8:2 hexanes–EtOAc); $[\alpha]22D$ = −191.6 (c 1.00, CHCl$_3$); ^{1}H NMR (CDCl$_3$, 400 MHz) δ 7.37–7.27 (m, 5H), 5.82 (ddt, J = 15.6, 6.4, 1.2 Hz, 1H), 5.50 (ddt, J = 15.2, 6.0, 1.2 Hz, 1H), 5.39 (ddd, J = 10.6, 6.8, 4 Hz, 1H), 4.79 (dq, J = 6.8, 3.2 Hz, 1H), 4.59–4.54 (m, 1H), 3.37 (dd, J = 11.6, 6.8 Hz, 1H), 3.24 (dd, J = 13.2, 4.0 Hz, 1H), 3.04 (dd, J = 13.2, 10.4 Hz, 1H), 2.88 (d, J = 11.6 Hz, 1H), 2.74 (d, J = 2.8 Hz, 1H), 2.08 (app. quint, J = 7.2, 2H), 1.19 (d, J = 6.8 Hz, 3H), 1.01 (t, J = 7.6 Hz, 3H); ^{13}C NMR (CDCl$_3$, 100 MHz) δ 201.8, 177.8, 136.6, 135.0, 129.6, 129.1, 127.9, 127.4, 72.5, 69.1, 43.5, 37.1, 31.9, 25.5, 13.6, 11.6; HRMS (ESI+) m/z calcd for $C_{18}H_{23}NO_2S_2Na^+$ [M + Na]$^+$ 372.1062, found 372.1087 (error 6.7 ppm).

(4R)-4-Benzyl-3-[(2R,3R,4E)-3-hydroxy-2-methylhept-4-enoyl]thiazolidine-2-thione (**19**)

To a solution of **17** (0.150 g, 0.566 mmol, 1.00 equiv) in anhydrous EtOAc (1.4 mL) were sequentially added anhydrous $MgBr_2$•OEt$_2$ (14.6 mg, 0.0566 mmol, 0.100 equiv), 2-pentenaldehyde (60.9 μL, 0.623 mmol, 1.10 equiv), Et$_3$N (0.158 mmol, 1.13 mmol, 2.00 equiv)

and Me₃SiCl (0.108 mL, 0.849 mmol, 1.50 equiv), which all had been freshly distilled. The reaction mixture was stirred at 23 °C for 26 h, then filtered through a silica gel plug (2.00 cm), washing with Et₂O (20 mL), and the filtrate was concentrated under reduced pressure. The crude residue was dissolved in a biphasic mixture of THF (10 mL) and aqueous hydrochloric acid (1 N, 2 mL) and vigorously stirred at 23 °C for 2 h. The reaction was then quenched with saturated aqueous sodium bicarbonate (10 mL) and the biphasic solution was separated. The aqueous layer was extracted with EtOAc (3 × 15 mL) and the combined organic fractions were dried (Na₂SO₄), filtered, and concentrated under reduced pressure. Purification by silica gel flash chromatography (8:2 hexane–EtOAc) afforded the title compound (35.8 mg, 17%) as a viscous, yellow oil: R_f = 0.28 (8:2 hexane–EtOAc); [α]24D = −297.1 (c 1.00, CHCl₃); ¹H NMR (CDCl₃, 400 MHz) δ 7.37–7.27 (m, 5H), 5.79 (dt, J = 15.2, 5.6 Hz, 1H), 5.42 (ddt, J = 15.2, 7.2, 1.6 Hz, 1H), 5.25 (ddd, J = 10.8, 6.8, 3.6 Hz, 1H), 4.34 (dq, J = 7.6, 6.8 Hz, 1H), 4.26 (t, J = 7.6 Hz, 1H), 3.39 (dd, J = 11.2, 6.8 Hz, 1H), 3.26 (dd, J = 13.2, 3.6 Hz, 1H), 3.06 (dd, J = 12.8, 10.8 Hz, 1H), 2.90 (d, J = 11.6 Hz, 1H), 2.16 (br, 1H), 2.06 (app. quint, J = 6.4, 2H), 1.22 (d, J = 6.8 Hz, 3H), 1.00 (t, J = 7.2 Hz, 3H); ¹³C NMR (CDCl₃, 100 MHz) δ 201.5, 178.2, 136.7, 136.3, 129.6, 129.3, 129.0, 127.3, 76.7, 69.2, 45.2, 36.8, 32.8, 25.4, 14.9, 13.5; HRMS (ESI+) m/z calcd for C₁₈H₂₃NO₂S₂Na⁺ [M + Na]⁺ 372.1062, found 372.1049 (error 3.5 ppm).

S-(2-Acetamidoethyl) (2R,3R,4E)-3-hydroxy-2-methylhept-4-enethioate (**3**)

To a solution of **19** (31.1 mg, 0.0890 mmol, 1.00 equiv) in CH₂Cl₂ (4.00 mL) was added imidazole (18.2 mg, 0.267 mmol, 3.00 equiv) and *N*-acetylcysteamine (10.4 μL, 0.0980 mmol, 1.10 equiv). The reaction mixture was vigorously stirred at 23 °C for 21 h. The crude reaction mixture was concentrated under reduced pressure and directly purified by flash chromatography (95:5 CH₂Cl₂–MeOH) to afford the title compound (16.8 mg, 67%) as a light yellow, viscous oil:

*R*ƒ = 0.30 (95:5 CH₂Cl₂–MeOH); [α]24D = −34.5 (*c* 0.29, CHCl₃); ¹H NMR (CDCl₃, 400 MHz) δ 6.00 (br s, 1H), 5.76 (dt, *J* = 15.6, 6.0 Hz, 1H), 5.40 (ddt, *J* = 15.6, 6.4, 1.2 Hz, 1H), 4.19 (t, *J* = 7.6 Hz, 1H), 3.55–3.37 (m, 2H), 3.13–2.98 (m, 2H), 2.76 (app. quint, *J* = 7.2 Hz, 1H), 2.42 (br s, 1H), 2.06 (app. quint, *J* = 7.6 Hz, 2H), 1.94 (s, 3H), 1.11 (d, *J* = 6.8 Hz, 3H), 1.00 (t, *J* = 7.6 Hz, 3H); ¹³C NMR (CDCl₃, 100 MHz) δ 203.6, 170.6, 136.6, 128.8, 75.5, 54.5, 39.5, 28.7, 25.4, 23.3, 15.1, 13.5; HRMS (ESI+) *m/z* calcd for C₁₂H₂₁NO₃SNa⁺ [M + Na]⁺ 282.1134, found 282.1153 (error 6.7 ppm).

(*4S*)-3-[(*3R,4E,6E*)-3-Hydroxy-4-methylnona-4,6-dienoyl]-4-isopropylthiazolidine-2-thione (*ent*-15).
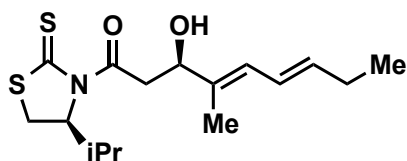
The title compound was prepared from *ent*-14 and 13 following the procedure described for compound 15 and isolated (112.0 mg, 75%) as a bright yellow oil, whose ¹H and ¹³C NMR data were identical to its enantiomer: $[\alpha]_D^{24}$ = +233.2 (*c* 1.00, CHCl₃).

S-(2-Acetamidoethyl) (*3R,4E,6E*)-3-hydroxy-4-methylnona-4,6-dienethioate (2).
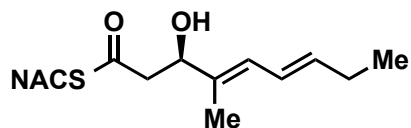
The title compound was prepared from *ent*-15 following the general thiazolidinethione displacement procedure and isolated (6.8 mg, 24%) as a yellow oil, whose ¹H and ¹³C NMR data were identical to its enantiomer: $[\alpha]_D^{24}$ = 17.1 (*c* 1.00, CHCl₃).

(*4S*)-4-Benzyl-3-[(*2R,3S,4E*)-3-hydroxy-2-methylhept-4-enoyl)]thiazolidine-2-thione (*ent*-**18**).
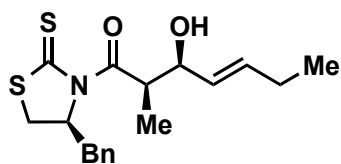
The desired aldol product was obtained an analogous method as the enantiomer, **18** and isolated (0.257 g, 78%) as a yellow oil: $R_f = 0.20$ (8:2 hexanes–EtOAc); $[\alpha]_D^{24} {}_D^{23} = +199.3$ (*c* 1.00, CHCl$_3$); ^{1}H NMR (CDCl$_3$, 400 MHz) δ 7.38–7.27 (m, 5H), 5.82 (ddt, J = 15.6, 6.4, 1.2 Hz, 1H), 5.50 (ddt, J = 15.2, 6.0, 1.2 Hz, 1H), 5.39 (ddd, J = 10.6, 6.8, 4 Hz, 1H), 4.79 (dq, J = 6.8, 3.2 Hz, 1H), 4.59–4.54 (m, 1H), 3.37 (dd, J = 11.6, 6.8 Hz, 1H), 3.24 (dd, J = 13.2, 4.0 Hz, 1H), 3.04 (dd, J = 13.2, 10.4 Hz, 1H), 2.88 (d, J = 11.6 Hz, 1H), 2.74 (d, J = 2.8 Hz, 1H), 2.08 (app. quint, J = 7.2, 2H), 1.19 (d, J = 6.8 Hz, 3H), 1.01 (t, J = 7.6 Hz, 3H); ^{13}C NMR (CDCl$_3$, 100 MHz) δ 201.8, 177.7, 136.5, 135.0, 129.6, 129.1, 128.0, 127.4, 72.5, 69.1, 43.4, 37.1, 31.9, 25.5, 13.6, 11.5; HRMS (ESI+) *m/z* calcd for C$_{18}$H$_{23}$NO$_2$S$_2$Na$^+$ [M + Na]$^+$ 372.1062, found 372.1081 (error 5.1 ppm).

(*4S*)-4-Benzyl-3-[(*2S,3S,4E*)-3-hydroxy-2-methylhept-4-enoyl)]thiazolidine-2-thione (*ent*-**19**).
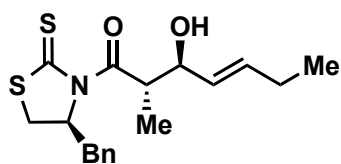
The desired aldol product was obtained an analogous method as the enantiomer, **19**, affording the product as a viscous yellow oil (20.6 mg, 10%): R_f = 0.28 (8:2 hexanes–EtOAc); $[\alpha]_D^{23} = +302.6$ (*c* 1.00, CHCl$_3$); ^{1}H NMR (CDCl$_3$, 400 MHz) δ 7.37–7.24 (m, 5H), 5.79 (dt, J = 15.2, 5.6 Hz, 1H), 5.42 (ddt, J = 15.2, 7.2, 1.6 Hz, 1H), 5.25 (ddd, J = 10.8, 6.8, 4 Hz, 1H), 4.34 (dq, J = 7.6, 6.8 Hz, 1H), 4.26 (t, J = 7.6 Hz, 1H), 3.39 (dd, J = 11.2, 6.8 Hz, 1H), 3.26 (dd, J = 13.2, 3.6 Hz, 1H), 3.06 (dd, J = 12.8, 10.8 Hz, 1H), 2.90 (d, J = 11.6 Hz, 1H), 2.16 (br, 1H), 2.06 (app. quint, J = 6.4, 2H), 1.22 (d, J = 6.8 Hz, 3H), 1.00 (t, J = 7.2 Hz, 3H); ^{13}C NMR (CDCl$_3$, 100 MHz) δ 201.5, 178.2, 136.7,

136.3, 129.6, 129.3, 129.0, 127.3, 76.7, 69.2, 45.2, 36.8, 32.8, 25.4, 14.9, 13.5; HRMS (ESI+) m/z

calcd for $C_{18}H_{23}NO_2S_2Na^+$ [M + Na]$^+$ 372.1062, found 372.1041 (error 5.6 ppm).

S-(2-Acetamidoethyl) (2*S*,3*R*,4*E*)-3-hydroxy-2-methylhept-4-enethioate (**4**).
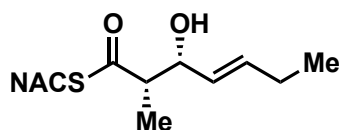
To a solution of aldol adduct **18** (25.2 mg, 0.0721 mmol, 1.00 equiv) dissolved in CH_2Cl_2 (5.00 mL) was added with *N*-acetylcysteamine (8.43 μL, 1.10 equiv) and imidazole (14.7 mg, 0.216 mmol, 3.00 equiv). The reaction mixture was stirred at 23 °C for 21 h. The resulting solution was evaporated under nitrogen stream and the crude residue was purified by flash chromatography (95:5 CH_2Cl_2–MeOH), furnishing the title compound (16.9 mg, 0.0652 mmol, 90%) as a colorless, viscous oil: R_f = 0.20 (95:5 CH_2Cl_2–MeOH); $[\alpha]_D^{24}$ = 27.6 (*c* 0.87, CHCl$_3$); ^{1}H NMR (CDCl$_3$, 400 MHz) 5.79 (br, 1H), 5.77 (ddt, *J* = 15.2, 6.4, 1.2 Hz, 1H), 5.44 (ddt, *J* = 15.2, 6.8, 1.6 Hz, 1H), 4.37 (br, 1H), 3.52–3.34 (m, 2H), 3.10–2.96 (m, 2H), 2.84–2.75 (m, 1H), 2.06 (app. quint, *J* = 6.8 Hz, 2H), 1.96 (s, 3H), 1.22 (d, *J* = 6.4 Hz, 3H), 0.99 (t, *J* = 7.2 Hz, 3H); ^{13}C NMR (CDCl$_3$, 100 MHz) δ 203.6, 170.5, 135.7, 128.0, 73.6, 54.0, 39.6, 28.7, 25.4, 23.4, 13.5, 12.0; HRMS (ESI+) *m/z* calcd for $C_{12}H_{21}NO_3SNa^+$ [M + Na]$^+$ 282.1134, found 282.1136 (error 0.71 ppm).

S-(2-Acetamidoethyl) (2*R*,3*S*,4*E*)-3-hydroxy-2-methylhept-4-enethioate (**5**).
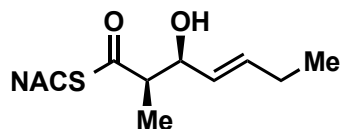
The thioester **5** was synthesized in an analogous manner to that of the thioester **4** yielding a colorless oil (14.5 mg, 63%): R_f = 0.19 (95:5 CH_2Cl_2–MeOH); $[\alpha]_D^{24}$ = -24.1 (*c* 0.58, CHCl$_3$); ^{1}H NMR (CDCl$_3$, 400 MHz) δ 5.91–5.67 (m, 2H), 5.52–5.37 (m, 1H), 4.37 (br s, 1H), 3.54–3.35 (m, 2H), 3.10–2.95 (m, 2H), 2.87–2.75 (m, 1H),

2.06 (app. quint, $J = 6.8$ Hz, 2H), 1.96 (s, 3H), 1.22 (d, $J = 7.2$ Hz, 3H), 0.99 (t, $J = 7.6$ Hz, 3H);

^{13}C NMR (CDCl$_3$, 100 MHz) δ 203.6, 170.5, 135.6, 128.0, 73.6, 54.0, 39.6, 28.7, 25.4, 23.4, 13.6,

12.0; HRMS (ESI+) *m/z* calcd for $C_{12}H_{21}NO_3SNa^+$ [M + Na]$^+$ 282.1134, found 282.1152 (error

6.4 ppm).

S-(2-Acetamidoethyl) (2*S*,3*S*,4*E*)-3-hydroxy-2-methylhept-4-enethioate (**6**).
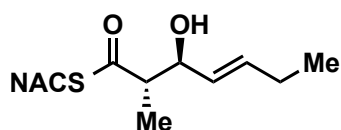
The thioester **6** was synthesized in an analogous manner to that of the prior thioester **3** furnishing the desired product as a colorless oil (3.24

mg, 42%): R_f = 0.30 (95:5 CH$_2$Cl$_2$–MeOH); $[\alpha]_D^{24}$ = 37.3 (*c* 0.35, CHCl$_3$); ^{1}H NMR (CDCl$_3$, 400

MHz) δ 5.88 (br s, 1H), 5.79 (dt, $J = 15.6$, 6.0 Hz, 1H), 5.40 (ddt, $J = 15.6$, 6.4, 1.2 Hz, 1H), 4.21

(t, $J = 7.6$ Hz, 1H), 3.55–3.37 (m, 2H), 3.13–2.98 (m, 2H), 2.76 (app. quint, $J = 7.2$ Hz, 1H), 2.07

(app. quint, $J = 7.6$ Hz, 2H), 1.96 (s, 3H), 1.13 (d, $J = 6.8$ Hz, 3H), 1.00 (t, $J = 7.6$ Hz, 3H); ^{13}C

NMR (CDCl$_3$, 100 MHz) δ 203.7, 170.6, 136.8, 128.8, 75.6, 54.5, 39.7, 28.7, 25.4, 23.3, 15.2,

13.5; HRMS (ESI+) *m/z* calcd for $C_{12}H_{21}NO_3SNa^+$ [M + Na]$^+$ 282.1134, found 282.1157 (error 8.2

ppm).

S-(2-Acetamidoethyl) 2-(diethoxyphosphoryl)propanethioate (**S2**).
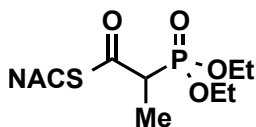
To a flask containing H$_2$O (2.00 mL) was added triethyl 2-phosphonopropionate (1.00 mL, 4.66 mmol, 1.00 equiv). The clear, colorless solution was cooled via ice water bath (0 °C). To the chilled

mixture was slowly added a cooled (4 °C), aqueous NaOH solution (10.0 N, 0.490 ml, 4.90 mmol,

1.05 equiv). The reaction mixture was allowed to slowly warm to 23 °C and stirred for 20 h. The

reaction was quenched with aqueous HCl (1 N) until the pH was 1.00. The resulting solution was

saturated with solid NaCl and extracted with CH$_2$Cl$_2$ (4 × 10 mL). The combined organic layers

were dried (Na$_2$SO$_4$), filtered and the solvent removed under reduced pressure. The crude residue was dissolved in CH$_2$Cl$_2$ (40 mL) and cooled by placing in an ice water bath (0 °C). To the chilled solution was added 4-dimethylaminopyridine (57.0 mg, 0.467 mmol, 0.100 equiv) and *N,N'*-dicyclohexylcarbodiimide (1.01 g, 4.89 mmol, 1.05 equiv). After stirring for 2 min, *N*-acetylcysteamine (0.644 mL, 6.06 mmol, 1.30 equiv) was added to the reaction mixture. The resulting solution was allowed to warm to 23 °C and stirred 22 h. The reaction mixture was diluted with Et$_2$O (40 mL) and filtered to remove the urea precipitate. The filtrate was concentrated under reduced pressure and purified by flash chromatography (EtOAc) affording the title compound (1.36 g, 4.37 mmol, 94%) as a clear colorless oil: R_f = 0.15 (EtOAc); ^{1}H NMR (CDCl$_3$, 400 MHz) δ 6.30 (br, 1H), 4.21–4.09 (m, 4H), 3.54–3.37 (m, 2H), 3.29 (dq, J = 22.4, 7.2 Hz, 1H), 3.20–3.12 (m, 1H), 3.04–2.95 (m, 1H), 1.96 (s, 3H), 1.45 (dd, J = 18.0, 7.2 Hz, 3H), 1.34 (t, J = 7.2 Hz, 6H); ^{13}C NMR (CDCl$_3$, 100 MHz) δ 196.1, 196.0, 170.6, 63.34, 63.27, 63.0, 62.9, 49.2, 47.9, 39.2, 29.4, 23.2, 16.54, 16.48, 12.51, 12.45; HRMS (ESI+) *m/z* calcd for C$_{11}$H$_{22}$NO$_5$PSNa$^+$ [M + Na]$^+$ 334.0849, found 334.0847 (error 0.60 ppm).

S-(2-Acetamidoethyl) (2*E*,4*E*)-2-methylhepta-2,4-dienethioate (**8**).
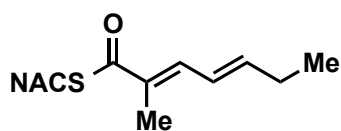
To a solution of LiBr (0.132 g, 1.52 mmol, 3.16 equiv) in THF (6.00 mL) was added the phophono-thioester **S2** (0.150 g, 0.482 mmol, 1.00 equiv). The solution was stirred vigorously at 23 °C for 10 min. To the reaction mixture was Et$_3$N (0.212 mL, 1.52 mmol, 3.16 equiv) resulting in the formation of a cloudy, colorless solution that was stirred at 23 °C for 15 min. To the reaction vessel was added freshly distilled 2-pentenaldehyde **9**[19] (99.0 µL, 1.02 mmol, 2.11 equiv) in a drop wise fashion. After stirring for 24 h, the reaction mixture was quenched upon addition of H$_2$O (30 mL). The biphasic solution was separated, and the aqueous layer was extracted with EtOAc (4 × 10 mL). The combined organic fractions were

dried (Na_2SO_4), filtered and concentrated under reduced pressure. The crude product residue was purified by wet-loading onto silica flash column (1:1 hexanes–EtoAc) yielding the title compound (49.5 mg, 0.205 mmol, 43%) as a cloudy oil: R_f = 0.30 (95:5 CH_2Cl_2–MeOH); ^{1}H NMR ($CDCl_3$, 400 MHz) δ 7.17 (d, J = 10.8 Hz, 1H), 6.35 (dd, J = 14.8, 11.2 Hz, 1H), 6.22 (dt, J = 5.6, 15.2 Hz, 1H), 6.01 (br, 1H), 3.52–340 (m, 2H), 3.15–3.03 (m, 2H), 2.30–2.16 (m, 2H), 1.97 (s, 6H), 1.07 (t, J = 6.8 Hz, 3H); ^{13}C NMR ($CDCl_3$, 100 MHz) δ 193.9, 170.8, 146.9, 138.5, 132.6, 124.8, 40.2, 28.5, 26.7, 23.4, 13.2, 12.7; HRMS (ESI+) m/z calcd for $C_{12}H_{19}NO_2SNa^+$ [M + Na]$^+$ 264.1029, found 264.1043 (error 5.3 ppm).

(*4S*)-3-((*5R,2E*)-5-Hydroxy-2-methylhept-2-enoyl)-4-isopropyloxazolidin-2-one (**S5**).
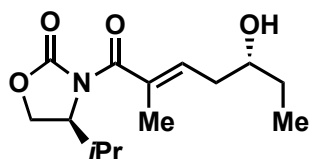
A solution of freshly distilled propionaldehyde[19] (0.443 mL, 6.14 mmol, 2.00 equiv) in CH_2Cl_2 (15.0 mL) was cooled via dry ice–acetone bath (-78 °C). To the reaction mixture was added $TiCl_4$ (0.338 mL, 3.07 mmol, 1.00 equiv). To the resulting yellow reaction mixture was slowly added the *N,O*-silyl ketene acetal **S4**[21] (1.00 g, 3.07 mmol, 1.00 equiv) as a solution in CH_2Cl_2 (14.6 mL). The reaction mixture was transferred to an MeCN–dry ice bath (-40 °C) and stirred for 7 h. The reaction was halted via sequential addition of a saturated, aqueous potassium sodium tartrate (10 mL) and a saturated, aqueous $NaHCO_3$ solution (10 mL). The resulting cloudy mixture was vigorously stirred at 23 °C for 1 h. The biphasic solution was separated, and the aqueous layer was extracted with CH_2Cl_2 (3 × 20 mL). The combined organic layers were dried (Na_2SO_4), filtered and concentrated under reduced pressure. The crude product residue was purified by flash chromatography (7:3 hexanes–

EtOAc) affording the title compound (0.673 g, 2.49 mmol, 81%) as an amorphous white solid: R_f = 0.20 (7:3 hexanes–EtOAc); $[\alpha]_D^{24}$ = 46.0 (c 1.00, CHCl₃); ¹H NMR (CDCl₃, 400 MHz) δ 6.03 (t, J = 7.6 Hz, 1H), 4.56 (dt, J = 8.8, 4.8 Hz, 1H), 4.33 (t, J = 8.8 Hz, 1H), 4.9 (dd, J = 8.8, 5.2 Hz, 1H), 3.70–3.60 (m, 1H), 2.53 (br, 1H), 2.43–2.26 (m, 3H), 1.94 (s, 3H), 1.65–1.47 (m, 2H), 0.98 (t, J = 7.6 Hz, 3H), 0.92 (t, J = 6.8 Hz, 6H); ¹³C NMR (CDCl₃, 100 MHz) δ 171.7, 154.4, 135.4, 133.2, 72.2, 63.6, 58.3, 36.5, 29.9, 28.5, 18.0, 15.3, 13.9, 10.4, 7.3; HRMS (ESI+) m/z calcd for $C_{14}H_{23}NO_4Na^+$ [M + Na]⁺ 292.1519, found 292.1529 (error 3.4 ppm).

S-(2-Acetamidoethyl) (5*R*,2*E*)-5-hydroxy-2-methylhept-2-enethioate (**21**).
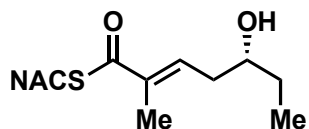
A solution of imide **S5** (0.190 g, 0.707 mmol, 1.00 equiv) dissolved in a THF–H₂O (2:1, 6.43 mL) was vigorously stirred in ice water bath (0 °C). To the chilled reaction mixture was added H₂O₂ (30% in water, 0.219 mL, 1.93 mmol, 3.00 equiv) followed by LiOH•H₂O (80.9 mg, 1.93 mmol, 3.00 equiv). The reaction mixture was vigorously stirred for 24 h, slowly warming to 23 °C. An additional aliquot of H₂O₂ (80.0 μL, 0.707 mmol, 1.00 equiv) and LiOH•H₂O (29.7 mg, 0.707 mmol, 1.00 equiv) were added to the reaction mixture at 0 °C. The reaction mixture was allowed to warm to 23 °C and stirred for 36 h. The crude solution was concentrated under reduced pressure and the resulting aqueous solution was portioned treated with aqueous, saturated NaHCO₃ (1 mL) and washed with Et₂O (2 × 10 mL). The aqueous fraction was acidified with aqueous HCl (2 M) to pH 2 and extracted with Et₂O (4 × 10 mL). The combined organics were concentrated to dryness under reduced pressure and the crude colorless oil (0.112 g) was submitted directly to the next reaction.

The crude acid **S6** (82.2 mg, 0.520 mmol, 1.00 equiv) in DMF (2.73 mL) was cooled via ice–water bath (0 °C). To the chilled solution was sequentially added diphenylphophoryl azide

(0.168 mL, 0.780 mmol, 1.50 equiv) and Et₃N (145 μL, 1.04 mmol, 2.00 equiv). The reaction mixture was stirred for 2 h at 0 °C. An aliquot of *N*-acetylcysteamine (55.3 μL, 0.520 mmol, 1.00 equiv) was added to the reaction mixture at 0°C. The slightly yellow solution was allowed to gradually warm to 23 °C and stirred 5.5 h. The reaction mixture was quenched upon addition of H₂O (3 mL) and EtOAc (10 mL) and the biphasic solution was separated. The aqueous layer was extracted with EtOAc (4 × 10 mL). The combined organic fractions were dried (Na₂SO₄), filtered and concentrated under reduced pressure. The crude product residue was purified by flash chromatography (95:5 to 9:1 CH₂Cl₂–MeOH) yielding the title compound (92.6 mg, 0.357 mmol, 69% over 2 steps) as a clear, colorless oil: R_f = 0.20 (95:5 CH₂Cl₂–MeOH); $[\alpha]_D^{24}$ = –15.3 (*c* 1.00, CHCl₃); ¹H NMR (CDCl₃, 400 MHz) δ 6.86 (t, *J* = 7.2 Hz, 1H), 5.87 (br, 1H), 3.78–3.69 (m, 1H), 3.45 (q, *J* = 6.0 Hz, 2H), 3.07 (t, *J* = 6.4 Hz, 2H), 2.47–2.32 (m, 2H), 1.97 (s, 3H), 1.91 (s, 3H), 1.60–1.46 (m, 2H), 0.98 (t, *J* = 7.2, 3H); ¹³C NMR (CDCl₃, 100 MHz) δ 194.0, 170.4, 138.0, 137.8, 72,5, 39.9, 36.4, 30.3, 28.7, 23.4, 12.9, 10.0; HRMS (ESI+) *m/z* calcd for C₁₂H₂₁NO₃SNa⁺ [M + Na]⁺ 282.1134, found 282.1236 (error 0.71 ppm).

The above compound matches that synthesized by another alternative and previously reported route in all respects[22].

(4*R*)-3-((5*S*,2*E*)-5-Hydroxy-2-methylhept-2-enoyl)-4-isopropyloxazolidin-2-one (**ent-S5**).
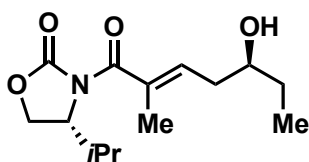
The target alcohol was synthesized from *N*, *O*-vinyl ketene acetal **ent-S4** via an analogous route to that of the enantiomer, **S5**: The product was produced as a clear, colorless oil (0.574 g, 88%). $[\alpha]_D^{24}$ = -44.5 (*c* 1.00, CHCl₃). Additional properties matched those of the enantiomer **S5**.

S-(2-Acetamidoethyl) (*5S,2E*)-5-hydroxy-2-methylhept-2-enethioate (**20**).
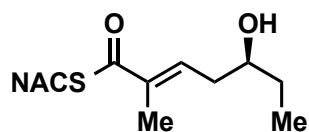
The thioenoate substrate **20** was synthesized in an analogous route to that of the enantiomer **21** starting from acyl oxazolidinone ***ent*-S5**. The desired SNAC-thioester was furnished as a clear, colorless oil (0.103 g, 69% over 2 steps): $[\alpha]_D^{24}$ = -14.0 (*c* 1.00, CHCl$_3$). All other properties matched those of the enantiomer, compound **21**.

General biology

All chemical reagents were purchased from Sigma-Aldrich and were used directly without further purification. *E. coli* BL21(DE3) cells were from New England BioLabs. IPTG was acquired through Gold Biotechnology. His60 Ni Superflow resin was purchased from Clontech Laboratories, Inc. OD$_{600}$ was measured on an Eppendorf BioPhotometer. Sonication was carried out with a Branson Sonifier 450. Gel filtration purification was performed on HiLoad 16/600 Superdex 200 pg column (GE Healthcare). The protein mass spectra data was obtained on a Bruker BioTOF II mass spectrometer. LC–MS/MS was conducted with an AB Sciex QTRAP 5500 mass spectrometer and Shimadzu LC system.

Protein purification and crystallization

DHs were purified as described previously[10]. For co-crystallization of substrates with inactive CurJ DH variants, the protein was pre-incubated 2 hr on ice in 5 mM substrate, and then crystallized at 20°C by sitting-drop vapor diffusion from a 1:1 mixture of protein stock (15 mg/mL DH, 5 mM substrate, 50 mM Tris pH 7.5, 150 mM NaCl, 10% glycerol) with well

solution (18% polyethylene glycol (PEG) 3350, 5% 1,4-butanediol, 250 mM NaCl, 100 mM Bis-Tris propane pH 6.5). Crystals were harvested directly from drops into liquid N_2.

Data collection and structure determination

Data were collected at the Advanced Photon Source (APS, Argonne National Laboratory) on GM/CA beamline 23ID-D. CurJ H978F crystals diffracted to 2.4 Å in the presence of 5 mM substrate. The crystals were nearly isomorphous with the previously reported crystals of wild-type CurJ DH[10]. Data were processed using XDS[23]. The structure was solved by molecular replacement in PHENIX[24] using the wild-type CurJ (PDB 3KG8) as a search model. Refinement was accomplished in PHENIX and model building with coot[25]. Ligand restraint files were built using eLBOW[26] in PHENIX. The structure was validated with MolProbity[27]; figures were generated with PyMOL[28].

Steady-state kinetic studies of CurK-DH

Incubation and sample preparation

Substrate **1** (0.25–6.0 mM) was incubated with recombinant CurK-DH (20 nM) and reaction buffer (50 mM Tris, 150 mM NaCl, pH 8.0) in a total volume of 50 μL at 23 °C. The reaction was quenched at 4 min by transfer of 5 μL of the reaction mixture into 495 μL of quench solution (1:1 MeCN–H_2O). The quenched mixture was briefly vortexed and centrifuged (21,000 × g, 5 min). A portion of the centrifuged supernatant (60 μL) was transferred to an HPLC vial containing the internal standard (10 μL of a 320 nM solution of diene **8**), mixed, injected and analyzed by LC–tandem MS.

Instrumentation

Reverse-phase liquid chromatography was conducted on a Shimadzu UFLC XR, SIL-20AC autosampler and Prominence CTO-20A column oven. A SCIEX QTRAP 5500 (Framingham, MA) was used for mass detection with an electrospray ionization source. All instrumentation was run using Analyst Software (1.5.2, AB SCIEX)
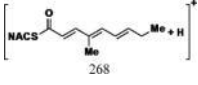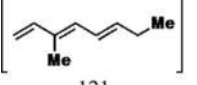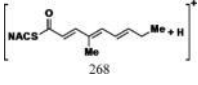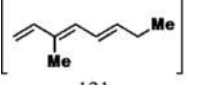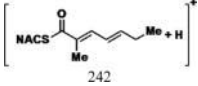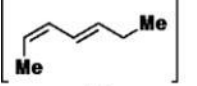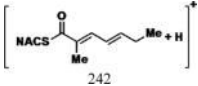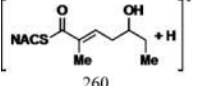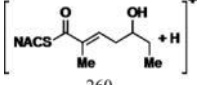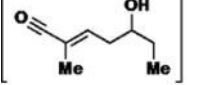
Chromatography

Reverse phase HPLC was conducted using a Kinetix reverse-phase C_{18} column (50 mm × 2.1 mm, 2.6 μm, Phenomenex®, Torrance, CA) operated at 0.4 mL min^{-1} with a column temperature of 35 °C. The mobile phase A (0.1% formic acid in H_2O) and mobile phase B (acetonitrile) were run at the following gradient program: 0 min, 5% B; 2 min, 5% B; 7 min, 55% B; 8 min, 70% B; 9 min, 70% B; 10.5 min, 5% B; 12 min, 5% B, STOP. The injection volume was 10 μL.

Mass spectrometry

Analytes were analyzed by MS in positive ionization mode by Multiple Reaction Monitoring (MRM). Optimal MRM settings were determined by direct infusion of the analyte solution (10 nM, 1:1 H_2O–MeCN with 0.1% formic acid) onto the MS by a syringe pump at a flow of 10 μL/min. The transitions and retention times are displayed in Table 4.1.

Table 4.1 LC-MS/MS transitions, parameters and retention times for 1-8, 20 and 21

Cmpd	Precursor Ion (*m/z*)	Product Ion (*m/z*)	DP[a] (V)	CE[a] (V)	CXP[a] (V)	Retention Time (min)
1, 2	268	121	35	25	15	6.17
7	268	121	35	25	15	7.44
3, 4, 5, 6	242	95	35	30	15	5.52 (**3** and **6**) 5.24 (**4** and **5**)
6	242	260	35	30	15	6.80
20, 21	260	141	35	17	15	5.11

[a]Mass Spectrometry parameter abbreviations: DP = de-clustering potential, CE = collision energy, CXP = collision cell exit potential

Standard curve and data analysis

A standard curve for the triene product **7** was generated by injecting the authentic standard at varying concentrations with a fixed concentration of internal standard **8** (Fig. 4.3). Transitions and retention times are given in Tables 4.2 and 4.3. Analyte and internals standard peak areas were calculated using MultiQuant software (version 2.0.2). Each analyte peak area was normalized to internal standard (**8**) peak area and converted to an analyte concentration using the standard curve equation. Each reaction was performed in duplicate. The calculated initial velocity at each substrate concentration was used to generate a Michaelis-Menten curve (eq.1, Fig.4.4) utilizing Prism 5 software (Version 5.0b) (Figure 4.4):

(eq. 1)

$$v = \frac{V_{max}[S]}{K_M + [S]}$$

where v is the reaction rate, V_{max} is the maximum enzymatic reaction rate, $[S]$ is the concentration of substrate and K_M is the Michaelis-Menten constant.

Table 4.2 CurK DH standard curve data

Conc. 3.7 (nM)	Transition (g/mol)	Peak Area	Area Ratio (3.7/4.6)
0	268→ 121	7362.665	0.008408595
0	242→ 95	875611.851	
20	268→ 121	22332.363	0.025029893
20	242→ 95	892227.710	
40	268→ 121	31796.445	0.037390844
40	242→ 95	850380.513	
80	268→ 121	59521.288	0.078705923
80	242→ 95	756249.172	
160	268→ 121	107466.167	0.145652283
160	242→ 95	737826.866	
320	268→ 121	228634.211	0.300539582
320	242→ 95	760745.754	
640	268→ 121	425896.088	0.569489824
640	242→ 95	747855.484	
1280	268→ 121	730462.476	1.025132203
1280	242→ 95	712554.414	

Scatter plot with axis label "Area Ratio (P/IS)" (y-axis) versus "Substrate Concentration (nM)" (x-axis), showing fitted line:

$$y = 0.000805x + 0.018269$$
$$R^2 = 0.996836$$
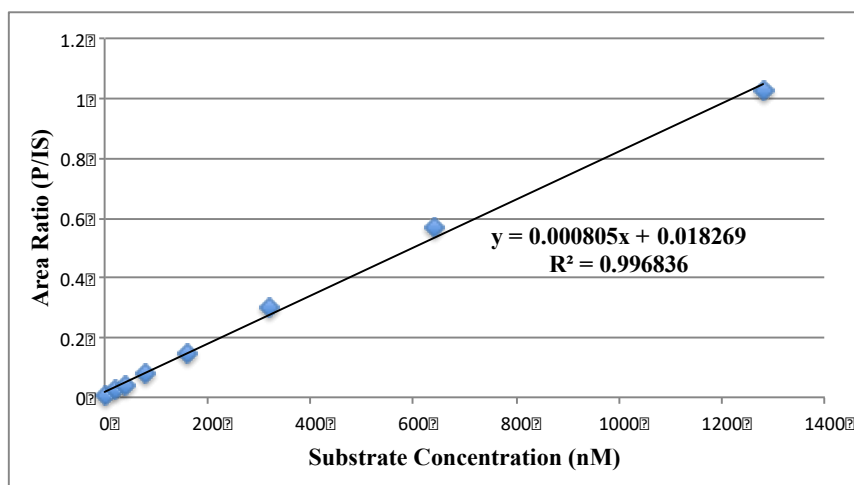
Figure 4.3 LC-MS/MS standard curve of 7.

Each point is the result of an area ratio of 7 and internal standard 8.

Table 4.3 LC-MS/MS data for CurK DH substrate 1

Conc. 3.5 (nM)	Transition (g/mol)	Peak Area	Area Ratio (3.7/4.6)	Conc. 3.7 (nM)	Velocity (nM/min)	×100 (dil.)	Velocity (μM/min)
Blank	268→121	9949.448					
Blank	242→95	23056.428					
Blank	268→121	27593.916					
Blank	242→95	69868.674					
0.25	268→121	45799.656	0.0487	37.8	9.45	945.4	0.945
0.25	242→95	940210.259					
0.25	268→121	51390.985	0.0558	46.6	11.7	1166.1	1.166
0.25	242→95	920671.740					
0.50	268→121	153218.239	0.164	181.4	45.4	4535.9	4.536
0.50	242→95	932404.409					
0.50	268→121	88632.4536	0.0973	98.2	24.5	2455.3	2.455
0.50	242→95	910653.094					
1.00	268→121	154376.557	0.171	189.9	47.5	4746.6	4.747
1.00	242→95	902209.734					
1.00	268→121	177808.667	0.186	208.7	52.2	5217.6	5.218
1.00	242→95	954541.380					
2.00	268→121	359675.683	0.397	471.0	117.7	11774.6	11.775
2.00	242→95	905047.196					
2.00	268→121	425682.053	0.452	539.4	134.9	13485.8	13.486
2.00	242→95	940703.784					
3.00	268→121	587242.104	0.610	735.1	183.8	18378.3	18.378
3.00	242→95	962612.388					
3.00	268→121	551492.214	0.607	732.2	183.0	18304.5	18.305
3.00	242→95	907545.802					
6.00	268→121	1015127.87	1.03	1252.	313.0	31299.8	31.300
6.00	242→95	989286.137					
6.00	268→121	900205.392	0.841	1022.	255.6	25557.8	25.558
6.00	242→95	1070107.51					

Overnight incubation of CurDHs with synthetic NAC substrates

Incubations were carried out following a similar procedure to that of the kinetic analysis of CurK-DH. Briefly, substrates **1**–**6**, **20**–**21**, or product **8** (1 mM) were individually incubated with enzyme (5 μM) (CurF-DH, CurH-DH, CurJ-DH and CurK-DH) in reaction buffer (50 mM Tris, 150 mM NaCl, pH 8.0) at 23 °C for 14 h (or a set time period in the case of the CurK-DH time course experiment) in a total volume of 100 μL. Samples (5 μL) were quenched with 495 μL quench solution (1:1 MeCN–H_2O). The mixture was centrifuged, and the supernatant was directly analyzed by LC-MS/MS using the method described above. Chromatograms were generated by extraction of raw the LC-MS/MS data with Analyst software and plotted with Prism software (Fig. 4.4).
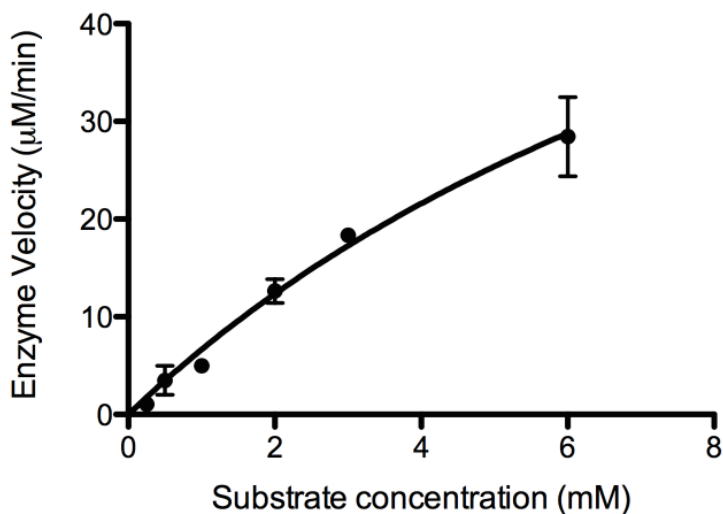
Figure 4.4 Michaelis-Menten Analysis of CurK-DH with substrate 1.

Chemoenzymatic synthesis of 1 by CurK-DH. S-(2-Acetamidoethyl) (2E,4E,6E)-4-methylnona-2,4,6-trienethioate (7)

A solution sterile H_2O (3.82 mL) and a small amount of $10\times$ TRIS buffer solution (1.50 M NaCl, 0.500M TRIS-HCl, pH 8.0) (0.600 mL) was briefly vortexed. To the buffered solution was added a DMSO– H_2O (1:1) stock solution (50 mM) of the β-hydroxy thioester substrate **1** (0.700 mL, 10.0 mg, 35.0 μmol). The mixture was vortexed to mix and the CurK dehydratase (8.19 mg/mL, 0.684 mL, 5.60 mg, 0.160 μmol) was added. The mixture was briefly inverted and covered with aluminum foil to shield from light. The reaction mixture was shaken (200 rpm) at 23 °C in the dark for 14 h. The reaction mixture was extracted with EtOAc (4×10.0 mL) and the combined extracts were dried (Na_2SO_4), filtered and concentrated under reduced pressure. The crude extract was purified by flash chromatography (95:5 CH_2Cl_2–MeOH) affording the title compound (2.52 mg, 25%) as a transparent light yellow oil: $R_f = 0.35$ (95:5 CH_2Cl_2–MeOH); ^{1}H NMR (CDCl$_3$, 400 MHz) δ 7.30 (d, $J = 15.6$ Hz, 1H), 6.46 (d, $J = 11.2$ Hz, 1H), 6.40 (app. t, $J = 13.6$ Hz, 1H), 6.15 (d, $J = 15.2$ Hz, 1H), 6.05 (dt, $J = 13.6, 6.4$ Hz, 1H), 5.98 (br, 1H), 3.48 (q, $J = 6.0$ Hz, 2H), 3.12 (t, $J = 6.4$ Hz, 2H), 2.22 (app. quint, $J = 6.8$ Hz, 2H), 1.97 (s, 3H), 1.87 (s, 3H), 1.06 (t, $J = 7.6$ Hz, 3H); ^{13}C NMR (CDCl$_3$, 100 MHz) δ 190.5, 170.6, 146.5, 143.6, 141.6, 131.2, 125.8, 122.8, 40.3, 28.5, 26.6, 23.4, 13.4, 12.5; HRMS (ESI+) *m/z* calcd for $C_{14}H_{21}NO_2SNa^+$ [M + Na]$^+$ 290.1185, found 290.1208 (error 7.9 ppm).

Results

Substrate design and synthesis

We set out to synthesize potential substrates to profile the dehydratase activity of the four DH domains in the pathway (Fig. 4.5). The distal thiazoline and cyclopropyl moieties were eliminated to reduce molecular complexity and enhance solubility of the substrates. Synthesis of the truncated CurK-DH tetraketide **1** began with a Horner-Wadsworth-Emmons reaction between *trans*-2-pentenaldehyde (**9**) and triethyl 2-phosphonopropionate (**10**) to afford the *trans-trans*-dienoate **11** in quantitative yield (Scheme 4.1). The dienoate was reduced with diisobutylaluminum hydride (DIBAL-H) and oxidized to aldehyde **13** employing MnO_2. Asymmetric aldol reaction of **13** with Nagao's D-valine-derived thiazolidinethione **14** provided alcohol **15** as a single diastereomer[29]. Facile displacement of the chiral auxiliary with *N*-acetylcysteamine (NAC) furnished **1**. The enantiomeric tetraketide **2** was prepared in an analogous fashion using the L-valine-derived thiazolidinethione. The CurK product **7** was obtained chemoenzymatically from **1** employing CurK-DH.

The truncated CurJ triketide substrates were synthesized using Crimmins' and Evans' aldol chemistry that allows access to all four possible stereoisomers from common intermediate **9** and the D-phenylalanine-derived thiazolidinethione **17** or its enantiomer by varying the Lewis acid and amine base (Scheme 4.1)[30-31]. The *syn*-aldol adduct **18** was obtained in a respectable 72% yield and converted to the required NAC thioester **4** by treatment with *N*-acetylcysteamine (Scheme 4.1B). The *anti*-aldol adduct **19** was isolated in 17% yield and analogously elaborated to the NAC thioester **3** (Scheme 4.1C). We attribute the consistently poor yield of the *anti*-aldol transformation to a limitation of the Evans' methodology when using aliphatic enals with an
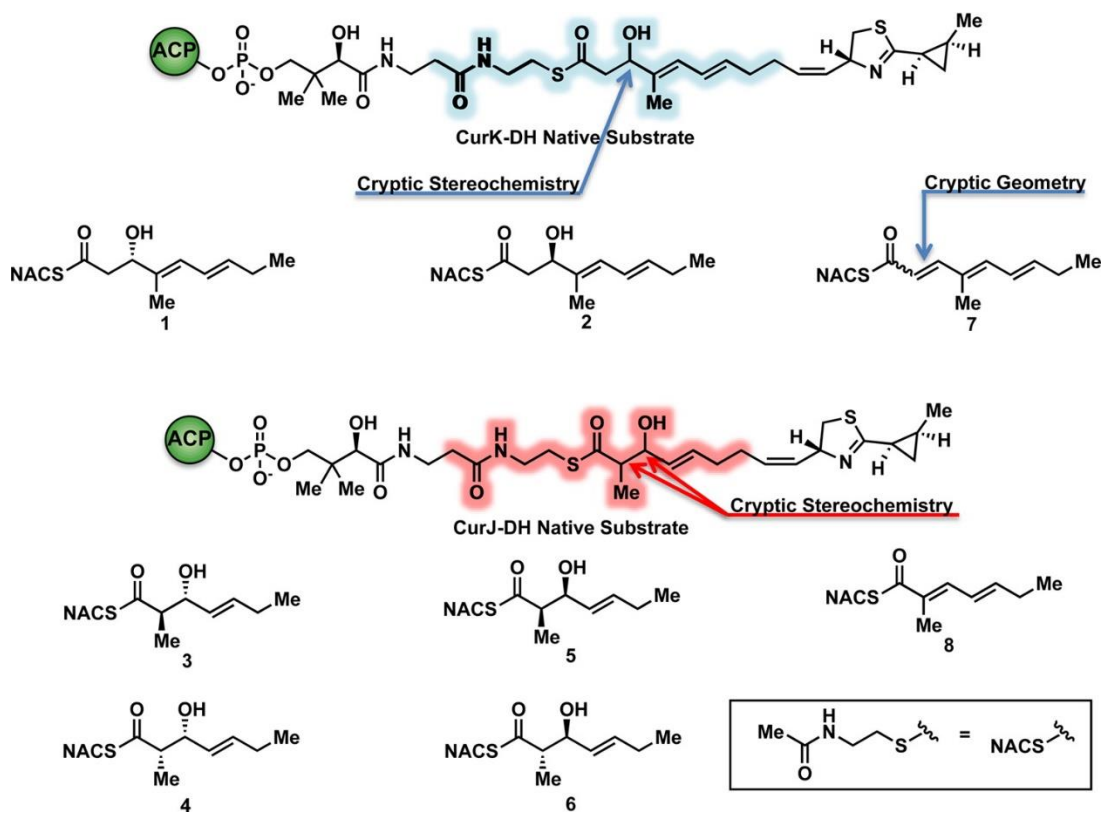
Figure 4.5 CurJ and CurK truncated substrates and products.
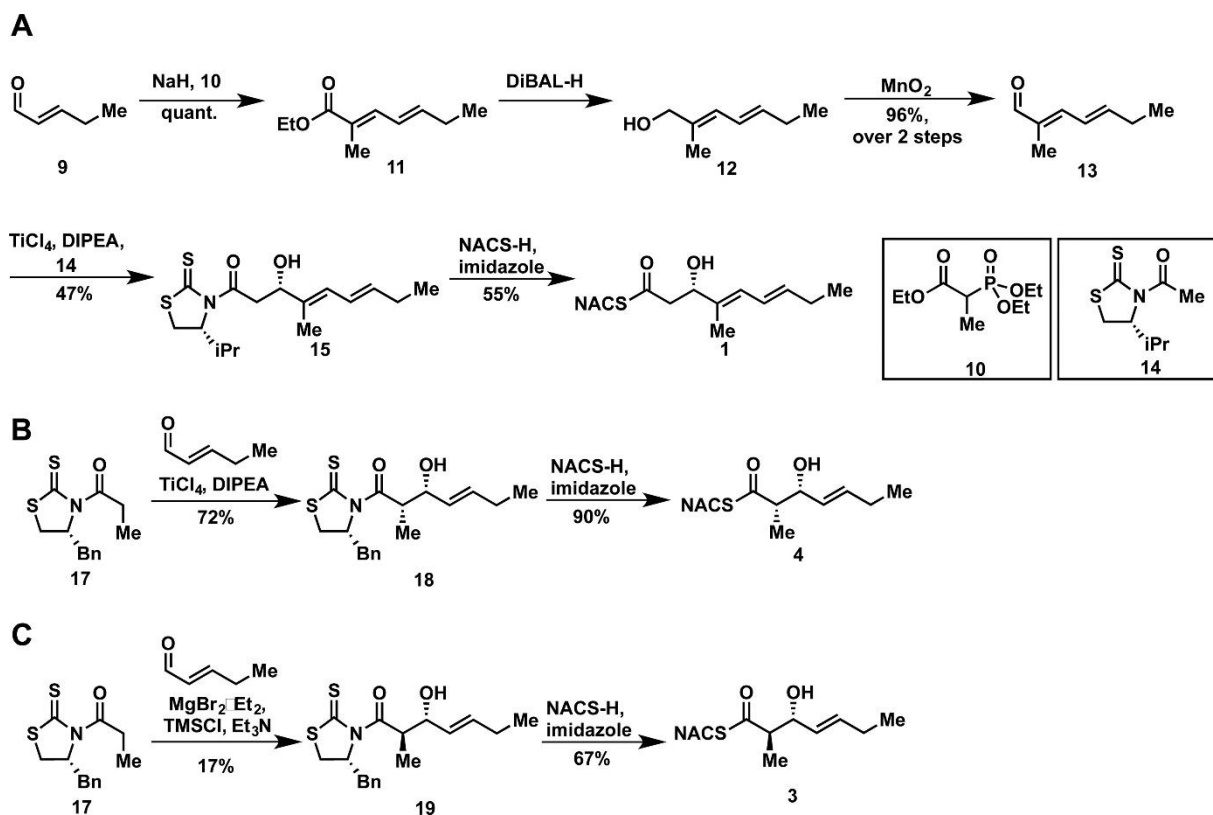
Scheme 4.1 Synthesis of CurK-DH substrate 1 and the CurJ substrates 3 and 4[a].

[a]Abbreviations: DIBAL-H, diisobutylaluminum hydride; DIPEA, diisopropylethylamine; NAC, N-acetylcysteamine

exchangeable γ-proton that may polymerize under the reaction conditions. The enantiomers of **3** and **4** were synthesized in an analogous way utilizing L-phenylalanine-derived thiazolidinethione auxiliary to afford **6** and **5**, respectively. Additionally, the truncated CurJ product **8** was synthesized through a Horner-Wadsworth Emmons reaction (Scheme 4.2)[32-33].
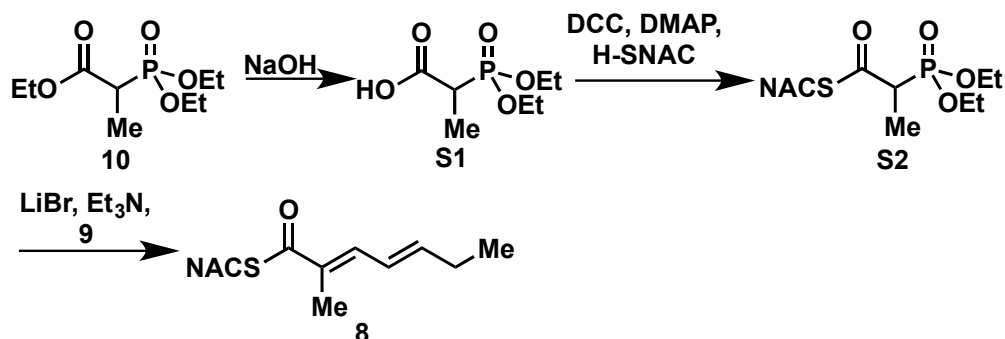
Scheme 4.2 Synthesis of diene 8.

Biochemical characterization of Cur DHs with 1 and 2

The four recombinant dehydratase domains (CurK-DH, CurJ-DH, CurH-DH, and CurF-DH) were individually incubated overnight at 37 °C with NAC esters **1** and **2** and analyzed via LC-MS/MS. CurK-DH dehydrated its truncated substrate in a completely stereospecific fashion, selectively acting only on the D-alcohol **1** with no turnover for L-alcohol **2**, whereas CurH-DH was unable to process either **1** or **2** (Figs. 4.6A, B). This matches the predicted stereospecificity of the CurK-KR containing the signature LDD motif for B-type ketoreductases[34]. Curiously, CurF-DH and CurJ-DH also turned over **1**, but not **2**, in a stereospecific fashion. While CurF-DH maintained comparable total conversions with that of CurK-DH (55% of CurK-DH), the CurJ-DH was drastically deficient in its ability to catalyze the same transformation (7% of CurK-DH) (Fig. 4.6C). A single reaction product from **1** and CurK-DH was observed, which was isolated in 25% overall yield from the overnight reaction mixture. The dehydrated substrate was analyzed

via ^{1}H and ^{13}C NMR and confirmed as the all *trans*-trienoate **7**. This result is consistent with the empirically based prediction that the enzymatic dehydration of D-alcohols affords *E*-olefins[35-36]. A time course study of the dehydration of **1** (1 mM) by CurK-DH (5 μM) revealed that the enzyme rapidly dehydrates nearly all of the substrate, reaching completion within 20 min (Fig. 4.6D). Steady-state kinetic analysis of the CurK-DH catalyzed dehydration of **1** to **7** was quantified by LC-MS/MS under initial velocity (v_0) conditions (Tables 4.2, 4.3, Figs. 4.3, 4.4). The resulting saturation curve (v_0 versus [**1**]) was fit to the Michaelis-Menten equation to provide an apparent K_M of 12.0 ± 4.7 mM and k_{cat} of 72 ± 21 s^{-1} resulting in a specificity constant (k_{cat}/K_M) of $(6.00 \pm 1.41) \times 10^3$ M^{-1} s^{-1}. While the K_M value is similar to other NAC thioester substrates with their cognate excised PKS DH domains, the k_{cat} value is nearly three orders of magnitude greater than any previously characterized PKS DH domain[37-38].
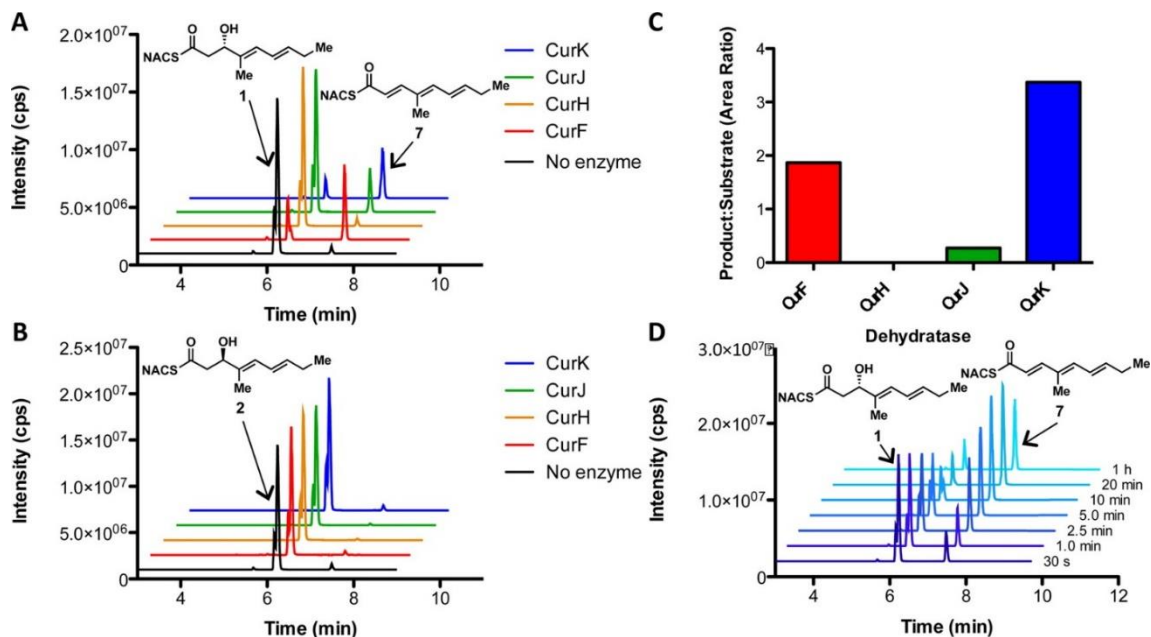
Figure 4.6 Incubation studies of synthetic CurK-DH substrates 1 and 2.

Extracted chromatograms of 14 h incubations of all curacin DH domains with substrates **1** (A) and **2** (B). CurF-DH, CurJ-DH, and CurK-DH all display stereospecificity for d-alcohol (**1**) over the l-alcohol (**2**). (C) Ratio of peak areas (**7**:**1**) for each curacin dehydratase enzyme subtracting negative control (no enzyme). CurF-DH and CurK-DH efficiently produce the triene **7**, with a lesser amount produced by CurJ-DH. (D) Time course extracted chromatograms of CurK-DH (5 μM) with substrate **1** (1 mM). The enzyme reaches equilibrium by 20 min. The transition m/z $268 \rightarrow 121$ was used to monitor both residual substrates (**1** and **2**) as well as product (**7**) formation for all extracted chromatograms due to spontaneous dehydration of the substrate under the MS ionization conditions. The recurring shoulder on compounds **1** and **2** is believed to be minor trans,cis-isomers arising from isomerization during assay conditions.

To probe the reaction mechanism and facilitate co-crystallization with substrates we prepared catalytically inactive point mutants His996Phe and Asp1169Asn of the His-Asp catalytic dyad in CurK-DH based on sequence alignment and the reported CurK-DH structure[10]. The His996Phe mutant was devoid of activity while the Asp1169Asn mutant retained small, but measurable activity showing 2–3% conversion of **1** to **7** after 12 hours. Crystal structures of both His996Phe and Asp1169Asn CurK-DH mutants were determined at 1.4 and 1.65 Å resolution, respectively (Tables 4.4 – 4.6, Figs. 4.7, 4.8)[10]. The structures of the mutant proteins were virtually identical to the wild type CurK-DH (RMSD of 0.11 Å for 509 Cα atoms) with no significant conformational changes in the active site. Co-crystallization trials of substrate **1** and either mutant of wild type CurK-DH resulted in no crystal growth under conditions that readily yielded crystals in absence of substrate. Crystal soaking experiments with **1** resulted in a rapid dissolution of the crystals, suggesting that substrate binding may induce a conformational change and destabilize the crystal form.

Table 4.4 Crystallographic summary for CurK DH

Data	CurK H996F	CurK D1169N
Space group	$P2_12_12_1$	$P2_12_12_1$
Unit cell a, b, c (Å)	38.11, 94.57, 152.00 (90, 90, 90)	38.22, 94.51, 151.70 (90, 90, 90)
Wavelength (Å)	1	1
$d_{min\,(Å)}$	1.428 (1.479 - 1.428)	1.648 (1.707 - 1.648)
Observations (#)	1,300,944 (96,298)	860, 172 (75,239)
Unique reflections	100,090 (8,843)	67,404 (6,535)
Mean I/σ_I	28.15 (2.74)	25.41 (2.07)
R_{merge}	0.04 (0.72)	0.05 (1.10)
$CC_{1/2}$	1 (0.83)	1 (0.70)
CC*	1 (0.95)	1 (0.91)
Completeness (%)	0.97 (0.87)	1 (0.99)
Wilson B ($Å^2$)	19.44	26.49
Refinement		
Reflections (#)	100,088 (8,843)	67,401 (6,535)
R_{work}	0.20 (0.25)	0.20 (0.28)
R_{free}	0.22 (0.29)	0.23 (0.31)
RMSD bonds (Å)	0.013	0.01
RMSD angles (Å)	1.32	1.21
Atoms (#)		
Protein	4,444	4436
Solvent	168	46
Ligand	0	0
Avg B-factors ($Å^2$)		
Protein	27.56	36.22
Solvent	30	30.39
Ligand	n/a	n/a
Ramachandran		
Favored (%)	98	97.4
Allowed (%)	1.64	2.6
Outliers (%)	0.36	0

* Values in parentheses refer to the outermost shell of data.
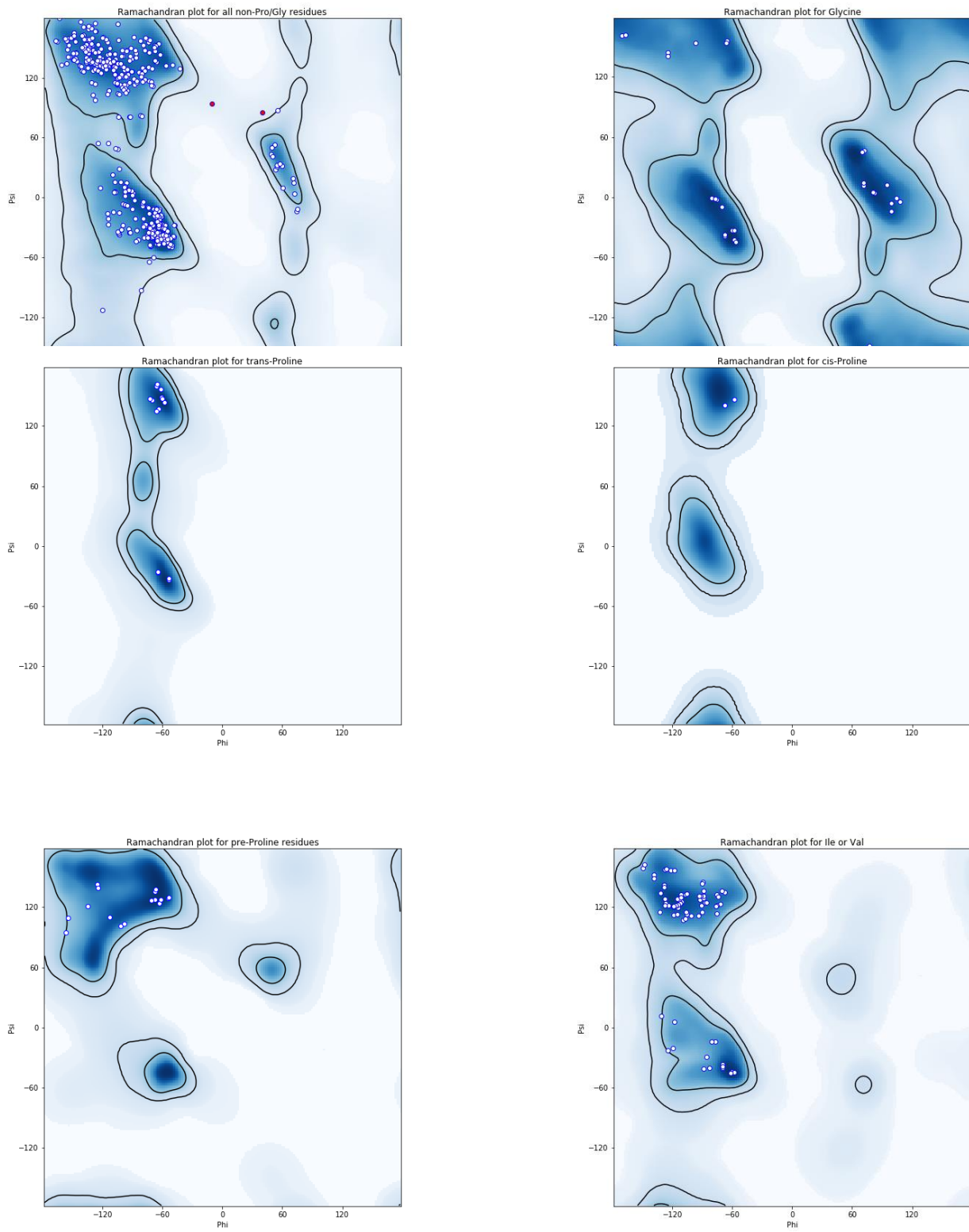
Figure 4.7 Ramachandran plots for CurK H996F
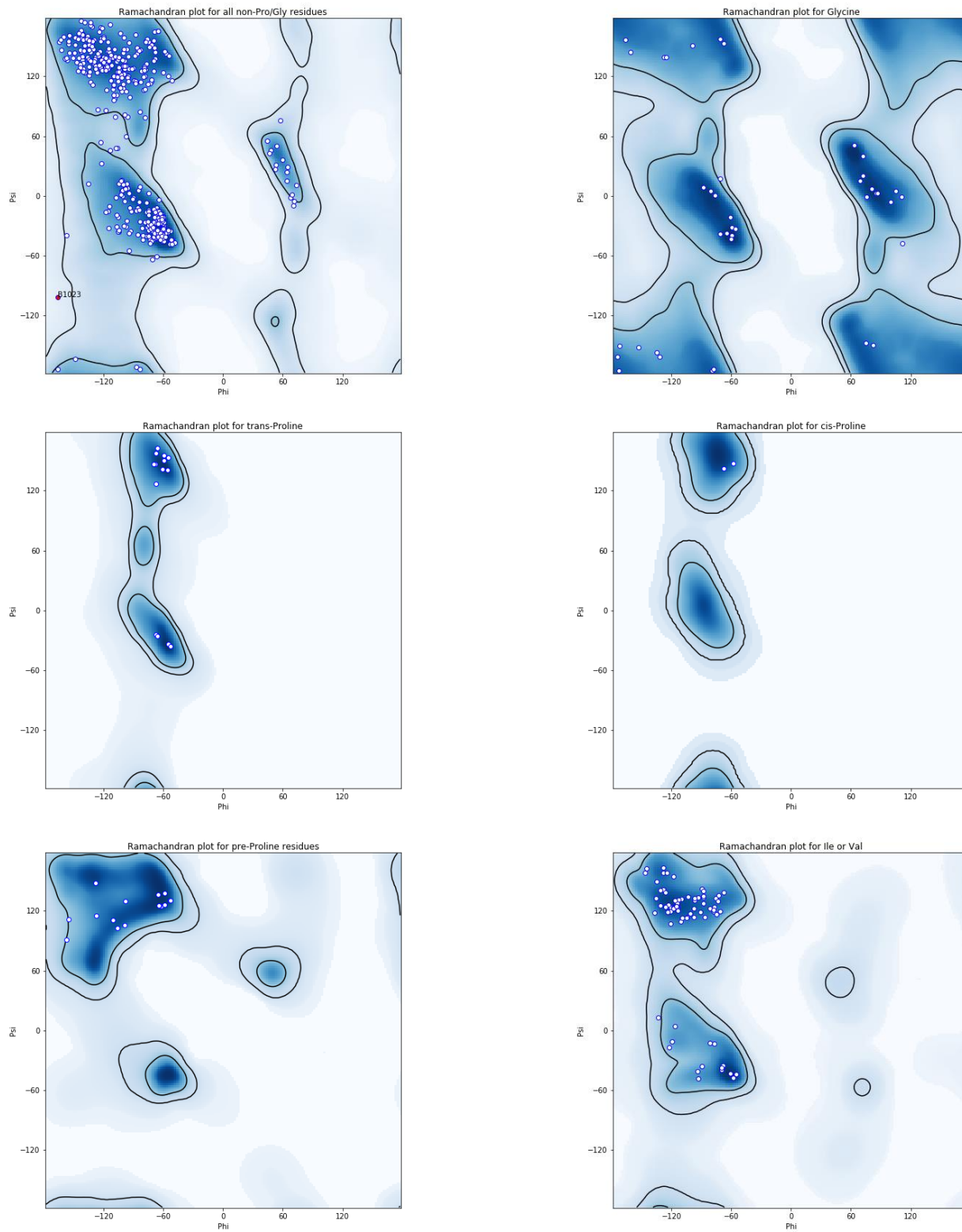
Figure 4.8 Ramachandran plots for CurK D1169N

Table 4.5 X-ray data statistics for CurK H996F

Resolution	N(obs)	N(uniq)	Mult.	Compl.	<I/sigma>	R-merge	R-meas	CC$_{1/2}$
47.31 - 3.08	131398	10759	12.21	99.84	61.9	0.033	0.034	1.000
3.08 - 2.45	136117	10340	13.16	99.55	51.9	0.04	0.041	0.999
2.45 - 2.14	135262	10199	13.26	99.23	42.8	0.049	0.051	0.999
2.14 - 1.94	135359	10112	13.39	98.53	32.9	0.063	0.066	0.999
1.94 - 1.80	132151	10013	13.2	98.39	21.3	0.098	0.102	0.997
1.80 - 1.70	137670	9947	13.84	97.62	15.3	0.144	0.149	0.995
1.70 - 1.61	129040	9955	12.96	97.8	9.9	0.22	0.229	0.987
1.61 - 1.54	133388	9860	13.53	97.25	7.2	0.311	0.323	0.978
1.54 - 1.48	130974	9799	13.37	96.83	4.7	0.472	0.491	0.952
1.48 - 1.43	99064	8961	11.06	88.7	2.7	0.716	0.75	0.835
47.28 - 1.43	1300423	99945	13.01	97.4	25.8	0.045	0.046	1.000

Table 4.6 X-ray data statistics for CurK D1169N

Resolution	N(obs)	N(uniq)	Mult.	Compl.	<I/sigma>	R-merge	R-meas	CC$_{1/2}$
47.28 - 3.55	82464	7100	11.61	99.87	65.1	0.029	0.031	1.000
3.55 - 2.82	84857	6814	12.45	99.99	50.8	0.039	0.041	0.999
2.82 - 2.46	89339	6773	13.19	100	34.8	0.063	0.066	0.999
2.46 - 2.24	86684	6662	13.01	100	25.5	0.089	0.092	0.998
2.24 - 2.08	87860	6709	13.1	100	18.5	0.128	0.133	0.996
2.08 - 1.96	90476	6677	13.55	100	12.7	0.195	0.203	0.992
1.96 - 1.86	84142	6643	12.67	100	7.1	0.345	0.359	0.974
1.86 - 1.78	87274	6648	13.13	100	4.5	0.547	0.569	0.940
1.78 - 1.71	88669	6607	13.42	100	3.2	0.784	0.815	0.881
1.71 - 1.65	77926	6613	11.78	99.95	2	1.09	1.14	0.733
44.59 - 1.65	859691	67246	12.78	99.98	22.8	0.053	0.056	1.000

CurK-DH and CurF-DH outcompete CurJ-DH in the dehydration of its predicted substrate

We next evaluated the diastereomeric triketide substrates **3–6** with all four Cur DHs (Fig. 4.3). Interestingly, only CurK-DH and CurF-DH were able to turn over the predicted CurJ-DH substrate **3**, arising from the B1-type CurJ-KR, affording the conjugated *trans-trans*-dienoate **8** (Fig. 4.9A)[39]. Neither of the *syn*-triketide substrates **4** and **5** nor the *anti*-triketide **6** were processed by any of the Cur DHs (Figs. 4.9B, C, D). This reaffirms the substrate specificity of CurF-DH and CurK-DH for D-configured alcohols at the β-position. The *trans*-olefin can only be formed through a *syn*-elimination of the α-proton and β-hydroxy group in **3** and thus provides the first confirmation for this mechanism for a PKS substrate lacking an α-substituent. From a biosynthetic perspective, the inability of CurJ-DH to process any of the truncated triketide substrates was unexpected, especially in light of the high activity of CurK-DH with its predicted truncated tetraketide substrate **1**. This is in stark contrast to CurJ-DH's ability to accommodate substrate **1**, a D-alcohol lacking an α-substituent, albeit with marginal catalytic efficacy. Furthermore, these results rule out the classic "stuttered" dehydration pathway because the same substrate would be used for the second elimination. As both CurH and CurJ immediately follow modules without DH domains (i.e. CurG and CurI) we sought an alternative hypothesis for dehydration.
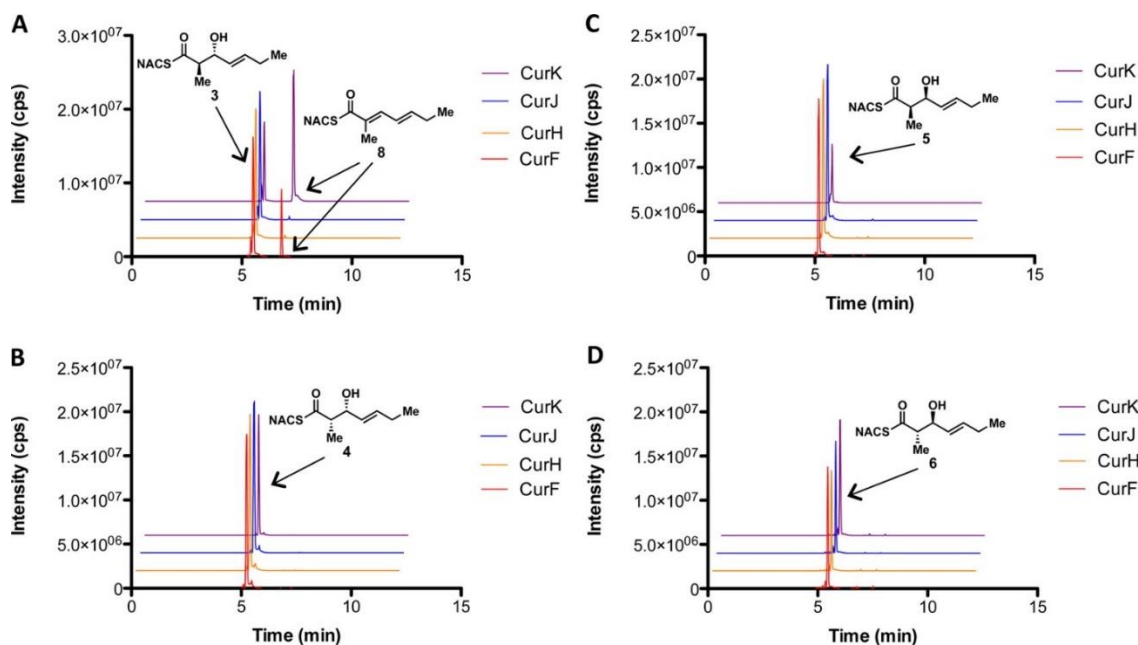
Figure 4.9 Overnight incubations of the putative triketide CurJ-DH substrates with all curacin PKS DHs.

LC-MS/MS extracted ion chromatograms with diastereomers **3** (A), **4** (B), **5** (C), and **6** (D). In each panel, the LC-MS/MS extracted ion chromatograms are stacked with the traces for each enzyme color-coded: red for CurF, orange for CurH, blue for CurJ, and purple for CurK. The transition m/z 242 → 95 was used to monitor both remaining substrate as well as product formation due to spontaneous dehydration under the MS ionization conditions. The anti-triketide **3** (panel A) is the only substrate that showed turnover by the appearance of a peak at 6.8 min corresponding to the dehydration product (this was only observed with CurK-DH and CurF-DH).

CurJ-DH and CurH-DH harbor vinylogous dehydration activity

The simplest proposal is that the KR products from modules lacking dehydratases are carried through to the next module. After extension and reduction, the resulting β,δ-dihydroxy thioester could first be eliminated in the normal fashion (α, β) followed by a vinylogous elimination (γ, δ) yielding the diene (Fig. 4.11). Truncated δ-hydroxy-α,β -unsaturated thioester substrates **20** and **21** were synthesized to test this hypothesis (Fig. 4.10, Scheme 4.3). No dehydration products were observed upon incubation with the L-alcohol substrate **20** (Fig. 4.11A). Overnight incubation with all four DH domains revealed that only CurH-DH and CurJ-DH were able to stereospecifically process the D-alcohol substrate **21** to afford the *trans-trans*-dienoate product **8** (Fig. 4.11B). Since the reaction is theoretically reversible, we next investigated the hydration reaction through incubation of *trans-trans*-dienoate **8** with each Cur DH domain. Consistent with the previous results, only CurH-DH and CurJ-DH were able to catalyze the reverse reaction, namely the regiospecific and stereospecific conversion of *trans-trans*-dienoate **8** exclusively to **21** when compared to controls, albeit at a low total conversion (<1%) (Fig. 4.11C). Both the inability of the enzyme to reach a stable equilibrium and markedly slow reaction rate compared to the α,β-dehydration catalyzed by CurK indicate that the truncations of substrate **21** severely attenuate enzyme reactivity. The mechanism of this novel elimination was then probed through site-directed mutagenesis of the His-Asp catalytic dyad in both CurH-DH and CurJ-DH. In this case, the catalytic histidine was mutated to alanine and phenylalanine to afford CurH(H971A), CurH(H971F), CurJ(H978A), and CurJ(H978F) mutants. Similarly, the catalytic aspartate was mutated to asparagine yielding CurH(D1136N) and CurJ(D1156N). All mutants were completely devoid of activity towards **21** highlighting their critical role in this novel elimination reaction (Fig. 4.11D).
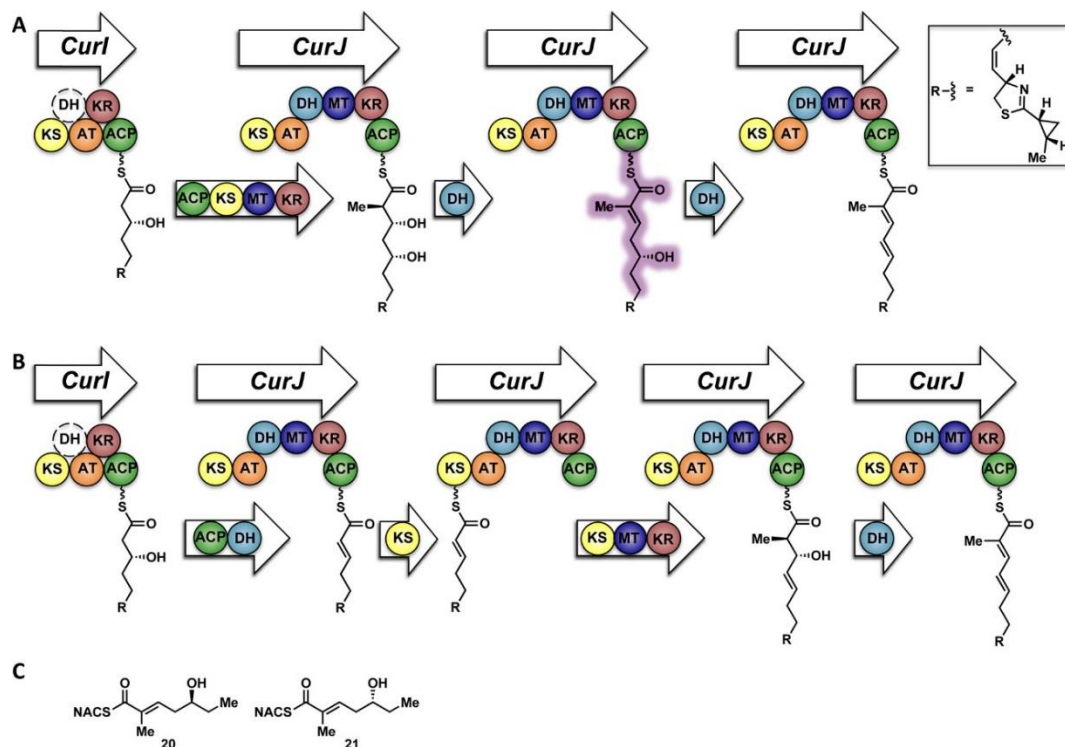
Figure 4.10 Proposed routes for elimination in the case of missing dehydratases.

(A) Our proposed vinylogous elimination route in module J. The polyketide intermediate from CurI is loaded onto CurJ for normal extension, methylation, and ketoreduction. The CurJ-DH eliminates the β-alcohol followed by a subsequent elimination of the δ-alcohol. (B) Classical stuttering mechanism based on predictions in other biosynthetic pathways. The polyketide intermediate from CurI is transferred directly onto the CurJ-ACP and dehydrated by the CurJ-DH. The ACP-bound intermediate is then transferred to the CurJ-KS for normal extension, methylation, and ketoreduction. A final dehydration by CurJ-DH furnishes the putative CurJ product. (C) Enantiomeric vinylogous CurJ-DH substrates 20 and 21. The design of the vinylogous substrates is based on the putative native substrate shown highlighted in violet in panel A.
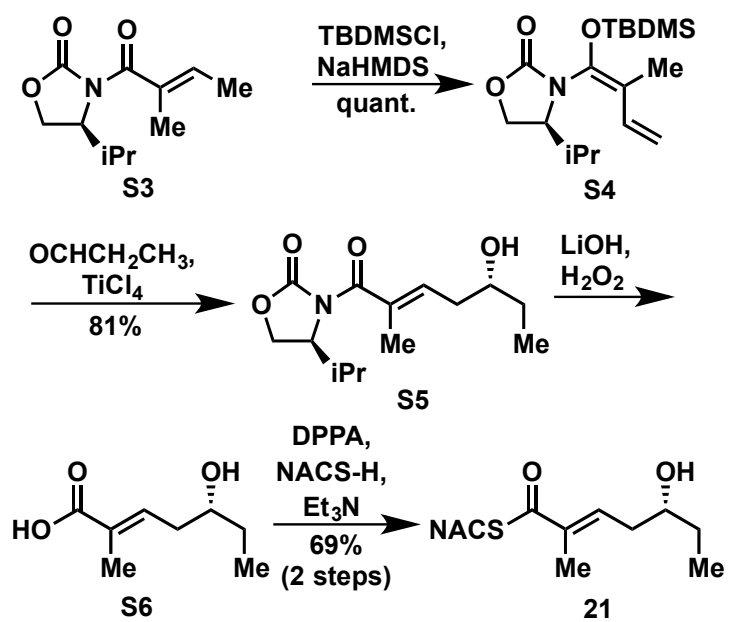
Scheme 4.3 Synthesis of vinylogous substrate 21.
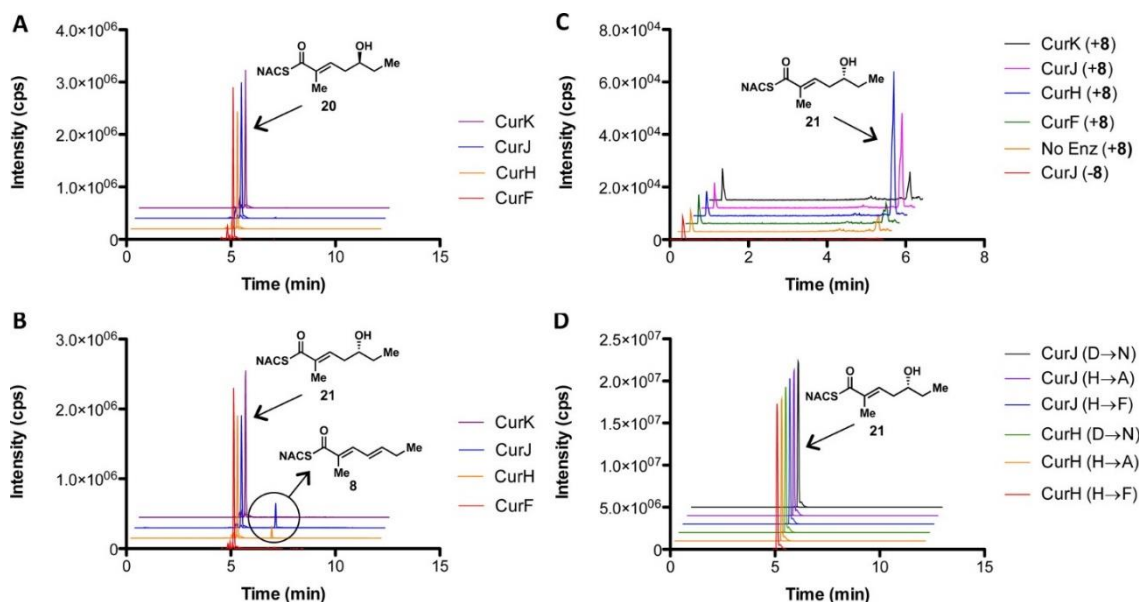
Figure 4.11 Vinylogous elimination of δ-hydroxy-α,β-unsaturated thioester substrates by curacin DH domains.

(A,B) LC-MS/MS extracted ion chromatograms obtained after overnight incubations of substrates 20 (A) and 21 (B) with each Cur DH monitoring the transition at m/z 242 → 95 for product dienoate 8 (peak at 6.8 min) and m/z 260 → 141 (peak at 5.1 min) for the residual substrates. In each panel, the LC-MS/MS extracted ion chromatograms are stacked with the traces for each enzyme color-coded: red for CurF-DH, orange for CurH-DH, blue for CurJ-DH, and purple for CurK-DH. The l-alcohol substrate 20 shown in panel A is not a substrate for any of the Cur DHs, whereas the d-alcohol substrate 21 shown in panel B is converted to the corresponding dienoate 8 only by CurJ-DH and CurH-DH. (C) Hydration of dienoate 8. Compared to negative control (without 8 or without CurJ-DH), only CurH-DH and CurJ-DH form 21 in the presence of 8. (D) Overnight incubation of the six CurJ-DH and CurH-DH catalytic dyad point mutants, scanning for the same transitions as previous panels. All mutants are devoid of activity, as evidenced by the absence of a peak at 6.8 min.

173

To visualize the binding of a vinylogous substrate to a DH, **21** was co-crystallized with the catalytically inactive H978F variant of the CurJ DH (Tables 4.7, 4.8, Fig. 4.12). Crystals grew more slowly in presence of compound (30 days compared to 2 days without substrate). In the 2.4-Å structure of the DH dimer, new density appeared in the active site of one monomer, adjacent to Asp1156 and within the hydrophobic substrate tunnel (Figs. 4.13, 4.14). Strong density was present for only the acyl portion of **21** and we assume that the polar *N*-acetylcysteamine was hydrolyzed during the long crystal growth period. The substitution of Phe for the catalytic His978 resulted in no change to the protein backbone conformation. The best fit of hydrolyzed **21** to the new density placed the δ-OH group within hydrogen bonding distance of Asp1156, in the same position as a water molecule in the free-enzyme structure[10]. The acid **21** was bound such that dehydration would proceed via the classic *syn* elimination mechanism of both PKS and FAS DHs.

Table 4.7 Crystallographic summary For CurJ DH

Data	CurJ H978F
Space group	$P2_12_12_1$
Unit cell a, b, c (Å)	47.55, 70.58, 176.02 (90, 90, 90)
Wavelength (Å)	1
$d_{min\ (Å)}$	2.4 (2.486 - 2.4)
Observations (#)	302,198 (30,140)
Unique reflections	23,985 (2,331)
Mean I/σ_I	18.08 (2.07)
R_{merge}	0.09 (1.44)
$CC_{1/2}$	0.99 (0.77)
CC^*	1 (0.93)
Completeness (%)	1 (1)
Wilson B (Å^2)	62.41
Refinement	
Reflections (#)	23,944 (2304)
R_{work}	0.188 (0.349)
R_{free}	0.242 (0.376)
RMSD bonds (Å)	0.009
RMSD angles (Å)	1.06
Atoms (#)	
Protein	4587
Solvent	22
Ligand	11
Avg B-factors (Å^2)	
Protein	111.02
Solvent	99.82
Ligand	62.58
Ramachandran	
Favored (%)	97.26
Allowed (%)	2.2
Outliers (%)	0.54

* Values in parentheses refer to the outermost shell of data.
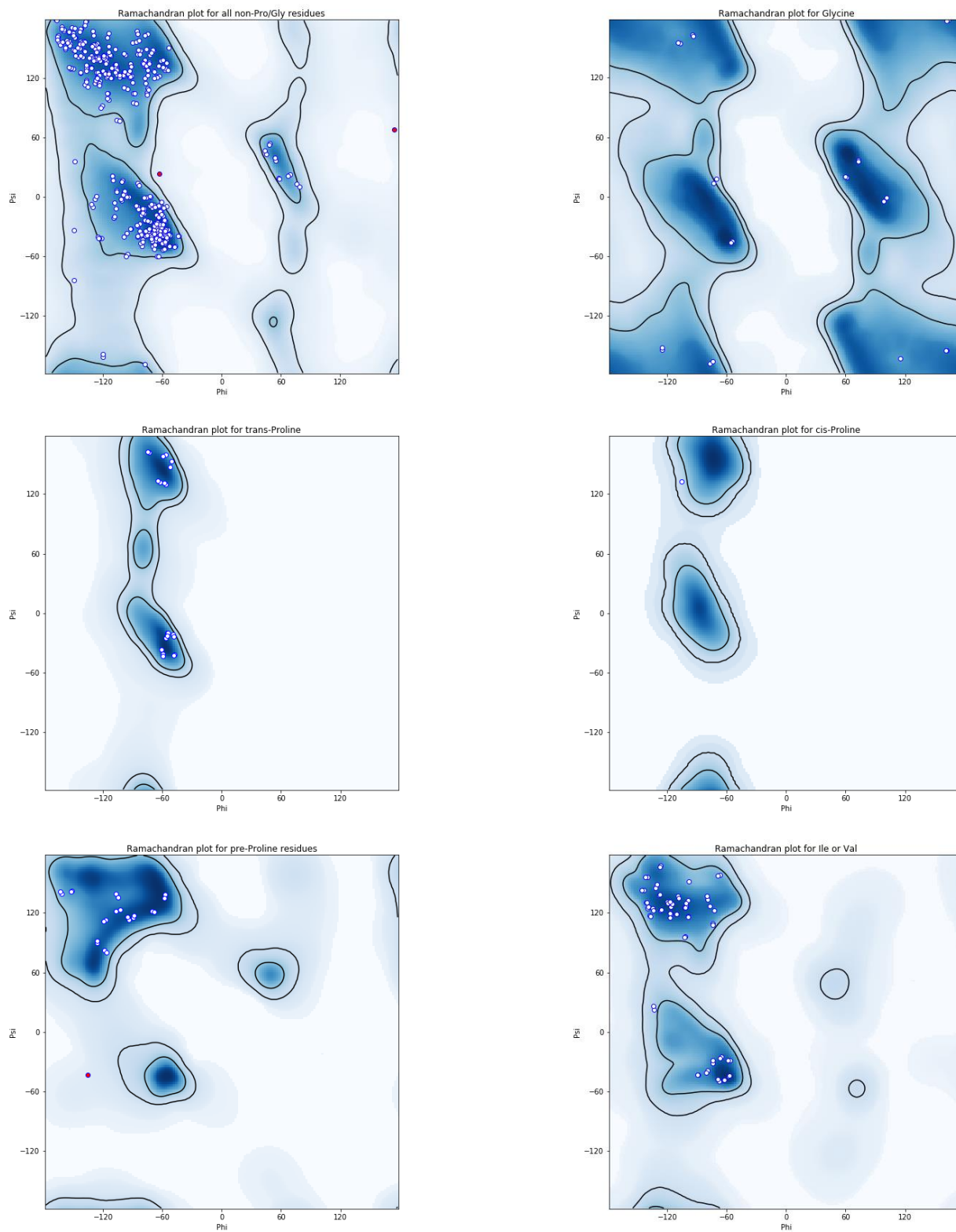
Figure 4.12 Ramachandran plots for CurJ H978F.

Table 4.8 X-ray data statistics for CurJ H978F

Resolution	N(obs)	N(uniq)	Mult.	Compl.	$\langle I/sigma \rangle$	R-merge	R-meas	$CC_{1/2}$
45.91 - 5.17	27490	2577	10.67	99.96	38.3	0.045	0.048	0.999
5.17 - 4.10	29081	2446	11.89	100	36.5	0.055	0.058	0.999
4.10 - 3.58	28639	2400	11.93	99.92	26.1	0.083	0.086	0.998
3.58 - 3.26	31360	2406	13.03	100	20	0.124	0.129	0.997
3.26 - 3.02	31547	2375	13.28	100	12.4	0.235	0.244	0.993
3.02 - 2.85	29903	2359	12.68	99.96	8.1	0.371	0.387	0.985
2.85 - 2.70	30720	2369	12.97	100	4.9	0.593	0.618	0.966
2.70 - 2.59	31433	2359	13.32	100	3.3	0.837	0.87	0.925
2.59 - 2.49	31885	2357	13.53	99.96	2.5	1.138	1.183	0.893
2.49 - 2.40	30163	2339	12.9	100	1.9	1.44	1.499	0.775
45.91 - 2.40	302221	23987	12.6	99.98	15.7	0.09	0.094	0.999
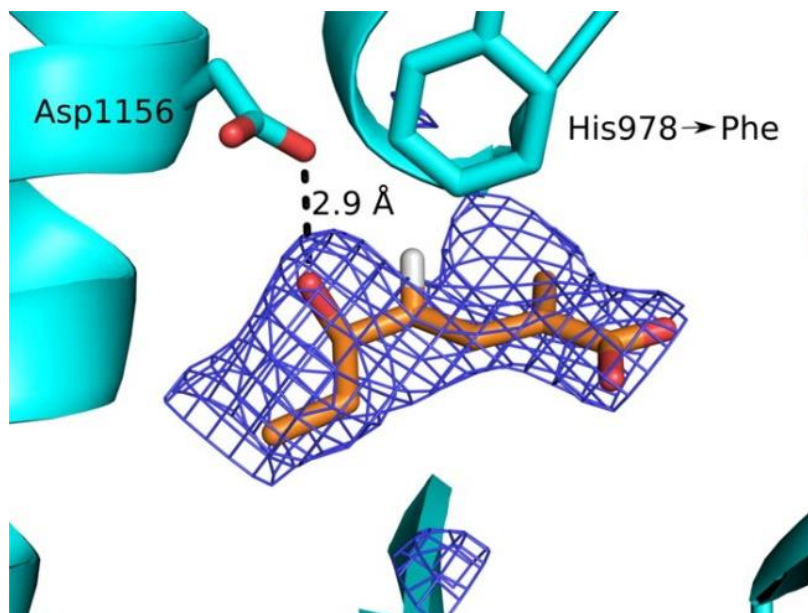
Figure 4.13 CurJ-DH H978F variant co-crystallized with the hydrolyzed form of compound 21.

The δ-hydroxyl group of carboxylate 21 is within hydrogen bonding distance of Asp1156 (blue SA omit electron density contoured at 2.5σ). Hydrolyzed 21 (sticks with atom coloring: orange, C; red, O; white, H; only the pro-R H atom is shown) is within 4 Å of the Phe substitution for His978 (sticks with cyan, C).
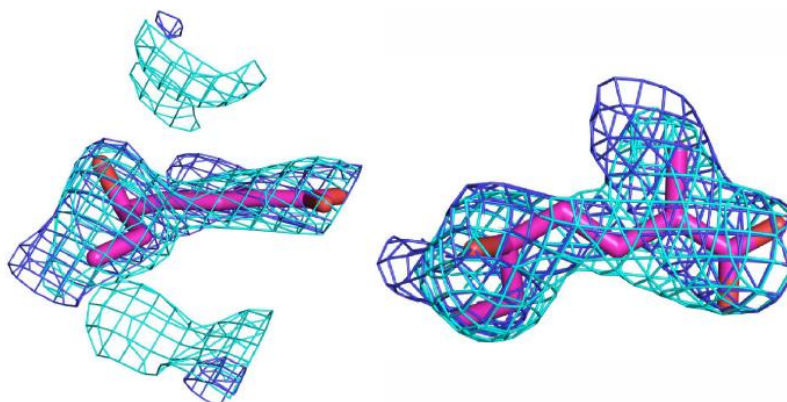
Figure 4.14 CurJ DH H978F variant co-crystallized with hydrolyzed compound 21.

SA omit density map around the carboxylate of **21** is shown in purple (2.5σ) and the 2Fo-Fc map is shown in cyan (1.0σ). In both maps, the hydrolyzed form of compound **21** fits the density well.

Discussion

Enigmatic dehydration in polyketide synthases

Curiously, there are numerous examples in the literature of missing DH domains when diene final products or intermediates are predicted. Notable cases come from the biosynthesis of columbamides, stigmatellin, epothilones, leinamycin, thuggacin, and the myxalamides (Fig. 4.15).[40-44] Unexpectedly, many of these anomalies involve the formation of a *cis*-alkene during the distal dehydration. The classic interpretations of these cases invoke either a *trans*-acting dehydratase, separate from the PKS pathway, or a stuttered dehydration process[40, 45]. Vinylogous dehydration of δ-hydroxy-α,β-unsaturated thioester substrates as described here provides an alternative mechanism.
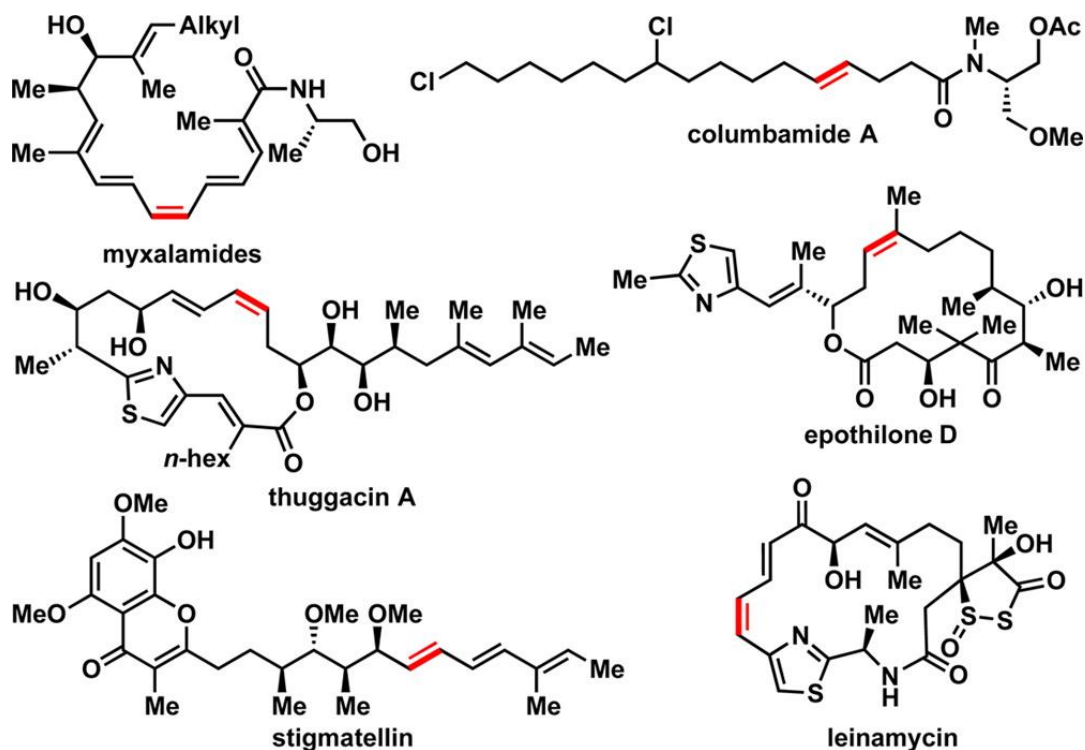
Figure 4.15 Select examples of sequential dehydration with a missing dehydratase domain.

Alkenes arising from modules lacking a DH are highlighted in red. The subsequent module contains an active DH, possibly capable of vinylogous dehydration.

Crystal structures and substrate specificity

The crystallization behavior of both CurK DH and CurJ DH in the presence of NAC-linked substrates is suggestive of a conformational change in the protein at the entrance to the substrate tunnel. For both DHs, crystals either did not grow in the presence of substrate or grew only after thioester hydrolysis. Similarly, pre-grown DH crystals dissolved when presented with substrate. The structure of CurJ DH H978F with the hydrolyzed **21** reveals an ideal orientation for hydrogen bonding of the catalytic Asp1156 carboxylate with the substrate hydroxyl. The site is occupied by a water molecule in structures of the DH free enzyme[10]. We found that the best fit of hydrolyzed **21** to the experimental density was in a conformation that would yield a *trans-cis* dienoate. As CurJ DH produced the *trans-trans* dienoate from **21** (Fig. 4.11B), we assume that hydrolysis of the NAC thioester accounts for the predominant bound conformation.

Mechanistic analogy to canonical eliminations in DH domains

Vinylogous dehydration by DH domains closely parallels canonical dehydrations. Stereospecificity appears to be maintained between the two events in the module. Moreover, the empirical trend that D-alcohols form *E*-substituted olefins holds true in this distal elimination. The catalytic His-Asp dyad is essential for this novel, second transformation by the dehydratase domain as the respective point mutants are catalytically incompetent. Given these results, we predict the reaction is a net *syn*-elimination as previously established in α,β-dehydrations in PKS and FAS systems[46-47]. The proposed mechanism shares similarities to three reported biosynthetic enzymes: FabA, an isomerizing DH involved in corallopyronin A biosynthesis, and a recently characterized isomerase (Fig. 4.16)[18, 48-49]. The first step involves deprotonation of the γ–proton, *pro*-(*R*) in the case of FabA, by a general base (likely the catalytic His) to afford a vinylogous enolate.[50] Until this point, the reaction mechanism mirrors that of a classic isomerase. Instead of

suprafacial protonation at the α-position, the subsequent elimination occurs with simultaneous protonation of the δ-hydroxyl group by the catalytic aspartic acid residue, forming the γ,δ-olefin. The dual activities would require that the substrate shift in the active site tunnel first to place the α-position by the catalytic His and the β-hydroxy by the catalytic Asp for the canonical dehydration, and then the γ-position by the catalytic His and δ-hydroxy by the catalytic Asp for the vinylogous dehydration.
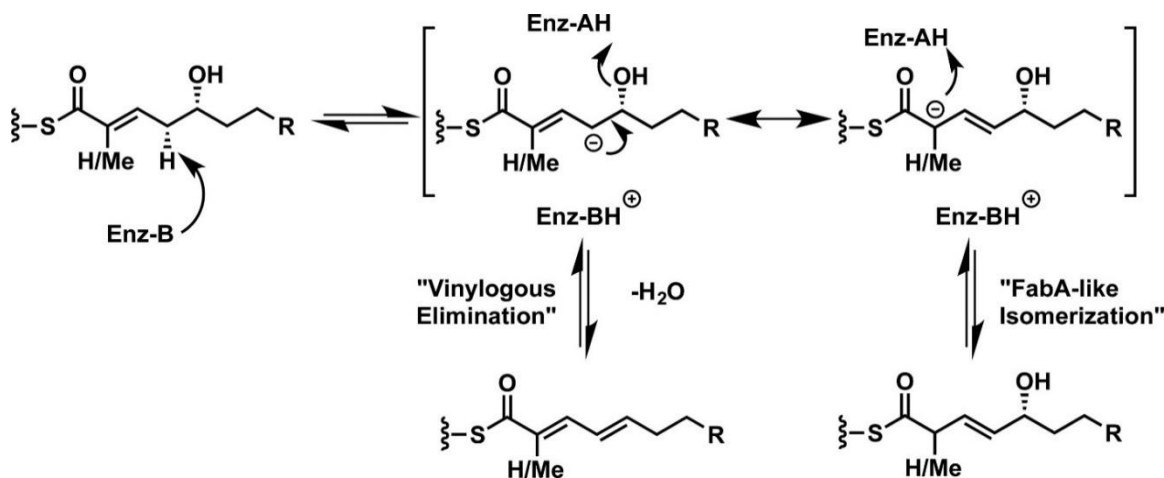
Figure 4.16 FabA isomerization mechanism and proposed mechanism of vinylogous dehydration by curacin J and H dehydratases.

The two events share a common intermediary vinylogous enolate and differ only in the final re-protonation or elimination. Site-directed mutagenesis of the catalytic dyad indicates that the canonical histidine and aspartic residues are the general base and acid, respectively. FabA (Escherichia coli β-hydroxydecanoyl thiol ester dehydrase) catalyzes elimination and bond isomerization in fatty acid biosynthesis.

In the present study, we found that CurF-DH activity unexpectedly closely mirrors that of the CurK-DH in its stereospecific processing of **1** over **2**. This seemingly nonsensical mimicry of dehydration activity is puzzling due to the fact that CurK-DH is predicted to process the longest dehydratase substrate in the Cur pathway, and CurF DH has no known function. By analyzing CurF polyketide cassette (ER-KS-AT-DH) against other possible pathways in the producing organism, we found that JamJ from the jamaicamide pathway has high homology (>72% identical) and the predicted action in its pathway matches that of the extra modules in CurF (i.e.

181

a complete reductive processing sequence to form an alkane intermediate). The majority of the modules needed for jamaicamide synthesis appear to be vestigial in CurF, and *vice versa*. For example, the ER domain is responsible for cyclopropane formation in curacin biosynthesis, whereas the vestigial JamJ ER domain has no activity with the natural jamaicamide β,γ-olefin intermediate but has robust reductive activity with α,β-olefin substrates[2]. Additionally, there is an NRPS module set (PCP-A-Cy) for thiazoline production appended to the end of the vestigial CurF PKS module. Genetic analysis of several PKS biosynthetic clusters has recently revealed that analogous instances of surplus DH domains present in a pathway compared to a predicted activity is a more common occurrence than missing DH domains. This often arises due to two unique evolutionary pressures: The necessity to retain a hydroxyl group in the pathway for the final natural product or the duplication and insertion of a full or partial module cassette to fulfill another pathway role. In the former case, the DH domain is often catalytically inactivated by a knockout mutation in the catalytic region. Classic examples include rifamycin (DH2 and 5), amphotericin B (DH15, 17 and 18) and FK506 (DH3, 4 and 8)[51-53]. The latter case is often harder to interpret biosynthetically as the partial module harbors necessary activity for the natural product biosynthesis (i.e. CurF ER), but also a superfluous and active DH domain (i.e. CurF DH). Examples include rifamycin (DH6, 7 and 8), epothilone A and B (DH7 and 8) and FK506 (DH2)[25, 51, 53-54]. Our results indicate this may be diagnosed by both sequence comparison to other modules in the organism and substrate-dehydratase interrogation, looking for high sequence identity and unexpected substrate selectivity, respectively.

Conclusion

   The curacin biosynthetic pathway continues to provide unique insight into non-canonical PKS enzymology. The present study focused on the mechanism and timing of DH-catalyzed processing in assembly of the polyketide segment introduced by the five Cur PKS monomodules CurG-CurK. Retrobiosynthetic analysis indicated five dehydrations are required; however, DH domains are missing in both CurG and CurI while an extraneous DH domain is present in CurF. To uncover the anomalous biosynthetic features of DH-catalysis in this segment of the polyketide, we employed diffusible small-molecule truncated NAC thioester substrates in conjunction with LC-MS/MS analysis, site-directed mutagenesis, and co-crystallization studies.

   We initially focused on the dehydration event in CurK using a tetraketide substrate and showed that CurK processed its predicted D-alcohol substrate **1** to the all *trans*-trienoate **7** more than three-orders of magnitude greater than any previously reported DH with its native substrate[37-38], highlighting the high intrinsic activity of Cur DHs when presented with their native substrates. Therefore, the inability of the CurJ-DH, which is the DH domain in the preceding module, to turn over any of the four diastereomeric triketide substrates including **21**, with the bioinformatically predicted *2R*, *3S* stereochemistry, suggested an alternative substrate. We hypothesized that CurJ may be responsible for a double dehydration of a β,δ-dihydroxy thioester substrate since the antecedent DH domain is absent in CurI. This would require a canonical dehydration to form a δ-hydroxy-α,β-unsaturated thioester intermediate, which would then undergo a second vinylogous elimination, at the same active site, to afford the *trans-trans*-dienoate product. Using a synthetic triketide δ-hydroxy-α,β-unsaturated thioester substrate, we unequivocally demonstrated that CurJ can catalyze this novel vinylogous elimination as well as the reverse hydration reaction in a completely stereospecific and regiospecific manner. The

183

vinylogous elimination required the His-Asp catalytic dyad as point mutations to either of these residues completely abolished activity. CurH analogously lacks a DH domain in the preceding module and was also shown to catalyze a vinylogous elimination. By contrast, CurK does not catalyze the vinylogous elimination, but only the canonical dehydration as expected based on the collinear organization of CurJ and CurK, which both contain functional DH domains. Interestingly, the substrate specificity of CurF-DH mirrored that of CurK-DH, suggesting CurF-DH is vestigial and may have evolutionary arisen from an earlier gene duplication event.

To provide a structural framework for the novel vinylogous elimination, we co-crystallized a mutagenized CurJ(H978F) with δ-hydroxy-α,β-unsaturated thioester **21**. The binding pose shows that the catalytic Asp1156 side chain is positioned to hydrogen bond with a hydroxyl group - or water molecule, as in the free-enzyme structures - and that this could be either a β-hydroxy or a δ-hydroxy.

The vinylogous elimination mechanism, catalyzed by both CurH-DH and CurJ-DH, compensates for the two modules lacking dehydratases (CurG and CurI) offering an alternative to the stuttered module hypothesis. The proposed mechanism closely resembles that of FabA in *E. coli*, which catalyzes α,β to γ,δ-isomerization of unsaturated fatty acids utilizing a His-Asp catalytic dyad. This discovery expands the growing number of known transformations carried out by the hotdog-fold family of enzymes. More broadly this new mechanism may be operative in other PKS systems missing DH domains.

Bibliography

1.   Gerwick, W. H., Proteau, P. J., Nagle, D. G., Hamel, E., Blokhin, A., Slate, D. L., Structure of curacin A, a novel antimitotic, antiproliferative and brine shrimp toxic natural product from the marine cyanobacterium *Lyngbya majuscula*. *The Journal of organic chemistry* **1994,** *59* (6), 1243-1245.

2.   Gu, L., Wang, B., Kulkarni, A., Geders, T. W., Grindberg, R. V., Gerwick, L., Håkansson, K., Wipf, P., Smith, J. L., Gerwick, W. H., Metamorphic enzyme assembly in polyketide diversification. *Nature* **2009,** *459* (7247), 731.

3.   Gu, L., Wang, B., Kulkarni, A., Gehret, J. J., Lloyd, K. R., Gerwick, L., Gerwick, W. H., Wipf, P., Håkansson, K., Smith, J. L., Polyketide decarboxylative chain termination preceded by O-sulfonation in curacin A biosynthesis. *Journal of the American Chemical Society* **2009,** *131* (44), 16033-16035.

4.   Gu, L., Eisman, E. B., Dutta, S., Franzmann, T. M., Walter, S., Gerwick, W. H., Skiniotis, G., Sherman, D. H., Tandem acyl carrier proteins in the curacin biosynthetic pathway promote consecutive multienzyme reactions with a synergistic effect. *Angewandte Chemie International Edition* **2011,** *50* (12), 2795-2798.

5.   McCarthy, J. G., Eisman, E. B., Kulkarni, S., Gerwick, L., Gerwick, W. H., Wipf, P., Sherman, D. H., Smith, J. L., Structural basis of functional group activation by sulfotransferases in complex metabolic pathways. *ACS chemical biology* **2012,** *7* (12), 1994-2003.

6.   Khare, D., Wang, B., Gu, L., Razelun, J., Sherman, D. H., Gerwick, W. H., Håkansson, K., Smith, J. L., Conformational switch triggered by α-ketoglutarate in a halogenase of curacin A biosynthesis. *Proceedings of the National Academy of Sciences* **2010,** *107* (32), 14099-14104.

7.   Khare, D., Hale, W. A., Tripathi, A., Gu, L., Sherman, D. H., Gerwick, W. H., Håkansson, K., Smith, J. L., Structural basis for cyclopropanation by a unique enoyl-acyl carrier protein reductase. *Structure* **2015,** *23* (12), 2213-2223.

8.   Gu, L., Geders, T. W., Wang, B., Gerwick, W. H., Håkansson, K., Smith, J. L., Sherman, D. H., GNAT-like strategy for polyketide chain initiation. *Science* **2007,** *318* (5852), 970-974.

9.   Whicher, J. R., Smaga, S. S., Hansen, D. A., Brown, W. C., Gerwick, W. H., Sherman, D. H., Smith, J. L., Cyanobacterial polyketide synthase docking domains: a tool for engineering natural product biosynthesis. *Chemistry & biology* **2013,** *20* (11), 1340-1351.

10.   Akey, D. L., Razelun, J. R., Tehranisa, J., Sherman, D. H., Gerwick, W. H., Smith, J. L., Crystal structures of dehydratase domains from the curacin polyketide biosynthetic pathway. *Structure* **2010,** *18* (1), 94-105.

11.   Gehret, J. J., Gu, L., Gerwick, W. H., Wipf, P., Sherman, D. H., Smith, J. L., Terminal alkene formation by the thioesterase of curacin A biosynthesis structure of a decarboxylating thioesterase. *Journal of Biological Chemistry* **2011,** *286* (16), 14445-14454.

12.   Geders, T. W., Gu, L., Mowers, J. C., Liu, H., Gerwick, W. H., Håkansson, K., Sherman, D. H., Smith, J. L., Crystal Structure of the ECH2 Catalytic Domain of CurF from *Lyngbya majuscula* insights into a decarboxylase involved in polyketide chain β-branching. *Journal of Biological Chemistry* **2007,** *282* (49), 35954-35963.

13.   Akey, D. L., Gehret, J. J., Khare, D., Smith, J. L., Insights from the sea: Structural biology of marine polyketide synthases. *Natural product reports* **2012,** *29* (10), 1038-1049.

14.   Yoo, H.-D., Gerwick, W. H., Curacins B and C, new antimitotic natural products from the marine cyanobacterium *Lyngbya majuscula*. *Journal of natural products* **1995,** *58* (12), 1961-1965.

15.   Chang, Z., Sitachitta, N., Rossi, J. V., Roberts, M. A., Flatt, P. M., Jia, J., Sherman, D. H., Gerwick, W. H., Biosynthetic Pathway and Gene Cluster Analysis of Curacin A, an Antitubulin Natural Product from the Tropical Marine Cyanobacterium *Lyngbya majuscula*. *Journal of natural products* **2004,** *67* (8), 1356-1367.

16.   Moss, S. J., Martin, C. J., Wilkinson, B., Loss of co-linearity by modular polyketide synthases: a mechanism for the evolution of chemical diversity. *Natural product reports* **2004,** *21* (5), 575-593.

17.   Helmkamp, G. M., Bloch, K., β-Hydroxydecanoyl Thioester Dehydrase studies on molecular structure and active site. *Journal of Biological Chemistry* **1969,** *244* (21), 6014-6022.

18.   Leesong, M., Henderson, B. S., Gillig, J. R., Schwab, J. M., Smith, J. L., Structure of a dehydratase–isomerase from the bacterial pathway for biosynthesis of unsaturated fatty acids: two catalytic activities in one active site. *Structure* **1996,** *4* (3), 253-264.

19.   Armarego, W. L. F., Perrin, D. D., *Purification of laboratory chemicals*. 4th ed.; Butterworth Heinemann: Oxford ; Boston, 1996; p xi, 529 p.

20.   Verdier-Pinard, P., Lai, J.-Y., Yoo, H.-D., Yu, J., Marquez, B., Nagle, D. G., Nambu, M., White, J. D., Falck, J., Gerwick, W. H., Structure-activity analysis of the interaction of curacin A, the potent colchicine site antimitotic agent, with tubulin and effects of analogs on the growth of MCF-7 breast cancer cells. *Molecular pharmacology* **1998,** *53* (1), 62-76.

21.   Shirokawa, S.-i., Kamiyama, M., Nakamura, T., Okada, M., Nakazaki, A., Hosokawa, S., Kobayashi, S., Remote Asymmetric Induction with Vinylketene Silyl N,O-Acetal. *J. Am. Chem. Soc.* **2004,** *126* (42), 13604-13605.

22.   Kinoshita, K., G Williard, P., Khosla, C., Cane, D. E., Precursor-Directed Biosynthesis of 16-Membered Macrolides by the Erythromycin Polyketide Synthase. *J. Am. Chem. Soc.* **2001,** *123* (11), 2495-2502.

23.   Kabsch, W., Integration, scaling, space-group assignment and post-refinement. *Acta Crystallographica Section D: Biological Crystallography* **2010,** *66* (2), 133-144.

24.   Adams, P. D., Afonine, P. V., Bunkóczi, G., Chen, V. B., Davis, I. W., Echols, N., Headd, J. J., Hung, L.-W., Kapral, G. J., Grosse-Kunstleve, R. W., PHENIX: a comprehensive Python-based system for macromolecular structure solution. *Acta Crystallographica Section D: Biological Crystallography* **2010,** *66* (2), 213-221.

25.   Emsley, P., Lohkamp, B., Scott, W. G., Cowtan, K., Features and development of Coot. *Acta Crystallographica Section D: Biological Crystallography* **2010,** *66* (4), 486-501.

26.   Moriarty, N. W., Grosse-Kunstleve, R. W., Adams, P. D., electronic Ligand Builder and Optimization Workbench (eLBOW): a tool for ligand coordinate and restraint generation. *Acta Crystallographica Section D: Biological Crystallography* **2009,** *65* (10), 1074-1080.

27.   Chen, V. B., Arendall, W. B., Headd, J. J., Keedy, D. A., Immormino, R. M., Kapral, G. J., Murray, L. W., Richardson, J. S., Richardson, D. C., MolProbity: all-atom structure validation for macromolecular crystallography. *Acta Crystallographica Section D: Biological Crystallography* **2010,** *66* (1), 12-21.

28.   Kabsch, W., Xds. *Acta Crystallographica Section D: Biological Crystallography* **2010,** *66* (2), 125-132.

29.   Nagao, Y., Hagiwara, Y., Kumagai, T., Ochiai, M., Inoue, T., Hashimoto, K., Fujita, E., New C-4-chiral 1, 3-thiazolidine-2-thiones: excellent chiral auxiliaries for highly diastereo-controlled aldol-type reactions of acetic acid and α,β-unsaturated aldehydes. *The Journal of Organic Chemistry* **1986,** *51* (12), 2391-2393.

30.   Crimmins, M. T., Chaudhary, K., Titanium enolates of thiazolidinethione chiral auxiliaries: Versatile tools for asymmetric aldol additions. *Organic letters* **2000,** *2* (6), 775-777.

31.   Evans, D. A., Downey, C. W., Shaw, J. T., Tedrow, J. S., Magnesium halide-catalyzed anti-aldol reactions of chiral N-acylthiazolidinethiones. *Organic letters* **2002,** *4* (7), 1127-1130.

32.   Wadsworth, W. S., Emmons, W. D., The utility of phosphonate carbanions in olefin synthesis. *Journal of the American Chemical Society* **1961,** *83* (7), 1733-1738.

33.   Rathke, M. W., Nowak, M., The Horner-Wadsworth-Emmons modification of the Wittig reaction using triethylamine and lithium or magnesium salts. *The Journal of Organic Chemistry* **1985,** *50* (15), 2624-2626.

34.   Zheng, J., Taylor, C. A., Piasecki, S. K., Keatinge-Clay, A. T., Structural and functional analysis of A-type ketoreductases from the amphotericin modular polyketide synthase. *Structure* **2010,** *18* (8), 913-922.

35.   Caffrey, P., Conserved amino acid residues correlating with ketoreductase stereospecificity in modular polyketide synthases. *ChemBioChem* **2003,** *4* (7), 654-657.

36.   Reid, R., Piagentini, M., Rodriguez, E., Ashley, G., Viswanathan, N., Carney, J., Santi, D. V., Hutchinson, C. R., McDaniel, R., A model of structure and catalysis for ketoreductase domains in modular polyketide synthases. *Biochemistry* **2003,** *42* (1), 72-79.

37.   Fiers, W. D., Dodge, G. J., Li, Y., Smith, J. L., Fecik, R. A., Aldrich, C. C., Tylosin polyketide synthase module 3: stereospecificity, stereoselectivity and steady-state kinetic analysis of β-processing domains via diffusible, synthetic substrates. *Chemical science* **2015,** *6* (8), 5027-5033.

38.   Li, Y., Dodge, G. J., Fiers, W. D., Fecik, R. A., Smith, J. L., Aldrich, C. C., Functional characterization of a dehydratase domain from the pikromycin polyketide synthase. *Journal of the American Chemical Society* **2015,** *137* (22), 7003-7006.

39.   Keatinge-Clay, A. T., A tylosin ketoreductase reveals how chirality is determined in polyketides. *Chemistry & biology* **2007,** *14* (8), 898-908.

40.   Tang, L., Ward, S., Chung, L., Carney, J. R., Li, Y., Reid, R., Katz, L., Elucidating the mechanism of *cis* double bond formation in epothilone biosynthesis. *Journal of the American Chemical Society* **2004,** *126* (1), 46-47.

41.   Tang, G.-L., Cheng, Y.-Q., Shen, B., Leinamycin biosynthesis revealing unprecedented architectural complexity for a hybrid polyketide synthase and nonribosomal peptide synthetase. *Chemistry & biology* **2004,** *11* (1), 33-45.

42.   Buntin, K., Irschik, H., Weissman, K. J., Luxenburger, E., Blöcker, H., Müller, R., Biosynthesis of thuggacins in myxobacteria: comparative cluster analysis reveals basis for natural product structural diversity. *Chemistry & biology* **2010,** *17* (4), 342-356.

43.   Gaitatzis, N., Silakowski, B., Kunze, B., Nordsiek, G., Blöcker, H., Höfle, G., Müller, R., The biosynthesis of the aromatic myxobacterial electron transport inhibitor stigmatellin is directed by a novel type of modular polyketide synthase. *Journal of Biological Chemistry* **2002,** *277* (15), 13082-13090.

44.   Kleigrewe, K., Almaliti, J., Tian, I. Y., Kinnel, R. B., Korobeynikov, A., Monroe, E. A., Duggan, B. M., Di Marzo, V., Sherman, D. H., Dorrestein, P. C., Combining mass spectrometric metabolic profiling with genomic analysis: a powerful approach for discovering natural products from cyanobacteria. *Journal of natural products* **2015,** *78* (7), 1671-1682.

45.   Dickschat, J. S., Vergnolle, O., Hong, H., Garner, S., Bidgood, S. R., Dooley, H. C., Deng, Z., Leadlay, P. F., Sun, Y., An Additional Dehydratase-Like Activity is Required for Lankacidin Antibiotic Biosynthesis. *ChemBioChem* **2011,** *12* (16), 2408-2412.

46.   Castonguay, R., Valenzano, C. R., Chen, A. Y., Keatinge-Clay, A., Khosla, C., Cane, D. E., Stereospecificity of ketoreductase domains 1 and 2 of the tylactone modular polyketide synthase. *Journal of the American Chemical Society* **2008,** *130* (35), 11598-11599.

47.   Sedgwick, B., Morris, C., French, S. J., Stereochemical course of dehydration catalysed by the yeast fatty acid synthetase. *Journal of the Chemical Society, Chemical Communications* **1978,** (5), 193-194.

48.   Gay, D. C., Spear, P. J., Keatinge-Clay, A. T., A double-hotdog with a new trick: structure and mechanism of the trans-acyltransferase polyketide synthase enoyl-isomerase. *ACS chemical biology* **2014,** *9* (10), 2374-2381.

49.   Lohr, F., Jenniches, I., Frizler, M., Meehan, M. J., Sylvester, M., Schmitz, A., Gütschow, M., Dorrestein, P. C., König, G. M., Schäberle, T. F., α, β→ β, γ double bond migration in corallopyronin A biosynthesis. *Chemical Science* **2013,** *4* (11), 4175-4180.

50.   Schwab, J. M., Klassen, J. B., Steric course of the allylic rearrangement catalyzed by β-hydroxydecanoylthioester dehydrase. Mechanistic implications. *Journal of the American Chemical Society* **1984,** *106* (23), 7217-7227.

51.   Schupp, T., Toupet, C., Engel, N., Goff, S., Cloning and sequence analysis of the putative rifamycin polyketide synthase gene cluster from *Amycolatopsis mediterranei*. *FEMS microbiology letters* **1998,** *159* (2), 201-207.

52.   Caffrey, P., Lynch, S., Flood, E., Finnan, S., Oliynyk, M., Amphotericin biosynthesis in *Streptomyces nodosus*: deductions from analysis of polyketide synthase and late genes. *Chemistry & biology* **2001,** *8* (7), 713-723.

53.   Motamedi, H., Shafiee, A., The biosynthetic gene cluster for the macrolactone ring of the immunosuppressant FK506. *The FEBS Journal* **1998,** *256* (3), 528-534.

54.   Molnar, I., Schupp, T., Ono, M., Zirkle, R., Milnamow, M., Nowak-Thompson, B., Engel, N., Toupet, C., Stratmann, A., Cyr, D., The biosynthetic gene cluster for the microtubule-stabilizing agents epothilones A and B from *Sorangium cellulosum* So ce90. *Chemistry & biology* **2000,** *7* (2), 97-109.

Chapter 5. Molecular basis for olefin rearrangement in gephyronic acid polyketide synthase

Summary

Polyketide synthase (PKS) are a rich source of natural products of varied chemical composition and biological significance. Here, we report the characterization of an atypical dehydratase (DH) domain from the PKS pathway for gephyronic acid, an inhibitor of eukaryotic protein synthesis. Using a library of synthetic substrate mimics, the reaction course, stereospecificity, and tolerance to non-native substrates of GphF DH1 are probed via LC-MS analysis. Taken together, the studies establish GphF DH1 as a dual-function dehydratase/isomerase that installs an odd-to-even double bond and yields a product consistent with the structure of gephyronic acid. The studies also reveal an unexpected C2 epimerase function in catalytic turnover with the native substrate. A 1.55-Å crystal structure of GphF DH1 guided mutagenesis experiments to elucidate the roles of key amino acids in the multi-step DH1 catalysis, identifying critical functions for leucine and tyrosine side chains. The mutagenesis results were applied to add a secondary isomerase functionality to a non-isomerizing DH in the first successful gain-of-function engineering of a PKS DH. Our studies of GphF DH1 catalysis highlight the versatility of the DH active site and adaptation for a specific catalytic outcome with a specific substrate.

Introduction

Polyketide synthases (PKS) produce a plethora of bioactive and chemically diverse compounds. The bacterial modular type I PKS are among the most versatile, as each module contains a set of distinct catalytic domains individually responsible for a single step during the elongation and modification of polyketide intermediates. In so-called *cis*-AT pathways, each module includes a ketosynthase (KS), an acyltransferase (AT), and an acyl carrier protein (ACP) at a minimum, whereas in *trans*-AT pathways, a separate AT polypeptide delivers a common building block to all modules. A module may also contain one or more modification domains such as ketoreductase (KR), dehydratase (DH), *O*-methyltransferase (OMT), *C*-methyltransferase (CMT), and enoylreductase (ER).

The DH domain generates a 2-enoyl thioester intermediate via *syn*-elimination of a 3-hydroxy group, resulting in the production of alkenes in even-to-odd positions in the final polyketide structure[1-9]. DHs are notable for a strict stereospecificity of the 3-hydroxy substrate, which is correlated with the geometry of the product double bond[1-3, 10]. Despite high-resolution crystal structures of several type-I PKS DHs, the structural basis for substrate specificity and product selectivity remains unclear[4, 11-14]. While "A" and "B" sequence motifs within KR domains predict the sterochemical configuration of the 3-hydroxy group[15], no such motifs have been identified in PKS DHs[3]. To date, only DHs that act on A-type KR products have been shown to produce *cis* double bonds[3], whereas B-type KR reduction followed by DH dehydration leads to *trans* double bonds in most cases[1-2, 4-5], with notable exceptions[4, 6, 16-17].

Like other PKS enzymes, DH homologs exist in both type I and type II fatty acid synthase (FAS). The type II FAS of many bacteria, including *Escherichia coli*, employ two DHs,

FabA and FabZ[18]. FabZ catalyzes a general β-elimination reaction like PKS DHs, acting on a variety of fatty acyl chain lengths to produce a 2-enoyl intermediate that is subsequently reduced and subject to further elongation cycles. FabA is specific for decanoyl substrates, and initially produces a *trans* double bond ((*E*)-2-decenoyl, even-to-odd) in a manner analogous to PKS DHs and FabZ. However, FabA also catalyzes a subsequent double-bond migration to produce an odd-to-even olefin in the *cis* configuration ((*Z*)-3-decenoyl)[7]. The final products of type II FAS with FabA include fatty acids with a *cis*, odd-to-even alkene situated six carbons from the terminal methyl group. An analogous system from *Enterococcus faecalis* has been characterized in which FabN, a dehydratase more similar to FabZ than FabA, dehydrates and isomerizes a 3-hydroxydecanoyl-ACP substrate to an odd-to-even (*Z*)-3-decenoyl product[19]. FabZ, FabA and PKS DHs possess conserved histidine and aspartate (or glutamate) catalytic amino acids and similar active site structures[4, 11-14, 20-21]. The catalytic groups presumably interact identically with the 3-hydroxy substrate in all these enzymes, but the structural basis for their differing activities is unknown.

While many modular PKS pathways include DHs, the products of these pathways rarely contain odd-to-even unsaturated products. Nevertheless, a number of interesting natural products of unknown biosynthetic origin contain odd-to-even double bonds including the tedanolides, candidaspongiolides and myriaporones[22-24]. Two distinct mechanisms for generation of odd-to-even unsaturation have been identified in *trans*-AT PKS. In the related pathways for chloronotil and anthracimycin, the formation of odd-to-even unsaturation has been attributed to multifunctional DHs[25]. In other pathways, DH-related enoyl isomerases (EIs) generate 3-enoyl intermediates from 2-enoyl substrates[26-27]. The best characterized is the EI from module 14 of the

bacillaene pathway (PksEI14), which catalyzes isomerization using only a catalytic histidine[27], in stark contrast to FabA, where isomerization requires both the catalytic histidine and aspartate[28].

Olefin rearrangement has been characterized in only two *cis*-AT PKS systems[8, 29]. In the ansamitocin pathway, feeding studies implicated DH-containing module 3 in the formation of a conjugated 2,4-dienoyl product via a proposed vinylogous dehydration[29]. An interesting DH from the ambruticin pathway catalyzes a novel three-step reaction in which a 3,4-olefin is generated only after epimerization of a 4-methyl substituent[8]. To date, no structures are available for any PKS DH predicted to catalyze both dehydration and isomerization. Gephyronic acid (**1**) is a eukaryotic translation inhibitor produced by a *cis*-AT PKS in the myxobacterium *Cystobacter violaceus*[30]. An odd-to-even double bond in **1** is apparently installed by the first extension module of the Gph PKS (Fig. 5.1A). The GphF tri-module polypeptide includes module 1, which extends an isobutyryl starter unit from the loading module to produce an intermediate containing a 3-enoyl (odd-to-even) intermediate (Fig. 5.1A). In addition to the DH, module 1 contains CMT and KR modification domains, which act first and present to the DH a 2-methyl-3-hydroxy substrate[31]. Here we determine that the module 1 DH domain (GphF DH1) is the source of the odd-to-even unsaturation in gephyronic acid. Biochemical characterization and a crystal structure of GphF DH1 establish its role as a bifunctional dehydratase-isomerase and reveal an unexpected C2 epimerization activity. Additionally, we identify tyrosine and leucine amino acids that are key to the isomerase activity.
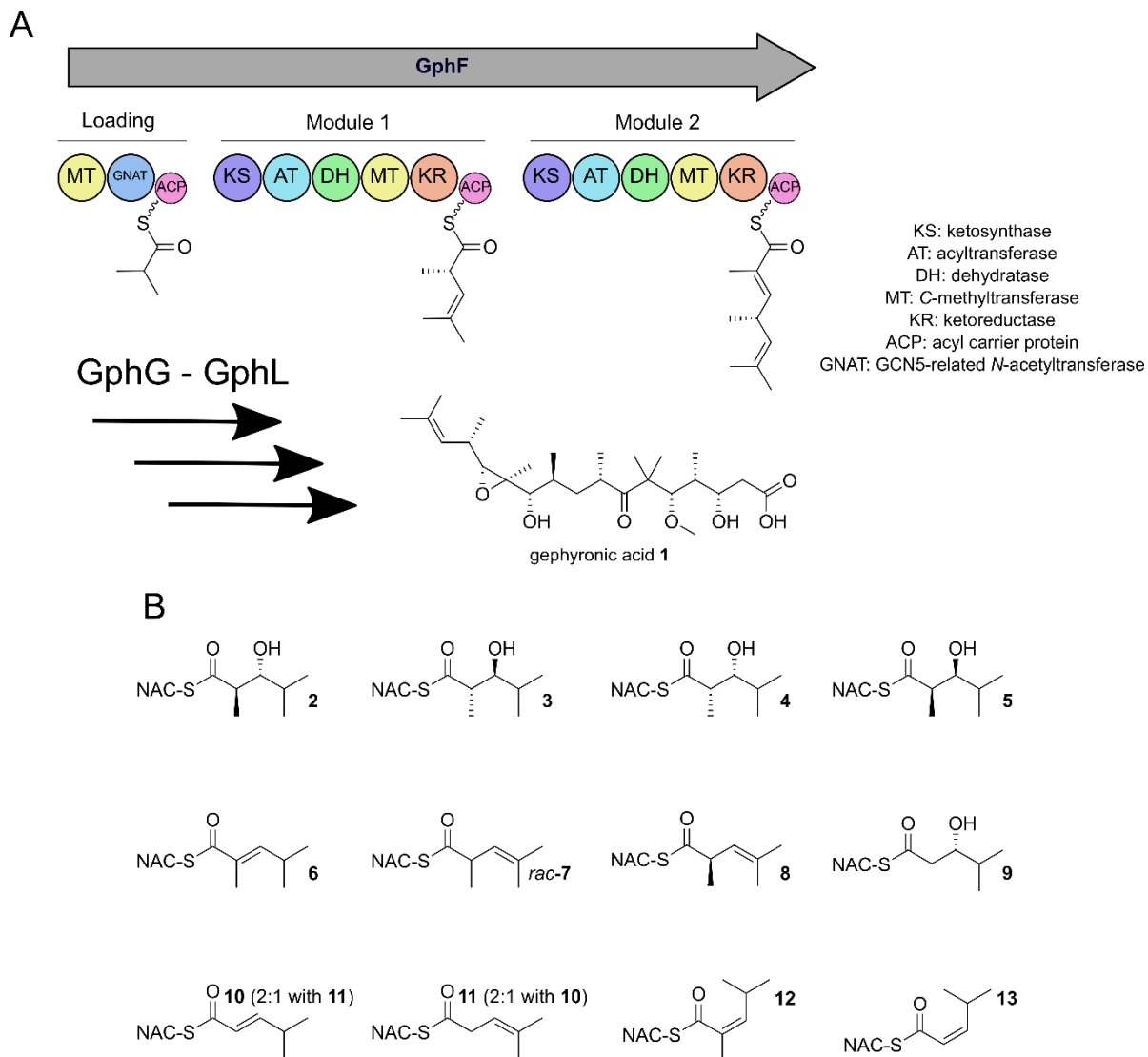
Figure 5.1 Domain architecture of GphF and substrate mimics used for assay.

A: Domain architecture of GphF, the first gene in the gephyronic acid PKS. Gephyronic acid **1** contains an unusual odd-to-even double bond, apparently installed by module 1. **B**: Library of *N*-acetylcysteamine (NAC) substrate mimics used to assess the function of GphF DH1. The library was designed specifically to test the stereospecificity of the DH by sampling each diastereomer of the predicted substrates (**2**, **3**, **4**, **5**).

Methods

A. Chemical synthesis

All synthesis experiments were run by Danialle Ronnow.

Unless otherwise noted, all materials were used as received from a commercial supplier without further purification. All anhydrous reactions were performed using oven-dried or flame-dried glassware under an atmosphere of nitrogen or argon; unless otherwise indicated, all reactions where performed under anhydrous conditions. Tetrahydrofuran (THF), diethyl ether (Et_2O), and dichloromethane (DCM), were filtered through activated alumina under nitrogen prior to use. All reactions were monitored by either E. Merck (Kenilworth, NJ, USA) analytical thin layer chromatography (TLC) plates (silica gel 60 GF, glass back) analyzed with 254 nm UV light and/or *p*-anisaldehyde/sulfuric acid or potassium permanganate treatment. Silica gel for column chromatography was purchased from E. Merck (Silica Gel 60, 230–400 mesh). All ^{1}H and 13C NMR spectra were obtained either on a Bruker ADVANCE III HD 400 (operating at 400.130 MHz for ^{1}H and 100.613 MHz for ^{13}C). Chemical shifts are reported as δ-values in parts per million (ppm) using residual $CHCl_3$ as internal reference (^{1}H: δ = 7.27 ppm, ^{13}C: δ = 77.23 ppm) and coupling constants (*J*) are reported in Hertz (Hz). Peak multiplicities are indicated as follows: s (singlet), d (doublet), t (triplet), q (quartet), m (multiplet) and br (broad). Optical rotation data was obtained on a Perkin–Elmer polarimeter model 343 with a Na lamp.

A.1 (2R,3R)-3-hydroxy-2,4-dimethyl-pentanoyl-SNAc (**2**)
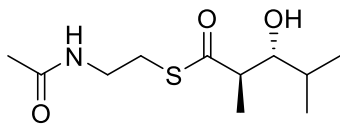
To a stirred solution of (2R,3R)-3-hydroxy-2,4-dimethyl-pentanoic acid[32] (50 mg, 0.34 mmol) in DCM (1.1 mL) was added N-acetylcyteamine (0.040 mL, 0.41 mmol) and DMAP (4.2 mg, 0.030 mmol), followed by DCC (106 mg, 0.510 mmol) at 0 °C. The reaction was allowed to warm to RT and was stirred for 4 hours. The reaction was quenched with 10 ml of 1M aqueous HCl, filtered and the aqueous layer was extracted with DCM (3 x 10 ml). The combined DCM extracts were washed with aqueous 0.5 M HCl (10 ml), washed with saturated aqueous $NaHCO_3$ (10 ml) and finally washed with saturated aqueous NaCl (20 ml). The organic layer was dried over Na_2SO_4 and then filtered and concentrated under reduced pressure. The residue was then purified by chromatography (3% MeOH/DCM) to yield (2R,3R)-3-hydroxy-2,4-dimethyl-pentanoyl-SNAc (39 mg,0.17 mmol, 47 % yield). $[\alpha]^{20}_D$ = -12.7 (c = 0.49, CHCl$_3$) ^{1}H NMR (CDCl$_3$, 400 MHz) δ ppm: 6.01 (br s, 1H), 3.49 – 3.35 (m, 3 H), 3.02 (m, 2H), 2.85 (qn, J = 7.3 Hz, 1H), 2.21 (br s, 1H), 1.95 (s, 3H), 1.79 – 1.65 (m, 1H), 1.18 (d, J = 7.1 Hz, 3 H), 0.96 (d, J = 6.8 Hz, 3H), 0.89 (d, J = 6.7 Hz, 3H); ^{13}C NMR (CDCl$_3$, 100 MHz) δ ppm 204.6, 170.5, 78.5, 51.6, 39.4, 30.7, 28.6, 23.2, 19.9, 15.9, 15.5; HRMS (FAB) m/z (M+H)+ calcd for $C_{11}H_{21}NO_3S$, 248.1320; obsd 248.1295

A.2 (2S,3S)-3-hydroxy-2,4-dimethylpentanoyl-SNAc (**3**)
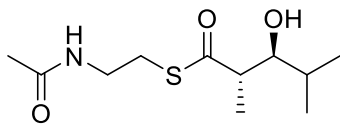
Synthesized via literature protocol [33]

A.3 (2S,3R)-3-hydroxy-2,4-dimethyl-pentanoyl-SNAc (**4**)
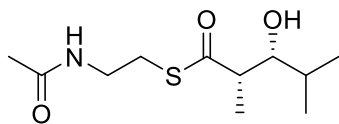
To a stirred solution of (2S,3R)-3-hydroxy-2,4-dimethyl-pentanoic acid (50 mg, 0.34 mmol) in DCM (1.1 mL) was added N-acetylcyteamine (0.045 mL, 0.41 mmol) and DMAP (4 mg, 0.030 mmol), followed by DCC (110 mg, 0.51 mmol) at 0 °C. The reaction was allowed to warm to RT and stirred for 4 hours. The reaction was quenched with 10 ml of 1M HCl and then filtered. The combined DCM extracts (3 x 30ml) were washed with 0.5 M HCl (10ml), washed with saturated aqueous NaHCO$_3$ (10ml) and finally washed with 20ml saturated aqueous NaCl. The combined organic extracts were dried and then concentrated under reduced pressure. The residue is then purified by chromatography (3% MeOH/DCM) to yield (2S,3R)-3-hydroxy-2,4-dimethyl-pentanoyl-SNAc (21 mg, 0.09 mmol, 25 % yield). Spectral data for compound 2 matched the data previously reported in the literature.[34]

A.4 (2R,3S)-3-hydroxy-2,4-dimethylpentanoic acid
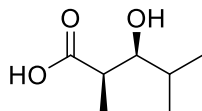
To a solution of (3S)-3-benzyl-2-[(2R,3S)-3-hydroxy-2,4-dimethyl-pentanoyl]cyclopentanone[35] (590 mg, 1.95 mmol) in THF (9.8 mL) and water (1.2 mL) was added H_2O_2 (1.17 ml, 11.7 mmol) followed by $LiOH \cdot H_2O$ (163.9 mg, 3.9 mmol). The reaction mixture was stirred at 0 ˚C for 1hr and then a 0.5 M solution of Na_2SO_3 (270.5 mg, 2.15 mmol) was added. After being buffered to pH 9 with aqueous $NaHCO_3$, the THF was removed with a rotary evaporator. The aqueous solution was washed with CH_2Cl_2. After acidification to pH 6 with 10% HCl, the aqueous phase was extracted with EtOAc, the combined organics dried over MgSO4, filtered and concentrated *in vacuo* and used directly in the next step.

A.5 (2R,3S)-3-hydroxy-2,4-dimethylpentanoyl-SNAc (**5**)
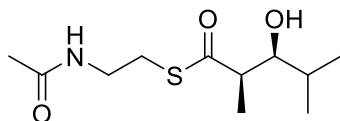
To a stirred solution of (2R,3S)-3-hydroxy-2,4-dimethyl-pentanoic acid (20 mg, 0.14 mmol) in DCM (0.45 mL) was added N-acetylcyteamine (0.020 mL, 0.16 mmol) and DMAP (2 mg, 0.01 mmol), followed by DCC (42 mg, 0.21 mmol) at 0 °C. The reaction was allowed to warm to rt and stirred for 4 hours. The reaction was quenched with 10 ml of 1M aq. HCl and then filtered. The combined DCM extracts (3 x 10ml) were washed with aq. 0.5 M HCl (10ml), washed with saturated aqueous $NaHCO_3$ (10ml) and finally washed with 20ml saturated aqueous NaCl. The combined organic extracts were dried and then concentrated under reduced pressure. The residue is then purified by chromatography (3% MeOH/DCM) to afford (2R,3S)-3-hydroxy-2,4-

dimethylpentanoyl-SNAc (21 mg, 0.084 mmol, 61% yield). $[\alpha]^{20}_D = -5.6$ (c 0.5, CHCl$_3$). ^{1}H NMR (CDCl$_3$, 400 MHz) δ ppm: 5.81 (br s, 1H), 3.58 (dd, J = 7.5, 3.7 1H), 3.46 (m, 2H), 3.02 (m, 2H), 2.85 (m, 1H), 2.33 (br s, 1H), 1.95 (s, 3H), 1.72 – 1.63 (m, 1H), 1.20 (d, J = 7.0 Hz, 3 H), 1.00 (d, J = 6.3 Hz, 3H), 0.88 (d, J = 6.8 Hz, 3H); ^{13}C NMR (CDCl$_3$, 100 MHz) δ ppm: 204.5, 170.4, 77.3, 50.8, 39.5, 30.9, 28.6, 23.2, 19.2, 18.5, 10.8; HRMS (FAB) m/z (M+H)+ calcd for C$_{11}$H$_{21}$NO$_3$S, 248.1320; obsd 248.1297

A.6 (E)-2,4-dimethylpent-2-enoyl-SNAc (**6**)
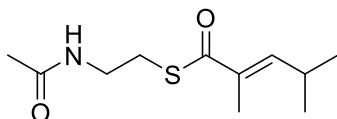
(E)-2,4-dimethylpent-2-enoic acid (105 mg, 0.820 mmol) was dissolved in DCM (3.12 mL) and cooled to 0 ˚C before N-acetylcyteamine (0.100 mL, 0.980 mmol) was added followed by DMAP (10.0 mg, 0.0800 mmol) and EDC-HCl (236 mg, 1.23 mmol). The reaction was allowed to warm to RT and stirred for 4 hours. Upon consumption of the starting material, saturated aqueous NH4Cl solution (5 ml) was added, and the organic phase was separated. The aqueous phase was extracted with diethyl ether (3 × 10 ml), and the combined organic phases were dried over anhydrous Na$_2$SO$_4$ and concentrated under reduced pressure. The residue was purified by silica gel column chromatography (60% EtOAc/hexane) to give (E)-2,4-dimethylpent-2-enoyl-SNAc (154 mg, 0.672 mmol, 82.0 % yield). ^{1}H NMR (CDCl$_3$, 400 MHz) δ ppm: 6.57 (dq, J = 9.5, 1.3 Hz, 1H), 5.90 (br s, 1H), 3.45 (q, J = 6.1 Hz, 2H), 3.06 (q, J = 6.2, 2H), 2.67 (m, 1H), 1.97 (s, 3H), 1.88 (d, J = 1.3 Hz, 3H) 1.05 (6, J = 6.7 Hz, 6H); ^{13}C NMR (CDCl$_3$, 100 MHz) δ ppm: 194.3, 170.3, 148.4, 133.6, 39.8, 28.4, 28.1, 23.2, 21.8, 12.4; HRMS (FAB) m/z (M+H)+ calcd for C$_{11}$H$_{19}$NO$_2$S, 230.1215; obsd 230.1220

A.7 *t*-butyl 2,4-dimethylpent-3-enoate
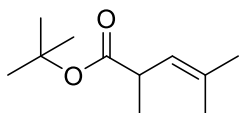
In a glove box, LiHMDS (627 mg, 3.75 mmol) and [PdP(tBu)₃Br]₂ (29.0 mg, 0.038 mmol) was added to a 10-mL crimp cap vial containing a stir bar. The vial was crimped, Toluene (6.0 mL) was added, and the vial was taken out of the glove box and stirred at 22°C. *t*-butyl propionate (225 µl, 1.5 mmol) was added dropwise to the stirred solution. After 5 min, 1-bromo-2-methylpropene (160 µl, 1.58 mmol) was added and stirred at 22°C for 3 h. The reaction mixture was diluted with ethyl acetate (5 ml), passed through a silica plug with ethyl acetate as eluent (20 ml), and concentrated. The residue was purified by silica gel column chromatography (3% EtOAc/hexane) to afford *t*-butyl 2,4-dimethylpent-3-enoate (200 mg, 1.09 mmol, 74% yield). Spectral data for the compound 6 matched the data previously reported in the literature.[36]

A.8 *rac*-2,4-dimethylpent-3-enoic acid
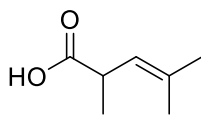
TFA (0.69 mL, 9.0 mmol) was added dropwise to a solution of *t*-butyl 2,4-dimethylpent-3-enoate (55 mg, 0.30 mmol) in DCM (7.5 mL) at 0 ˚C. The mixture was stirred at 0 ˚C for 30 mins before warming up to RT and stirred until starting material was consumed. The reaction was then concentrated in vacuo, mixed with DCM and 1% aqueous NaOH and extracted with DCM. The DCM layer was discarded. The aqueous layer was acidified with 10% HCl and extracted 3 times with DCM. The organic phase was dried over Na₂SO₄ and concentrated to afford 2,4-dimethylpent-3-enoic acid (32mg,0.2497mmol, 83.653% yield) that was carried on crude to the next step. Spectral data for the acid matched the data previously reported in the literature.[37]

A.9 2,4-dimethylpent-3-enoyl-SNAc (*rac*-**7**)
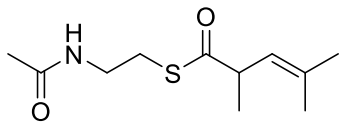
To a stirred solution of 2,4-dimethylpent-3-enoic acid (14 mg, 0.11 mmol) in DCM (0.39 mL) was added N-acetylcyteamine (14 µL, 0.13 mmol) and DMAP (1.0 mg, 0.010 mmol), followed by DCC (34 mg, 0.16 mmol) at 0 °C. The reaction was allowed to warm to RT and stirred for 4 hours. The reaction was quenched with 10 ml of 1M HCl and then filtered. The combined DCM extracts (3 x 5 ml) were washed with 0.5 M HCl (5 ml), washed with saturated aqueous $NaHCO_3$ (5 ml) and finally washed with 10 ml saturated aqueous NaCl. The combined organic extracts were dried and then concentrated under reduced pressure. The residue was purified by chromatography (60% EtOAc/hexanes) to afford S-(2-acetamidoethyl) 2,4-dimethylpent-3-enethioate (15 mg, 0.067 mmol, 62 % yield) as a clear oil. ^{1}H NMR ($CDCl_3$, 400 MHz) δ ppm: 5.86 (br s, 1H), 5.07 (dt, J = 9.4, 2.7 Hz, 1H), 3.45 (m, 1H), 3.39 (q, J = 6.2, 2H), 2.95 (t, J = 6.4 Hz, 2H), 1.93 (s, 3H), 1.72 (d, J = 1.0 Hz, 3H) 1.66 (d, J = 1.1 Hz, 3H), 1.19 (d, J = 6.8 Hz, 3H); ^{13}C NMR ($CDCl_3$, 100 MHz) δ ppm: 203.0, 170.2, 136.1, 123.2, 47.9, 39.8, 28.4, 25.8, 23.2, 18.3, 18.1; HRMS (FAB) m/z (M+H)+ calcd for $C_{11}H_{19}NO_2S$, 230.1215; obsd 230.1220

A.10 (2R)-2,4-dimethylpent-3-enoyl-SNAc (**8**)
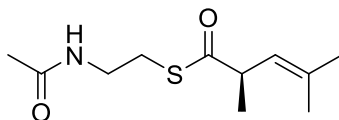
 (2R)-2,4-dimethylpent-3-enoic acid[38] (40 mg, 0.31 mmol) was dissolved in DCM (2.1 mL) and cooled to 0 ˚C before N-acetylcyteamine (0.040 mL, 0.37 mmol) was added followed by DMAP

(3.8 mg, 0.030 mmol) and EDC-HCl (90 mg, 0.47 mmol). The reaction was allowed to warm to RT and stirred for 4 hours. Upon consumption of the starting material, saturated aqueous NH$_4$Cl solution (5 ml) was added, and the organic phase was separated. The aqueous phase was extracted with diethyl ether (3 × 5 ml), and the combined organic phases were dried over anhydrous Na$_2$SO$_4$ and concentrated under reduced pressure. The residue was purified by silica gel column chromatography (60% EtOAc/n-hexane) to give (2R)-2,4-dimethylpent-3-enoyl-SNAc (58 mg,0.25 mmol, 81 % yield).). [α]^{20}$_D$ = -203.5 (c 1.0, CHCl$_3$)^{1}H NMR (CDCl$_3$, 400 MHz) δ ppm: 5.80 (br s, 1H), 5.09 (dt, J = 9.4, 1.3 Hz, 1H), 3.48 (m, 1H), 3.42 (q, J = 6.2, 2H), 2.98 (t, J = 6.4 Hz, 2H), 1.95 (s, 3H), 1.75 (d, J = 1.0 Hz, 3H) 1.68 (d, J = 1.1 Hz, 3H), 1.22 (d, J = 6.9 Hz, 3H); ^{13}C NMR (CDCl3, 100 MHz) δ ppm: 203.0, 170.2, 136.1, 123.2, 47.9, 39.8, 28.3, 25.8, 23.2, 18.3, 18.1; HRMS (FAB) m/z (M+H)+ calcd for C$_{11}$H$_{19}$NO$_2$S, 230.1215; obsd 230.1216

A.11 (3S)-3-hydroxy-4-methyl-pentanoyl-SNAc (**9**)
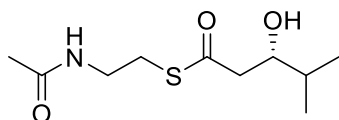
To a stirred solution of (3S)-3-hydroxy-4-methyl-pentanoic acid[39] (48.mg, 0.36mmol) in DCM (1.2 mL) was added N-acetylcyteamine (0.05 mL, 0.44mmol) and DMAP (4 mg, 0.04mmol), followed by DCC (112 mg, 0.54mmol) at 0 °C. The reaction was allowed to warm to rt and stirred for 4 hours. The reaction was quenched with 5 ml of 1M aq. HCl and then filtered. The combined DCM extracts (3 x 10ml) were washed with aq. 0.5 M HCl (10ml), washed with saturated aqueous NaHCO$_3$ (10ml) and finally washed with saturated aqueous NaCl (20 ml). The combined organic extracts were dried and then concentrated under reduced pressure. The residue is then purified by chromatography (3% MeOH/DCM) to afford (3S)-3-hydroxy-4-methyl-

pentanoyl-SNAc (23 mg, 0.10 mmol, 27% yield). $[\alpha]^{20}_D = 19.8$ (c 1.0, CHCl$_3$) . ^{1}H NMR (CDCl$_3$, 400 MHz) δ ppm: 5.31 (br s, 1H), 3.85 (m, 1H), 3.44 (m, 2H), 3.05 (m, 2H), 2.75 (dd, J = 15.4, 3.0 Hz, 1H), 2.68 (dd, J = 15.4, 9.3, 1H), 1.97 (s, 3H), 1.76 (br s, 1H), 1.71 (m. 1H), 0.95 (d, J = 6.9 Hz, 3H), 0.93 (d, J = 6.9 Hz, 3H); ^{13}C NMR (CDCl$_3$, 100 MHz) δ ppm 200.0, 170.5, 73.5, 48.3, 39.3, 33.4, 28.9, 23.2, 18.4, 17.6; HRMS (FAB) m/z (M+H)+ calcd for C$_{10}$H$_{19}$NO$_3$S, 234.1164; obsd 234.1131

A.12 (E)-4-methylpent-2-enoyl-SNAc (**10**)
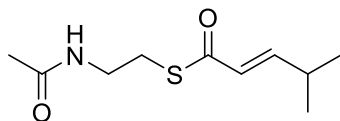
(E)-4-methylpent-2-enoic acid (70 mg, 0.31 mmol) was dissolved in DCM (2.0 mL) and cooled to 0 ˚C before N-acetylcyteamine (0.040 mL, 0.37 mmol) was added followed by DMAP (3.8 mg, 0.030 mmol) and EDC-HCl (89 mg, 0.46 mmol). The reaction was allowed to warm to RT and stirred for 4 hours. Upon consumption of the starting material, saturated aqueous NH$_4$Cl solution (5 ml) was added, and the organic phase was separated. The aqueous phase was extracted with diethyl ether (3 × 5ml), and the combined organic phases were dried over anhydrous Na$_2$SO$_4$, filtered and concentrated under reduced pressure. The residue was purified by silica gel column chromatography (60% EtOAc/n-hexane) to give (E)-4-methylpent-2-enoyl-SNAc (55 mg, 0.128 mmol, 41.2 % yield). Spectral data for compound 8 matched the data previously reported in the literature.[37]

A.13 4-methylpent-3-enoyl-SNAc (**11**)
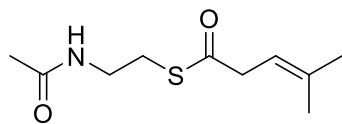
4-methylpent-3-enoic acid[38] (100 mg, 0.880 mmol) was dissolved in DCM (3.00 mL) and cooled

to 0 ˚C before N-acetylcyteamine (0.110 mL, 1.05 mmol) was added followed by DMAP (10.7

mg, 0.0900 mmol) and EDC-HCl (252 mg, 1.31 mmol). The reaction was allowed to warm to

RT and stirred for 4 hours. Upon consumption of the starting material, saturated aqueous NH_4Cl

solution (5 ml) was added, and the organic phase was separated. The aqueous phase was

extracted with diethyl ether (3 × 5 ml), and the combined organic phases were dried over

anhydrous Na_2SO_4, filtered and concentrated under reduced pressure. The residue was purified

by silica gel column chromatography (60% EtOAc/n-hexane) to give 4-methylpent-3-enoyl-

SNAc (103 mg, 0.478 mmol, 54.6 % yield). ^{1}H NMR ($CDCl_3$, 400 MHz) δ ppm: 5.85 (br s, 1H),

5.26 (m, 1H), 3.43 (q, J = 6.2 Hz, 2H), 3.26 (d, J = 7.4, 2H), 3.00 (t, J = 6.4 Hz, 2H), 1.95 (s,

3H), 1.76 (s, 3H) 1.66 (s, 3H); ^{13}C NMR ($CDCl_3$, 100 MHz) δ ppm: 199.1, 170.3, 137.8, 115.1,

43.4, 39.7, 28.5, 25.8, 23.2, 18.1; HRMS (FAB) m/z (M+H)+ calcd for $C_{10}H_{17}NO_2S$, 216.1058;

obsd 216.1052

A.14 (Z)-2,4-dimethylpent-2-enoyl-SNAc (**12**)
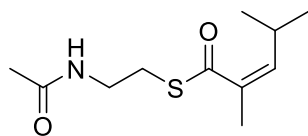
(Z)-2,4-dimethylpent-2-enoic acid[40] (61 mg, 0.48 mmol) was dissolved in DCM (1.5 mL) and

cooled to 0 ˚C before N-acetylcysteamine (0.060 mL, 0.57 mmol) was added followed by DMAP

(6.1 mg, 0.050 mmol) and EDC-HCl (137 mg, 0.71 mmol). The reaction was allowed to warm to

RT and stirred for 4 hours. Upon consumption of the starting material, saturated aqueous NH_4Cl

solution (10 ml) was added, and the organic phase was separated. The aqueous phase was extracted with diethyl ether (3 × 10 ml), and the combined organic phases were dried over anhydrous Na_2SO_4, filtered and concentrated under reduced pressure. The residue was purified by silica gel column chromatography (60% EtOAc/hexane) to give (Z)-2,4-dimethylpent-2-enoyl-SNAc (65 mg,0.28 mmol, 60% yield). ^{1}H NMR ($CDCl_3$, 400 MHz) δ ppm: 5.98 (br s, 1H), 5.49 (dq, J = 10.0, 1.4 Hz, 1H), 3.43 (q, J = 6.2, 2H), 3.05 (t, J = 6.4 Hz, 2H), 3.01 – 2.95 (m,1H), 1.94 (s, 3H), 1.93 (d, J = 1.4 Hz, 3H), 0.96 (d, J = 6.8 Hz, 6H); ^{13}C NMR ($CDCl_3$, 100 MHz) δ ppm: 194.9, 170.3, 146.2, 131.3, 39.8, 28.6, 28.4, 23.2, 22.7, 21.8, 20.7; HRMS (FAB) m/z (M+H)+ calcd for $C_{11}H_{19}NO_2S$, 230.1215; obsd 230.1207

A.15 (Z)-4-methylpent-2-enoyl-SNAc (**13**)
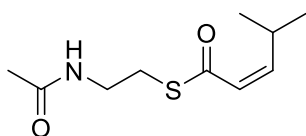
(Z)-4-methylpent-2-enoic acid[41] (50.mg, 0.4400mmol) was dissolved in DCM (1.5 mL) and cooled to 0 ˚C before N-(2-sulfanylethyl)acetamide (0.060 mL, 0.5300 mmol) was added followed by DMAP (2 mg, 0.0400mmol) and EDC-HCl (126 mg, 0.6600mmol). The reaction was allowed to warm to RT and stirred for 4 hours. Upon consumption of the starting material, saturated aqueous NH4Cl solution (10 ml) was added and the organic phase was separated. The aqueous phase was extracted with diethyl ether (3 × 10 ml), and the combined organic phases were dried over anhydrous Na2SO4 and concentrated under reduced pressure. The residue was purified by silica gel column chromatography (60% EtOAc/n-hexane) to give (Z)-4-methylpent-2-enoyl-SNAc (65 mg,0.30 mmol, 68.916% yield) δH (CDCl3, 400 MHz) 6.89 (dd, 15.6, 6.6 Hz.

1H), 6.07 (dd, 15.6, 1.5 Hz, 1H), 5.91 (br s, 1H), 3.45 (q, 6.0 Hz, 2H), 3.08 (t, 6.4 Hz, 2H), 2.46 (m, 1H), 1.96 (s, 3H), 1.05 (d, 6.8 Hz, 6H); ^{13}C NMR (CDCl$_3$, 100 MHz) δ ppm: 190.7, 170.3, 152.6, 125.7, 39.8, 31.0, 28.3, 23.2, 21.1; HRMS (FAB) m/z (M+H)+ calcd for C$_{10}$H$_{17}$NO$_2$S, 216.1058; obsd 216.1051

B. Biological protocols

B.1 Cloning and expression

A construct encoding amino acids 1697-1984 from *GphF* of the gephyronic acid PKS was codon optimized for expression in *E. coli.* Synthetic cDNA was cloned into a pMocr-based expression vector[26] to create pGJD013. Cells of *E. coli* strain BL21(DE3) pRARE AI were transformed with pGJD013. The starter culture was transferred to a 2 L baffled flask containing 0.5 L 4% glycerol Terrific Broth media (BD) with 100 mg/L ampicillin and 50 mg/L spectinomycin, grown at 37°C to an OD$_{600}$ of 1.5, cooled to 20°C, induced by addition of isopropyl β-D-1-thiogalactopyranoside (IPTG) to 0.2 mM and 1 g solid (L)-arabinose, and incubated 18 hr. Cells were harvested via centrifugation, transferred to 50 mL falcon tubes and immediately frozen at -20°C. Plasmids encoding CurK DH (wild type and P1005V) were expressed in *E. coli* as described previously.[11]

B.2 Mutagenesis

Site-directed mutagenesis of GphF DH1 and CurK DH was done via PCR of pGJD013 and pJRR198[11], respectively, using primers designed with the QuikChange primer design tool website (Agilent) (Table 5.1). Forward and reverse primers are shown below with the mutated codons underlined. Sequences of the coding regions of all plasmids were confirmed by Sanger sequencing.

Table 5.1 Primers for mutagenesis

Mutant	Primers (5' – 3')
GphF DH1 H1735Q	catcataaacccactgttcacccagatatgccgga tccggcatatctgggtgaacagtgggtttatgatg
GphF DH1 D1898N	cactgaaaacaggcattcagcagtgccggatgc gcatccggcactgctgaatgcctgttttcagtg
GphF DH1 L1744P	catttccagataggtaacacccggaacaacaattgcatcataaac gtttatgatgcaattgttgttccgggtgttacctatctggaaatg
GphF DH1 Y1856F	agacgcggaccaaaatagatgcgcatacgttcataa ttatgaacgtatgcgcatctattttggtccgcgtct
CurK P1005V	aatagcctgtggctacaaagagcaccttgttaaatacttggtg caccaagtatttaacaaggtgctctttgtagccacaggctatt

B.3 Protein Purification

All purification steps were performed at 4°C. Cells were resuspended in buffer A (50 mM Tris

pH 7.5, 300 mM NaCl, 10% glycerol) with 15 mM imidazole (4 mL/g cell pellet), incubated 1 hr

on ice in lysis buffer (Buffer A + 2 mM $MgCl_2$, 0.5 mg/mL DNaseI, and 0.06 mg/mL lysozyme),

and lysed by sonication. The lysate was cleared via centrifugation. The supernatant was filtered

through a 0.2 μm filter, and loaded onto a 5 mL His Trap column (GE Healthcare). The column

was washed with 10 volumes buffer A with 15 mM imidazole, and protein was eluted with a

linear gradient from 15 mM to 400 mM imidazole. Peak fractions were pooled, and the His-Mocr

tag was removed by overnight incubation with tobacco etch virus (TEV) protease (1:50

TEV:Mocr-GphF DH) with dialysis against Buffer A. The dialysate was re-loaded onto a His-trap column, and the flow-through and wash fractions were pooled, concentrated, and loaded on a Superdex 16/60 S200 gel filtration column (GE Healthcare) equilibrated with buffer A. GphF DH eluted as a monomer with an apparent molecular weight of 29 kDa (Calculated MW 32.6 kDa). Fractions with GphF DH1 were pooled, the protein was concentrated to 15 mg/mL, and flash frozen in liquid N_2.

B.4 Crystallography

Crystals were grown by sitting-drop vapor diffusion in 1:1 mix of 15 mg/mL protein stock and crystallization solution (01.M trisodium citrate, 20% polyethylene glycol 4K, 22% 1,4-butanediol, 10 mM Hepes pH 7.3). Crystals formed in 2-3 hours and were fully grown after 2 days. Crystals were harvested directly from drops and flash-cooled in liquid N_2. Data were collected at the Advanced Photon Source (APS, Argonne National Laboratory) on GM/CA beamline 23-ID-A. GphF DH crystals diffracted to 1.55 Å and were in orthorhombic space group $P2_12_12_1$ with one polypeptide per asymmetric unit. Data were processed using XDS[42]. The structure was solved via molecular replacement in phaser[43] using a search model generated using the chainsaw[44] program in CCP4[45] based on a dehydratase in the curacin biosynthetic pathway (CurK DH[11], PDB 3KG9). The CurK DH search model was truncated to the closest common carbon to the GphF DH. Refinement was done with PHENIX[46], and model building in coot[47]. The refined model was validated with MolProbity[48]. The superior crystallization properties of DH1/P1711L are explained by a lattice contact of the Leu1711 side chain with an outward-facing Ala side chain on a helix in an adjacent molecule in the crystal lattice.

B.5 Enzyme Assay

Reaction mixtures containing 200 µM substrate, 50 mM Hepes pH 7.5, 200 mM NaCl, 5% glycerol and GphF DH to a final concentration of 7.5 mg/mL (204.6 µM) in a total volume of 80 µL were mixed by brief pipetting and incubated overnight at 37°C. Reactions were quenched by addition of 150 µL methanol. After precipitated proteins were removed via centrifugation, 0.5 µL of the supernatant from each reaction were analyzed by mass spectrometry on an Agilent 6250 Q-TOF LC/MS. Separation was achieved using a Kinetix reverse-phase C_{18} column (50 mm x 2.1 mm, 2.6 um, Phenomenex) with a gradient from 0-95% H_2O:acetonitrile. Serial dilution of authentic standards was used to determine the minimum sensitivity for each compound, standard curves were used for quantitation. Additionally, 10 µL of the same samples were separated by HPLC (Agilent 1200) and analyzed by ultraviolet absorbance at 225 nm. Separation was achieved using a Kinetix reverse-phase C_{18} column (50 mm x 2.1 mm, 2.6 um, Phenomenex) with a gradient of 0-95% acetonitrile in water. A_{225} values were quantitated from the peak areas based on extinction coefficients of standards, and LC/MS EIC values via standard curves of standards. CurK DH was assayed identically to the procedure used for GphF DH1, but with a final enzyme concentration of 10 mg/mL (313.68 µM) and a 30 hour incubation at 37°C. Chiral separation was achieved using a reverse-phase Lux cellulose 3 5 µm column (Phenomenex) with a gradient from 30-85% H_2O:acetonitrile.

Results

Synthesis of Gph1 DH substrate candidates

All synthesis experiments were run by Danialle Ronnow

To investigate both the reactivity and specificity of GphF DH1, we systematically examined features of both the native diketide and the potential intermediates crucial for recognition and processing (Fig. 5.1B). Four potential 2-methyl-3-hydroxy substrates (**2-5**), a potential (*E*)-2-methyl-2-enoyl dehydration product (**6**), and two potential 2-methyl-3-enoyl elimination products (*rac*-**7**, **8**) were synthesized in an effort to explore the effect of stereochemistry on GphF DH function (Fig. 5.1B). To explore the importance of the 2-methyl group, a 3-hydroxy substrate (**9**), a potential (*E*)-2-enoyl dehydration product (**10**), and a potential 3-enoyl elimination product (**11**) were synthesized (Fig. 5.1B). Finally, as some DHs can act on (*Z*) configured alkenes[3, 10], (*Z*)-2-methyl-2-enoyl (**12**) and (*Z*)-2-enoyl (**13**) compounds were synthesized. All thioester analogs were synthesized by coupling the corresponding carboxylic acids to *N*-acetylcysteamine (NAC) except potential elimination product *rac*-**7**, which was synthesized in an expedient manner via a palladium-catalyzed alkenylation followed by routine conversion to the NAC thioester. All synthetic substrates had distinct retention times in chromatographic separation excepting the **2**/**3** , the **4**/**5** enantiomers and the *E*/*Z* regioisomers **6**/**12** and **11**/**13** (Figs. 5.2, 5.3, 5.4, Table 5.2).
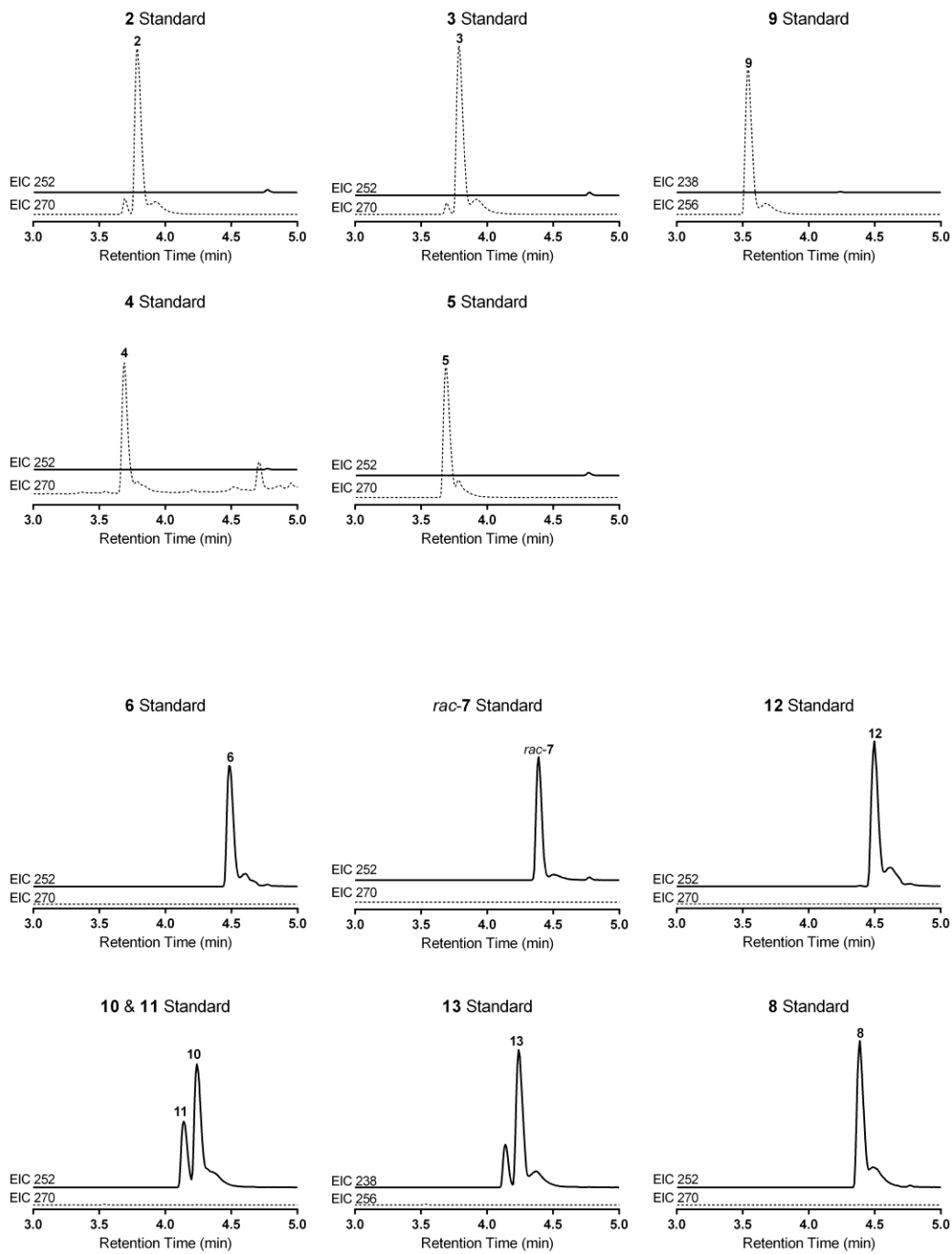
Figure 5.2 LCMS EICs for 2-13. Distinct retention times are observed for all non-enantiomeric species.
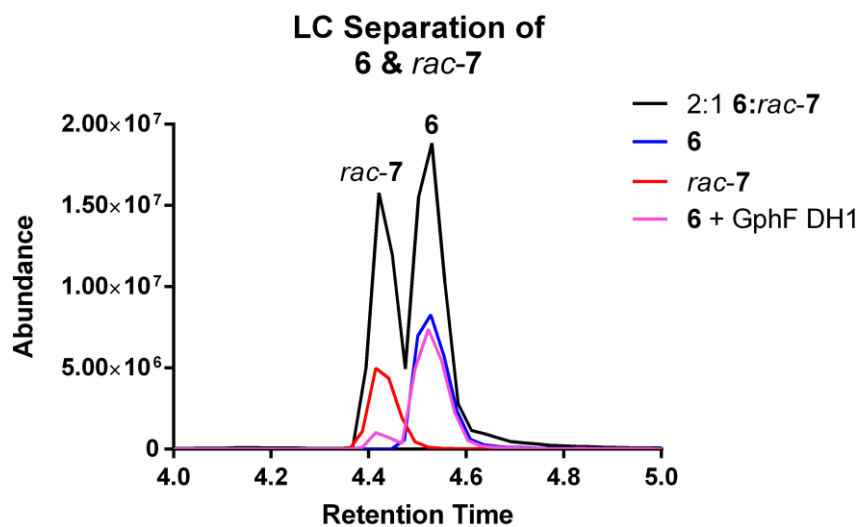
Figure 5.3 LC separation of 6 and 7.

Standards of 6 (blue) and 7 (red) were analyzed separately and in a 2:1 ratio of 6:7 (black) by
LCMS. The retention times observed in this experiment match those observed in the dehydration of
2 and 3 by GphF DH1.
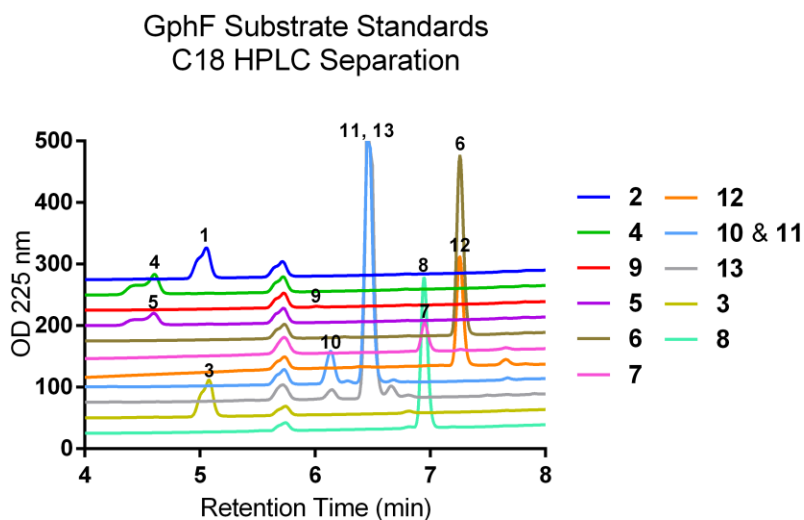
**Figure 5.4 HPLC/UV traces of GphF substrate mimic
standards.**

Table 5.2 LC/MS Retention Times

C18 column	
Compound	Retention Time
2	3.78
3	3.78
4	3.7
5	3.7
6	4.47
rac-**7**	4.35
8	4.35
9	3.54
10 & 11	4.23, 4.13
12	4.47
13	4.22

Chiral cellulose column	
Compound	Retention Time
6	10.80
8	10.21
14	10.41

Catalytic assay

**GphF DH1
Superdex S200**
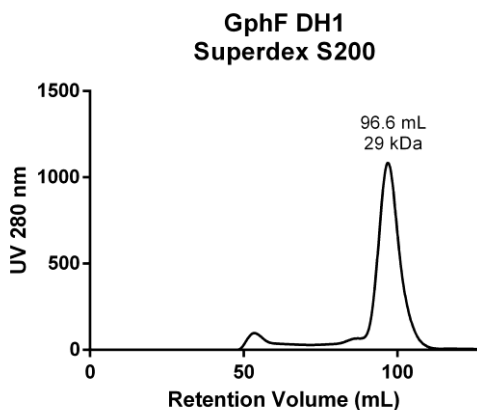
Figure 5.5 Superdex S200 gel filtration profile of Purified GphF DH1.

The apparent molecular weight of the excised domain is 29 kDa, indicating DH1 is monomeric in solution. The calculated molecular weight of GphF DH1 is 32.6 kDa.

Amino acids 1697-1984 of GphF were selected as the boundaries of the DH1 domain based on homology to PKS DH domains of known structure[4, 11-14], and the excised DH was produced in *E. coli*. The purified, recombinant GphF DH1 was monomeric in solution with an apparent molecular weight of 29 kDa by size-exclusion chromatography (calculated molecular weight 32.6 kDa), in contrast to other module-embedded DH domains, which are dimeric in solution (Fig.

5.5).[4, 11-13] GphF DH1 was assayed using NAC-linked test substrates **2-13** (Fig. 5.1B). Following removal of protein by methanol precipitation, reaction mixtures were separated by HPLC and analyzed by both absorbance at 225 nm (Table 5.3) and mass spectrometry. Quantitation based on **2**-**13** authentic standards yielded highly consistent results with A_{225} and LC/MS analysis, but owing to the low ultraviolet absorbance of **2-13**, the MS analysis had greater precision. Total ion counts (TIC) of the LC elution profiles of the test substrates and reaction mixes were monitored, and extracted ion chromatograms (EICs) were generated from individual peaks and used to quantitate the extent of catalysis. GphF DH1 catalyzed reactions with all compounds except **5** and **8**.

Table 5.3 GphF DH1 activity by UV absorbance

	Distribution of substrate & products (%)		
3-hydroxy substrate	3-hydroxy	2-enoyl	3-enoyl
2	$70.3 \pm 2.6^*$	27.7 ± 2.3	1.9 ± 7.4
3	83.4 ± 4.1	14.5 ± 4.3	2 ± 17
4	99.9 ± 4.5	0	0
5	99.9 ± 3.4	0	0
9	N.D.†	63.3 ± 1.3	36.7 ± 1.5
Unsaturated Substrate	3-hydroxy	2-enoyl	3-enoyl
6	0.4 ± 5.1	97.77 ± 0.04	1.81 ± 0.05
rac-**7**	0	20.6 ± 0.7	79.4 ± 0.7
8	0	0	99.9 ± 2.0
10 & 11	N.D.	32.0 ± 4.0	67.9 ± 4.2
12	0	99.9 ± 6.9	0
13	N.D.	33.6 ± 4.3	66.4 ± 4.3

* Quantitation of substrate/product distribution is based on HPLC separation
and absorbance at 225 nm by comparison to authentic standards.
†**9** (rehydration product of **10**, **11** or **13**) does not absorb at 225 nm and cannot
be detected in the UV absorbance assay.

Table 5.4 Activity of Wild-type GphF DH1

3-hydroxy substrate	Distribution of substrate & products (%)		
	3-hydroxy	2-enoyl	3-enoyl
2	71.6 ± 0.5*	27.7 ± 0.5	0.6 ± 0.1
3	81.6 ± 0.4	18.0 ± 0.3	0.3 ± 0.1
4	99.9 ± 0.1	0.5 ± 0.1	< 0.01
5	99.9 ± 0.1	< 0.01	< 0.01
9	87.5 ± 0.2	5.4 ± 0.1	7.1 ± 0.1
Unsaturated substrate	3-hydroxy	2-enoyl	3-enoyl
6	1.3 ± 0.1	89.4 ± 0.1	9.3 ± 0.1
rac-**7**	< 0.01	12.9 ± 0.2	87.0 ± 0.2 $(37 + 50)$
8	< 0.01	< 0.01	99.9 ± 0.1
10 & **11** (2:1)	5.9 ± 0.3	38 ± 2	56 ± 2
12	0.3 ± 0.1	96.6 ± 0.1	3.1 ± 0.1
13	6.3 ± 0.2	37.1 ± 0.4	56.7 ± 0.6

* Quantitation of substrate/product distribution is based on LC/MS separation and extracted ion counts for each species, as described in Methods. The starting substrate concentration in all assays was 200 μM.

Dehydratase activity

Based on the biosynthetic pathway deduced from the *gph* gene cluster[30] and on the established intermediates and products of homologous PKS modules, the GphF DH1 natural substrate is predicted to be (2*R*,3*R*)-3-hydroxy-2,4-dimethylpentanoyl-ACP, as the GphF CMT has been shown to act before the GphF KR1[31], and the "B-type" KR1 should produce an (*R*)-2-hydroxy product[15] PKS DHs have been predicted to catalyze *syn*-elimination [1-2, 49], as could occur with the (2R,3R)-2-methyl-3-hydroxy substrate **2**, or its enantiomer **3**. This prediction is based on PKS DH similarity to FAS DHs, where syn-elimination has been demonstrated[50-51], and on the activity of DH domains with 2-methyl substituents [4, 49]. Consistent with this prediction, recent studies on the stereospecificity of CMT domains from *trans*-AT PKS found that CMT domains installed (*R*)-2-methyl groups[52]. However, based on the structure of **1**, the methyl group installed by GphF MT1 is predicted to be in the (*S*)-configuration[30]. Thus we investigated GphF DH1 reactivity with NAC-linked thioesters of all four diastereomers of the predicted natural substrate (**2**, **3**, **4**, **5**) (Figs. 5.1B, 5.6, Table 5.4). Dehydrated products were detected for the enantiomers **2** and **3**, which are competent for *syn* elimination, whereas only trace amounts of dehydrated product were detected with **4**, and

none with **5**. Greatest activity was detected with **2** (28% conversion to **6**), whereas **3** was less

reactive (18% conversion to **6**) under our assay conditions. This indicates that the natural

substrate for GphF DH1 is likely (2*R*,3*R*)-3-hydroxy-2,4-dimethylpentanoyl-ACP and that GphF

DH1 catalyzes a *syn* elimination.
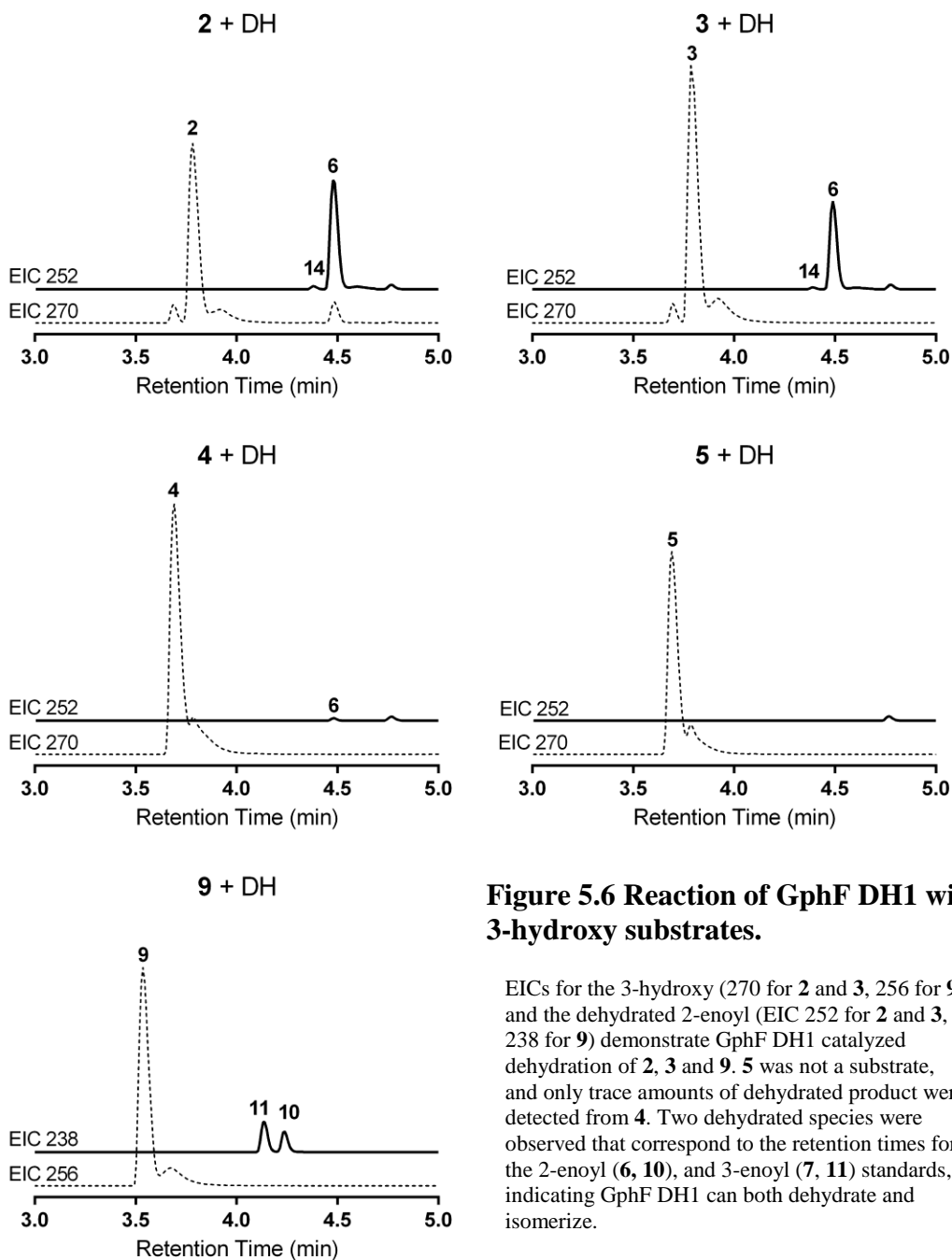
Figure 5.6 Reaction of GphF DH1 with 3-hydroxy substrates.

EICs for the 3-hydroxy (270 for **2** and **3**, 256 for **9**) and the dehydrated 2-enoyl (EIC 252 for **2** and **3**, 238 for **9**) demonstrate GphF DH1 catalyzed dehydration of **2**, **3** and **9**. **5** was not a substrate, and only trace amounts of dehydrated product were detected from **4**. Two dehydrated species were observed that correspond to the retention times for the 2-enoyl (**6, 10**), and 3-enoyl (**7**, **11**) standards, indicating GphF DH1 can both dehydrate and isomerize.

217

Isomerase activity

Reaction of **2** or **3** with GphF DH1 resulted in two dehydrated products with retention times of 4.47 min for the major product, and 4.35 min for the minor product (Fig. 5.6, Table 5.4). The masses and elution times of these products exactly match those of authentic **6** and *rac*-**7** prepared independently (Fig. 5.4). Thus, GphF DH1 possesses both dehydration and isomerization activities, and dehydration of a 2-hydroxy substrate may be followed by isomerization of the resulting 2-enoyl **6** to 3-enoyl *rac*-**7**, similar to the catalytic route of FabA. The isomerase activity was easily detected, but less 3-enoyl than 2-enoyl product accumulated under our assay conditions. In the reaction of GphF DH1 with **4**, we detected only trace amounts of the 2-enoyl product (retention time 4.47 min, Table 5.2) and the low turnover may have precluded detection of any 3-enoyl product.

When exposed to an (*E*)-2-enoyl NAC substrate, the *E. coli* FAS DH FabA produced an equilibrium mixture of 68% 3-hydroxy, 29% (*E*)-2-enoyl and 3% (*Z*)-3-enoyl products[7]. In an analogous manner, we used **6** and *rac*-**7** to assess the mixture of dehydration and isomerization products of GphF DH1 (Fig. 5.7, Table 5.4). Incubation with **6** resulted in 9% conversion to the 2-methyl-3-enoyl **7** (retention time 4.35 min), but only 1% re-hydration to substrate **2** or **3** (retention time 3.78 min). Similarly, GphF DH1 isomerized 13% of **7** to **6**, but **2/3** was not detected. These results provide additional support for a sequential mechanism of dehydration followed by isomerization and demonstrated strong forward equilibrium for the dehydration reaction, implying that the 2-methyl olefins **6** and **8/14** may have difficulty binding simultaneously with a water molecule in a manner competent for re-hydration.
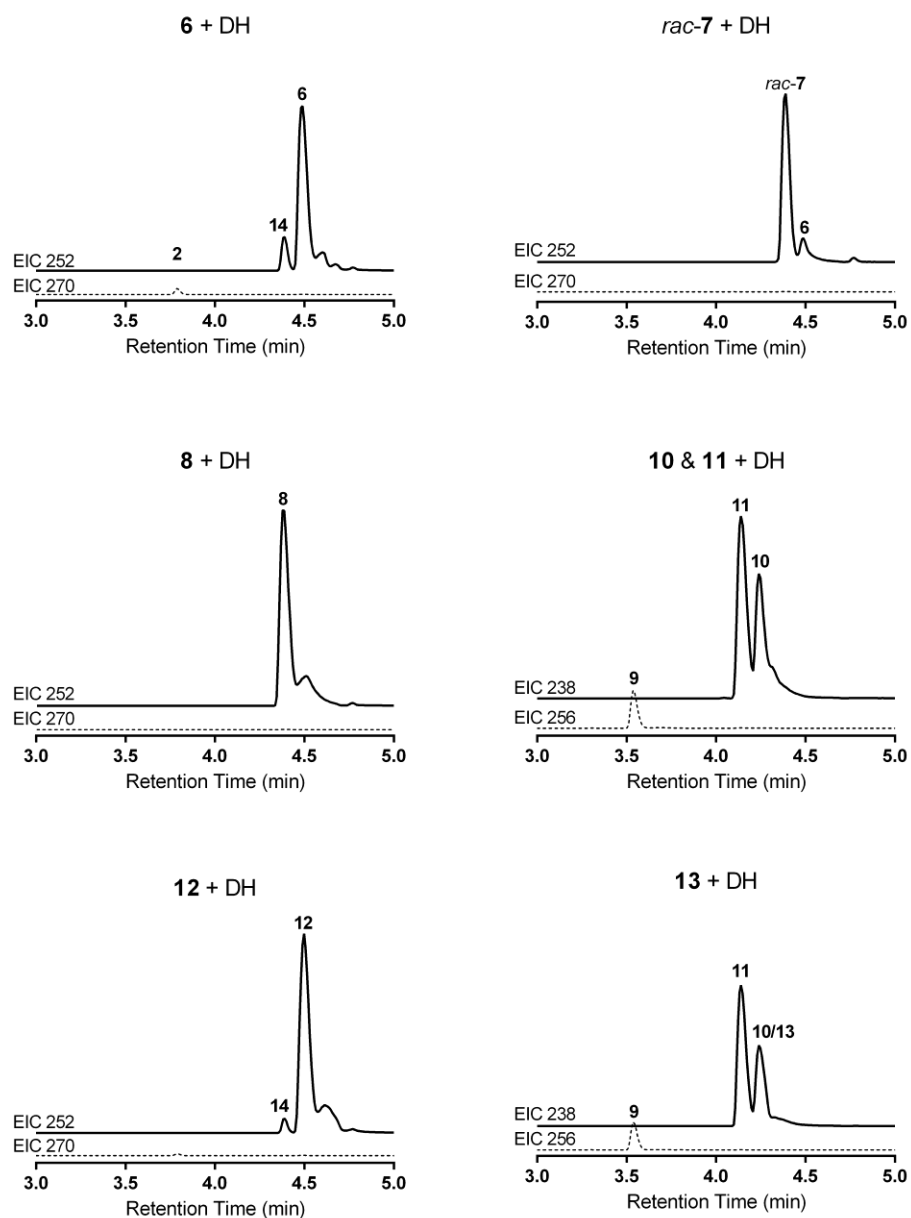
Figure 5.7 Reaction of GphF DH1 with unsaturated intermediates and products.

EICs are shown for both substrates and products. GphF DH1 was active on **6**, **7**, **12**, **13**, and a 2:1 mix of **10** & **11.** These results establish that like FabA, GphF DH utilizes a two-step mechanism in which the 2-enoly intermediate formed by dehydration is subsequently isomerized to give the final 3-enoyl product. Enantiomerically pure **8** is not turned over by DH1, while racemic 2-methyl-3-enoyl **7** is isomerized to **6**.

219

Specificity at C2 and epimerase activity

We used the (*R*)-configured **8** to assess GphF DH1 stereospecificity at C2 (Fig. 5.6, Table 5.1). No products were detected in reactions of GphF DH1 with **8** (Fig. 5.7, 5.8, Table 5.4), indicating that isomerization of **6** yielded the (*S*)-2-methyl product **14**. This was confirmed by chiral-LC/MS analysis (Fig. 5.8, Table 5.2) The *rac*-**7** standard was partially resolved into a species with an identical retention time to **8** (10.21 min) and a second species (10.41 min) corresponding to its enantiomer **14** (Fig. 5.8, Table 5.2). When incubated with **6**, GphF DH1 generated a product whose retention time matched that of **14**, and co-injection of **8** with the **6** + GphF DH1 reaction mixture clearly demonstrated that the isomerization product was **14** and not **8** (Fig. 5.8, Table 5.2) These results confirm a C2 epimerase function in the overall transformation of **2** to **14**. The effective epimerization requires either different catalytic residues for dehydration and epimerization, or substrate rearrangement in the active site to position **6** with the pro-*R* face of C2 towards the presumed proton donor (His1735).
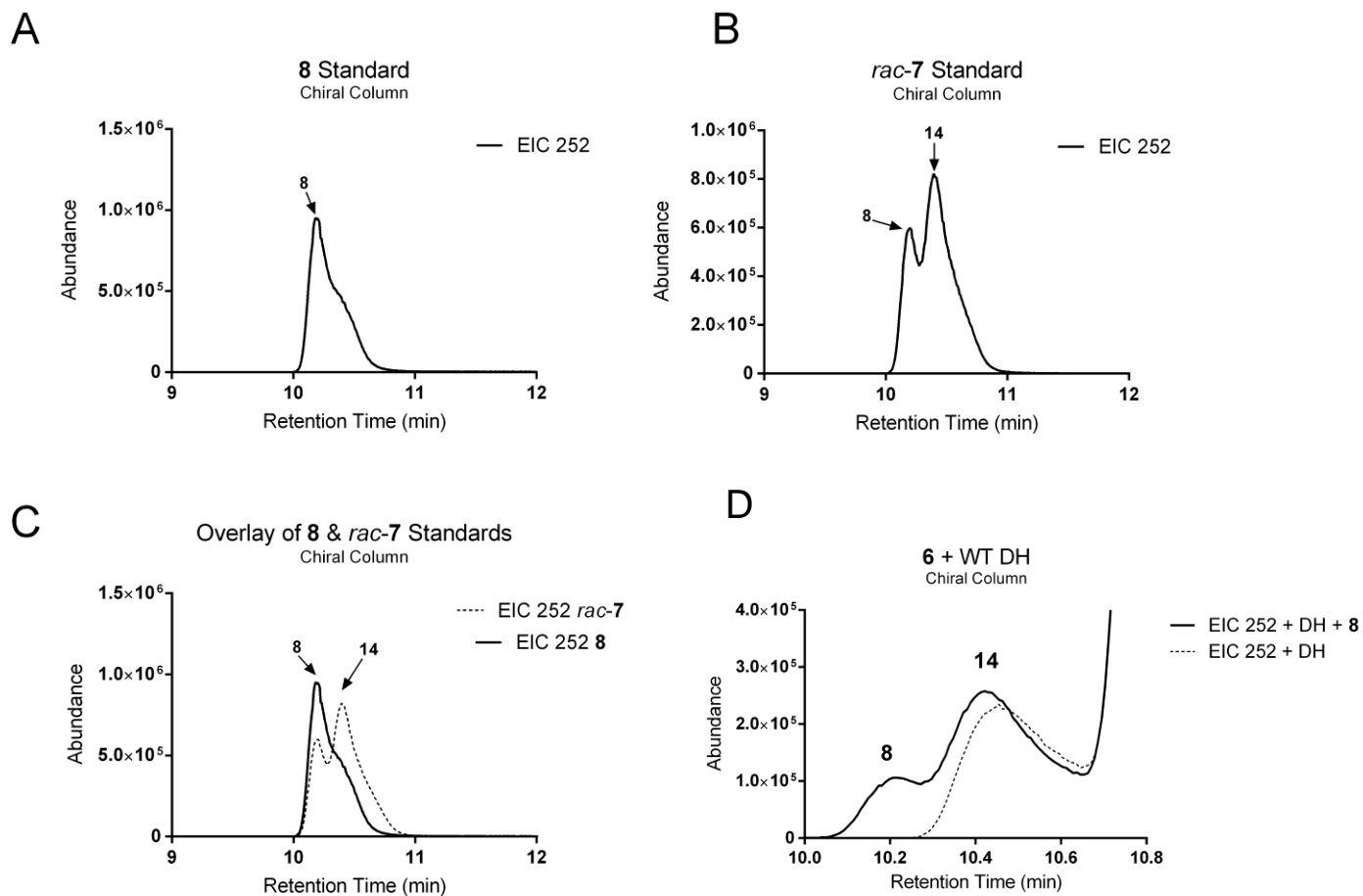
Figure 5.8 Chiral-LC/MS analysis of GphF DH1 isomerization/epimerization reaction.

EICs ([M + Na]$^+$) are shown for unsaturated intermediates/products. The 2*R* and 2*S* enantiomers **8** and **14** had distinct retention times (10.2 and 10.4 min, respectively). GphF DH1 selectively produced the 2*S* configured **14** from **6**, confirming epimerization activity.

We also tested the tolerance of GphF DH1 for non-methylated substrates using **9**, which resulted in products with retention times of 4.23 min and 4.13 min, identical to those of authentic standards for dehydration product **10** and elimination product **11**, respectively, which were available as a 2:1 mixture (Figs. 5., 5.7 Table 5.4). Thus, the dual-functionality of GphF DH1 is not strictly dependent on the presence of a 2-methyl substituent. Nevertheless, GphF DH1 preferred 2-methyl substrates: **9** was a poorer dehydration substrate than were **2** and **3** (13% dehydration for **9** *vs*. 28% for **2** and 18% for **3**, Table 5.4). This is consistent with the demonstration that 2-methylation by GphF CMT precedes KR1 reduction[31]. While lower levels of dehydrated intermediate **10** accumulated with non-methylated substrate **9** (5% **10**, compared to 28% **6** from methylated **2**), the isomerization was more effective, as **9** yielded significant quantities of the 3-enoyl product **11** (7%, compared to <1% 7 from the methylated **2** or **3**). Additionally, GphF DH1 converted the 67%:33% mixture of **10**:**11** to a 38%:56%:6% mixture of **10**:**11**:**9** (Fig. 5.7, Table 5.4).

E vs. *Z* selectivity

To further explore the relaxed substrate selectivity, we also evaluated the tolerance of GphF DH1 for (*Z*)-2-enoyl substrates **12** and **13** (Fig. 5.7, Table 5.4). The (*Z*)-configured **13** was converted to a mixture of elimination product **10** (57%) and hydrated product **9** (6%).In contrast, GphF DH1 had very low activity with the (*Z*)-2-methyl substrate **12** (3% isomerized to **7**, <1% hydrated to **2**/**3**), illustrating again that a 2-methyl substituent is detrimental to isomerization and effectively blocks hydration of 2-enoyl substrates. Activity with a (Z)-configured substrate is additional evidence for the relaxed substrate specificity and intermediate regiospecificity of GphF DH1, although it is unlikely that the activity observed here represents a biologically

relevant function, as neither **12** nor **13** is predicted to be a native substrate or intermediate[30]. Some PKS DHs are predicted to produce a (*Z*)-2-enoyl product, and this has been demonstrated in one case[3].

GphF DH1 crystal structure

Purified, recombinant GphF DH1 yielded single crystals that diffracted to 1.6 Å, but they were difficult to reproduce and grew slowly (Tables 5.5, 5.6, Figs. 5.10, 5.12A). A P1711L variant had identical activity to the wild type DH (Fig. 5.11) and resulted in reproducible growth of crystals of a different form that diffracted to 1.55 Å (Fig. 5.11, Tables 5.5, 5.7).GphF DH1 has the canonical double-hotdog fold of PKS DHs (Cα superposition results in RMSD values of 1.0 – 2.1 Å, Fig. 5.12B)[4, 11-14], but does not form a dimer in crystals, in agreement with the monomeric state in solution (Fig. 5.5). The active site, identified by the catalytic His1735 and Asp1898 side chains, is at the start of a hydrophobic substrate pocket (~7 Å wide and ~14 Å long) that extends from the catalytic His-Asp dyad along the central hotdog helix, and has a bi-lobed shape that could accommodate the substrate terminal methyl groups. The GphF DH1 pocket is shorter than the pockets of the curacin and erythromycin DHs, which have longer substrates[11-12] (Fig. 5.13).

Table 5.5 Crystallographic summary for WT GphF DH1 and P1711L variant

Diffraction data	GphF DH1 WT	GphF DH1 P1711L
Space group	$P2_12_12_1$	$P2_12_12_1$
Unit cell a, b, c (Å)	41.9, 74.42, 86.84	53.4, 71.6, 78.1
Wavelength (Å)	1.033	1.033
d_{min} (Å)	1.55 (1.605 – 1.55)	1.85 (1.91-1.85)*
Observations (#)	209,337 (6,450)	181,621 (12,129)
Unique reflections (#)	37,411 (2,556)	26,020 (2,380)
Mean I/σ_I	22.32 (1.99)	17.7 (1.67)
R_{merge}	0.044 (0.489)	0.076 (0.937)
$CC_{1/2}$	0.99 (0.62)	0.99 (0.56)
CC*	1.00	1.00
Completeness (%)	0.93 (0.65)	0.99 (0.92)
Wilson B (Å^2)	19.4	25.7
Refinement		
Reflections (#)	37,374	26,014
R_{work}	0.19	0.18
R_{free}	0.22	0.22
RMSD bonds (Å)	0.009	0.011
RMSD angles (°)	1.27	1.33
Atoms (#)		
Protein	2,241	2,266
Solvent	271	1163
Ligand	n/a	19
Avg B-factors (Å^2)		
Protein	26.9	37.4
Solvent	36.1	43.7
Ligand		52.7
Ramachandran		
Favored (%)	98.9	98.6
Allowed (%)	1.1	1.4
Outliers (%)	0	0

* Values in parentheses refer to the outermost shell of data.

Table 5.6 X-ray data statistics for GphF DH1 WT

Resolution	N(obs)	N(uniq)	Mult.	Compl.	<I/sigma>	R-merge	R-meas	R-pim	CC1/2
44.32 – 3.32	27,411	4,296	6.4	1.00	56.2	0.025	0.028	0.011	0.999
3.32 – 2.64	27,084	4,130	6.6	1.00	40.9	0.033	0.035	0.014	0.999
2.64 – 2.31	27,849	4,075	6.8	1.00	29.1	0.049	0.053	0.020	0.999
2.31 – 2.09	24,957	4,008	6.2	0.99	21.4	0.073	0.080	0.032	0.996
2.09 – 1.94	27,091	4,067	6.7	1.00	15.5	0.120	0.130	0.051	0.993
1.94 – 1.83	25,431	3,966	6.4	0.99	9.6	0.204	0.223	0.089	0.982
1.83 – 1.74	20,955	3,964	5.3	0.99	6.1	0.252	0.281	0.120	0.958
1.74 – 1.66	13,541	3,553	3.8	0.88	3.5	0.335	0.387	0.187	0.905
1.66 – 1.60	9,230	3,028	3.0	0.76	2.4	0.416	0.496	0.264	0.822
1.60 – 1.54	6,143	2,506	2.5	0.63	1.7	0.503	0.629	0.368	0.614
All	209,692	37,593	5.6	0.92	20.3	0.044	0.049	0.020	0.999

Table 5.7 X-ray data statistics for GphF DH1 P1711L

Resolution	N(obs)	N(uniq)	Mult.	Compl.	<I/sigma>	R-merge	R-meas	R-pim	CC1/2
44.10 – 3.99	18,806	2,782	6.8	1.00	47.3	0.028	0.031	0.012	0.999
3.99 – 3.17	18,849	2,656	7.1	1.00	36.7	0.041	0.045	0.017	0.999
3.17 – 2.77	18,925	2,615	7.2	1.00	22.6	0.071	0.076	0.028	0.998
2.77 – 2.51	19,127	2,619	7.3	1.00	13.7	0.123	0.133	0.049	0.995
2.51 – 2.33	19,006	2,594	7.3	1.00	9.9	0.176	0.189	0.070	0.992
12.33 – 2.20	18,963	2,588	7.3	1.00	7.7	0.226	0.243	0.089	0.987
2.20 – 2.09	18,961	2,589	7.3	1.00	5.7	0.315	0.339	0.124	0.978
2.09 – 2.00	18,853	2,569	7.3	1.00	3.9	0.474	0.510	0.186	0.941
2.00 – 1.92	18,005	2,566	7.0	1.00	2.4	0.756	0.817	0.305	0.882
1.92 – 1.85	12,949	2,454	5.3	0.96	1.4	1.058	1.176	0.502	0.633
All	182,444	26,032	7.0	1.00	15.5	0.071	0.077	0.029	0.999
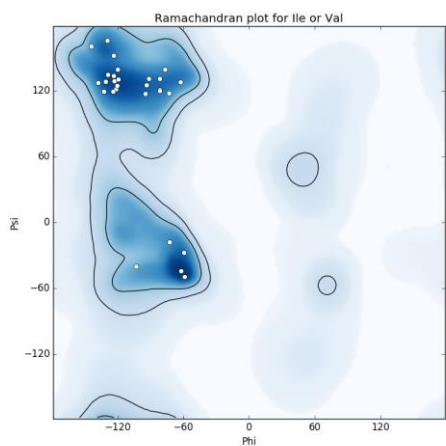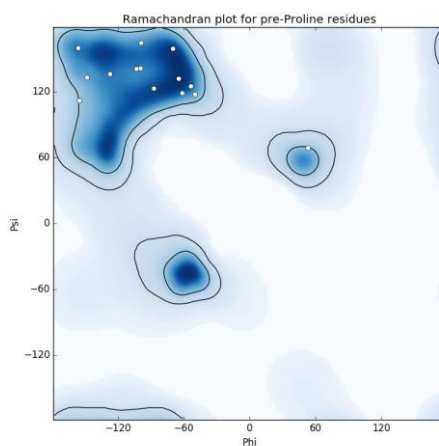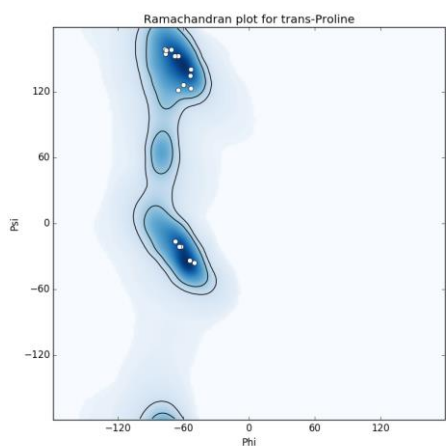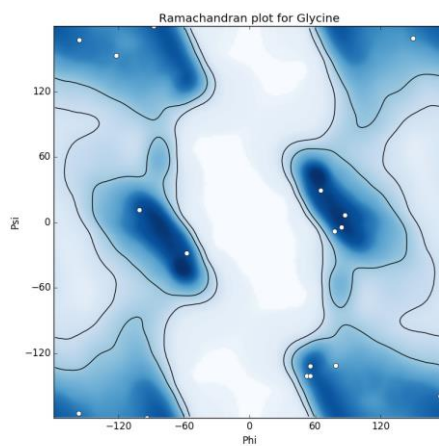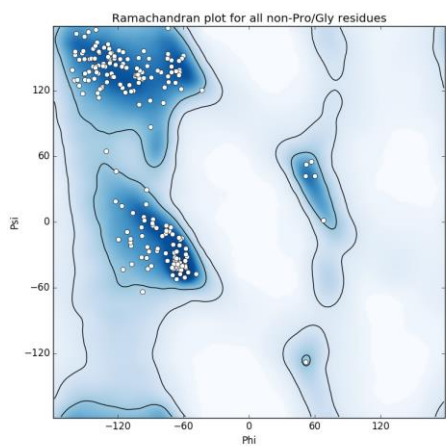
Figure 5.9 Ramachandran plots for GphF DH1 WT.
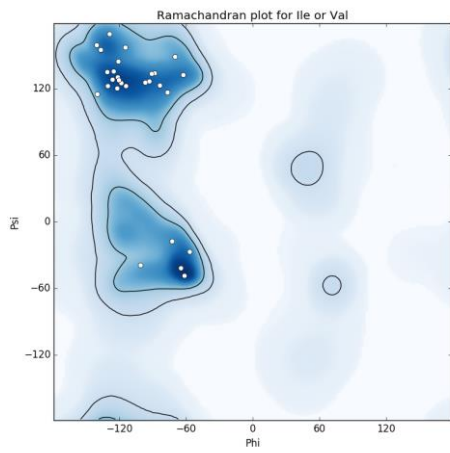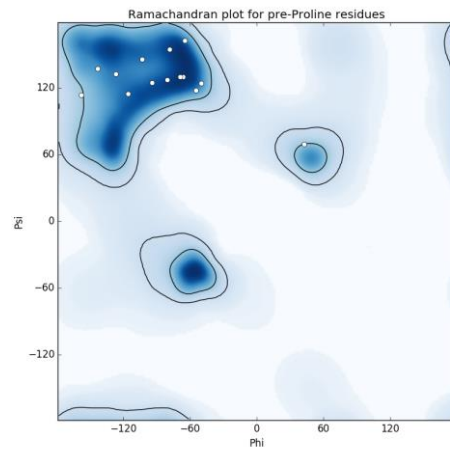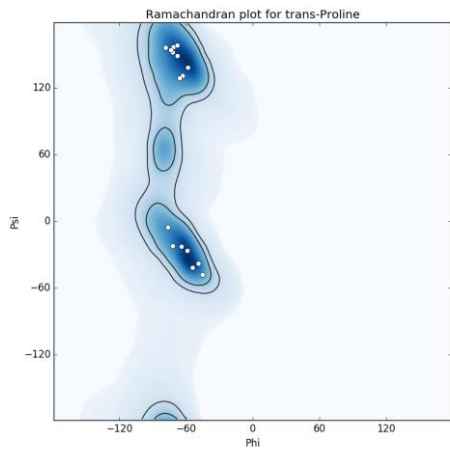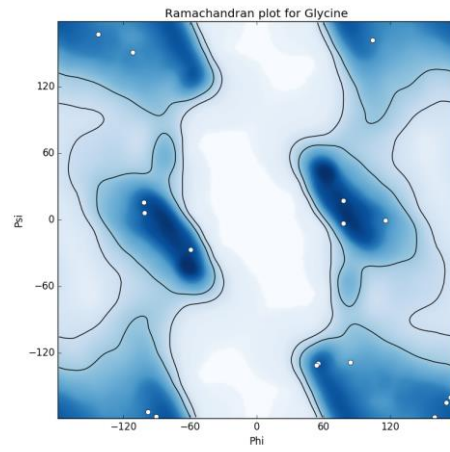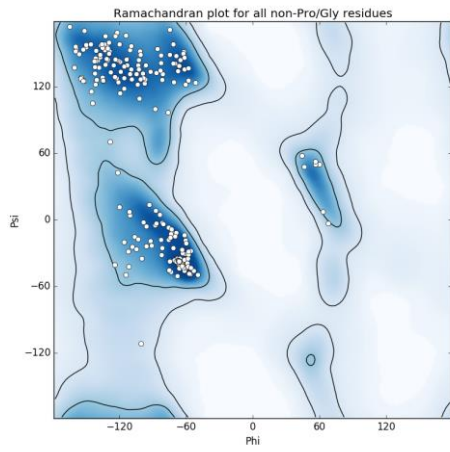
Figure 5.10 Ramachandran plots for GphF DH1 P1711L.
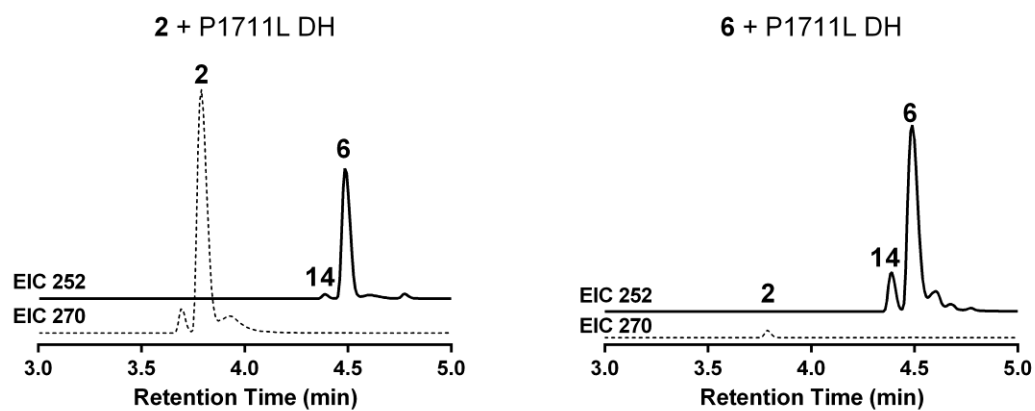
Figure 5.11 GphF DH1/P1711L Assay.

The variant used to reproducibly generate crystals exhibits identical activity to WT GphF DH1 using both **2** and **6**.
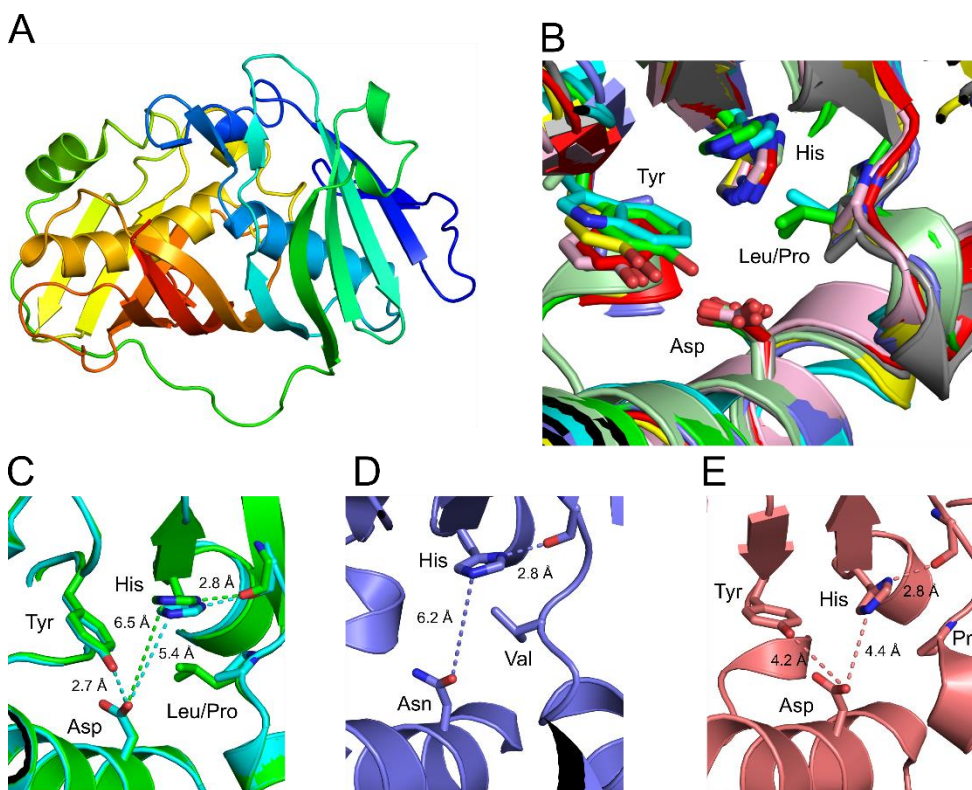
Figure 5.12 GphF DH1 structure.

A: Overall structure. B: Superposition of GphF DH1 (green), PksEI14 (cyan), and several non-isomerizing PKS DHs (DEBS yellow, Rif tan, CurK red, CurH white, CurJ purple, AmbDH3 light green). The catalytic His of GphF DH1 and Pks EI is further from the catalytic Asp than in the non-isomerizing DHs, correlated with a branched-chain amino acid in lieu of Pro. Protrusion of the Leu or Val into the active site also influences the Asp position. C. Superposition of WT GphF DH1 (Green) with L1744P GphF DH1 (Cyan). A modest shift in the position of the catalytic histidine is observed in the L1744P variant, reducing the distance between the catalytic His and Asp to 5.7 Å from 6.4 Å. Although this difference appears minor from a structural perspective, the L1744P variant is inactive as an isomerase, while retaining dehydration activity. D. The active site architecture of PksEI with relevant amino acids shown as sticks. The active site of PKSEI is very similar to that of GphF DH1. E. Active site architecture of the CurK DH with relevant amino acids shown as sticks. CurK DH is representative of a typical monofunctional PKS DH. The catalytic His and Asp are much closer than in GphF DH1, and the distance between the catalytic Asp and a conserved Tyr is well outside of hydrogen-bond length.

Superposition of active site structures revealed distinct differences between PKS enzymes capable of isomerization (GphF DH1 and PksEI14[27]) and the non-isomerizing DHs[4, 11-13] (Figs. 5.12B). Like the FAS DHs, all these enzymes have a hydrogen bond from the catalytic His-Nδ to a backbone carbonyl (Val1742), making the His-Nε atom available for acid-base chemistry. The most striking difference is a nearly 2 Å greater separation of the catalytic His and Asp functional groups in the isomerizing enzymes than in non-isomerizing PKS DHs[4, 11-13],
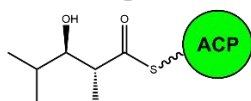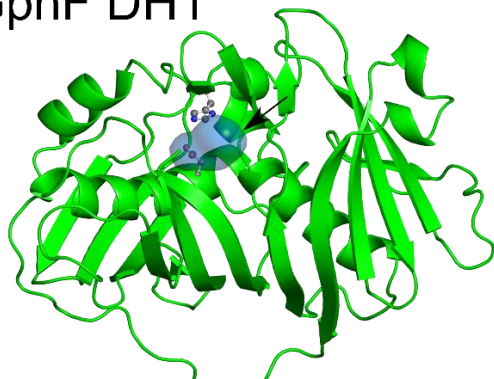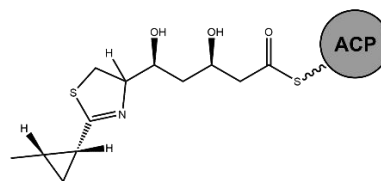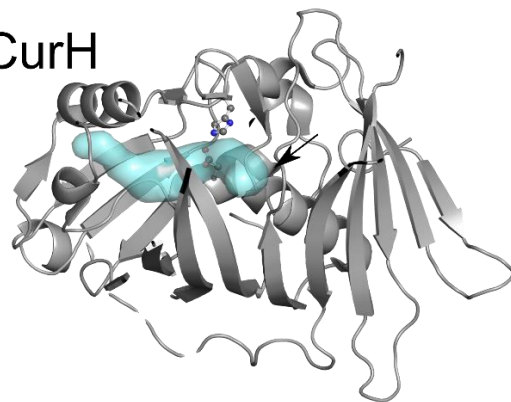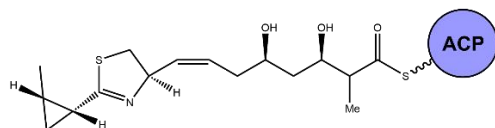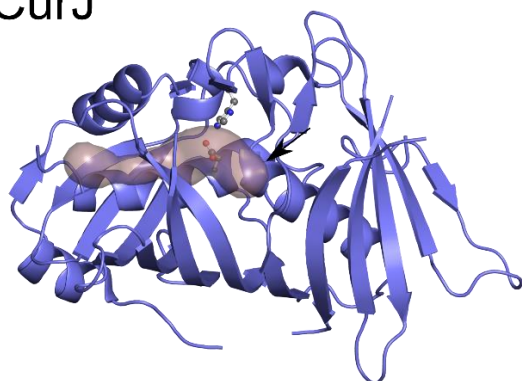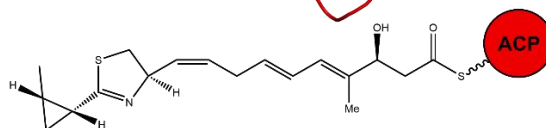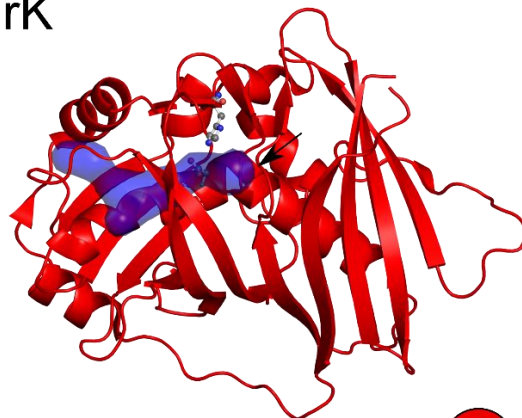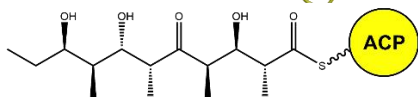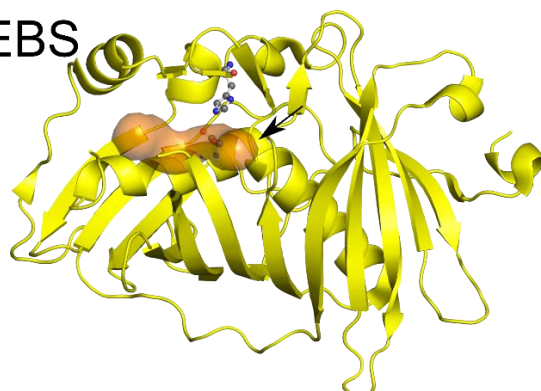
Figure 5.13 Comparison of PKS DH structures and substrates.

Active site entrances indicated by arrows, binding pockets shown as transparent surface. Comparison of these DHs highlights the similarity of the overall structure of PKS DHs, while active site renderings show how this fold is used as a scaffold to bind a variety of chemically diverse substrates.

and 1.3 Å longer than in FabA[20] (Fig. 5.12C, D). The extended distance may be due to a branched-chain amino acid near the catalytic His (GphF DH1 Leu1744, PksEI14 Val27) (Figs. 5.12C, D). As noted previously[27], a branched amino acid exists at this position in most presumed isomerizing DHs, whereas it is proline in non-isomerizing PKS DHs (Fig. 5.14). To investigate the importance of Leu1744 to the active site structure, we solved a crystal structure of GphF DH1/L1744P (Figs. 5.12C, 5.14, Tables 5.8, 5.9). In this structure, the catalytic His1735 Nε is 0.7 Å closer to Asp1898 than in the wild-type DH, but still further than in non-isomerizing DHs (Fig. 5.12E). Thus, the bulkier Leu side chain does not solely account for the longer distance between the catalytic side chains of GphF DH1.

A second striking difference of GphF DH1 to the non-isomerizing DHs is a hydrogen bond from the conserved Tyr1856 hydroxy to the catalytic Asp1898 carboxylate, a unique feature of GphF DH1 (Figs. 5.12C, E). The hydroxy-carboxylate contact does not occur in the non-isomerizing DHs due to the position the Asp side chain, which in GphF DH1 is affected by the branched side chain at Leu1744. An analogous hydrogen bond does not exist in the PksEI14 where the Asp is replaced with Asn and the Tyr with Trp (Figs. 5.12B, D 5.14)[27]. The Tyr1856 - Asp1898 hydrogen bond is especially interesting in light of the unusual GphF DH1 chemistry to affect an epimerization during sequential dehydration and isomerization reactions.

Assessment of Dual-Enzyme Functionality

We first tested the role of the His-Asp dyad in the dual DH activities. When the catalytic His1735 was substituted with Gln, no products were detected with **2**, **6**, **9**, or **10** & **11**, and substitution of the catalytic Asp1898 with Asn was similarly unreactive with **2** or **6**. Thus, like FabA, both His1735 and Asp1898 are required for each of the dehydration and isomerization

231

reactions (Fig. 5.16)[28]. In contrast, the isomerase activity of the PksEI14 required only the catalytic His[27].
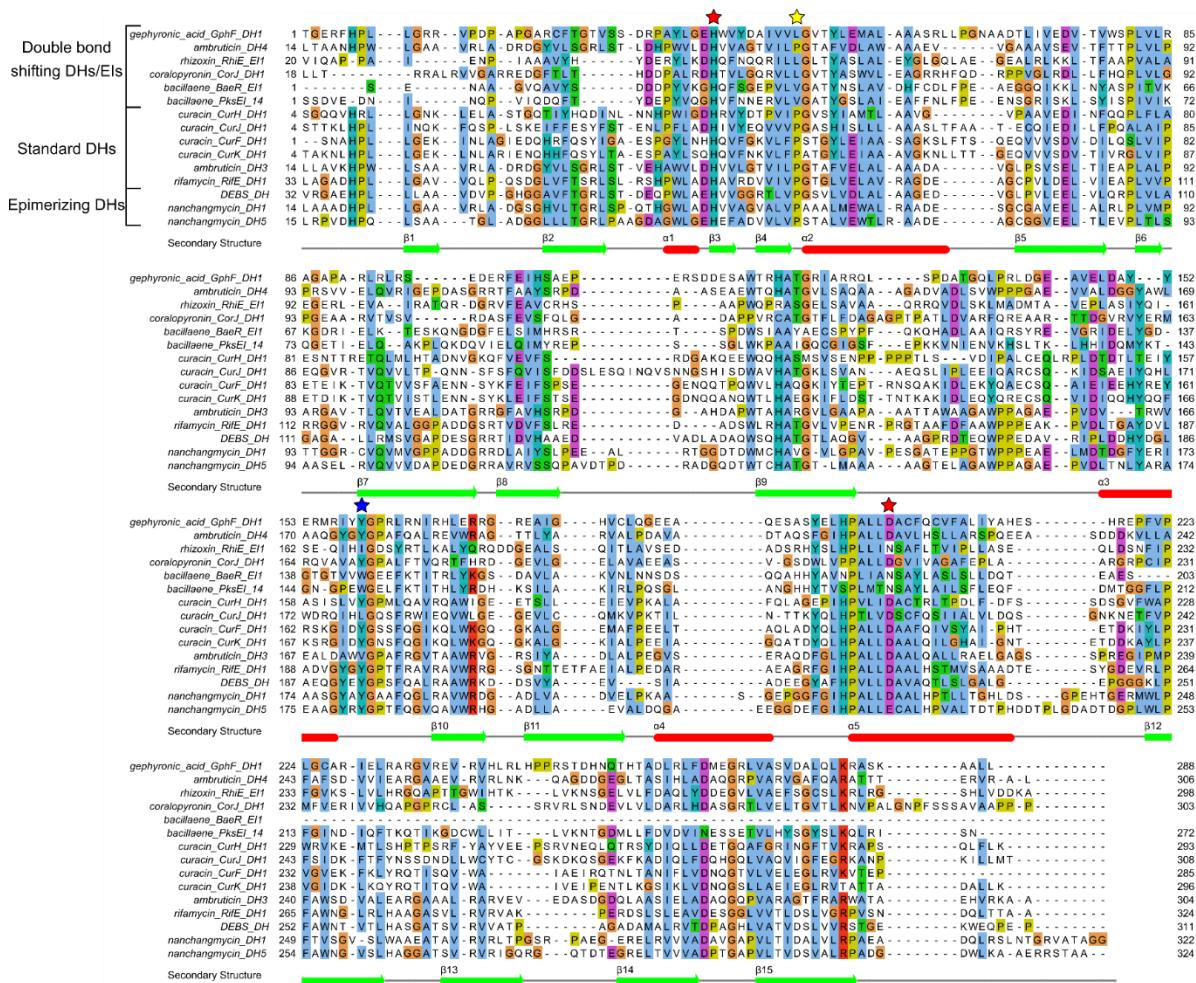
Figure 5.14 Sequence alignment of PKS DHs.

Red stars denote catalytic His and Asp, yellow star denotes the differentially conserved Leu(Val)/Pro, blue star denotes the mostly conserved tyrosine. In most DHs predicted to catalyze olefin shifts, there is a conserved branched-chain amino acid found nine residues after the catalytic His. In standard DHs, this position contains a conserved Pro.

Table 5.8 Crystallographic summary for GphF DH1 L1744P

Diffraction data	GphF DH1 P1711L, L1744P
Space group	$P2_12_12_1$
Unit cell a, b, c (Å)	34.9, 53.3, 147.1
Wavelength (Å)	1.033
d_{min} (Å)	1.7 (1.76 – 1.70)
Observations (#)	177,269 (8,583)
Unique reflections (#)	29,918 (2,268)
Mean I/σ_I	11.61 (0.96)
R_{merge}	0.082 (0.879)
$CC_{1/2}$	0.988 (0.531)
CC*	1.00
Completeness (%)	0.95 (0.73)
Wilson B ($Å^2$)	25.7
Refinement	
Reflections (#)	29,911
R_{work}	0.18
R_{free}	0.21
RMSD bonds (Å)	0.013
RMSD angles (°)	1.35
Atoms (#)	
Protein	2,305
Solvent	235
Ligand	n/a
Avg B-factors ($Å^2$)	
Protein	34.6
Solvent	40.3
Ligand	
Ramachandran	
Favored (%)	96.8
Allowed (%)	3.2
Outliers (%)	0.4

Table 5.9 X-ray data statistics for GphF DH1 P1711L, L1744P

Resolution	N(obs)	N(uniq)	Mult.	Compl.	<I/sigma>	R-merge	R-meas	R-pim	CC1/2
43.20 – 3.65	20,073	3,365	6.0	0.99	26.4	0.053	0.058	0.023	0.997
3.65 – 2.90	19,462	3,174	3.1	1.00	21.2	0.066	0.072	0.029	0.996
2.90 – 2.53	20,154	3,160	6.4	1.00	14.9	0.095	0.104	0.041	0.994
2.53 – 2.30	20,672	3,144	6.6	1.00	11.2	0.129	0.140	0.054	0.990
2.30 – 2.14	20,246	3,093	6.5	1.00	8.2	0.175	0.191	0.074	0.986
2.14 – 2.01	20,259	3,147	6.4	1.00	6.2	0.231	0.252	0.099	0.969
2.01 – 1.91	20,410	3,065	6.7	1.00	3.9	0.353	0.384	0.148	0.934
1.91 – 1.83	16,576	3,025	5.5	0.98	2.2	0.508	0.516	0.234	0.860
1.83 – 1.76	11,595	2,668	4.3	0.86	1.4	0.669	0.758	0.347	0.745
1.76 – 1.70	7,977	2,145	3.7	0.69	0.9	0.899	1.039	0.508	0.498
All	177,424	29,986	5.9	0.95	10.0	0.083	0.091	0.036	0.998
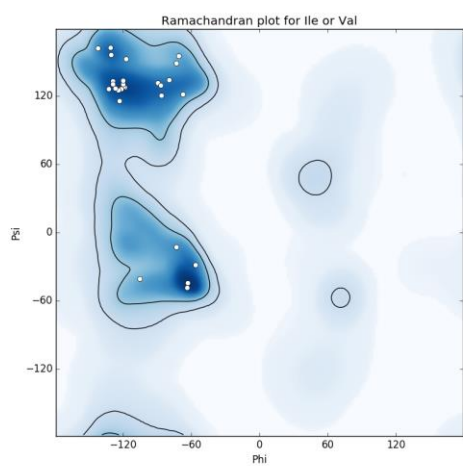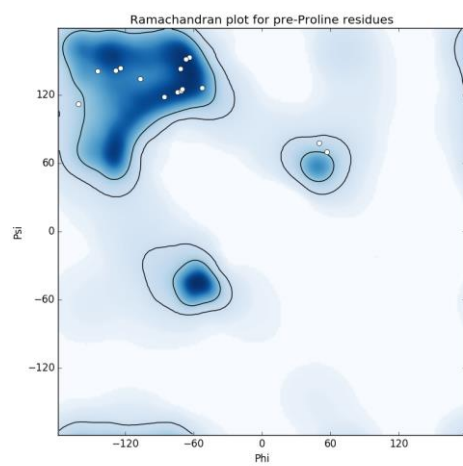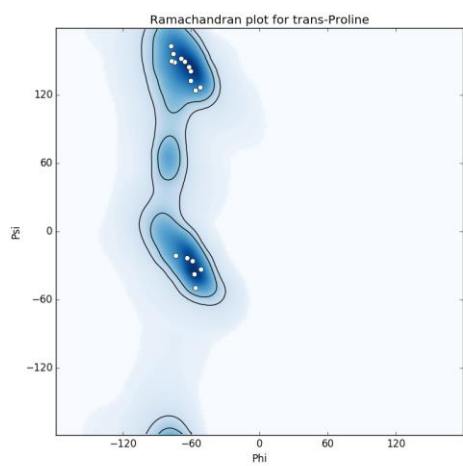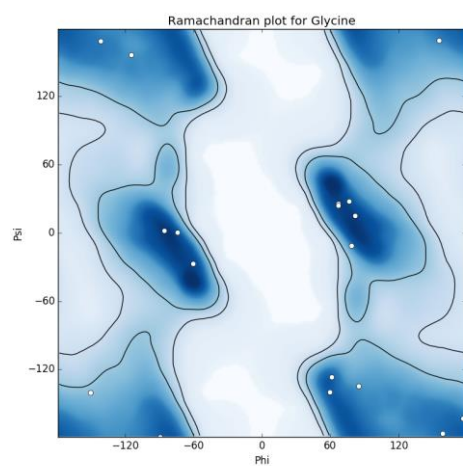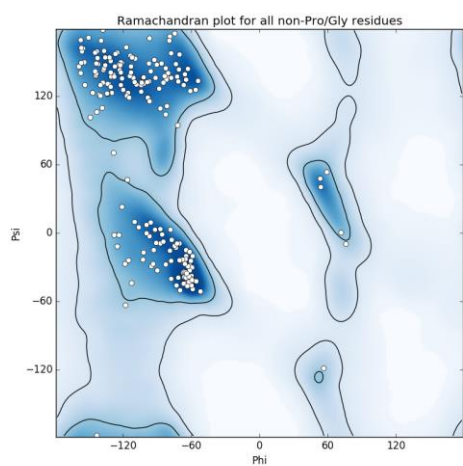
Figure 5.15 Ramachandran plots for GphF DH1 P1711L, L1744P.
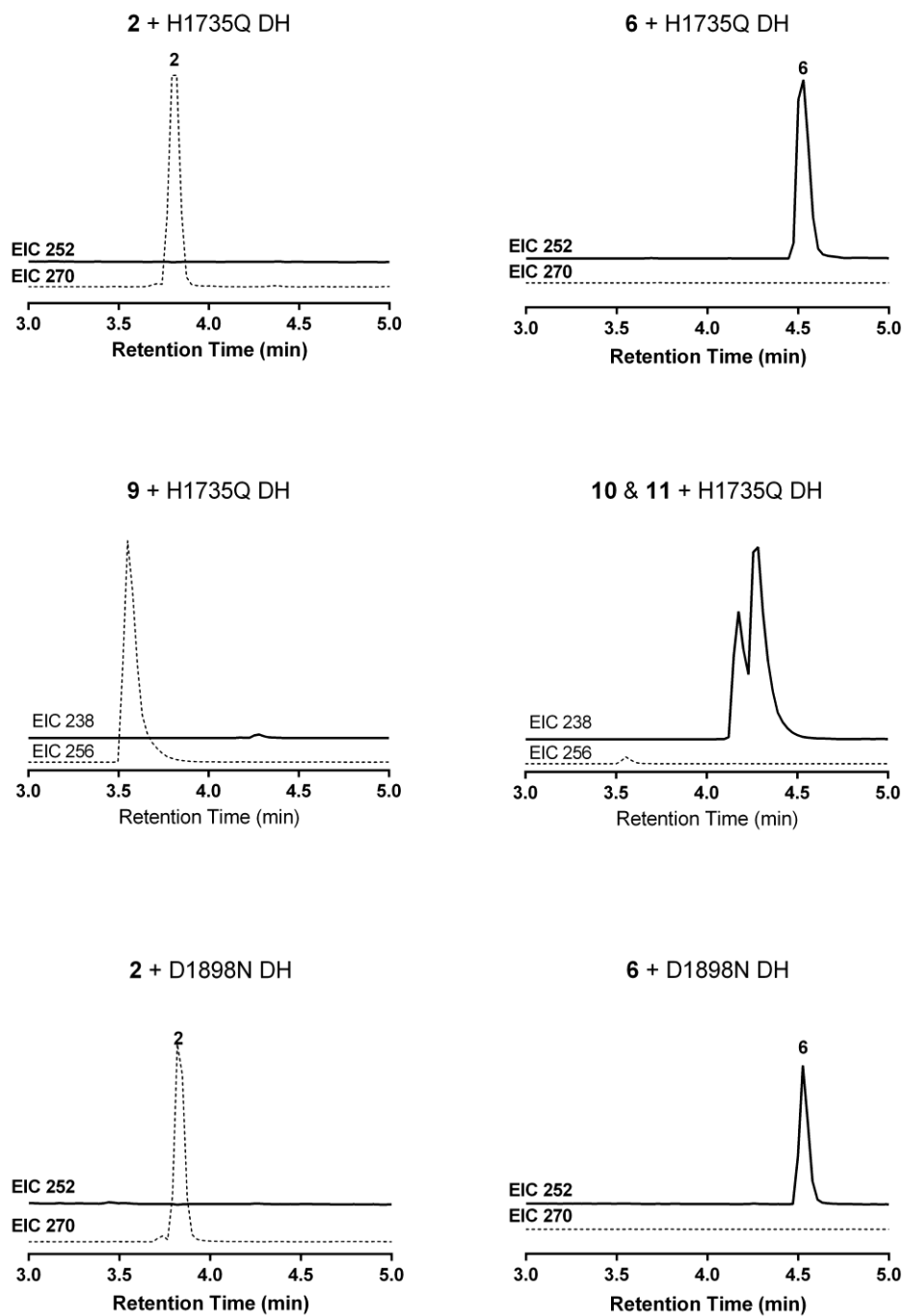
Figure 5.16 Mutagenesis of GphF DH1 catalytic residues.

Substrate and product EICs shown **2, 6, 9**, and **10** & **11**. For both the H1735Q variant and the D1898N variant, neither dehydration nor isomerization are observed. This result contrasts with the Pks EI, which can isomerize a 2-enoyl intermediate using only a catalytic His.

Table 5.10 Activity of GphF DH1/L1744P

	Distribution of substrate & products (%)		
3-hydroxy substrate	3-hydroxy	2-enoyl	3-enoyl
2	51.4 ± 0.4	48.8 ± 0.4	< 0.01
3	50.3 ± 0.6	49.6 ± 0.5	< 0.01
4	95.4 ± 0.1	0.5 ± 0.1	< 0.01
5	99.9 ± 0.1	< 0.01	< 0.01
9	58.9 ± 0.1	39.1 ± 0.5	2.0 ± 0.1
Unsaturated substrate	3-hydroxy	2-enoyl	3-enoyl
6	12.9 ± 0.2	87.1 ± 0.2	< 0.01
rac-7	< 0.01	< 0.01	99.9 ± 0.1
8	< 0.01	< 0.01	99.9 ± 0.1
10 & **11** (2:1)	35.1 ± 0.2	35.8 ± 0.8	29.1 ± 0.5
12	4.3 ± 0.1	95.6 ± 0.1	< 0.01
13	39.7 ± 0.6	40.7 ± 0.5	19.6 ± 0.2

We next investigated the role of the branched-chain amino acid near His1735. GphF DH1/L1744P had substantially increased dehydration activity relative to wild type DH1 (Table 5.9), but it lacked detectable isomerase activity with any of the 2-methyl substrates (**2**, **3**, **6**, *rac*-**7**, **12** ;Fig. 5.16; Table 5.10). In contrast, isomerase activity was retained with the substrates lacking a 2-methyl substituent (**9**, **10**, **11**, **13**). Thus, the effect of the branched side chain in the DH1 active site is specific to 2-methyl substrates. Additionally, DH1/L1744P had greater rehydration activity with **6** (13% *vs*. 1%) and with the **10**/**11** mixture (35% *vs*. 6%) than did the wild type. The increase in dehydration and rehydration with DH1/L1744P indicates that the branched side chain at position 1744 enables isomerization at the cost of reduced dehydration and rehydration activities.

2 + L1744P DH

EIC 252
EIC 270

6 + L1744P DH

EIC 252
EIC 270

10 & **11** + L1744P DH

EIC 238
EIC 256
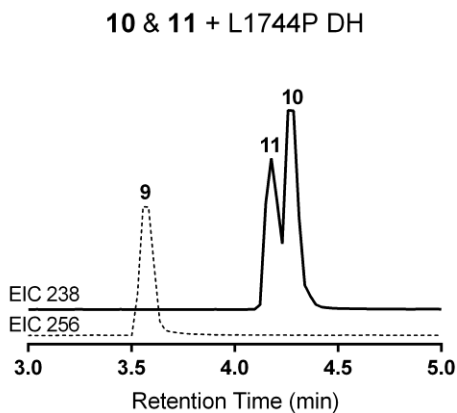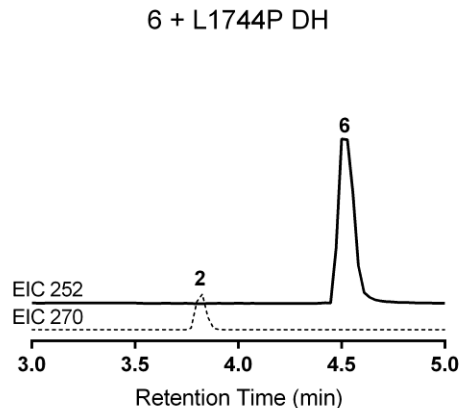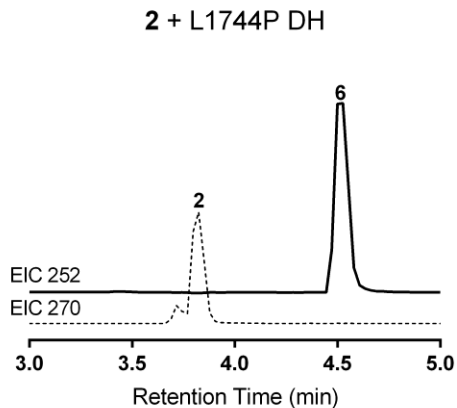
Figure 5.17 Assay of GphF DH1/L1744P using 2, 6, and a 2:1 mix of 10 & 11.

Substrate and product EICs are shown. DH1/L1744P dehydrated **2** and rehydrated **6** and **10** but did not form **7** or perturb the ratio of **10**:**11**. This demonstrates that for GphF DH1, Leu1744 is essential for isomerization activity, but plays no role in dehydration.

Table 5.11 Activity of GphF DH1/Y1856F

	Distribution of substrate & products (%)		
3-hydroxy substrate	3-hydroxy	2-enoyl	3-enoyl
2	83.2 ± 0.6	16.1 ± 0.7	< 0.01
3	80.5 ± 0.4	19.5 ± 0.4	< 0.01
4	99.4 ± 0.1	0.6 ± 0.1	< 0.01
5	99.9 ± 0.1	< 0.01	< 0.01
9	61.4 ± 0.6	31.9 ± 0.5	6.6 ± 0.3
Unsaturated substrate	3-hydroxy	2-enoyl	3-enoyl
6	2.3 ± 0.3	97.7 ± 0.3	< 0.01
7 (racemic)	< 0.01	< 0.01	99.9 ± 0.1
8	< 0.01	< 0.01	99.9 ± 0.1
10 & **11** (2:1)	31.1 ± 0.3	38.5 ± 0.4	30.4 ± 0.2
12	0.6 ± 0.1	99.3 ± 0.1	< 0.01
13	33.8 ± 0.1	39.9 ± 0.2	26.3 ± 0.2

To investigate the role of Tyr1856, we generated a Phe substitution. Tyr is conserved at this position in most, but not all, PKS DHs but, uniquely in GphF DH1, the side chain hydroxy is hydrogen bonded to the catalytic Asp1898 carboxylate (Figs. 5.12C, E 5.14, Table 5.11)[4, 11-12, 27]. GphFDH1/Y1856F catalyzed dehydration at a comparable rate to the wild type, but lacked any detectable isomerase activity with the 2-methyl substrates (**2**, **3**, **6**, *rac*-**7**, **12**; Fig. 5.17; Table 5.11). However, with substrates lacking a 2-methyl substituent (**9**, **10**, **11**, **13**), GphF DH1/Y1856F retained isomerase activity. Thus, while Asp1898 is critical to both dehydratase and isomerase activity, Tyr1856 plays an essential role in isomerization of 2-methyl substrates.
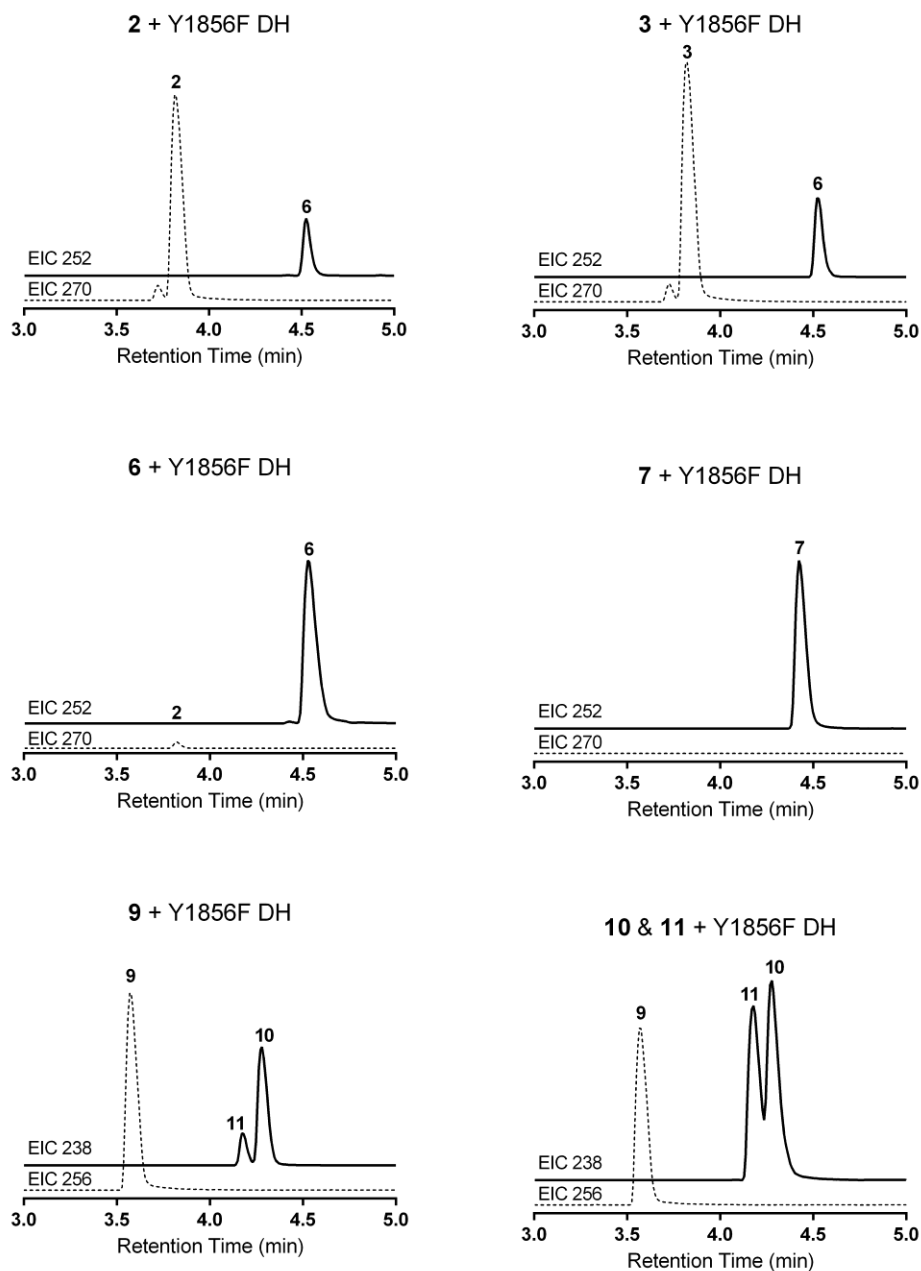
Figure 5.18 Assay of GphF DH1/Y1856F using 1, 3, 6, *rac*-7, 9, and a 2:1 mix of 10 & 11.

Substrate and product EICs are shown. DH1/Y1856F dehydrated **2** and **3**, as well as hydrated **6** and **10**. However, DH1/Y1856F was unable to form **7** or perturb the ratio of **10**:**11**, demonstrating that Tyr1856 is essential for isomerase activity, but not for dehydration.

Engineering a curacin DH/isomerase

Table 5.12 CurK DH activity

	Distribution of substrate & products (%)		
	3-hydroxy	2-enoyl	3-enoyl
Wild type			
3-hydroxy **9**	49.1 ± 0.2	50.9 ± 0.2	< 0.01
2-enoyl **10** & 3-enoyl **11** (2:1)	34.8 ± 0.3	34.9 ± 0.1	30.3 ± 0.3
P1005V			
3-hydroxy **9**	60.2 ± 0.3	38.4 ± 0.2	1.4 ± 0.2
2-enoyl **10** & 3-enoyl **11** (2:1)	34.9 ± 0.3	36.9 ± 0.5	28.2 ± 0.7

To investigate the hypothesis that the His-proximal branched-chain amino acid is essential for isomerization activity, we created an analogous P1005V variant of the non-isomerizing CurK DH. The natural CurK DH substrate has a 4-methyl substituent but lacks a 2-methyl, so **9** was used as a surrogate substrate. The wild-type CurK DH readily dehydrated **9**, producing only the 2-enoyl species **10**. CurK DH/P1005V also dehydrated **9**, but produced both the 2-enoyl species **10**, and the 3-enoyl **11** (Fig. 5.18, Table 5.12).
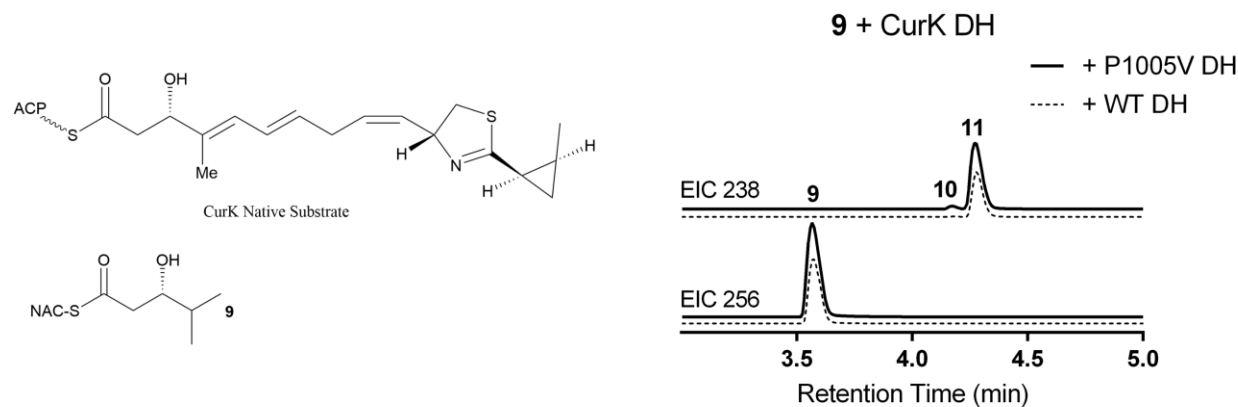
Figure 5.19 Engineering a dual-function PKS DH.

Left: **9** is a mimic of the acyl chain of the CurK DH substrate (top). **Right:** Assay of curK DH with **9.** Dashed lines show EICs for wild-type (WT) CurK DH, solid lines show EICs for CurK DH/P1005V variant. Both WT and P1005V dehydrated **3**, as shown by the production of 2-enoyl **10**. A second peak corresponding to 3-enoyl **11** is observed in the product EIC for DH/P1005V, establishing that a single amino acid substitution is sufficient to impart isomerase

Discussion:

Multifunctional PKS dehydratases:

Here, we describe the formation of an odd-to-even double bond by the GphF DH1 through dual dehydratase and isomerase activities. The (*S*)-2,4-dimethyl-3-pentenoyl thioester product is consistent with the structure of gephyronic acid **1**, the natural product of the Gph PKS pathway[30]. GphF DH1 had dehydratase activity only with compounds capable of *syn* elimination (**2**, **3** and **9**), in agreement with previously characterized DHs. DH1 exhibited relaxed substrate selectivity for both the dehydration and isomerization reactions. It dehydrated both 2-methyl-3-hydroxy enantiomers **2** and **3** as well as the non-methylated **9** to produce an (*E*)-2-enoyl product. DH1 was an isomerase for substrates with and without a 2-methyl substituent and even acted on (*Z*)-2-enoyl substrates. The FabA of bacterial fatty acid synthesis also catalyzes sequential dehydration and isomerization reactions, but it is specific for a 3-hydroxydecanoyl substrate and forms a (*Z*)-3-decenoyl product[7].

The crystal structure of GphF DH1, the first for an isomerizing PKS DH, offers clues to the basis for the dual catalytic activities. The active site His is assumed to be the sole catalytic base in all DH family members (FabA dual dehydratase/isomerase, PksEI4 and non-isomerizing DHs). As in other DHs, His1735 and Asp1898 together catalyze *syn* dehydration and therefore must be on the same face of the natural (2*R*,3*R*)-2-methyl-3-hydroxy substrate **2**. The His-Asp catalytic dyad and Tyr1856 are all required for isomerization of the (*E*)-2-methyl-2-enoyl dehydration product **6**. Thus, we propose that Asp1898 activates Tyr1856 to remove a C4 proton, creating a dienolate intermediate, and that His1735 re-protonates C2 to form the (*S*)-2-methyl-3-enoyl product (enantiomer of **8**) (Scheme 5.1). Tyr1856 is conserved in most PKS DHs (Fig.
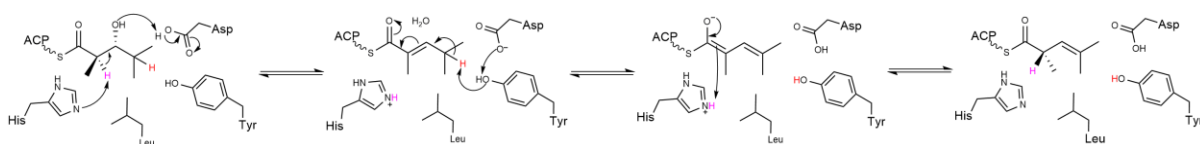
Scheme 5.1 Proposed mechanism for GphF DH1 activity on substrates containing a 2-methyl group.

After dehydration, Asp1898 activates Tyr1856, which abstracts a proton from C4, generating a dienolate intermediate. His1735 then reprotonates C2, setting the methyl in the (*S*) configuration.

5.14). Among those of known structure, only GphF DH1 Tyr1856 forms a hydrogen bond with catalytic Asp1898 and only GphF DH1 catalyzes isomerization[4, 11-14].

Despite the relaxed substrate selectivity of both the dehydratase and isomerase reactions, the mutagenesis data revealed a striking divergence of isomerase mechanism between substrates with a 2-methyl substituent (**2**, **3**, **6**, and *rac*-**7**) and those without (**9**, **10/11**). Whereas both the branched side chain of Leu1744 and the hydroxy group of Tyr1856 were essential to isomerase activity with any 2-methyl substrate, neither with the branched side chain nore the Tyr hydroxy was essential to isomerization of substrates lacking a 2-methyl. The Leu1744 side chain protrudes into the active site further than does a Pro side chain (Figs. 5.12B, C), and thus imposes greater conformational and positional constraints on binding of (*E*)-2-methyl-2enoyl **6** than on the binding of (*E*)-2-enoyl **10**. With the 2-methyl substrate, these constraints are evidently needed to position , the C4 appropriately for abstraction of a proton during the isomerization reaction. In contrast, the isomerase activity of GphF DH1/Y1856F with non-methylated **10** may be due to C4 deprotonation by Asp1898, directly or through a water molecule.

The importance of the branched side chain to substrate positioning for isomerization is clear from the data on CurK DH, a typical non-isomerizing DH with His, Asp, Pro and Tyr side chains in the active site and a substrate without a 2-methyl substituent. CurK DH dehydrated **9** but had no detectable isomerase activity (Fig 5.18, Table 5.12). However, when the active-site

243

Pro1005 was replaced with the branched amino acid Val, the CurK DH acquired isomerase activity with **9** (Fig. 5.18, Table 5.12).

Epimerization at C2

We made the unexpected discovery that GphF DH1 acts as a 2-methyl epimerase through sequential dehydration and isomerization reactions. The preferred (and anticipated natural) substrate was (2*R*,3*R*)-2-methyl-3-hydroxy **2**, although both **1** and the odd-to-even olefin product **14** have an (*S*)-methyl at this position. Epimerization requires removal of the (2*S*)-proton in the dehydration step and addition of a (2*R*)-proton in the isomerization step, implying substantial re-positioning of the substrate in the active site. While GphF DH1 epimerizes the C2 position of its substrate, FabA catalysis involves only the *pro*-2S proton[50]. Despite the similar overall structures, many details of the GphF DH1 and FabA active sites differ, which may explain the differences in the sterochemical course of reaction catalyzed by the two DHs. Notably, the analog of Tyr1856 is Pro in FabA, as is the analog of Leu1744.

We note that several non-isomerizing PKS DH homologs function as C2 epimerases for 2-methyl-3-keto substrates, which are not dehydration substrates[53]. These enzymes and GphF DH1 have the common problem of deprotonating and reprotonating opposite faces of the substrate C2 position. In all cases where epimerase activity has been reported, the DHs also have a Tyr analog of Tyr1856 in GphF DH1. While these DH homologs do not catalyze isomerization, they may use both His and Tyr for epimerization. In contrast, for the PksEI14, where the Asp1898 analog is Asn and the Tyr1856 analog is Trp, the acidity of the C4 proton is enhanced by a double bond to C5. No base was identified for deprotonation of the substrate C4 and it was concluded that the catalytic His is responsible for all proton transfers[27].

Of the *cis*-AT DHs predicted to produce odd-to-even unsaturated final products, DH4 from the ambruticin pathway catalyzes sequential dehydration, epimerization and isomerization reactions on a (3*S*,4*S*)-3-hydroxy-4-methyl substrate in which epimerization of the 4-methyl occurs after dehydration to a 4-methyl-2-enoyl intermediate and before double bond shift to the 4-methyl-3-enoyl product (Scheme 5.2).[8] The Amb DH4 is most similar to non-isomerizing DHs with His, Asp, Pro and Tyr amino acids in the active site (Fig. 5.14). It is tempting to speculate that the His and Tyr may be involved in the epimerization step.
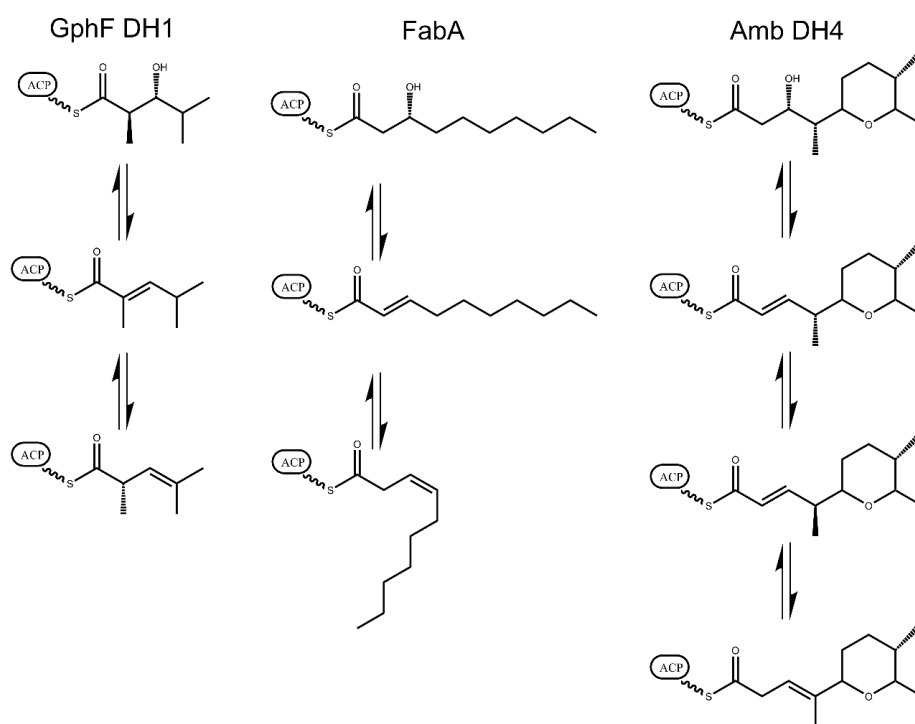
Scheme 5.2 Comparison of multifunctional DH reaction schemes.

Each DH catalyzes an initial dehydration at the β position, but diverge in their secondary function. GphF isomerizes the 2-enoyl intermediate and resets the newly formed stereocenter to the (2*S*) configuration. FabA forms a (*Z*)-3-decenoyl final product and is highly specific for C10 substrates. Amb DH4 catalyzes an epimerization at C4 prior to isomerization, forming a 3-enoyl product that is subsequently methylated by a standalone MT.

Isomerase activity and pathway throughput

In both GphF DH1 and FabA, the isomerization reaction is thermodynamically unfavorable as it shifts a double bond out of resonance with the thioester carbonyl. In biochemical assays, both enzymes produce low levels of the 3-enoyl elimination product[7] (Table 5.4). While the level of the (Z)-3-decenoyl final product from FabA (3%) appears too low to support the critical biological requirement for unsaturated fatty acid biosynthesis, *E. coli* drives the equilibrium in the forward direction by co-expression of *fabA* with *fabB*, a gene encoding a specialized KS for elongation of a (Z)-3-decenoyl product[54]. We anticipate that the KS of GphF module 2 drives gephyronic acid biosynthesis in a similar manner. In contrast to GphF DH1 and FabA, the PksEI14 isomerization is more thermodynamically favorable, as the double bond shift forms a conjugated triene with double bonds at C5 and C7.

Rational engineering in PKS DHs

We conclude that GphF DH1 had a non-isomerizing DH ancestor that may have acted on a 2-methyl substrate. Introduction of a branched side chain in the active site led to selective 2-methyl epimerization relative to the (2*R*,3*R*)-2-methyl-3-hydroxy product of the module KR.

The presence of a branched-chain amino acid in the PKS DH active site is correlated with a capability for double-bond migration[27], although the Amb DH4 is an exception[8]. We show that substitution of a branched chain-amino acid at this position in a non-isomerizing DH from the curacin A PKS resulted in a 3-enoyl product. These experiments may represent a stepping-stone for PKS engineering. Attempts to engineer isomerization activity in bacterial FAS DHs required swapping large domains between FabZ and FabN (a FabZ homolog capable of isomerization)[55]. In contrast, the PKS DHs evolved a secondary isomerase function in a simpler manner, but at some expense to dehydration efficiency. If secondary isomerase activity is to be developed for

246

chemoenzymatic synthesis, then a scheme such as a capture enzyme may be needed to drive an unfavorable raction forward.

In summary, GphF DH1 is a novel addition to the versatility of the DH and DH-like domains in PKS systems, expanding the repertoire of reactions catalyzed by these fascinating enzymes. The biochemical characterization and crystal structure together shed light on the molecular requirements for secondary function in PKS DHs. Both the substrate structure and the arrangement of Leu1744 and Tyr1856 adjacent to the His1735/Asp1898 catalytic dyad control isomerization subsequent to dehydration. The results of these experiments facilitated rational engineering of an isomerizing variant of the CurK DH, representing a step towards a more nuanced approach to PKS engineering. As the overall fold and general catalytic machinery of PKS DHs are highly conserved, we anticipate that additional secondary functions will be driven, in an analogous manner to GphF DH1, via subtle alterations to the active site that are specific to the natural DH substrate, as for the dehydratase-cyclase Amb DH3[14].

Bibliography

1.   Fiers, W. D., Dodge, G. J., Li, Y., Smith, J. L., Fecik, R. A., Aldrich, C. C., Tylosin polyketide synthase module 3: stereospecificity, stereoselectivity and steady-state kinetic analysis of β-processing domains via diffusible, synthetic substrates. *Chem. Sci.* **2015,** *6* (8), 5027-5033.
2.   Li, Y., Dodge, G. J., Fiers, W. D., Fecik, R. A., Smith, J. L., Aldrich, C. C., Functional characterization of a dehydratase domain from the pikromycin polyketide synthase. *J. Am. Chem. Soc.* **2015,** *137* (22), 7003-7006.
3.   Shah, D. D., You, Y. O., Cane, D. E., Stereospecific formation of *E*- and *Z*-disubstituted double bonds by dehydratase domains from modules 1 and 2 of the fostriecin polyketide synthase. *J. Am. Chem. Soc.* **2017,** *139* (40), 14322-14330.
4.   Gay, D., You, Y.-O., Keatinge-Clay, A., Cane, D. E., Structure and stereospecificity of the dehydratase domain from the terminal module of the rifamycin polyketide synthase. *Biochemistry* **2013,** *52* (49), 8916-8928.
5.   Fiers, W. D., Dodge, G. J., Sherman, D. H., Smith, J. L., Aldrich, C. C., Vinylogous dehydration by a polyketide dehydratase domain in curacin biosynthesis. *J. Am. Chem. Soc.* **2016,** *138* (49), 16024-16036.

6.   Vergnolle, O., Hahn, F., Baerga-Ortiz, A., Leadlay, P. F., Andexer, J. N., Stereoselectivity of isolated dehydratase domains of the borrelidin polyketide synthase: implications for *cis* double bond formation. *ChemBioChem* **2011,** *12* (7), 1011-1014.

7.   Brock, D. J., Kass, L. R., Bloch, K., β-hydroxydecanoyl thioester dehydrase. II. Mode of action. *J. Biol. Chem.* **1967,** *242* (19), 4432-4440.

8.   Berkhan, G., Merten, C., Holec, C., Hahn, F., The interplay between a multifunctional dehydratase domain and a *C*-methyltransferase effects olefin shift in ambruticin biosynthesis. *Angew. Chem., Int. Ed. Engl.* **2016,** *55* (43), 13589-13592.

9.   Berkhan, G., Hahn, F., A dehydratase domain in ambruticin biosynthesis displays additional activity as a pyran-forming cyclase. *Angew. Chem., Int. Ed. Engl.* **2014,** *53* (51), 14240-14244.

10.   Alhamadsheh, M. M., Palaniappan, N., DasChouduri, S., Reynolds, K. A., Modular polyketide synthases and *cis* double bond formation: establishment of activated *cis*-3-cyclohexylpropenoic acid as the diketide intermediate in phoslactomycin biosynthesis. *J. Am. Chem. Soc.* **2007,** *129* (7), 1910-1911.

11.   Akey, D. L., Razelun, J. R., Tehranisa, J., Sherman, D. H., Gerwick, W. H., Smith, J. L., Crystal structures of dehydratase domains from the curacin polyketide biosynthetic pathway. *Structure* **2010,** *18* (1), 94-105.

12.   Keatinge-Clay, A., Crystal structure of the erythromycin polyketide synthase dehydratase. *J. Mol. Biol.* **2008,** *384* (4), 941-953.

13.   Faille, A., Gavalda, S., Slama, N., Lherbet, C., Maveyraud, L., Guillet, V., Laval, F., Quémard, A., Mourey, L., Pedelacq, J. D., Insights into substrate modification by dehydratases from type I polyketide synthases. *J. Mol. Biol.* **2017,** *429* (10), 1554-1569.

14.   Sung, K. H., Berkhan, G., Hollmann, T., Wagner, L., Blankenfeldt, W., Hahn, F., Insights into the dual activity of a bifunctional dehydratase-cyclase domain. *Angew. Chem., Int. Ed. Engl.* **2018,** *57* (1), 343-347.

15.   Caffrey, P., Conserved amino acid residues correlating with ketoreductase stereospecificity in modular polyketide synthases. *ChemBioChem* **2003,** *4* (7), 654-657.

16.   Tohyama, S., Kakinuma, K., Eguchi, T., The complete biosynthetic gene cluster of the 28-membered polyketide macrolactones, halstoctacosanolides, from Streptomyces halstedii HC34. *The Journal of antibiotics* **2006,** *59* (1), 44.

17.   Kandziora, N., Andexer, J. N., Moss, S. J., Wilkinson, B., Leadlay, P. F., Hahn, F., Uncovering the origin of Z-configured double bonds in polyketides: intermediate E-double bond formation during borrelidin biosynthesis. *Chem. Sci.* **2014,** *5* (9), 3563-3567.

18.   Heath, R. J., Rock, C. O., Roles of the FabA and FabZ β-hydroxyacyl-acyl carrier protein dehydratases in *Escherichia coli* fatty acid biosynthesis. *J. Biol. Chem.* **1996,** *271* (44), 27795-27801.

19.   Wang, H., Cronan, J. E., Functional replacement of the FabA and FabB proteins of *Escherichia coli* fatty acid synthesis by *Enterococcus faecalis* FabZ and FabF homologues. *J. Biol. Chem.* **2004,** *279* (33), 34489-34495.

20.   Leesong, M., Henderson, B. S., Gillig, J. R., Schwab, J. M., Smith, J. L., Structure of a dehydratase-isomerase from the bacterial pathway for biosynthesis of unsaturated fatty acids: two catalytic activities in one active site. *Structure* **1996,** *4* (3), 253-264.

21.   Kimber, M. S., Martin, F., Lu, Y., Houston, S., Vedadi, M., Dharamsi, A., Fiebig, K. M., Schmid, M., Rock, C. O., The structure of (3R)-hydroxyacyl-acyl carrier protein dehydratase (FabZ) from *Pseudomonas aeruginosa*. *J. Biol. Chem.* **2004,** *279* (50), 52593-52602.

22.   Cheng, J. F., Lee, J. S., Sakai, R., Jares-Erijman, E. A., Silva, M. V., Rinehart, K. L., Myriaporones 1-4, cytotoxic metabolites from the Mediterranean bryozoan *Myriapora truncata*. *J. Nat. Prod.* **2007,** *70* (3), 332-336.

23.   Meragelman, T. L., Willis, R. H., Woldemichael, G. M., Heaton, A., Murphy, P. T., Snader, K. M., Newman, D. J., van Soest, R., Boyd, M. R., Cardellina, J. H., 2nd, McKee, T. C., Candidaspongiolides, distinctive analogues of tedanolide from sponges of the genus *Candidaspongia*. *J. Nat. Prod.* **2007,** *70* (7), 1133-1138.

24.   Schmitz, F. J., Gunasekera, S. P., Yalamanchili, G., Hossain, M. B., Van der Helm, D., Tedanolide: a potent cytotoxic macrolide from the Caribbean sponge *Tedania ignis*. *J. Am. Chem. Soc.* **1984,** *106* (23), 7251-7252.

25.   Jungmann, K., Jansen, R., Gerth, K., Huch, V., Krug, D., Fenical, W., Müller, R., Two of a kind-the biosynthetic pathways of chlorotonil and anthracimycin. *ACS Chem. Biol.* **2015,** *10* (11), 2480-2490.

26.   Kusebauch, B., Busch, B., Scherlach, K., Roth, M., Hertweck, C., Functionally distinct modules operate two consecutive α,β→β,γ double-bond shifts in the rhizoxin polyketide assembly line. *Angew. Chem., Int. Ed. Engl.* **2010,** *49* (8), 1460-1464.

27.   Gay, D. C., Spear, P. J., Keatinge-Clay, A. T., A double-hotdog with a new trick: structure and mechanism of the *trans*-acyltransferase polyketide synthase enoyl-isomerase. *ACS Chem. Biol.* **2014,** *9* (10), 2374-2381.

28.   Moynié, L., Leckie, S. M., McMahon, S. A., Duthie, F. G., Koehnke, A., Taylor, J. W., Alphey, M. S., Structural insights into the mechanism and inhibition of the β-hydroxydecanoyl-acyl carrier protein dehydratase from *Pseudomonas aeruginosa*. *J. Mol. Biol.* **2013,** *425* (2), 365-377.

29.   Taft, F., Brünjes, M., Knobloch, T., Floss, H. G., Kirschning, A., Timing of the Δ(10,12)-Δ(11,13) double bond migration during ansamitocin biosynthesis in *Actinosynnema pretiosum*. *J. Am. Chem. Soc.* **2009,** *131* (11), 3812-3813.

30.   Young, J., Stevens, D. C., Carmichael, R., Tan, J., Rachid, S., Boddy, C. N., Müller, R., Taylor, R. E., Elucidation of gephyronic acid biosynthetic pathway revealed unexpected SAM-dependent methylations. *J. Nat. Prod.* **2013,** *76* (12), 2269-2276.

31.   Wagner, D. T., Stevens, D. C., Mehaffey, M. R., Manion, H. R., Taylor, R. E., Brodbelt, J. S., Keatinge-Clay, A. T., α-Methylation follows condensation in the gephyronic acid modular polyketide synthase. *Chem. Commun. (Cambridge, U. K.)* **2016,** *52* (57), 8822-8825.

32.   Galobardes, M., Gascón, M., Mena, M., Romea, P., Urpí, F., Vilarrasa, J., Enolization of chiral α-silyloxy ketones with dicyclohexylchloroborane. application to stereoselective aldol reactions. *Organic letters* **2000,** *2* (17), 2599-2602.

33.   Fanjul, S., Hulme, A. N., White, J. W., Achieving high selectivity and facile displacement with a new thiol auxiliary for boron-mediated aldol reactions. *Organic letters* **2006,** *8* (19), 4219-4222.

34.   Harris, R., Cutter, A., Weissman, K., Enantiospecific synthesis of analogues of the diketide intermediate of the erythromycin polyketide synthase (PKS). *Journal of Chemical Research* **1998,** (6), 283-283.

35.   Evans, D. A., Connell, B. T., Synthesis of the antifungal macrolide antibiotic (+)-roxaticin. *Journal of the American Chemical Society* **2003,** *125* (36), 10899-10905.

36.   Piva, O., Mortezaei, R., Henin, F., Muzart, J., Pete, J. P., Highly enantioselective photodeconjugation of α,β-unsaturated esters. Origin of the chiral discrimination. *Journal of the American Chemical Society* **1990,** *112* (25), 9263-9272.

37.   Kapferer, T., Brückner, R., Asymmetric dihydroxylation of β,γ-unsaturated carboxylic esters with trisubstituted C=C bonds–enantioselective syntheses of trisubstituted γ-butyrolactones. *European journal of organic chemistry* **2006,** *2006* (9), 2119-2133.

38.   Garnier, J.-M., Robin, S., Guillot, R., Rousseau, G., Preparation of enantiopure 3, 5, 5-trialkyl-γ-butyrolactones by diastereospecific 5-endo halo lactonizations. *Tetrahedron: Asymmetry* **2007,** *18* (12), 1434-1442.

39.   Gabriel, T., Wessjohann, L., The chromium—Reformatsky reaction: Asymmetric synthesis of the aldol fragment of the cytotoxic epothilons from 3-(2-bromoacyl)-2-oxazolidinones. *Tetrahedron Letters* **1997,** *38* (8), 1363-1366.

40.   Etemad-Moghadam, G., Seyden-Penne, J., Synthese stereoselective d'esters α,β-ethyleniques α-methyles Z ou E par la reaction de wittig-horner a partir de phosphonates ou d'oxydes de phosphine. *Tetrahedron* **1984,** *40* (24), 5153-5166.

41.   Grisé, C. M., Tessier, G., Barriault, L., Synthesis of the tricyclic core of vinigrol via an intramolecular Diels− Alder reaction. *Organic letters* **2007,** *9* (8), 1545-1548.

42.   Kabsch, W., Xds. *Acta Crystallographica, Section D: Biological Crystallography* **2010,** *66* (Pt 2), 125-32.

43.   McCoy, A. J., Grosse-Kunstleve, R. W., Adams, P. D., Winn, M. D., Storoni, L. C., Read, R. J., Phaser crystallographic software. *Journal of Applied Crystallography* **2007,** *40* (Pt 4), 658-674.

44.   Stein, N., CHAINSAW: a program for mutating pdb files used as templates in molecular replacement. *Journal of Applied Crystallography* **2008,** *41* (3), 641-643.

45.   Winn, M. D., Ballard, C. C., Cowtan, K. D., Dodson, E. J., Emsley, P., Evans, P. R., Keegan, R. M., Krissinel, E. B., Leslie, A. G., McCoy, A., McNicholas, S. J., Murshudov, G. N., Pannu, N. S., Potterton, E. A., Powell, H. R., Read, R. J., Vagin, A., Wilson, K. S., Overview of the CCP4 suite and current developments. *Acta Crystallographica, Section D: Biological Crystallography* **2011,** *67* (Pt 4), 235-42.

46.   Adams, P. D., Afonine, P. V., Bunkoczi, G., Chen, V. B., Davis, I. W., Echols, N., Headd, J. J., Hung, L. W., Kapral, G. J., Grosse-Kunstleve, R. W., McCoy, A. J., Moriarty, N. W., Oeffner, R., Read, R. J., Richardson, D. C., Richardson, J. S., Terwilliger, T. C., Zwart, P. H., PHENIX: a comprehensive Python-based system for macromolecular structure solution. *Acta Crystallographica, Section D: Biological Crystallography* **2010,** *66* (Pt 2), 213-21.

47.   Emsley, P., Lohkamp, B., Scott, W. G., Cowtan, K., Features and development of Coot. *Acta Crystallographica, Section D: Biological Crystallography* **2010,** *66* (Pt 4), 486-501.

48.   Chen, V. B., Arendall, W. B., 3rd, Headd, J. J., Keedy, D. A., Immormino, R. M., Kapral, G. J., Murray, L. W., Richardson, J. S., Richardson, D. C., MolProbity: all-atom structure validation for macromolecular crystallography. *Acta Crystallographica, Section D: Biological Crystallography* **2010,** *66* (Pt 1), 12-21.

49.   Valenzano, C. R., You, Y.-O., Garg, A., Keatinge-Clay, A., Khosla, C., Cane, D. E., Stereospecificity of the dehydratase domain of the erythromycin polyketide synthase. *J. Am. Chem. Soc.* **2010,** *132* (42), 14697-14699.

50.   Schwab, J. M., Klassen, J. B., Steric course of the allylic rearrangement catalyzed by β-hydroxydecanoylthioester dehydrase. Mechanistic implications. *J. Am. Chem. Soc.* **1984,** *106* (23), 7217-7227.

51.   Schwab, J. M., Klassen, J. B., Habib, A., Stereochemical course of the hydration reaction catalysed by β-hydroxydecanoylthioester dehydrase. *J. Chem. Soc.* **1986,** (4), 357-358.

52.   Xie, X., Khosla, C., Cane, D. E., Elucidation of the stereospecificity of *C*-methyltransferases from *trans*-AT polyketide synthases. *J. Am. Chem. Soc.* **2017,** *139* (17), 6102-6105.

53.   Xie, X., Garg, A., Khosla, C., Cane, D. E., Elucidation of the cryptic methyl group epimerase activity of dehydratase domains from modular polyketide synthases using a tandem modules epimerase assay. *J. Am. Chem. Soc.* **2017,** *139* (28), 9507-9510.

54.   Cronan, J. J., Rock, C. O., Biosynthesis of membrane lipids. *EcoSal Plus* **2008,** *3* (1).

55.   Lu, Y. J., White, S. W., Rock, C. O., Domain swapping between *Enterococcus faecalis* FabN and FabZ proteins localizes the structural determinants for isomerase activity. *J. Biol. Chem.* **2005,** *280* (34), 30342-30348.

Chapter 6. AcpP-FabZ crystal structure elucidates differences in activity and substrate selectivity of *E. coli* dehydratases, FabA and FabZ

Summary

Fatty acid biosynthesis in α- and γ-proteobacteria requires two functionally distinct dehydratases (DHs), FabA and FabZ. Here, mechanistic crosslinking facilitates the first structural characterization of a stable hexameric complex of *E. coli* FabZ with six AcpP acyl carrier proteins (ACP). The crystal structure sheds light on the divergent substrate selectivity of FabA and FabZ by revealing front and back "gating" residues along with distinct conformations of the binding pocket. Molecular dynamics simulations demonstrate differential biasing of substrate orientations within the active sites of FabA and FabZ such that FabZ is pre-organized to catalyze only dehydration, while FabA is primed for both dehydration and isomerization.

Introduction

In order to maintain membrane phospholipid homeostasis and modulate membrane fluidity, all organisms must regulate the synthesis of unsaturated fatty acids (UFAs).[1-2] α- and γ-proteobacteria, including *Escherichia coli, Yersinia* pestis, and *Pseudomonas aeruginosa* produce UFAs during *de novo* biosynthesis through the coordinated action of two dehydratases (DHs), FabA and FabZ.[6-7] This system of UFA biosynthesis is unique to bacteria, and is of interest as an antibiotic target. FabA and FabZ are part of the type II fatty acid synthase (FAS), in which discrete enzymes synthesize fatty acids in a stepwise manner. Through this process the growing fatty acid

remains tethered to an acyl carrier protein (ACP), AcpP, for stability and transport (Figure 6.1A).

Therefore, protein-protein interactions between AcpP and partner enzymes is essential to fatty acid

synthesis. Both FabZ and FabA catalyze the dehydration of β-hydroxyacyl-AcpP, but they have

varying substrate selectivity (C8-C12 substrates for FabA, and C6 and C12+ substrates for FabZ)

(Figure 6.1B).[7] FabA has an additional allylic-rearrangement activity that converts *trans*-dec-2-

enoyl-AcpP, the immediate product of dehydration, into *cis*-dec-3-enoyl-AcpP, the precursor to *E.*

coli UFAs. FabZ is incapable of isomerization. While the activities of FabA and FabZ have been

the subject of intense mechanistic study for decades,[7-12] the structure-function relationships of

these enzymes have not been established definitively. *E. coli* FabA and FabZ share 23% amino

acid identity (41% similarity), but a crystal structure is available for only FabA.[13] Crystal

structures have been reported for both FabA and FabZ from *Pseudomonas aeruginosa*,[14-15] but

the similar active site pockets do not reveal the molecular basis for the selective activity of FabA

as an isomerase, and the structures lack an associated acyl-AcpP. Recently, the crystal structure of

a complex of phosphopantetheinyl-AcpP (*holo*-AcpP) and FabZ from *Helicobacter pylori* was

described, but the ACP lacked an acyl group, limiting conclusions regarding the distinct activities

and substrate preferences of FabA and FabZ.[16]

The reason many structures are without an associated acyl-AcpP is that AcpP-partner

protein interactions are fleeting. We previously circumvented the challenge of transient ACP-DH

interactions by employing mechanism-based crosslinking probes to trap FabA in functional

association with acyl-AcpP and solve the crystal structure (AcpP=FabA).[5] Here, we apply this

crosslinking strategy in combination with new fusion-protein methods to trap *E. coli* AcpP and

FabZ (AcpP=FabZ), and report the crystal structure of the complex. The AcpP=FabZ and
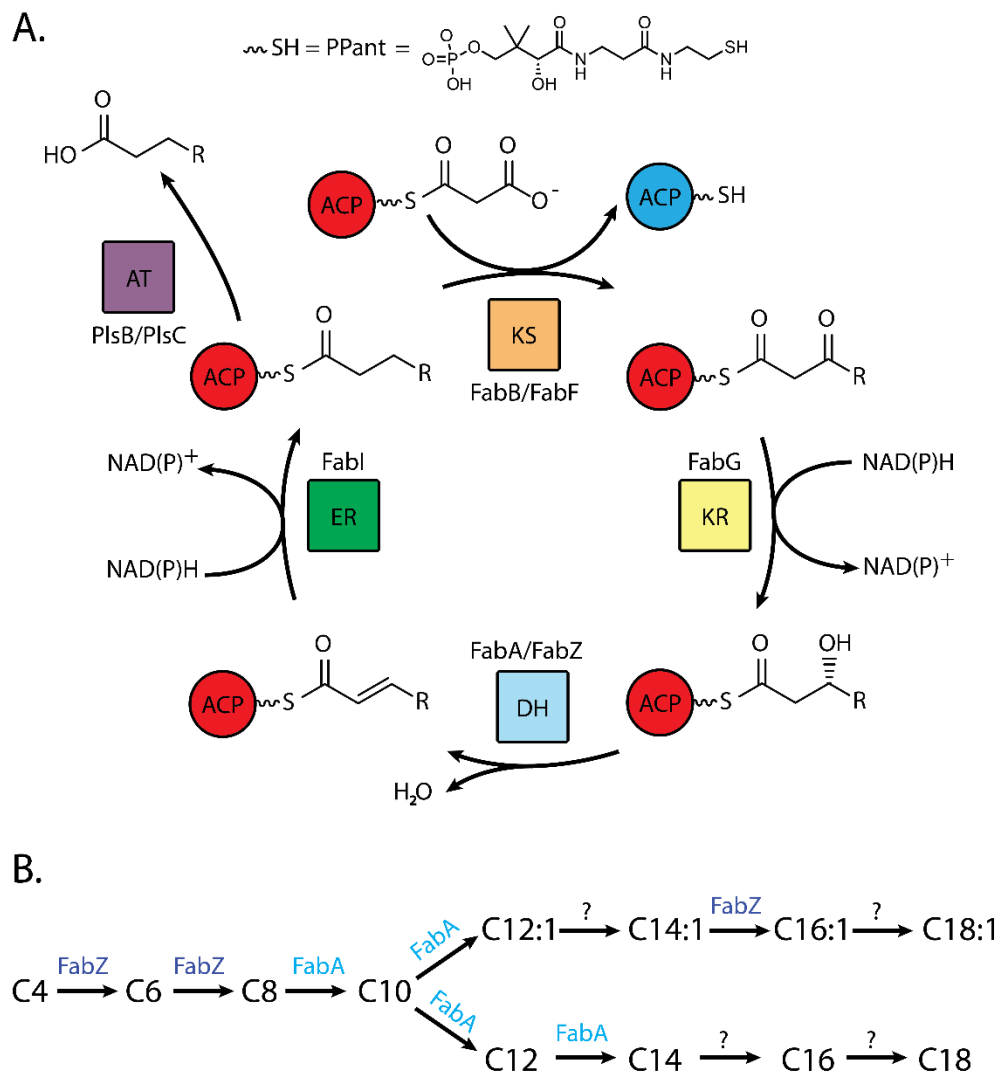
Figure 6.1 Fatty acid biosynthesis and FabA/FabZ substrate preference.

A. Fatty acids are biosynthesized in an iterative fashion, with the growing substrate always tethered to the acyl carrier protein (ACP). In *E. coli*, the substrate is extended by two carbons by ketosynthase (KS) FabB or FabF, reduced by ketoreductase (KR) FabG, dehydrated by dehydratase (DH) FabA or FabZ, and reduced by enoyl reductase (ER) FabI. When at the optimal length, the substrate is transferred by acyl transferase (AT) PlsB and PlsC. **B.** FabA and FabZ have distinct substrate preferences. FabZ has much higher activity on C4 and C6 substrates than FabA, whereas FabA has a preference for intermediate chain lengths C8-C12. Only FabA can perform the isomerization step to initiate the unsaturated fatty acid branch of the pathway. FabA and FabZ both have poor activity on C14 and C16 substrates, making it unclear which acts on those substrates. FabZ almost exclusively acts on C14:1. It was proposed that after the initial isomerization step by FabA, only FabZ can act on the unsaturated substrates C12:1-C16:1, but this has not been demonstrated experimentally for C12:1 or C16:1.

254

AcpP=FabA structures enabled us to perform molecular dynamics (MD) simulations of the of

acyl-AcpP•FabA and acyl-AcpP•FabZ complexes to evaluate the mechanisms of dehydration

catalyzed

by FabA and FabZ. Simulation results provide for the first time a structural rationale for the

unique isomerase activity of FabA, accounting for the *de novo* synthesis of UFAs in *E. coli.* The

simulations also recapitulated the established substrate preferences of FabA and FabZ. Together

these findings reveal the molecular basis for the differential activity of FabA and FabZ, a critical

component of bacterial phospholipid metabolism.

Methods

A. Chemical and biological protocols

A.1. Cloning and protein expression

FabZ: Previous reports indicated *E. coli* FabZ was soluble when expressed recombinantly with a

C-terminal His tag[17]. For this work, an optimized construct encoding an N-terminal Mocr fusion

protein[18] and residues 2-150 of *E. coli* FabZ was cloned into a pMocr-based expression vector to

create pGJD026 (Table 6.1). The insert was confirmed via sequencing. *E. coli* strain BL21

pRARE AI was transformed with pGJD026. A 0.5 L culture in 4% glycerol Terrific Broth media

(BD) with 100 mg/L ampicillin and 50 mg/L spectinomycin was grown at 37°C to an OD_{600} of

1.5, cooled to 20°C, induced by the addition of isopropyl β-D-1-thiogalactopyranoside (IPTG) to

0.2 mM and 1 g solid (L)-arabinose, and incubated 18 hr. Cells were harvested via

centrifugation. Cell pellets were transferred to 50 mL falcon tubes, immediately frozen and

stored at -20°C.

AcpP: *E.coli* AcpP was cloned into a pMCSG7-based expression vector to create pGJD042. The insert was confirmed via sequencing. *E. coli* strain BL21 pRARE AI was transformed with pGJD042. A 0.5 L culture in 4% glycerol Terrific Broth media (BD) with 100 mg/L ampicillin and 50 mg/L spectinomycin was grown at 37°C to an OD_{600} of 1.5, cooled to 20°C, induced by the addition of isopropyl β-D-1-thiogalactopyranoside (IPTG) to 0.2 mM and 1 g solid (L)-arabinose, and incubated 18 hr. Cells were harvested via centrifugation. Cell pellets were transferred to 50 mL falcon tubes, immediately frozen and stored at -20°C.

Table 6.1 Primers for Cloning

Primer	Primer Sequence 5' to 3'
fabz fwd LIC	TACTTCCAATCCAATGCNACCACCAATACCCATACCTTACAGATTG
fabz rev LIC	TTATCCACTTCCAATGTTATTATCCACTTCCAATGTTA

A.2. Protein purification

FabZ: All steps were performed at 4°C. Cell pellets were resuspended in buffer A (50 mM Tris pH 7.5, 300 mM NaCl, 15 mM imidazole, 10% glycerol) with 2 mM $MgCl_2$, 0.5 mg/mL DNase I, and 0.06 mg/mL lysozyme (4 mL per g cell pellet), incubated on ice for 1 hr, then sonicated. The lysate was cleared by centrifugation. The supernatant was passed through a 0.2 μm filter and loaded onto a 5 mL HisTrap column (GE Healthcare). The column was washed with 10 volumes buffer A, and protein was eluted with a linear gradient from 15 mM to 400 mM imidazole in buffer A. Peak fractions were pooled, concentrated, and loaded on a Superdex 16/60 S200 gel filtration column pre-equilibrated with buffer B (25 mM Tris pH 7.5, 150 mM NaCl, 10% glycerol). FabZ eluted as a hexamer, with an apparent molecular weight of 200 kDa (calculated MW 201 kDa). Peak fractions from were pooled and loaded onto a HiTrap Q column. The

column washed with 10 volumes buffer B, and protein was eluted with a linear gradient from 150 mM to 1 M NaCl in buffer B. Peak fractions were pooled, concentrated, and loaded on a Superdex 16/60 S200 gel filtration column pre-equilibrated with buffer B. Peak fractions were pooled, concentrated to 15 mg/mL, flash cooled in liquid N_2, and stored at -80°C.

AcpP: All steps were performed at 4°C. Cell pellets were resuspended in buffer A (50 mM Tris pH 7.5, 300 mM NaCl, 15 mM imidazole, 10% glycerol) with 2 mM $MgCl_2$, 0.5 mg/mL DNase I, and 0.06 mg/mL lysozyme (4 mL per g cell pellet), incubated on ice for 1 hr, then sonicated. The lysate was cleared by centrifugation. The supernatant was passed through a 0.2 μm filter, and loaded onto a 5 mL HisTrap column (GE Healthcare). The column was washed with 10 volumes buffer A, and protein was eluted with a linear gradient from 15 mM to 400 mM imidazole in buffer A. Peak fractions were pooled, concentrated, and loaded on a Superdex 16/60 S75 gel filtration column pre-equilibrated with buffer B (25 mM Tris pH 7.5, 150 mM NaCl, 10% glycerol). Peak fractions were pooled, concentrated, and loaded on a Superdex 16/60 S200 gel filtration column pre-equilibrated with buffer B. Peak fractions were pooled, concentrated to 15 mg/mL, flash cooled in liquid N_2, and stored at -80°C.

A.3. One-pot AcpP modification and FabZ crosslinking

Apo-AcpP was prepared from a mixture of apo- and holo-AcpP according to a previously published protocol[19]. The one-pot loading reactions were performed as previously reported[20]. Briefly, the 1-mL reaction mix contained 8 mM ATP, 0.5 μM CoaA, 0.7 μM CoaD, 0.6 μM CoaE, 1.5 μM Sfp, 0.4 mM apo-AcpP, 500 μM DH6 probe in Buffer D (100 mM phosphate pH 7.6, 100 mM NaCl, 10% glycerol). The mixture was rotated 24 hr at 37 °C. The formation of

257

crypto-AcpP was monitored by urea-PAGE gel and LCMS (ESI) analyses. The *crypto*-AcpP was purified by size exclusion (GE Healthcare Superdex S75) and concentrated using a 3-kDa ultra centrifugation filter (Amicon) and stored at -80°C until needed.

Crosslinking of His$_6$-tagged *crypto*-DH6-AcpP and Mocr-tagged FabZ was carried out in a 1.5:1 molar ratio. A 1-mL crosslinking reaction in buffer D contained 150 µM (subunit) Mocr-tagged FabZ, 225 µM His$_6$-tagged *crypto*-DH6-AcpP, and 0.5 mg/mL TEV protease, and was rotated 8 hr at 37 °C. The formation of Mocr-tagged crosslinked complex and protease cleavage of the Mocr fusion partner were monitored by SDS-PAGE. Reaction mixtures were loaded directly onto a Superdex S200 gel filtration column equilibrated with Buffer B. Peak fractions were pooled, combined and concentrated to 10 mg/mL.

A.4. Mocr-FabZ TEV protease cleavage turbidity

50 µM Mocr-FabZ was incubated in buffer C with TEV protease to a final concentration of 3.75 mg/mL in the presence of *apo*-AcpP at a final concentration of 0, 25, 50, 150, 300 or 500 µM. Cleavage reaction mixtures were incubated at 25 °C for 1 hr and turbidity was determined by optical density (OD) at 600 nm. Concentrations of Mocr-FabZ refer to the monomer subunit. Experiments were performed in triplicate.

A.5. Size exclusion chromatography with multi-angle light scattering

40 µM Mocr-FabZ was mixed with *apo*-AcpP to a final concentration of 200 (1:5), 400 (1:10) or 800 (1:20) µM AcpP. 40 µM Mocr-FabZ was mixed with *holo*-AcpP to a final concentration of 200 (1:5) or 400 (1:10) µM AcpP. 20 µM Mocr-FabZ was mixed with *holo*-AcpP to a final concentration of 200 (1:20) µM. All samples were incubated 1 hr at 25 °C. 50 µL

of each sample was loaded onto a KW-804 size exclusion column (Showdex) pre-equilibrated with buffer E (25 mM Tris pH 7.5, 100 mM NaCl) at a flow rate of 0.4 mL/min. The eluent was passed through both a DAWN HELEOS II multi-angle light scattering detector (Wyatt), and a T-rEX differential refractive index detector (Wyatt) pre-configured with a β-amylase standard. Data were analyzed using ASTRA software package (Wyatt). Concentrations of Mocr-FabZ refer to the subunit. Experiments were performed in duplicate.

A.6. Crystallography details

The AcpP-FabZ complex was crystallized at 20°C by hanging drop vapor diffusion in a 1:1 mix of 9.5 mg/mL protein stock and reservoir solution (100 mM Bis-Tris pH 6.5, 200 mM MgCl$_2$, 19% PEG 3350). Crystals were harvested without additional cryoprotection and flash-cooled in liquid N$_2$.

Data were collected at the Advanced Photon Source (APS, Argonne National Laboratory) on GM/CA beamline 23-ID-D. Crystals diffracted to 2.5 Å and were in orthorhombic space group $P2_12_12_1$ containing one AcpP=FabZ hexamer per asymmetric unit. Data were processed using XDS[21]. The AcpP-FabZ structure was solved by molecular replacement in phaser[22] using the *P. aeruginosa* FabZ as an initial search model (PDB: 1U1Z[14]). Six AcpPs were placed manually into electron density using the AcpP from the AcpP=FabA structure (PDB: 4KEH[23]) in coot[24]. The resulting atomic model was refined in PHENIX[25]. The refined model was validated with MolProbity[26]. Structure figures were generated in PyMOL[27]. Protein-protein interfaces were calculated using the PISA server[28].

B. Molecular dynamic simulation protocols

All simulations were carried out by Ashay Patel (UCSD)

Initial coordinates were prepared using the structure of AcpP=FabZ structure reported herein and the crystal structure of crosslinked AcpP=FabA[23]. Note that while the AcpP•FabZ is hexameric, a DH dimer was simulated for reasons of computational tractability. The phosphopantetheinylated serine bearing the acyl substrates (or product) in each system was treated as a nonstandard residue. Partial atomic charges for the nonstandard residues were determined using the restrained electrostatic potential (RESP) methodology[29]. The potential was computed at the HF/6-31G(d) level of theory using Gaussian 09[30]. AMBER (ff14SB)[31] and GAFF[32] type parameters were assigned to the atoms of these residues using ANTECHAMBER[33]. The protonation states of all systems were determined using the H++ webserver[34-37], assuming an external dielectric constant of 80, salinity of 0.150 M, and at pH 7.4. The protonation states of all histidine residues were manually confirmed. All acyl-ACP•DH complexes were solvated with TIP3P[38] water box large enough that no proteinogenic atom was within 12 Å of the box edge. Na^+ and Cl^- were added to the system to neutralize the anionic complex and to mimic the salt content of physiological systems (ca. 0.150 M). TLEAP was used to solvate and add counterions to these systems[39].

B1. Simulation details

Gaussian accelerated molecular dynamics[40-44] (GaMD) simulations were performed using Amber14[39]. The ff14SB[31] force field was employed in all simulation work. The SHAKE algorithm[45] was used to constrain all nonpolar bond involving hydrogen atoms, and a 2 fs time-step was used in the simulations. The Particle Mesh Ewald (PME) method[46] was used to treat long-range electrostatic interaction using a 10.0 Å cutoff for nonbonded interactions. Before

simulations of the complexes were performed, all systems were subjected to a two-step minimization. In the first step, the solvent was allowed to relax, while the atoms in the solute were restraint using a harmonic potential (500 kcal mol^{-1} A^{-2}). Subsequently, the entire system was minimized without constraints. After minimization, each system was slowly heated to 305 K over the course of a 3.5 ns canonical ensemble (NVT) MD simulation. These "heated" systems were subsequently equilibrated for 6 ns by performing unbiased isobaric-isothermal (NPT) simulations (at 305 K). In all simulations, temperature control was maintained using a Langevin thermostat ($\lambda = 1.0$ ps^{-1})[47]. For all NPT simulations, a Monte Carlo barostat was used.

Three independent 290 ns production-grade NPT GaMD simulations were performed of each acyl-AcpP•DH complex. The threshold energy was set to V_{max}. A 16 ns unbiased NPT simulation was used collect data to determine the maximum (V_{max}), minimum (V_{min}), average (V_{av}), and the standard deviation (σ_V) of the system potential. These data were not used in our analysis.

B2. Data analysis and molecular visualization

Coordinate data were written to disk every 0.5 ps. Analysis was performed using PYTRAJ, a Python-based front-end for the CPPTRAJ[48] software package, and MDTRAJ[49]. Gaussview 5,[50] Avogadro,[51] and PyMol v1.8.6[27] were used to prepare and visualize structures. PyMol was used to render the images shown herein[27]. Binding pockets were analyzed using POVME 3.[3]

Results and discussion

To compare catalytic selectivities and probe the structural basis of catalysis by natural FabA and FabZ partners, we sought to examine the *E. coli* FabZ in complex with AcpP. However,

unlike *E. coli* FabA, there are no reported structures of the *E. coli* FabZ, presumably due to the solubility challenges of FabZ. We produced highly pure, recombinant *E. coli* FabZ as an N-terminal fusion with the monomeric Mocr protein (Figure 6.2).[18] The Mocr-FabZ fusion protein was purified to homogeneity in a stable and soluble form; the Mocr fusion did not interfere with the expected hexameric association of FabZ (Figure 6.2). After proteolytic cleavage of the Mocr fusion partner, FabZ remained soluble (as assessed by turbidity) only if the cleavage reaction included equimolar or greater concentrations of AcpP, implying that, like the *H. pylori* FabZ, the *E. coli* FabZ may have inherent affinity for its carrier protein (Table 6.2).[52]
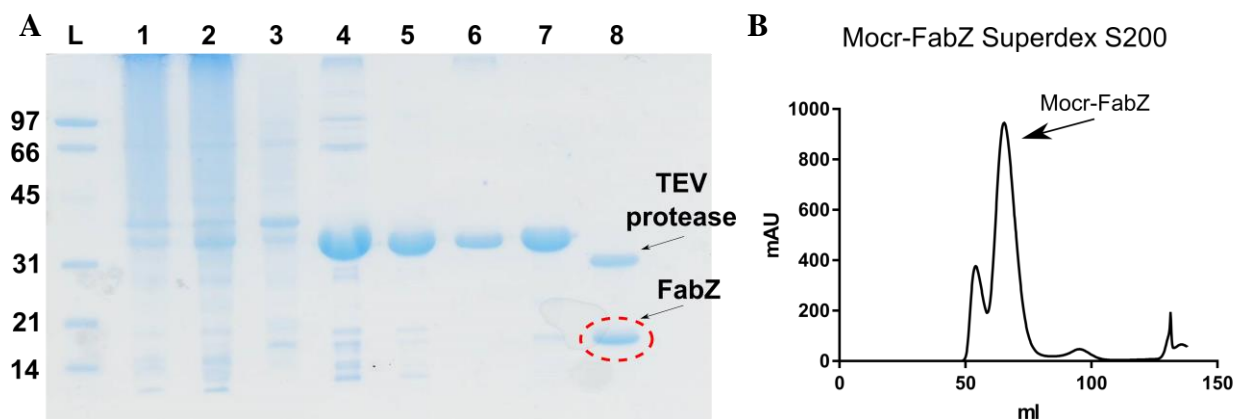
Figure 6.2 FabZ purification and solubilization.

A: SDS PAGE, Lane 1: Total lysate from production of recombinant Mocr-FabZ; Lane 2: Soluble fraction; Lane 3: Pellet fraction; Lane 4: Histrap elution; Lane 5: Superdex S200 #1; Lane 6: IonX; Lane 7: Superdex S200 #2; Lane 8: Resolubilized precipitated protein following TEV protease treatment. **B:** Superdex S200 gel filtration profile. Mocr-FabZ elutes as a hexamer with an apparent molecular weight of 201 kDa.

Table 6.2 Turbidity of Mocr-FabZ after TEV protease cleavage

	Mocr-FabZ*	+ 25 μM *apo*-AcpP	+ 50 μM *apo*-AcpP	+ 150 μM *apo*-AcpP	+ 300 μM *apo*-AcpP	+ 500 μM *apo*-AcpP
OD_{600}	0.07 ± 0.02	0.04 ± 0.01	0.03 ± 0.01	0.01 ± 0.01	0.01 ± 0.01	0.01 ± 0.01

We then used size exclusion chromatography (SEC) with multi-angle light scattering (MALS) to characterize the stoichiometry of complexes of Mocr-FabZ and *holo*-AcpP (with the

phosphopantetheine cofactor linked at Ser36) or *apo*-AcpP (lacking phosphopantetheine). All combinations of FabZ and AcpP resulted in complex formation with oligomeric states ranging from (AcpP$_1$-FabZ$_6$) to (AcpP$_6$-FabZ$_6$) (Figures 6.3A, 6.3B). The oligomer state was dependent on AcpP concentration, with a 20-fold molar excess of either *apo-* or *holo*-AcpP fully saturating Mocr-FabZ. The complexes had similar elution volumes to Mocr-FabZ in absence of AcpP, indicating a dynamic mixture of transient oligomeric states. This observation is consistent with a type II FAS system in which the AcpP must find and interact with each enzyme; should a tight, long lasting complex form with any one enzyme, FAS throughput would drop significantly.

We then sought to generate a soluble AcpP=FabZ complex suitable for crystallography by crosslinking AcpP prior to proteolytic cleavage of the Mocr fusion partner. As previously reported, 3-alkynyl-sulfone-pantethtine probes can be used to link AcpP and DHs.[4-5] Here, we chose a six-carbon probe (DH6) to mimic the optimal FabZ substrate, and appended it to AcpP (*crypto*-DH6-AcpP, Figure 6.4B).[7] Crosslinking trials with Mocr-FabZ and *crypto*-DH6-AcpP proceeded nearly to completion (Figures 6.3D, 6.4). In agreement with the previously reported substrate preference of FabZ,[7] less than 10% crosslinked complex formed with a probe mimicking the least-favored substrate, *crypto*-DH10-AcpP (AcpP loaded with a 10-carbon probe, Figure 6.4A). SEC-MALS analysis of DH6-AcpP=Mocr-FabZ indicated a stable complex with shorter retention time than the non-covalent complexes with *apo*-AcpP or *holo*-AcpP and a molecular weight corresponding to (AcpP$_6$=Mocr-FabZ$_6$) (Figures 6.2A, 6.2B). AcpP=FabZ was stable upon proteolytic cleavage of the Mocr fusion partner and had an apparent molecular weight of 160 kDa by SEC (Figure 6.5), again corresponding to an AcpP$_6$=FabZ$_6$ complex.
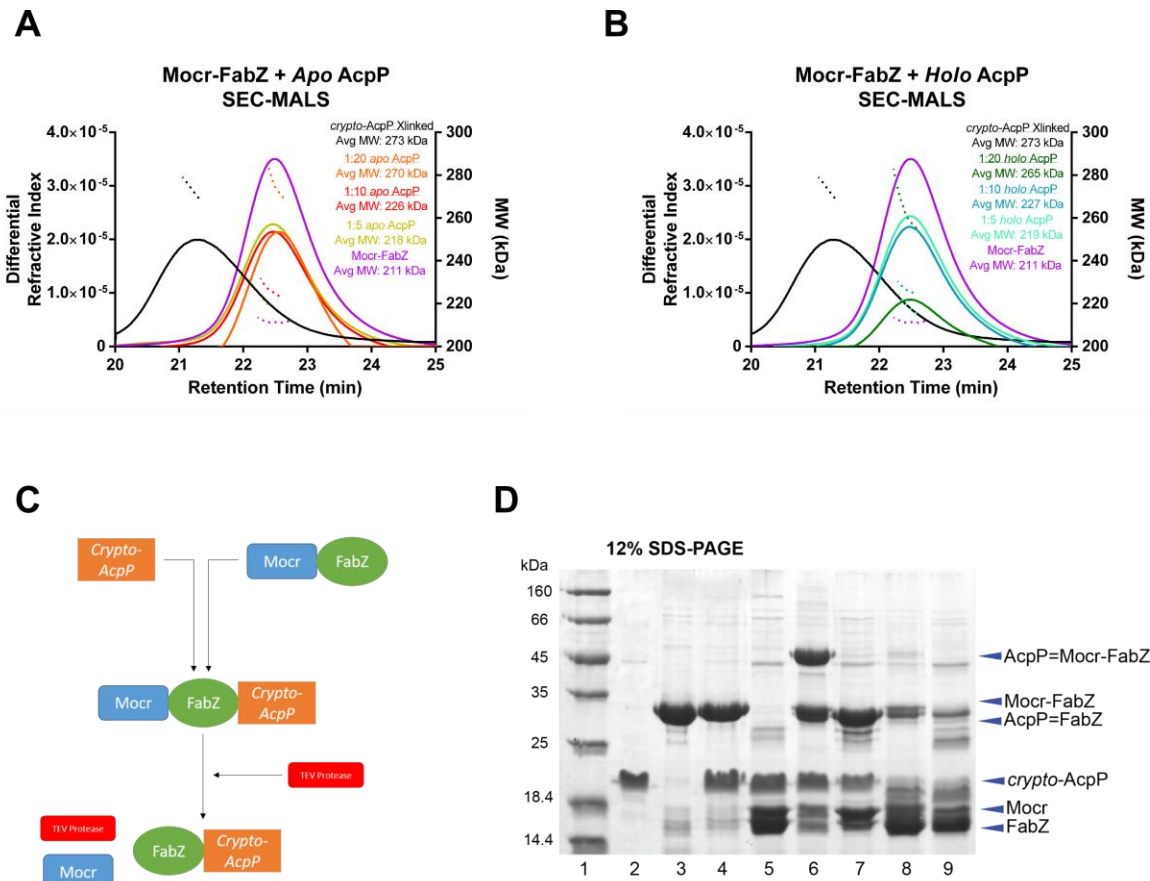
Figure 6.3 FabZ and AcpP crosslinking and biophysical analysis

A. Schematic of FabZ and crypto-AcpP crosslinking reaction and TEV protease cleavage. FabZ is insoluble when released from the Mocr fusion partner, but solubility is rescued when FabZ is crosslinked to acidic AcpP.

B. Denaturing gel (12% SDS) analysis of crosslinking reactions between AcpP and Mocr-FabZ. Lane 1: MW standards; Lane 2: apo-AcpP; Lane 3: Mocr-FabZ; Lane 4: apo-AcpP and Mocr-FabZ in crosslinking buffer; Lane 5: apo-AcpP and Mocr-FabZ in crosslinking buffer with TEV protease; Lane 6: crypto-DH6-AcpP and Mocr-FabZ crosslinking reaction; Lane 7: crypto-DH6-AcpP and Mocr-FabZ crosslinking reaction with TEV protease; 8: crypto-DH10-AcpP and Mocr-FabZ crosslinking reaction; Lane 9: crypto-DH10-AcpP and 20 Mocr-FabZ crosslinking reaction with TEV protease.

C, D. SEC-MALS traces of Mocr-FabZ and AcpP complexes. SEC elution profiles (differential refractive index) are shown in solid lines; MALS average molecular weight plots as dotted lines. C. SEC-MALS analysis of Mocr-FabZ in complex with apo-AcpP. Mocr-FabZ shown in purple, Mocr-FabZ=AcpP in black, 1:5 Mocr-FabZ:apo-AcpP in gold, 1:10 Mocr-FabZ:apo-AcpP in red, 1:20 Mocr-FabZ:apo-AcpP in orange. D. SEC-MALS analysis of Mocr-FabZ in complex with holo-AcpP. Mocr-FabZ shown in purple, Mocr-FabZ=AcpP in black, 1:5 Mocr-FabZ:holo-AcpP in cyan, 1:10 Mocr-FabZ:holo-AcpP in teal, 1:20 Mocr-FabZ:holo-AcpP in dark green. In both C and D, an AcpP concentration-dependent increase in average MW is observed, fully saturating the available Mocr-FabZ at a 20-fold excess. Data generated by Kara Jaremko

Figure 6.4 Crypto-DH6-AcpP and crypto-DH10-AcpP analysis.

Previously synthesized DH6 and DH10 probes [4] were loaded onto AcpP using "one-pot" methods, and the *crypto*-AcpPs purified by size exclusion chromatography, and analyzed by HPLC-MS (ESI) in positive mode and the charge distribution deconvoluted. (A) *Crypto*-DH10-AcpP analysis, showing LC trace (left) and mass analysis of the t=7.33 min protein peak (right, m/z). (B) *Crypto*-DH6-AcpP analysis, showing LC trace (left) and mass analysis of the t=7.09 min protein peak (right, m/z). Data Generated by Kara Jaremko

Figure 6.5 AcpP=FabZ purification and analysis.

Left: SDS PAGE, Lane 1: *crypto*-DH6-AcpP; Lane 2: Mocr-FabZ; Lanes 3-7: crosslinking reaction at several time points; Lane 8: Overnight crosslinking reaction with TEV protease; Lane 9: Overnight crosslinking reaction with TEV protease after concentrating with a 100K Amicon filter (Millipore); Lanes 10-12: Peaks from S200 superdex gel filtration column. FabZ=AcpP remained soluble following gel filtration. Mocr and TEV were readily separated from AcpP=FabZ via size exclusion chromatography. **Right:** Superdex S200 gel filtration profile of crosslinking reaction mix. FabZ=AcpP can be readily separated from the other components. The FabZ=AcpP peak height exhibits low signal at 280 nm due to the low molar absorptivity of the both FabZ (calculated $\varepsilon = 3,105$) and AcpP (calculated $\varepsilon = 1,490$), compared to Mocr (calculated $\varepsilon = 18,910$) and TEV protease (calculated $\varepsilon = 33,585$). FabZ=AcpP elutes as a hexamer with an apparent molecular weight of 160 kDa.

We crystallized the $AcpP_6=FabZ_6$ complex and obtained a 2.5-Å crystal structure with six AcpPs crosslinked with the FabZ hexamer (Figures 6.6, 6.7, Tables 6.3, 6.4). The FabZ hexamer is a trimer of FabA-like dimers, consistent with structures of other bacterial FabZ enzymes[14, 16, 53-55]. In the hexamer, an AcpP is crosslinked to the catalytic His54 of each FabZ monomer and contacts both subunits of the FabZ "dimer" but makes no contacts with the other two "dimers" or with any other AcpP (Figure 6.8).

The surface of AcpP helix α2 contacts the surface of the FabZ β-sheet via an interface comprised of several hydrophobic contacts surrounded by ionic interactions (Figure 6.8As with FabA, acidic residues on AcpP contact basic residues on FabZ surrounding the active site entrance. Interestingly, the majority of protein-protein contacts occur between AcpP and the subunit of the FabZ "dimer" to which it is not crosslinked (AcpP subunit A to FabZ subunit B, and AcpP subunit B to FabZ subunit A). Nevertheless, the crosslinked subunit also contributes to the interface, which buries 16% (745 Å^2) of the AcpP surface. The interface is significantly larger than the AcpP=FabA interface (~530 Å^2)[5, 56], in which AcpP has no contacts with the FabA monomer to which it is crosslinked (Figure 6.8). The six AcpP-FabZ interfaces are nearly identical, although two of the six AcpPs are shifted due to crystal contacts (Figure 6.9).

The AcpP-interacting surface of *E. coli* FabZ is strictly analogous to the AcpP-interacting surface of *H. pylori* FabZ.[16] However in contrast to our finding that the *E. coli* FabZ hexamer can interact productively with six AcpPs, a see-saw mechanism was proposed for the *H. pylori* FabZ in which only three AcpPs simultaneously engage the hexamer. The proposal was based on the crystal structure ($FabZ_6-AcpP_3$) where only one AcpP bound per dimer in the FabZ hexamer, together with analysis by SEC-MALS, small-angle X-ray scattering (SAXS) and micro-scale thermophoresis (MST)[16]. However, the *H. pylori* $FabZ_6-AcpP_3$ stoichiometry in the crystal
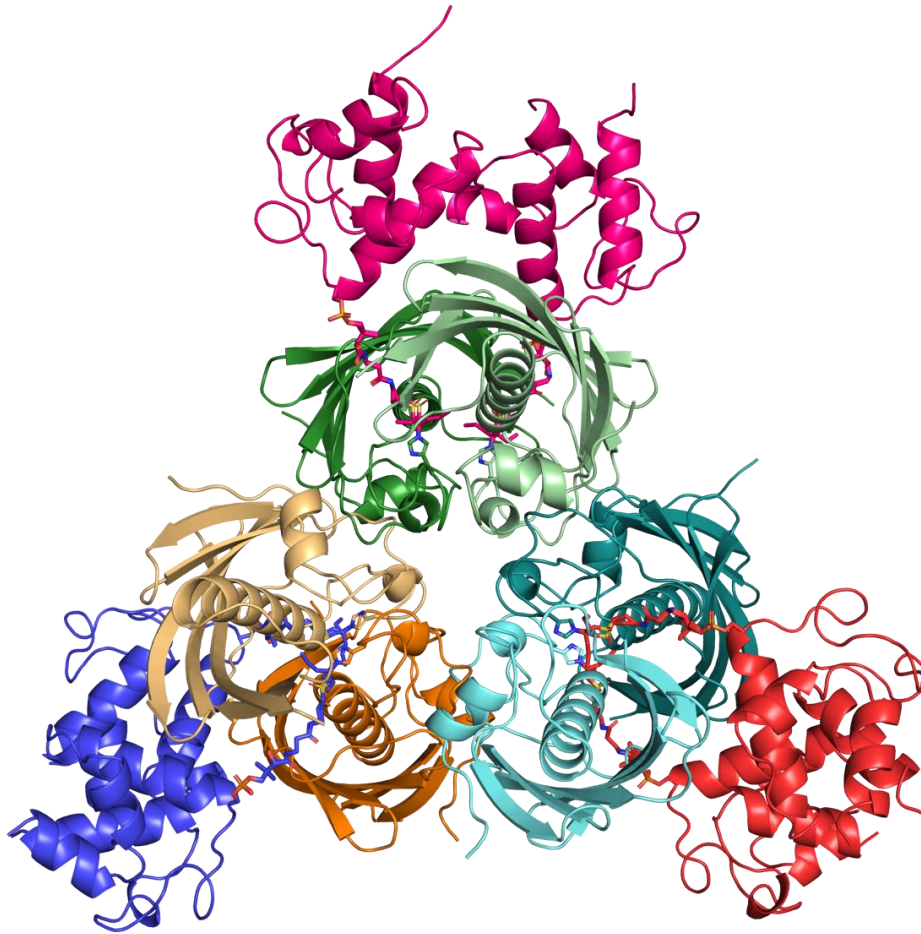
Figure 6.6 Structure of AcpP=FabZ.

The central FabZ hexamer is composed of three dimers (dark and light shades of green, orange, and cyan). The six AcpPs are at the periphery (dark and light shades of red, pink, and dark blue), each crosslinked to a FabZ subunit. The FabZ catalytic His54 and DH6 crosslinker are rendered as sticks in atomic coloring (blue N, red O, yellow S, and C colored as the respective protein).

Table 6.3 Crystallographic summary

Diffraction data	FabZ=HisAcpP
Space group	$P2_12_12_1$
Unit cell a, b, c (Å)	65.1, 136.2, 152.2
Wavelength (Å)	1.033
d_{min} (Å)	2.5 (2.59 – 2.50)*
Observations (#)	307,308 (29,936)
Unique reflections (#)	47,665 (4,689)
Mean I/σ_I	10.22 (1.12)
R_{merge}	0.150 (1.634)
$CC_{1/2}$	0.99 (0.479)
CC*	0.99 (0.805)
Completeness (%)	0.99 (0.99)
Wilson B ($Å^2$)	66.9

Refinement	
Reflections (#)	47,645
R_{work}	0.208
R_{free}	0.253
RMSD bonds (Å)	0.009
RMSD angles (°)	1.27
Atoms (#)	
Protein	10,369
Solvent	58
DH6 Probe	348
Avg B-factors ($Å^2$)	
Protein	84.2
Solvent	64.3
DH6 Probe	82.2
Ramachandran	
Favored (%)	94.7
Allowed (%)	5.1
Outliers (%)	0.2
# of TLS groups	82

* Values in parentheses refer to the outermost shell of data.

Table 6.4 X-ray data statistics for AcpP=FabZ

Resolution (Å)	N(obs)	N(uniq)	Mult.	Compl. (%)	$\langle I/sigma\rangle$	R-merge	R-meas	R-pim	$CC_{1/2}$
5.38 - 4.27	32,112	4,840	6.6	1.00	24.4	0.090	0.098	0.038	0.995
4.27 - 3.73	31,186	4,807	6.5	1.00	17.7	0.145	0.158	0.062	0.991
3.73 - 3.39	30,135	4,734	6.4	0.99	12.2	0.260	0.283	0.112	0.979
3.39 - 3.15	29,779	4,736	6.3	1.00	7.3	0.363	0.396	0.158	0.698
3.15 - 2.96	30,323	4,724	6.4	0.99	4.5	0.511	0.557	0.220	0.936
2.96 - 2.82	31,768	4,715	6.7	1.00	3.1	0.732	0.795	0.307	0.885
2.82 - 2.69	30,531	4,702	6.5	1.00	2.1	0.975	11.062	0.416	0.758
2.69 - 2.59	31,703	4,698	6.7	1.00	1.6	1.334	1.448	0.557	0.592
2.59 - 2.50	29,936	4,689	6.4	1.00	1.1	1.634	1.780	0.701	0.479
All	307,308	47,665	6.4	1.00	10.2	0.150	0.164	0.065	0.997
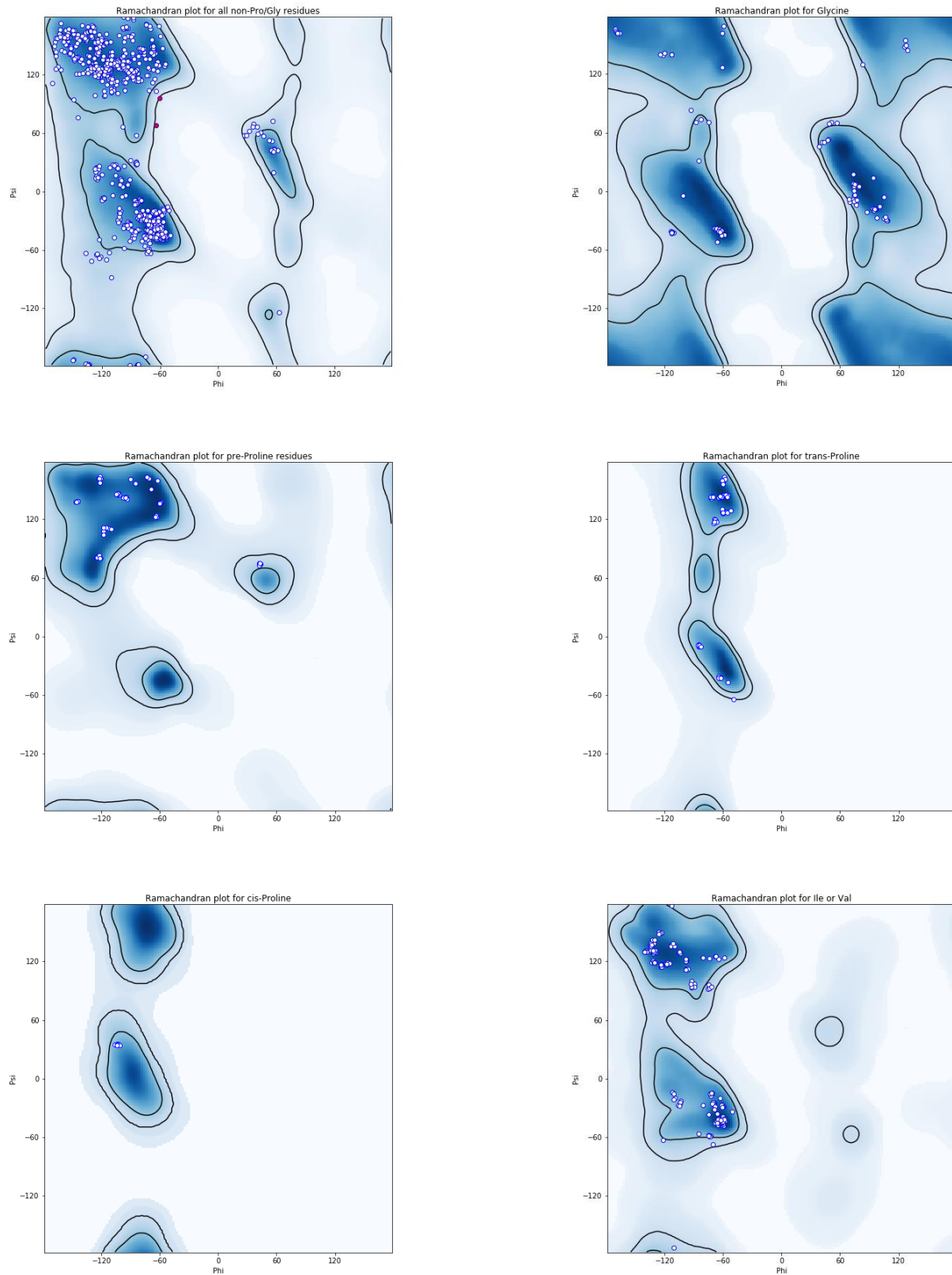
Figure 6.7 Ramachandran plots for AcpP=FabZ.
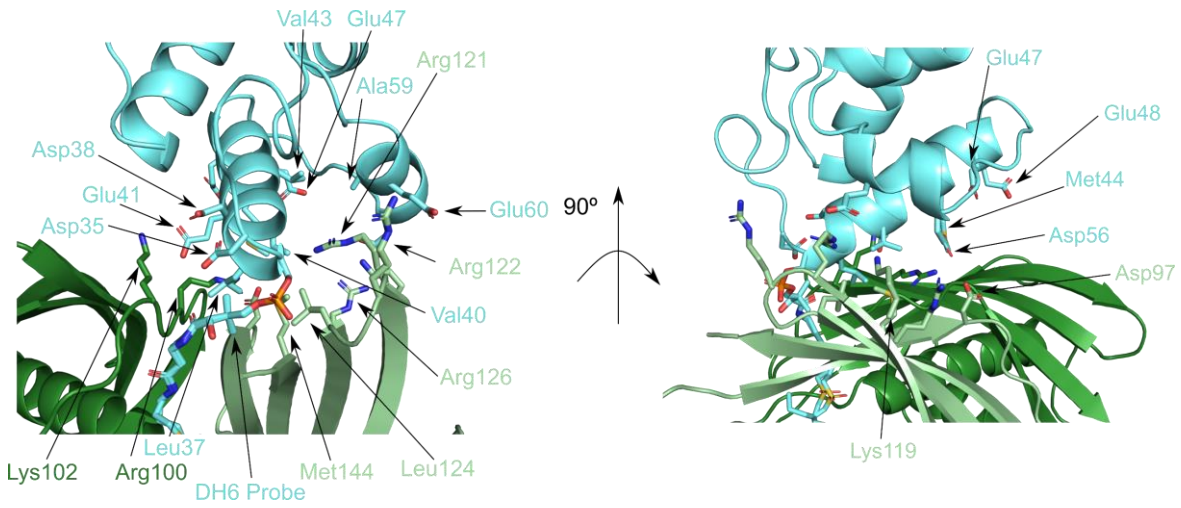
Figure 6.8 The AcpP - FabZ interaction.

The AcpP (cyan) is crosslinked to the dark green FabZ, but the protein-protein contacts with this subunit are limited to FabZ Arg100 and Lys102 (dark green sticks) and AcpP Asp35, Asp38, and Glu41 (cyan sticks). AcpP has far more contacts with the partner subunit (light green) of the FabZ dimer, where FabZ Lys119, Arg121, Arg122, Arg126, Leu124, Asp97 and Met144 (light green sticks) contact AcpP Leu37, Val40, Glu41, Val43, Met44 Glu47, Glu48, Asp56, Ala59 and Glu60). The reciprocal situation pertains to the AcpP crosslinked to the light green FabZ.
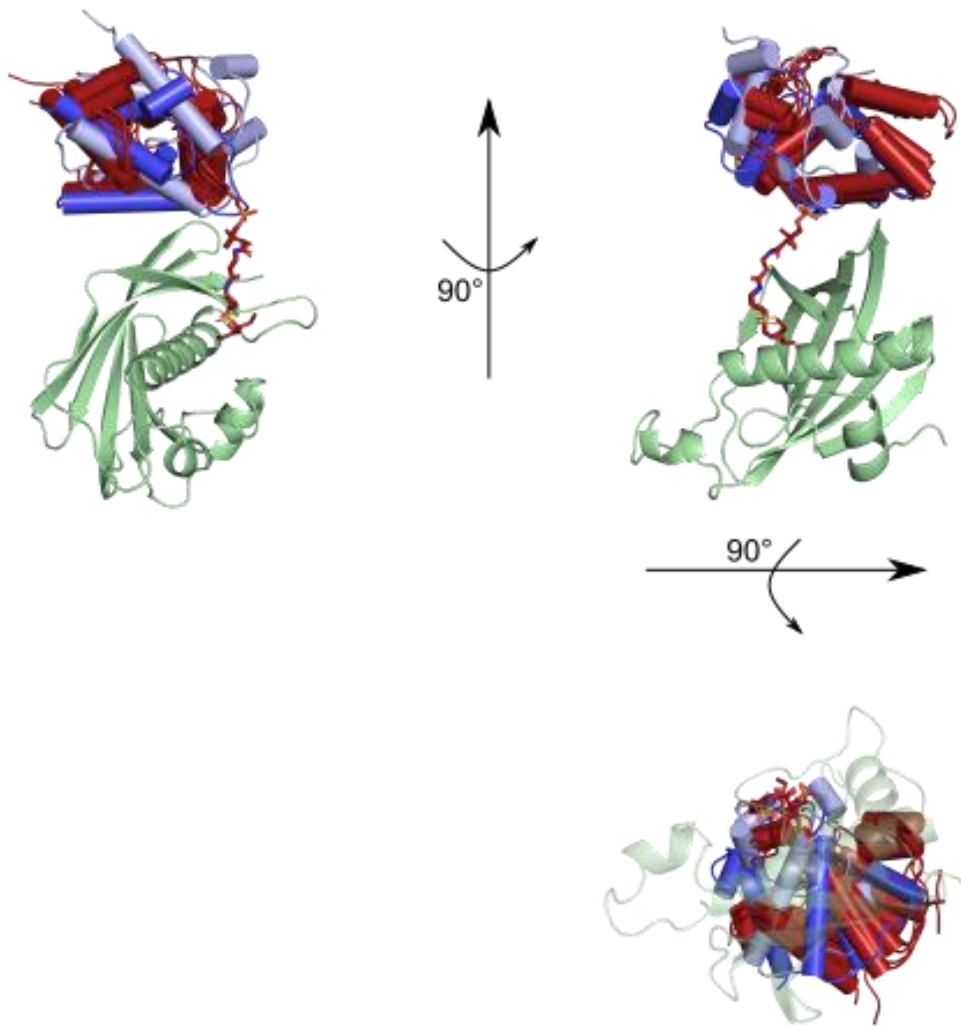
Figure 6.9 Position of crosslinked AcpP relative to the non-crosslinked DH monomer.

Shown in red, four of the six crosslinked AcpPs occupy similar positions. Shown in light and dark blue, the two remaining AcpPs are shifted about the DH6 crosslinker due to crystal packing. Non-crosslinked DH monomer shown in light green. DH6 crosslinker shown as red sticks.

structure is more simply explained by crystal lattice contacts that block the three unoccupied AcpP sites. Previous surface plasmon resonance (SPR) characterization of the H. pylori FabZ – AcpP interaction indicated a single Kd of 120 nM,[52] in contrast to the three weaker binding events deduced from MST data.[16] In our SEC-MALS analysis of the E. coli FabZ-AcpP interaction, higher-order complexes existed with an excess of either apo- or holo-AcpP, and a 20-fold excess AcpP fully saturated the Mocr-FabZ hexamer (Figure 6.3A, 6.3B). The crystal lattice of the H. pylori AcpP3-FabZ6 is incompatible with an equimolar complex, so it may be that a higher-order complex was missed in the study. Alternatively, the different oligomer states observed for the *E. coli* AcpP$_6$-FabZ$_6$ complex (this work) and the *H. pylori* ACP$_3$-FabZ$_6$ complex[16] may reflect a real difference in the two FabZ proteins, perhaps arising from distinct strategies for dehydration of β-hydroxyacyl-AcpPs during fatty acid biosynthesis. Indeed, the bacterial FAS DHs vary, for example the dual FabA – FabZ DH system exists in α- and γ-proteobacteria, whereas ε-proteobacteria such as *H. pylori* possess only FabZ and use a desaturase to synthesize unsaturated fatty acids.[57-58]

DHs possess a hydrophobic binding pocket that shields the fatty acyl substrate from solvent. In *E. coli* FabZ, the binding pocket abuts the central 'hotdog' helix (α3) and is bounded by amino acids in the α3-β3 loop (residues 85-90) and the α1-β1 loop. Phe79 in the hotdog helix (α3), Leu85 in the α3-β3 loop and Leu17 form a hydrophobic surface at the innermost end of the pocket, where substrates with chain lengths of 12 carbons or greater can bind. The binding pocket broadens beyond the C6 position and could easily accommodate longer substrates with a *cis* double bond installed by FabA. In contrast, the FabA substrate-binding pocket is narrower and of length to accommodate C10 or shorter substrates. These differences in pocket length and shape between FabA and FabZ are due to the structures and lengths of their α1-β1 and α3-β3 loops (Figures 6.10A,

6.10B, 6.11). The α1-β1 loop plays a much larger role in the substrate pocket of FabA, whereas the α3-β3 loop figures prominently in the FabZ pocket.

The α3-β3 loop of FabZ connects the distal end of the pocket (Figure 6.10A, 6.10C) and conserved Tyr92 at the substrate entrance. Tyr92 was proposed as a FabZ "gating residue" based on the reduced dehydration activity of an Ala substitution[54] and on the "open" and "closed" conformations of the Tyr side chain in FabZ crystal structures (Figure 6.10C)[14, 16, 53, 55, 59]. In the closed conformation, the Tyr92 side chain blocks the entrance of the substrate binding pocket[14, 53, 55, 59]. In the AcpP=FabZ complex, the Tyr92 gate is "open" in all six FabZ monomers, and the acylated phosphopantetheine extends into the binding pocket.

Interestingly, the α3-β3 loop is the least conserved region of FabZ and varies in length (7-10 amino acids, Figure 6.11). In FabZ structures with shorter α3-β3 loops, the loop is often poorly ordered or disordered. However, the shorter α3-β3 loop in the *E. coli* FabZ is well ordered with identical conformations in all six subunits of the AcpP=FabZ complex, suggesting that FabZ interactions with AcpP or the acyl group may facilitate the ordering the α3-β3 loop and formation of the substrate pocket. How this may occur is not apparent from the structure.
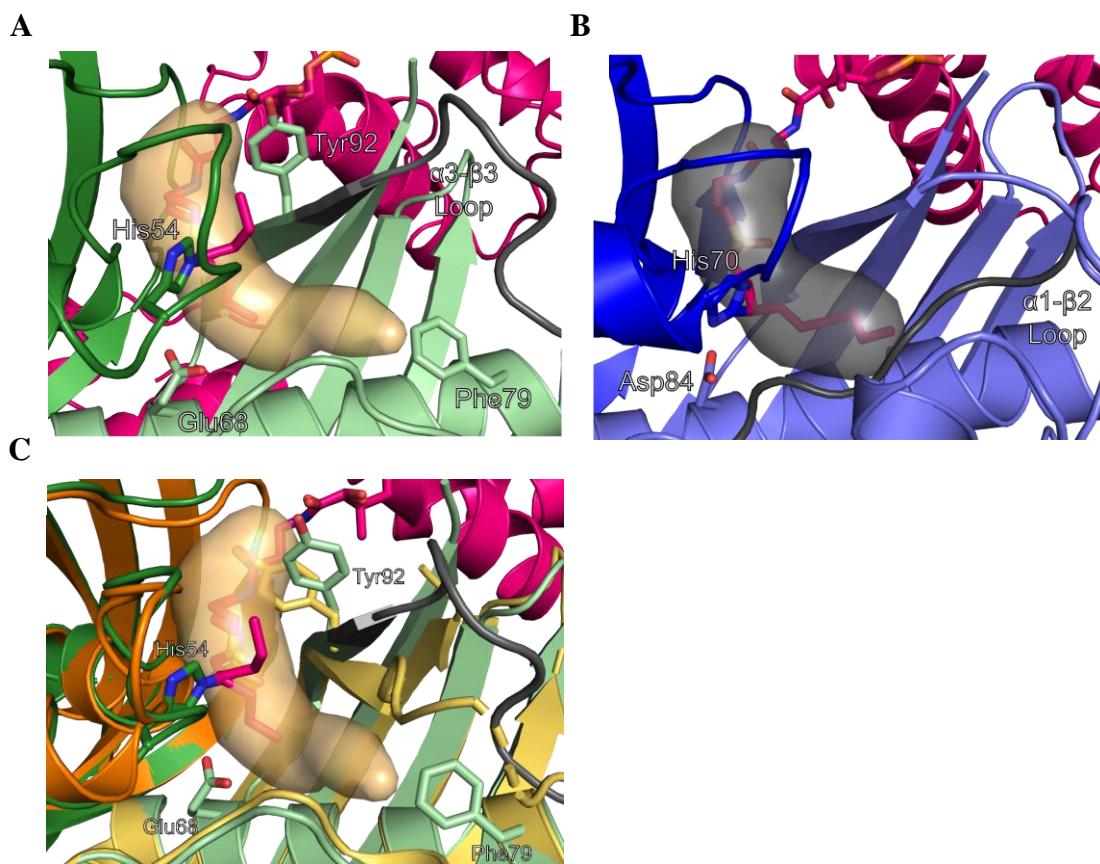
Figure 6.10 Comparison of E. coli FabZ and FabA substrate binding pockets.

A. FabZ (light and dark green) and AcpP (magenta) with an ordered α3-β3 loop (gray). The binding pocket (orange surface) is wide at the top with a narrow terminus and is long enough to for C14 substrates. Important amino acids and the C6 crosslinkers shown as sticks.

B. FabA (light and dark blue) and AcpP (magenta). The α1-β2 loop (gray) defines the end of the binding pocket (gray surface), which is optimal for C10 substrates. Important amino acids and the C10 crosslinker are shown as sticks.

C. Overlay of FabZ from *E. coli* (light/dark green) and *P. aeruginosa* (yellow/dark orange, PDB 1U1Z). In the AcpP=FabZ complex, the α3-β3 loop region (residues 85-90, gray) creates the distal end of the substrate pocket. The corresponding region of the *P. aeruginosa* FabZ is disordered in all subunits of the hexamer (dashed line). In absence of AcpP or a suitable ligand, the Tyr92 gate, which immediately follows the loop, blocks the entrance to the substrate pocket. The Tyr92 gate is open in the presence of acyl-ACP, which may order the loop and form the distal end of the substrate pocket.
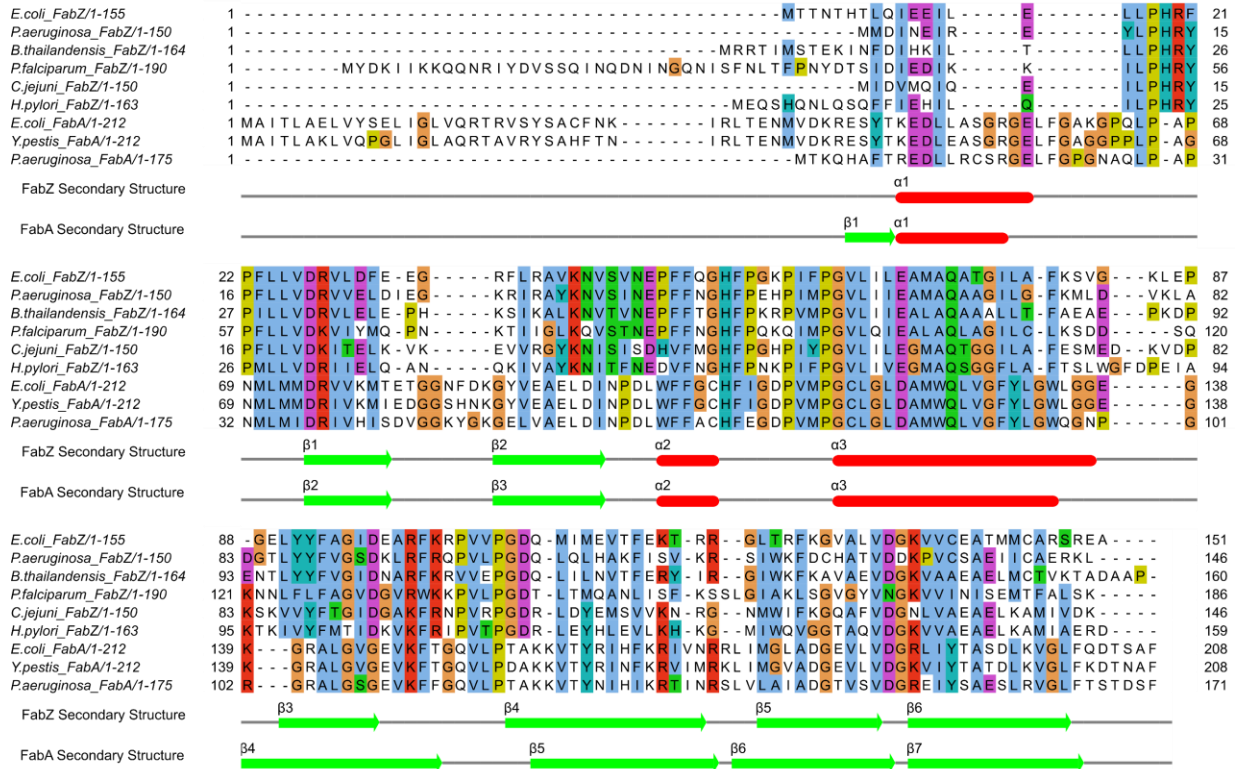
Figure 6.11 Sequence alignment of FabZ and FabA from select biological sources.

α-helical secondary structure denoted as red tubes, β-strands denoted by green arrows.

We next used MD simulations to evaluate how the protein structure imparts the mechanistic differences and substrate selectivities of the two enzymes. As AcpP=FabZ and AcpP=FabA represent the most accurate approximations of natural binding events at the moment of catalysis, these structures are ideally suited for MD simulations with modeled alternate substrates. Gaussian accelerated molecular dynamics (GaMD)[30] simulations of multiple [(R)-β-hydroxyhexanoyl-AcpP (C6), (R)-β-hydroxydecanoyl-acyl-AcpP (C10), α,β-trans-decenoyl-AcpP (trans-C10:1), β,γ-cis-decenoyl-AcpP (cis-C10:1), (R)-β-hydroxytetradecanoyl-AcpP (C14), and (R)-β-hydroxytetradec-7-cis-enoyl-AcpP (C14:1)] acyl-AcpP$_2$•FabZ$_2$ and acyl-AcpP$_2$•FabA$_2$ were performed and segregated into two mechanistic steps: β-hydroxy dehydration, as naturally catalyzed by both enzymes, and allylic rearrangement, as naturally catalyzed only by FabA. The β-hydroxy dehydration to form the trans-2-decenoate product can theoretically undergo 2 different mechanisms; a 2-step mechanism, where the conjugate base intermediate is stabilized by the carbonyl (E1cb), or a 1-step mechanism where no intermediates are formed (E2). Mechanistic studies of FabA support an E1cb-like mechanism (Scheme 6.1) ,[8, 60] and a similar conclusion was reached on the basis of the crystal structure of *P. aeruginosa* FabA in complex with a substrate mimic.[15] GaMD simulations of both β-hydroxydecanoyl-AcpP$_2$•FabA$_2$ and β-hydroxydecanoyl-AcpP$_2$•FabZ$_2$ agree with the proposed E1cb dehydration. In both simulations, a clear bias for the 60° Cα-Cβ dihedral was observed, which positions the substrate pro-R H$_α$ and β-hydroxy group ideally for E1cb elimination (Figures 6.12A, 6.12B). The -60° Cα-Cβ dihedral, which would pose the substrate for E2 elimination was not observed in simulations of either FabA or FabZ.

The production of *cis*-3-decenoyl-AcpP via allylic rearrangement has been unequivocally demonstrated to involve the intermediacy of *trans*-2-decenoyl-AcpP.[8] NMR isotope studies

rate-determining
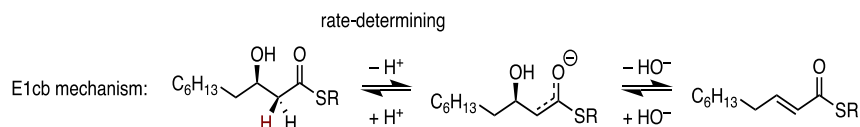
E1cb mechanism:

Scheme 6.1 Proposed mechanism of FabA-catalyzed dehydration of 3R-hydroxydecanoate NAC.

concluded that FabA abstracts the pro-*R* H$_\gamma$ of *trans*-2-decenoyl-AcpP in order to produce *cis*-3-decenoyl-AcpP.[12] Consequently, we performed GaMD simulations of *trans*-2-decenoyl-AcpP•FabA and *trans*-2-decenoyl-AcpP•FabZ and monitored the C$_\beta$–C$_\gamma$ dihedrals sampled in both enzymes. In the simulations, the substrate predominantly assumed one of four C$_\beta$–C$_\gamma$ rotameric states (Figure 6.13). In only one of the rotameric states sampled computationally, the (–) *gauche* conformer, is the pro-*R* H$_\gamma$ suitably positioned within the active site to be abstracted by the active site catalytic His70 base to initiate the allylic rearrangement. While both FabA and FabZ sampled the same four conformers, FabA showed a distinct preference for the (–) *gauche* conformer compared to FabZ (Figure 6.13). Thus, FabA isomerization may be a consequence of preorganizing the allylic substrate for pro-*R* H$_\gamma$ abstraction after dehydration. This analysis supports the critical influence of the shape and size of the FabA substrate pocket on the isomerase activity.

To evaluate the origins of chain length preferences, we performed simulations of both β-hydroxyhexanoyl-AcpP•FabA/Z and β-hydroxydecanoyl-AcpP•FabA/Z, the preferred substrates of FabZ (C6 and C14) and FabA (C10), respectively. Analysis of the simulation data demonstrated active site preorganization, as visualized by the distances between the catalytic His and substrate α carbon and between the catalytic Asp/Glu and the substrate β-hydroxy (Figures 6.14A, 6.14B). Throughout the simulation, FabZ maintained a hydrogen bond ($d < 3.0$ Å) between the carboxylate of Glu68 and the β-hydroxy substituent of β-hydroxyhexanoyl-AcpP, in agreement with the proposed Glu68 function as a general acid. In constrast, the FabA catalytic Asp84 formed a longer

279
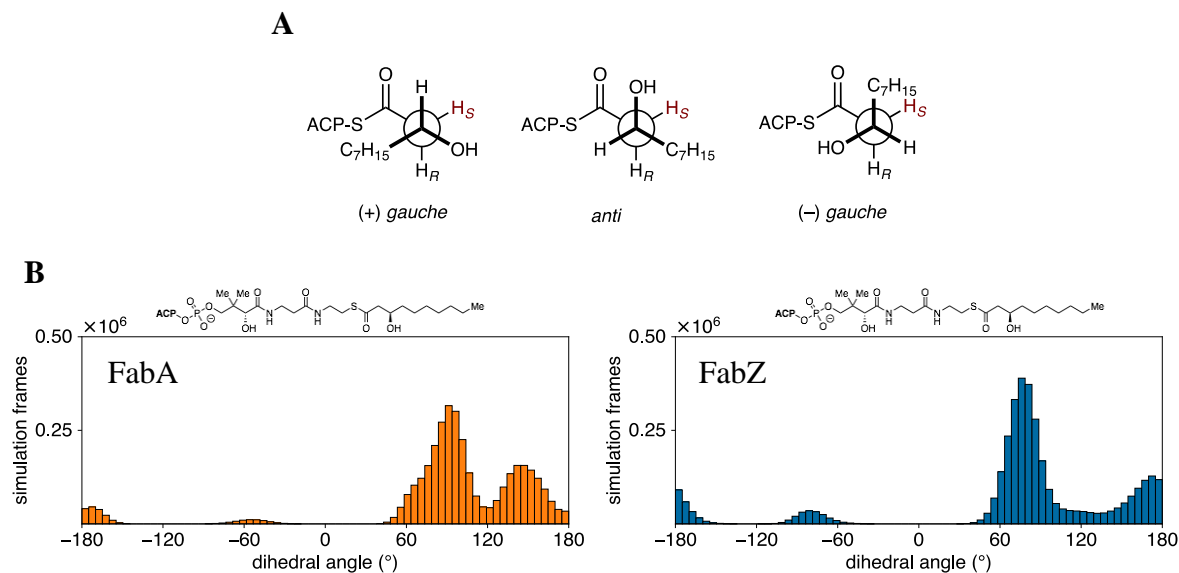
Figure 6.12 Distribution of dihedral angles for the C(O)–Cα–Cβ–Cγ torsion sampled throughout the course of GaMD simulations of β-hydroxydecanoyl-AcpP.

A: Newman projections along the Cα–Cβ bond of the (+) gauche (+60°), anti (180°), and (–) gauche (–60°) substrate rotamers of β-hydroxydecanoyl–AcpP. **B**: **Left** (orange): simulations of β-hydroxydecanol-AcpP•FabA. **Right** (blue): simulations of β-hydroxydecanol-AcpP•FabZ. Simulation data were written every 0.5 ps with a bin width of 5°. Data generated by Ashay Patel
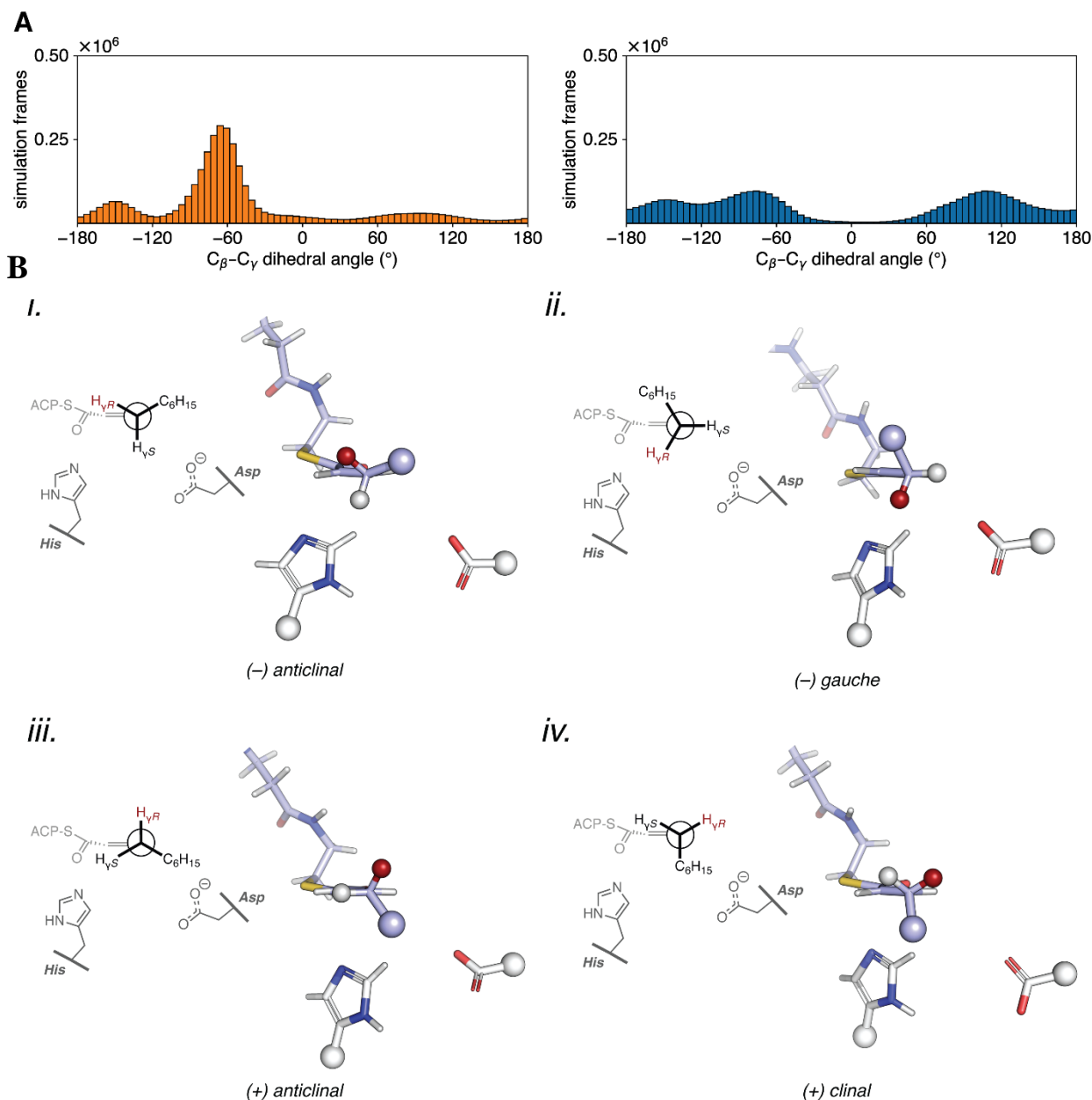
Figure 6.13 Analyis of MD simulations with trans-dec-2-enoyl-AcpP.

A.) Distribution of dihedral angles for the C_α–C_β–C_γ–C_δ torsion of the *trans*-dec-2-enoyl substrate sampled throughout the course of GaMD simulations of *trans*-dec-2-enoyl-AcpP•FabA (left-hand panel, in orange) and *trans*-dec-2-enoyl-AcpP•FabZ (right-hand panel, in blue). Simulation data written every 0.5 ps were binned to prepare histograms using a bin width of 5°. B.) Representative structures of the four C_β–C_γ rotamers sampled computationally. These structures were identified from the larger simulated ensemble of the *trans*-dec-2-enoyl-AcpP•FabA complex. Structures are oriented as Newman projections along the C_γ–C_β bond of the *trans*-dec-2-enoyl substrate (stick form with pale blue C, red O, blue N) within the active site of FabA (catalytic histidine and aspartate with white C). Large spheres indicate the portions of the substrate and catalytic residues omitted in the three-dimensional images. The smaller spheres found at C_γ show the pro-*R* (red) and pro-*S* (white) γ hydrogens; the pro-*R* H_γ is abstracted in the isomerization reaction. A two-dimensional representation of each structure is shown on the left of each panel.

281
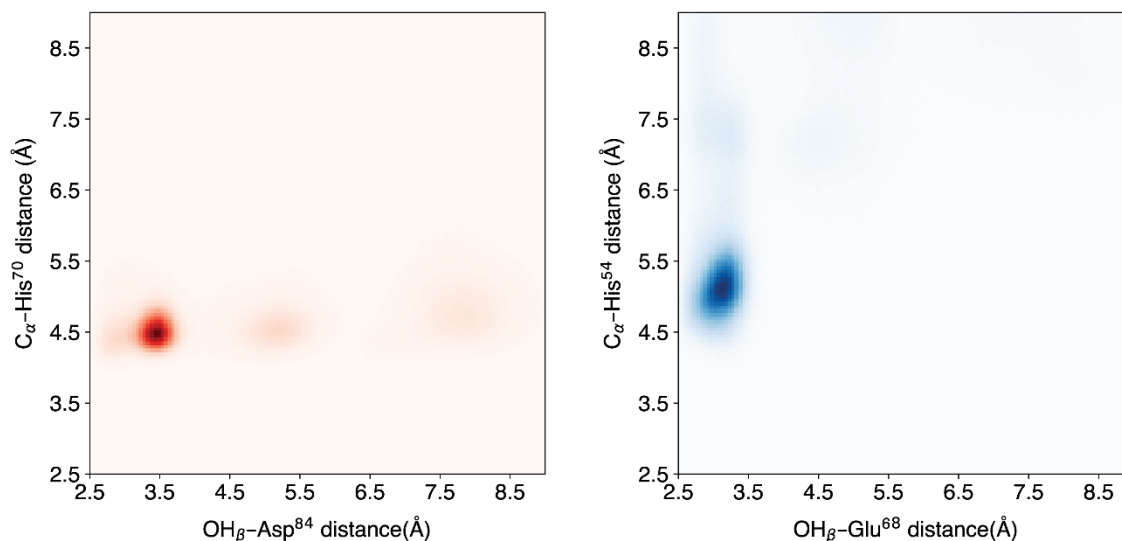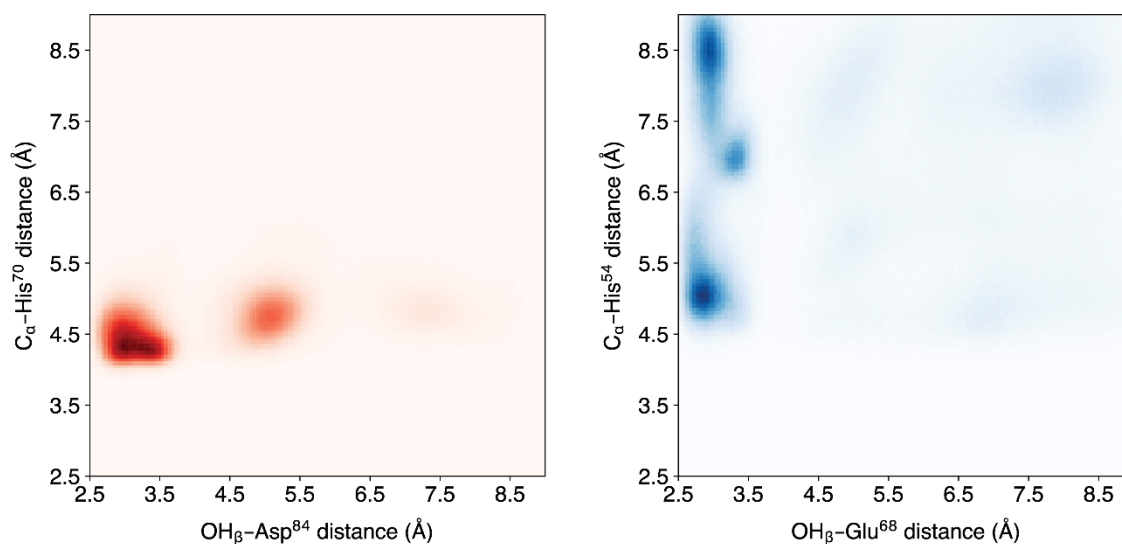
Figure 6.14 Distances between catalytic residues and key substrate positions during MD simulations.

Distances of substrate atoms and catalytic amino acids during MD simulations. The 2D histograms were created by binning simulation data for the complexes of saturated β-hydroxyacyl-AcpP•DHs with C6 and C10 substrate chain lengths. The distance between the substrate β-hydroxy O atom and the carboxylate sidechain of Asp[84] in FabA or Glu[68] in FabZ is represented on the horizontal axis, while the vertical axis depicts the distance between the substrate α C atom and the imidazole moiety of the catalytic histidine. A) Data from simulations of β-hydroxyhexanoyl-Acp•FabA (left) and β-hydroxyhexanoyl-Acp•FabZ (right). B) Data from simulations of β-hydroxydecanoyl-AcpP•FabA (left) and β-hydroxydecanoyl-AcpP•FabZ (right). Data generated by Ashay Patel.

hydrogen bond (3.0 Å $< d <$ 3.5 Å) with the β-hydroxy substituent in the simulations of β-hydroxyhexanoyl-AcpP•FabA. While the Asp/Glu of FabA and FabZ could form a hydrogen bond with the β-hydroxydecanoyl-AcpP, the FabA preferred substrate, the FabA active site histidine maintained contact with the substrate α-carbon throughout the simulation, whereas the FabZ catalytic histidine often disengaged (d > 6.0 Å) the substrate (Figure 6.14B).

Further analysis of the substrate binding pockets was performed by evaluating the shape of the pockets sampled over the course of the MD simulations (Figures 6.15, 6.16). The 10 carbon substrates of decanoyl-AcpP, *trans*-2-decenoyl-AcpP, and *cis*-3-decenoyl-AcpP were all accommodated within the FabA binding pocket with minimal reorganization of the pocket and were of ideal length to occupy its entirety. When hexanoyl-AcpP was bound, the pocket was similar in size and shape to that sampled during simulations of the decanoyl-AcpP•FabA complexes; but the shorter 6 carbon alkyl chain, left a void in the binding cavity that may be responsible for its lower activity with FabA. In contrast, the 14 carbon substrates of tetradecanoyl-AcpP and *cis*-7-tetradecanoyl-AcpP were too large for the FabA active site and not only forced the cavity to expand, but also increased the space between AcpP and FabA (Figure 6.15B, upper

regions of the isosurfaces of tetradecanoy-AcpP•FabA and *cis*-7-tetradecanoyl AcpP•FabA), presumably reducing their affinity for one another. Analysis of simulation data for acyl-AcpP•FabZ complexes demonstrated that the substrate binding pocket of FabZ was generally larger in volume and more dynamic than the FabA pocket (Figure 6.16). The relationship between simulated pocket volumes and substrate specificities is less obvious for FabZ than for FabA, as the preferred short6 carbon chain length substrate and intermediate 10 carbon chain length species (Figure 6.16B) occupied similar pockets during simulations. Interestingly, the simulations
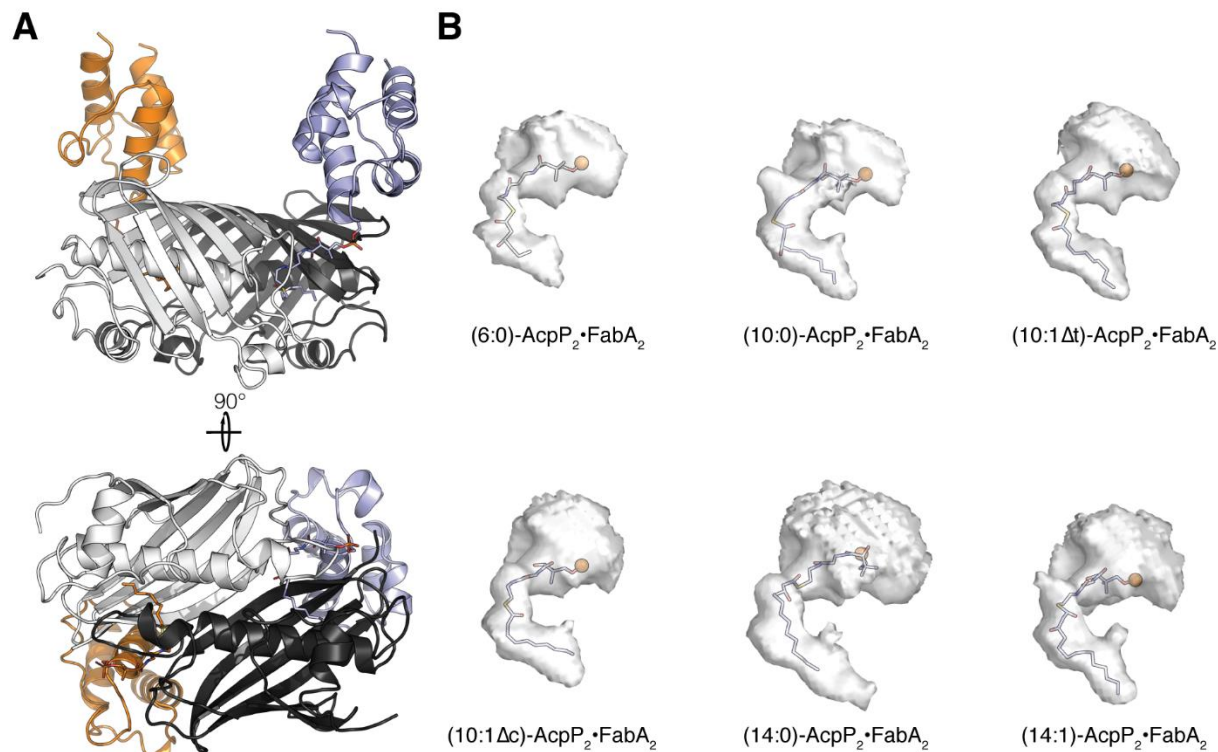
Figure 6.15 Analysis of binding pocket volume over the course of MD simulations with selected substrates for FabA.

Analysis of the FabA binding pocket size and shape for acyl substrates of varying length. Cavity volumes of the acyl-AcpP•FabA complexes were sampled computationally using POVME 3[3]. **A**. Structure of the AcpP=FabA dimer[5]. **B**. Isosurfaces of the acyl-AcpP•FabA complexes sampled via MD simulation. The views correspond to the blue acyl-AcpP in the lower image in A. The binding pocket is within the displayed volume in at least 10 percent of the simulation steps. The phosphantethiene prosthetic group and acyl substrate are shown as sticks (P atom as orange sphere). The computed cavities include unoccupied space (upper regions of isosurfaces) between AcpP and FabA. Data generated by Ashay Patel
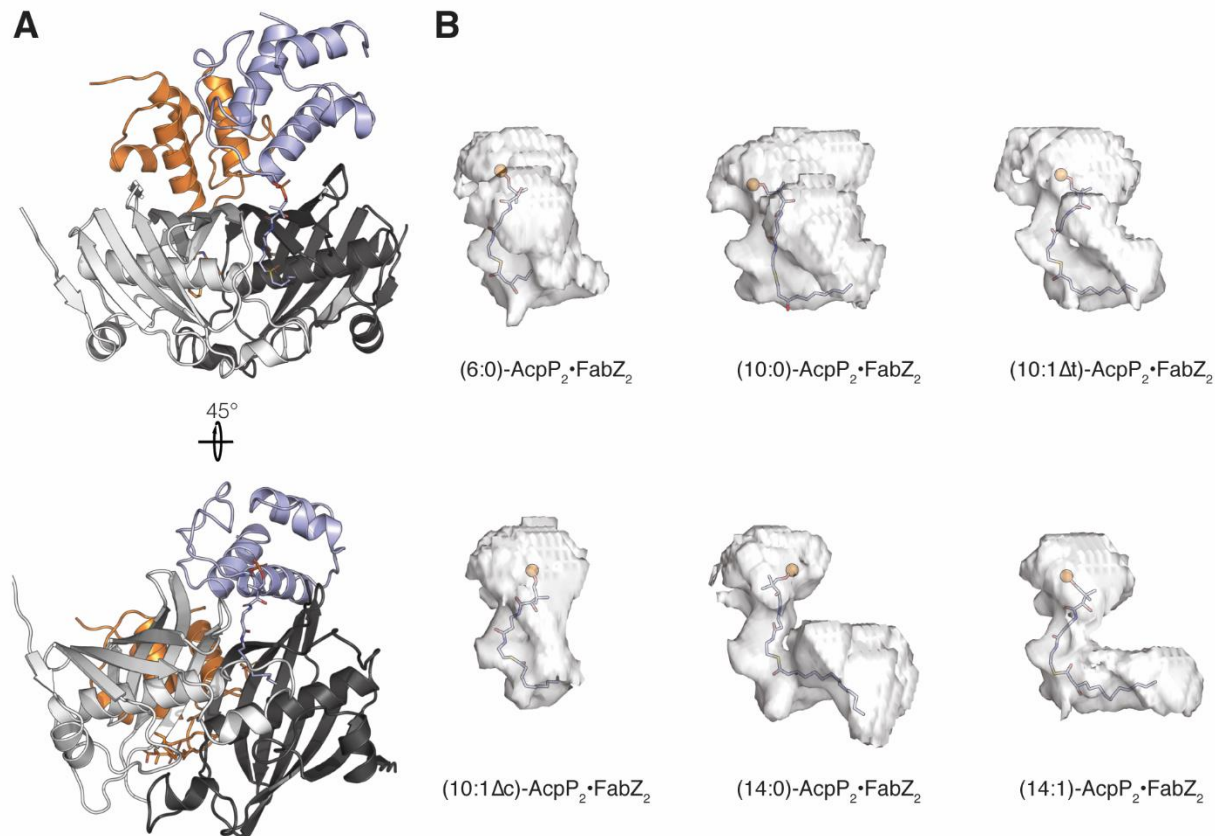
Figure 6.16 Analysis of binding pocket volume over the course of MD simulations with selected substrates for FabZ.

Analysis of the FabZ binding pocket size and shape for acyl substrates of varying length. Cavity volumes of the acyl-AcpP•FabZ complexes were sampled as in Figure 8. **A**. Structure of the AcpP=FabZ dimer. **B**. Isosurfaces of the acyl-AcpP•FabZ complexes sampled via MD simulation. The views correspond to the blue acyl-AcpP in the lower image in A. The binding pocket is within the displayed volume in at least 37.5% of the simulation steps. The phosphantethiene and acyl substrate are as in Figure 8. Note that the computed cavities includes unoccupied space (upper regions of isosurfaces) between AcpP and FabZ.

recapitulated the proposed FabZ reorganization of the substrate pocket when bound to longer-chain substrates (i.e, 14 carbon- acyl groups, Figure 6.16B).

In conclusion, we present a 2.5-Å crystal structure of the *E. coli* AcpP=FabZ complex, the first structure of the *E. coli* FabZ, with six AcpPs in functional association with the FabZ hexamer. The *E. coli* AcpP=FabZ crystal structure used the power of small molecule inhibitor-based mechanistic crosslinking probes to trap the native interaction, clearly demonstrating that all six FabZ monomers can functionally and simultaneously interact with AcpP. The structure reveals a broad FabZ substrate pocket in contrast to the narrow and straight pocket of FabA. The α3-β3 loop of FabZ that lines the distal end of the substrate pocket is well-ordered, forming a hydrophobic cleft that may allow the dehydration of long-chain acyl substrates, especially those with *cis*-unsaturation. By application of GaMD simulations to both the AcpP=FabZ and AcpP=FabA crosslinked structures, we corroborated these conclusions and recapitulated the known substrate preferences of both enzymes. GaMD further revealed how both enzyme pockets stabilize substrate rotamers to allow dehydration via an E1cb mechanism. Subsequently, simulations showed that only FabA stabilized the (–) *gauche* conformer of *trans*-2-decenoyl-AcpP for allylic rearrangement, in which the pro-*R* γ hydrogen is suitably positioned for abstraction to form *cis*-3-decenoyl-AcpP. These structural findings shed light on the divergent substrate preferences of *E. coli* FabA and FabZ and provide clarity for how the structure of each enzyme dictates mechanistic specificity.

Bibliography

1. Cronan, J. E., Jr., Gelmann, E. P., Physical properties of membrane lipids: biological relevance and regulation. *Bacteriol Rev* **1975,** *39* (3), 232-56.
2. Zhang, Y. M., Rock, C. O., Membrane lipid homeostasis in bacteria. *Nat. Rev. Microbiol.* **2008,** *6* (3), 222-33.
3. Wagner, J. R., Sørensen, J., Hensley, N., Wong, C., Zhu, C., Perison, T., Amaro, R. E., POVME 3.0: software for mapping binding pocket flexibility. *Journal of chemical theory and computation* **2017,** *13* (9), 4584-4592.
4. Ishikawa, F., Haushalter, R. W., Lee, D. J., Finzel, K., Burkart, M. D., Sulfonyl 3-alkynyl pantetheinamides as mechanism-based cross-linkers of acyl carrier protein dehydratase. *J. Am. Chem. Soc.* **2013,** *135* (24), 8846-8849.
5. Nguyen, C., Haushalter, R. W., Lee, D. J., Markwick, P. R., Bruegger, J., Caldara-Festin, G., Finzel, K., Jackson, D. R., Ishikawa, F., O'Dowd, B., Trapping the dynamic acyl carrier protein in fatty acid biosynthesis. *Nature* **2014,** *505* (7483), 427-431.
6. Cronan, J. J., Rock, C. O., Biosynthesis of membrane lipids. *EcoSal Plus* **2008,** *3* (1).
7. Heath, R. J., Rock, C. O., Roles of the FabA and FabZ β-hydroxyacyl-acyl carrier protein dehydratases in *Escherichia coli* fatty acid biosynthesis. *J. Biol. Chem.* **1996,** *271* (44), 27795-27801.
8. Brock, D. J., Kass, L. R., Bloch, K., β-hydroxydecanoyl thioester dehydrase. II. Mode of action. *J. Biol. Chem.* **1967,** *242* (19), 4432-4440.
9. Helmkamp, G. M., Jr., Brock, D. J., Bloch, K., β-hydroxydecanoly thioester dehydrase. Specificity of substrates and acetylenic inhibitors. *J. Biol. Chem.* **1968,** *243* (12), 3229-31.
10. Mohan, S., Kelly, T. M., Eveland, S. S., Raetz, C. R., Anderson, M. S., An *Escherichia coli* gene (FabZ) encoding (3R)-hydroxymyristoyl acyl carrier protein dehydrase. Relation to fabA and suppression of mutations in lipid A biosynthesis. *J. Biol. Chem.* **1994,** *269* (52), 32896-903.
11. Schwab, J. M., Klassen, J. B., Habib, A., Stereochemical course of the hydration reaction catalysed by β-hydroxydecanoylthioester dehydrase. *J. Chem. Soc., Chem. Commun.* **1986,** (4), 357-358.
12. Schwab, J. M., Klassen, J. B., Steric course of the allylic rearrangement catalyzed by β-hydroxydecanoylthioester dehydrase. Mechanistic implications. *J. Am. Chem. Soc.* **1984,** *106* (23), 7217-7227.
13. Leesong, M., Henderson, B. S., Gillig, J. R., Schwab, J. M., Smith, J. L., Structure of a dehydratase-isomerase from the bacterial pathway for biosynthesis of unsaturated fatty acids: Two catalytic activities in one active site. *Structure* **1996,** *4* (3), 253-264.
14. Kimber, M. S., Martin, F., Lu, Y., Houston, S., Vedadi, M., Dharamsi, A., Fiebig, K. M., Schmid, M., Rock, C. O., The structure of (3R)-hydroxyacyl-acyl carrier protein dehydratase (FabZ) from *Pseudomonas aeruginosa*. *J. Biol. Chem.* **2004,** *279* (50), 52593-52602.
15. Moynié, L., Leckie, S. M., McMahon, S. A., Duthie, F. G., Koehnke, A., Taylor, J. W., Alphey, M. S., Structural Insights into the Mechanism and Inhibition of the β-Hydroxydecanoyl-Acyl Carrier Protein Dehydratase from *Pseudomonas aeruginosa*. *J. Mol. Biol.* **2013,** *425* (2), 365-377.
16. Zhang, L., Xiao, J., Xu, J., Fu, T., Cao, Z., Zhu, L., Chen, H.-Z., Shen, X., Jiang, H., Zhang, L., Crystal structure of FabZ-ACP complex reveals a dynamic seesaw-like catalytic mechanism of dehydratase in fatty acid biosynthesis. *Cell Res.* **2016,** *26* (12), 1330-1344.

17.   Yu, X., Liu, T., Zhu, F., Khosla, C., In vitro reconstitution and steady-state analysis of the fatty acid synthase from *Escherichia coli*. *Proceedings of the National Academy of Sciences* **2011,** *108* (46), 18643-18648.

18.   DelProposto, J., Majmudar, C. Y., Smith, J. L., Brown, W. C., Mocr: A novel fusion tag for enhancing solubility that is compatible with structural biology applications. *Protein Expression Purif.* **2009,** *63* (1), 40-49.

19.   Kosa, N. M., Haushalter, R. W., Smith, A. R., Burkart, M. D., Reversible labeling of native and fusion-protein motifs. *Nat. Methods* **2012,** *9* (10), 981-984.

20.   Worthington, A. S., Rivera, H., Torpey, J. W., Alexander, M. D., Burkart, M. D., Mechanism-based protein cross-linking probes to investigate carrier protein-mediated biosynthesis. *ACS chemical biology* **2006,** *1* (11), 687-691.

21.   Kabsch, W., Xds. *Acta Crystallogr D Biol Crystallogr* **2010,** *66* (Pt 2), 125-32.

22.   McCoy, A. J., Grosse-Kunstleve, R. W., Adams, P. D., Winn, M. D., Storoni, L. C., Read, R. J., Phaser crystallographic software. *J. Appl. Crystallogr.* **2007,** *40* (4), 658-674.

23.   Nguyen, C., Haushalter, R. W., Lee, D. J., Markwick, P. R. L., Bruegger, J., Caldara-Festin, G., Finzel, K., Jackson, D. R., Ishikawa, F., O'Dowd, B., McCammon, J. A., Opella, S. J., Tsai, S.-C., Burkart, M. D., Trapping the dynamic acyl carrier protein in fatty acid biosynthesis. *Nature* **2014,** *505* (7483), 427-431.

24.   Emsley, P., Lohkamp, B., Scott, W. G., Cowtan, K., Features and development of Coot. *Acta Crystallogr. Sect. D. Biol. Crystallogr.* **2010,** *66* (4), 486-501.

25.   Adams, P. D., Afonine, P. V., Bunkóczi, G., Chen, V. B., Davis, I. W., Echols, N., Headd, J. J., Hung, L. W., Kapral, G. J., Grosse-Kunstleve, R. W., McCoy, A. J., Moriarty, N. W., Oeffner, R., Read, R. J., Richardson, D. C., Richardson, J. S., Terwilliger, T. C., Zwart, P. H., PHENIX: A comprehensive Python-based system for macromolecular structure solution. *Acta Crystallogr. Sect. D. Biol. Crystallogr.* **2010,** *66* (2), 213-221.

26.   Adams, P. D., Afonine, P. V., Bunkoczi, G., Chen, V. B., Davis, I. W., Echols, N., Headd, J. J., Hung, L. W., Kapral, G. J., Grosse-Kunstleve, R. W., McCoy, A. J., Moriarty, N. W., Oeffner, R., Read, R. J., Richardson, D. C., Richardson, J. S., Terwilliger, T. C., Zwart, P. H., PHENIX: a comprehensive Python-based system for macromolecular structure solution. *Acta Crystallographica, Section D: Biological Crystallography* **2010,** *66* (Pt 2), 213-21.

27.   Schrodinger, LLC, The PyMOL Molecular Graphics System, Version 1.8. 2015.

28.   Krissinel, E., Henrick, K., Inference of Macromolecular Assemblies from Crystalline State. *J. Mol. Biol.* **2007,** *372* (3), 774-797.

29.   Cieplak, P., Cornell, W. D., Bayly, C., Kollman, P. A., Application of the multimolecule and multiconformational RESP methodology to biopolymers: Charge derivation for DNA, RNA, and proteins. *J. Comput. Chem.* **1995,** *16* (11), 1357-1377.

30.   Frisch, M. J., Trucks, G. W., Schlegel, H. B., Scuseria, G. E., Robb, M. A., Cheeseman, J. R., Scalmani, G., Barone, V., Mennucci, B., Petersson, G. A., Nakatsuji, H., Caricato, M., Li, X., Hratchian, H. P., Izmaylov, A. F., Bloino, J., Zheng, G., Sonnenber, D. J., Gaussian 09 Revision D.01. *Gaussian, Inc. Wallingford CT* **2009**, 2-3.

31.   Maier, J. A., Martinez, C., Kasavajhala, K., Wickstrom, L., Hauser, K. E., Simmerling, C., ff14SB: Improving the Accuracy of Protein Side Chain and Backbone Parameters from ff99SB. *Journal of Chemical Theory and Computation* **2015,** *11* (8), 3696-3713.

32.   Wang, J., Wolf, R. M., Caldwell, J. W., Kollman, P. A., Case, D. A., Development and testing of a general Amber force field. *J. Comput. Chem.* **2004,** *25* (9), 1157-1174.

33.   Wang, J., Wang, W., Kollman, P. A., Case, D. A., Automatic atom type and bond type perception in molecular mechanical calculations. *J. Mol. Graphics Model.* **2006,** *25* (2), 247-260.

34.   Bashford, D., Karplus, M., pKa's of Ionizable Groups in Proteins: Atomic Detail from a Continuum Electrostatic Model. *Biochemistry* **1990,** *29* (44), 10219-10225.

35.   Gordon, J. C., Myers, J. B., Folta, T., Shoja, V., Heath, L. S., Onufriev, A., H++: A server for estimating pKas and adding missing hydrogens to macromolecules. *Nucleic Acids Res.* **2005,** *33* (SUPPL. 2), W368-W371.

36.   Myers, J., Grothaus, G., Narayanan, S., Onufriev, A., A simple clustering algorithm can be accurate enough for use in calculations of pKs in macromolecules. *Proteins: Structure, Function and Genetics* **2006,** *63* (4), 928-938.

37.   Anandakrishnan, R., Aguilar, B., Onufriev, A. V., H++ 3.0: Automating pK prediction and the preparation of biomolecular structures for atomistic molecular modeling and simulations. *Nucleic Acids Res.* **2012,** *40* (W1).

38.   Jorgensen, W. L., Chandrasekhar, J., Madura, J. D., Impey, R. W., Klein, M. L., Comparison of simple potential functions for simulating liquid water. *The Journal of Chemical Physics* **1983,** *79* (2), 926-935.

39.   Case, D. A., Babin, V., Berryman, J., Betz, R. M., Cai, Q., Cerutti, D. S., Cheatham III, T. E., Darden, T. A., Duke, R. E., Gohlke, H., Goetz, A. W., Gusarov, S., Homeyer, N., Janowski, P., Kaus, J., Kolossváry, I., Kovalenko, A., Lee, T. S., LeGrand, S., Luchko, T., Luo, R., Madej, B., Merz, K. M., Paesani, F., Roe, D. R., Roitberg, A., Sagui, C., Salomon-Ferrer, R., Seabra, G., Simmerling, C. L., Smith, W., Swails, J., Walker, R. C., Wang, J., Wolf, R. M., Wu, X., Kollman, P. A. *AMBER14*, University of California, San Francisco: 2014.

40.   Hamelberg, D., Mongan, J., McCammon, J. A., Accelerated molecular dynamics: A promising and efficient simulation method for biomolecules. *The Journal of Chemical Physics* **2004,** *120* (24), 11919-11929.

41.   Pierce, L. C. T., Salomon-Ferrer, R., Augusto F. De Oliveira, C., McCammon, J. A., Walker, R. C., Routine access to millisecond time scale events with accelerated molecular dynamics. *Journal of Chemical Theory and Computation* **2012,** *8* (9), 2997-3002.

42.   Salomon-Ferrer, R., Götz, A. W., Poole, D., Le Grand, S., Walker, R. C., Routine microsecond molecular dynamics simulations with AMBER on GPUs. 2. Explicit solvent particle mesh ewald. *Journal of Chemical Theory and Computation* **2013,** *9* (9), 3878-3888.

43.   Miao, Y., Feher, V. A., McCammon, J. A., Gaussian Accelerated Molecular Dynamics: Unconstrained Enhanced Sampling and Free Energy Calculation. *Journal of Chemical Theory and Computation* **2015,** *11* (8), 3584-3595.

44.   Miao, Y., Sinko, W., Pierce, L., Bucher, D., Walker, R. C., McCammon, J. A., Improved reweighting of accelerated molecular dynamics simulations for free energy calculation. *Journal of Chemical Theory and Computation* **2014,** *10* (7), 2677-2689.

45.   Ryckaert, J. P., Ciccotti, G., Berendsen, H. J. C., Numerical integration of the cartesian equations of motion of a system with constraints: molecular dynamics of n-alkanes. *Journal of Computational Physics* **1977,** *23* (3), 327-341.

46.   Darden, T., York, D., Pedersen, L., Particle mesh Ewald: An $N \cdot \log(N)$ method for Ewald sums in large systems. *The Journal of Chemical Physics* **1993,** *98* (12), 10089-10092.

47.   Loncharich, R. J., Brooks, B. R., Pastor, R. W., Langevin dynamics of peptides: The frictional dependence of isomerization rates of N-acetylalanyl-N′-methylamide. *Biopolymers* **1992,** *32* (5), 523-535.

48.   Roe, D. R., Cheatham, T. E., PTRAJ and CPPTRAJ: Software for processing and analysis of molecular dynamics trajectory data. *Journal of Chemical Theory and Computation* **2013,** *9* (7), 3084-3095.

49.   McGibbon, R. T., Beauchamp, K. A., Harrigan, M. P., Klein, C., Swails, J. M., Hernández, C. X., Schwantes, C. R., Wang, L. P., Lane, T. J., Pande, V. S., MDTraj: A Modern Open Library for the Analysis of Molecular Dynamics Trajectories. *Biophys. J.* **2015,** *109* (8), 1528-1532.

50.   Dennington, R., Keith, T., Millam, J. *Gaussview, Version 5*, 2016.

51.   Hanwell, M. D., Curtis, D. E., Lonie, D. C., Vandermeerschd, T., Zurek, E., Hutchison, G. R., Avogadro: An advanced semantic chemical editor, visualization, and analysis platform. *Journal of Cheminformatics* **2012,** *4* (17).

52.   Liu, W., Du, L., Zhang, L., Chen, J., Shen, X., Jiang, H., *Helicobacter pylori* acyl carrier protein: Expression, purification, and its interaction with β-hydroxyacyl-ACP dehydratase. *Protein Expression Purif.* **2007,** *52* (1), 74-81.

53.   McGillick, B. E., Kumaran, D., Vieni, C., Swaminathan, S., β-Hydroxyacyl-acyl Carrier Protein Dehydratase (FabZ) from *Francisella tularensis* and *Yersinia pestis*: Structure Determination, Enzymatic Characterization, and Cross-Inhibition Studies. *Biochemistry* **2016,** *55* (7), 1091-1099.

54.   Zhang, L., Liu, W., Hu, T., Du, L., Luo, C., Chen, K., Shen, X., Jiang, H., Structural basis for catalytic and inhibitory mechanisms of beta-hydroxyacyl-acyl carrier protein dehydratase (FabZ). *The Journal of biological chemistry* **2008,** *283* (9), 5370-5379.

55.   Kostrewa, D., Winkler, F. K., Folkers, G., Scapozza, L., Perozzo, R., The crystal structure of PfFabZ, the unique β-hydroxyacyl-ACP dehydratase involved in fatty acid biosynthesis of *Plasmodium falciparum. Protein Sci.* **2005,** *14* (6), 1570-1580.

56.   Finzel, K., Nguyen, C., Jackson, D. R., Gupta, A., Tsai, S. C., Burkart, M. D., Probing the Substrate Specificity and Protein-Protein Interactions of the *E. coli* Fatty Acid Dehydratase, FabA. *Chemistry and Biology* **2015,** *22* (11), 1453-1460.

57.   Wang, H., Cronan, J. E., Functional replacement of the FabA and FabB proteins of *Escherichia coli* fatty acid synthesis by *Enterococcus faecalis* FabZ and FabF homologues. *J. Biol. Chem.* **2004,** *279* (33), 34489-34495.

58.   Bi, H., Zhu, L., Jia, J., Zeng, L., Cronan, J. E., Unsaturated fatty acid synthesis in the gastric pathogen Helicobacter pylori proceeds via a backtracking mechanism. *Cell chemical biology* **2016,** *23* (12), 1480-1489.

59.   Kirkpatrick, A. S., Yokoyama, T., Choi, K.-J., Yeo, H.-J., *Campylobacter jejuni* fatty acid synthase II: Structural and functional analysis of β-hydroxyacyl-ACP dehydratase (FabZ). *Biochem. Biophys. Res. Commun.* **2009,** *380* (2), 407-412.

60.   Schwab, J. M., Habib, A., Klassen, J. B., A thorough study of the stereochemical consequences of the hydration/dehydration reaction catalyzed by β-hydroxydecanoyl thioester dehydrase. *J. Am. Chem. Soc.* **1986,** *108* (17), 5304-5308.

Chapter 7. Conclusions and future directions

Substrate stereospecificity and product stereoselectivity of DHs

Pikromycin DH2-KR2

Studies on the DH2-KR2 di-domain from the pikromycin biosynthetic pathway represent the first steady-state kinetic analysis of a PKS DH domain[1]. The results of these studies identified unexpected extreme stereospecificity at the β, γ, and δ positions on a library of thioether chiral substrate mimics. Assay results agreed with the empirical observation that DHs in modules containing B-type KRs produce *trans* olefins. pH profiling of catalytic efficiency identified a critical general base with a pK_a of 7.0, presumably His3611.

The unexpected specificity of Pik DH2 hints at a role for DHs as stereochemical filters within PKS modules, a result that has since been echoed in the literature[2-5]. While intriguing from a functional standpoint, this unexpected stereospecificity adds a new layer of complication to PKS engineering efforts, as neither the amino acid sequence nor a homology model of Pik DH2 reveal any distinguishing characteristics. Site-directed mutagenesis guided by a homology model highlighted the importance of a hydrophobic patch comprising two Phe residues, one of which is usually a Tyr in a YGP motif in most DHs[6]. The feasibility of alkyne crosslinking probes as covalent substrate mimics for PKS DHs was tested using a 3-decynoyl-*N*-acetylcysteamine. The probe inactivated PikDH2, implying that the crosslinking probes used to study substrate-protein interactions of FAS DHs[7-8] may also be viable for PKS DHs.

Tylosin DH3-KR3

Studies on the DH3-KR3 di-domain from the tylosin biosynthetic pathway aimed to understand the stereochemical course of the reaction catalyzed by KR3 and the stereospecificity of DH3 using thioester and thioether substrate mimics[4]. These studies were the first in which a diffusible substrate probe bearing the native acyl moiety was used to characterize a PKS di-domain. LC-MS/MS analysis showed strict stereospecificity of TylDH3 for the β-position, as well as at distal stereocenters. TylDH3 was also sensitive to the length of the substrate, exhibiting no dehydration activity on a truncated substrate mimic. These results agree with the PikDH2 studies mentioned above, and further reinforce the role of PKS DH as stereochemical filters within modules.

A puzzling result from these experiments was the unexpectedly high rate of dehydration of diffusible substrates bearing a β-keto group. LC-MS/MS assay of overnight reactions showed KR3 was active, and produced a (R)-configured product consistent with its classification as a B-type KR[9]. However, the ratio of β-hydroxy intermediate to α,β-unsaturated product was 1:22 for a thioester mimic and 1:102 for a thioether mimic. This unexpected distribution implies that KR3 is capable of shuttling its product to DH3, even in the absence of an ACP. Two mechanisms were proposed to understand this phenomenon, one in which the KR active site exit and the DH entrance are proximal, and another in which a conformation change during catalysis brings the two active sites together – a similar KR conformational change has been observed in cryoEM studies of the full PikAIII module[10]. It is difficult to fully interpret this finding in the absence of any corresponding structural information.

Curacin DHs

The curacin biosynthetic pathway is an example of a PKS pathway containing both *cis* and *trans* "orphan" double bonds[11-14]. Two sets of diffusible triketide substrate mimics were used to characterize each of the DH domains from this pathway to investigate this phenomenon[5]. CurK, CurF and CurJ DHs exhibited activity on a β-hydroxy diene triketide mimic of the native CurK substrate. CurF DH retained only 55% activity of CurK DH on the CurK substrate mimic, while CurJ maintained only 7% CurF DHs. Each of DHs were stereospecific for the D-alcohol, the expected product of a B-type KR.

Curiously, only CurF DH and CurK DH were active upon a triketide substrate designed to mimic the CurJ native substrate, containing both an α-methyl and a β-hydroxy group. The stereochemistry of this substrate is consistent with β-reduction by a B-type KR and has the necessary configuration for *syn* elimination of the α-proton and the β-hydroxy group by a DH. The CurK DH does not encounter an α-methyl on its native substrate, yet was still specific for the (2*S*,3*R*) CurJ substrate, implying that this DH is indeed specialized for *syn* elimination of a B-type KR product. The inability for CurJ DH to dehydrate any of the β-hydroxy substrate mimics was unexpected, but led to the discovery of a non-canonical DH reaction discussed below.

Gephyronic acid DH1

The stereospecificity and regioselectivity of GphF DH1 was investigated using a library of diffusible substrate mimics that sampled all the possible enantiomers of the DHs native substrate and products[15]. As with the pikromycin, curacin, and tylosin DHs, GphF DH1 catalyzed *syn* elimination, but exhibited a degree of flexibility compared to most PKS DHs in that it

dehydrated either the (2*S*,3*S*) or (2*R*,3*R*) enantiomers of the native substrate. There was a slight

(~10%) preference for the (2*R*,3*R*) which contained the proper β-hydroxy chirality predicted to

be set by the B-type Gphf KR1. The regioselectivity of GphF DH1 was assayed using a set of (*E*)

and (*Z*) configured α,β-unsaturated substrate mimics. Again, GphF DH1 showed a degree of

flexibility in terms of substrate scope, as both the (*E*) and (*Z*) configured versions of its native

product were rehydrated, with a 3:1 preference for the (*E*) regioisomer. The substrate scope of

GphF DH1 was interrogated using a set of substrate and product mimics lacking an α-methyl

group. Wild-type GphF DH1 had 5-fold reduced activity on a β-hydroxy substrate lacking an α-

methyl group. These results showed that like the PikDH2, TylDH3, and the Cur DHs, GphF DH1

has specificity for the stereochemical configuration and composition of its native substrate.

Non-canonical DH reactions

Curacin DHs

CurJ DHs lack of activity on its native substrate mimic and the complete lack of activity

of CurH DH prompted an expanded analysis of these domains[5]. Upon re-examination of the

biosynthetic pathway, it became apparent that CurJ DH could encounter a β,δ-dihydroxy

substrate as CurI lacks a DH. Using a δ-hydroxy-α,β-unsaturated triketide substrate, CurJ DH

was demonstrated to stereospecifically catalyze a vinylogous δ-elimination as well as

regiospecifically catalyze the reverse hydration. This novel reaction required the His-Asp

catalytic dyad, as confirmed by mutagenesis. CurH DH also follows a module lacking a DH and

was shown to catalyze vinylogous elimination in a manner identical to CurJ DH. The unexpected

vinylogous dehydration activity uncovered by these experiments highlights the functional

diversity of PKS DHs. From either sequence or structure analysis, there was no obvious

distinction between CurJ or CurH DHs and any characterized "standard" PKS DHs.

In an effort to better understand this novel activity structurally, a catalytically inactive variant of CurJ DH was co-crystallized with a thioester substrate mimic[5]. While only a portion of the density of the substrate was resolved, an obvious hydrogen bond between catalytic Asp1156 and a hydroxyl of the substrate was observed, providing the first visualization of the Asp – hydroxyl interaction between a PKS DH and its substrate.

GphF DH1

While there are examples of PKS DHs that catalyze multiple reactions[2-3, 16-17], the molecular mechanisms behind their secondary functions are only beginning to be understood. We investigated the putative isomerization function of GphF DH1 using LC-MS assay, structure and mutagenesis. Secondary isomerization function was confirmed in our initial assay of GphF DH1, with both the (2R,3R) and (2S,3S) substrates generating both 2,3- (α,β-) and 3,4-(β,γ-) olefin products. While only minor amounts of the 3,4-olefin were observed from the 2-methyl-3-hydroxy substrates, significant quantities were observed when GphF DH1 was assayed using the 2,3-unsaturated intermediate directly. This result clearly demonstrated the GphF was a multifunctional DH/isomerase and agrees closely with results from *E. coli* FAS DH/isomerase FabA[18].

Isomerization was also assessed using the substrates lacking an α-methyl group. GphF DH1 exhibited reduced dehydration of these compounds compared to substrates bearing an α-methyl group. Interestingly, GphF DH1 generated significantly higher quantities of isomerized β,γ-unsaturated final product from substrates without an α-methyl compared to those with an α-methyl. This molecular basis for this result remains puzzling in the absence of a structure of an enzyme – substrate complex, but may imply that the α-methyl moiety of the native substrate imposes a barrier to isomerization, perhaps via a steric effect.

Interestingly, the chirality of the α-methyl of the preferred substrate (R), and the chirality of the corresponding methyl group on gephyronic acid (S) are enantiomers[19]. This led to the hypothesis that GphF DH1 harbors a cryptic third functionality as an epimerase. This was assessed using a 3,4-unsaturated product mimic containing the "incorrect" (R) configured α-methyl group. No activity was observed using the ($2R$)-2-methyl-3,4-olefin, but significant isomerization of a racemic mixture of the ($2R$) and ($2S$) form of the 2-methyl-3,4-olefin was observed. This result showed that the ($2S$)-2-methyl-3,4-olefin was the final product of catalysis by GphF DH1, and that the enzyme had epimerized the α-methyl group in addition to the previously characterized dehydration and isomerization activity.

Finally, structure-guided mutagenesis identified the catalytic machinery required for GphF DH1 function. A His1738-Asp1898 dyad was required for both dehydration and isomerization, in agreement with the experiments on the Cur, Tyl, and Pik DHs. Isomerization function was pinpointed to two positions adjacent to the catalytic dyad: Leu1744 that is differentially conserved compared to most non-isomerizing DHs, where it is generally a Pro, and Tyr1856 that is repositioned in GphF DH1 to form a hydrogen bond with the catalytic Asp. Characterization of a Leu1744→Pro variant of GphF DH1 showed a drastic increase in dehydration efficiency at the cost of isomerization, while of a Tyr1856→Phe variant displayed no isomerization capacity, with wild-type levels of dehydration. These results facilitated a gain-of-function experiment in which isomerization activity was engineered into the CurK DH via a Pro1005→Val substitution. This represented the first successful rational engineering of a PKS DH.

E.coli **FabZ – AcpP complex**

Here, the first structure of the *E. coli* FAS DH FabZ was determined, in a 1:1 crosslinked complex with its carrier protein AcpP. The complex was characterized biophysically by SEC-MALS, which revealed that both *apo*-AcpP and *holo*-AcpP formed a 1:1 complex with FabZ, in agreement with crosslinking studies. Both the protein interaction surface between FabZ and AcpP and the position of the acyl moiety of the 6-carbon substrate mimic were visualized ina 2.5Å crystal structure. The AcpP=FabZ and AcpP=FabA[8] structures were used as starting models for GaMD simulations. These simulations revealed differences in preferred substrate chain length between FabA and FabZ and demonstrated that these FAS DHs differentially bias the conformations of substrate acyl chains. FabZ positioned substrates such that only dehydration could occur, while FabA biased the substrate towards conformations favorable for both dehydration and isomerization.

Future directions

PKS DH substrates and assay

Clearly, *N*-acetylcysteamine truncated substrate mimics have proven to be useful tools for studying PKS DHs. As the NAC moiety fails to fully mimic the Ppant arm that would be present in a native DH – ACP complex within a module, it is possible that the results demonstrated here may be expanded by using Ppant tethered substrates. While the DHs reported in this work all displayed activity on NAC-linked substrates, there are reports in the literature of those that do not accept such compounds[6]. However, neither NAC-linked nor Ppant-linked substrates will recapitulate the protein-protein interactions between a productive DH – ACP complex, an area that is critically underexplored in PKS DHs. There are also reports of DHs that exhibit different stereospecificity on NAC-linked substrates than ACP-linked substrates[20]. When assayed using

NAC-linked, Ppant-linked, and AcpP-linked substrate mimics bearing identical acyl chains, FabA displayed significantly different activities for each class of substrate[18]. Future experiments must be designed with both DH – Ppant and DH – ACP interactions in mind. ACP – DH interaction studies would be particularly valuable in the case of GphF DH1, where both the (2S,3S) and (2R,3R) substrates are tolerated. For the α-proton and β-hydroxy group of these enantiomers to be properly positioned for elimination, they must bind in the same binding pocket rotated 180° relative to one another. One could imagine GphF ACP1 may bias substrate delivery such that only the native (2R,3R) substrate can bind correctly.

DH substrate interactions

To date, there are no structures of a PKS DH in complex with a native substrate. The data reported here from the co-crystallization experiments with CurJ DH represent the first snapshot of a PKS DH interacting with a hydroxy-bearing truncated substrate fragment. A recently reported study of a DH from the phthiocerol dimycocerosate biosynthetic pathway (PpsC DH) utilized a catalytically inactive variant to trap PpsC DH in complex with both a C4:1 and C12:1 acyl-CoA unsaturated product mimic[21]. While the PpsC DH structure revealed the first snapshot of a long chain product mimic in complex with a PKS DH, the compounds used for co-crystallization contain relatively simple acyl chains compared to a typical PKS DH substrate. Thus, the structural basis for the extreme stereospecificity of the Pik, Tyl, Cur and Gph DHs remains unclear. As synthesis of PKS DH NAC- and Ppant-linked substrate mimics continues to improve, it may be worthwhile to screen libraries of compounds against DHs and catalytically inactive variants of DHs that behave well in crystallization. In the absence of a true enzyme – substrate complex structure, MD simulations may represent a viable alternative to generating meaningful data to further understand the structural determinants of PKS DH stereoselectivity.

DH ACP interactions

The *E. coli* FabZ studies here exemplify the use of chemical biology tools to study DH - ACP interactions. As demonstrated with PikDH2, alkyne-based mechanistic inhibitors are active against PKS DHs[1]. As such, a scheme similar to that which generated the AcpP=FabZ and AcpP=FabA complex may facilitate the generation of ACP=DH complexes from PKS. There are obvious hurdles to this approach, most notably the differences between Type-I and Type-II biosynthetic schemes. As Type-II systems comprise a set of discrete enzymes, the catalytic machinery must harbor an affinity for the carrier protein. This is not the case in type-I systems, where the ACP is found in *cis* with the catalytic domains. To date, there are no reports on the affinity for excised type-I DHs and their cognate ACPs. In both the AcpP=FabA and AcpP=FabZ structures, a large portion of the protein interaction surface on AcpP comprises acidic residues. While these residues are conserved amongst type-II FAS ACPs, type-I PKS DHs are less acidic[22], and thus may utilize different surfaces for protein interaction. Due to the DH specificity reported here, efforts to develop crosslinking probes that better mimic the acyl groups of native substrates may be worthwhile to take advantage of any affinity for native acyl chains presented on an ACP. Additionally, crosslinking may be improved by targeting DHs with long-chain substrates, taking advantage of any hydrophobic stabilization afforded by the DH substrate binding pocket[21, 23].

Multi-domain and full module studies

While a number of structures of excised PKS DHs have been reported[6, 12, 16, 20], there is only one reported multi-domain structure containing a DH from type-I PKS[24]. There are no structures of intact modules containing DHs. As the cost of synthetic DNA continues to decrease, crystallographic screening of libraries of PKS multi-domains will become more viable. Should

crosslinking methods be developed for trapping PKS DH – ACP complexes, these may be useful

for generating stable complexes between excised PKS multi-domains containing DHs and their

ACPs. With the rise of single particle cryo-electron microscopy (CryoEM), it has become easier

to structurally characterize large, dynamic proteins, such as PKS and NRPS modules[25-26].

cryoEM studies of PKS modules containing DH domains could yield critical information in

regard to protein-protein interactions between DHs and other domains within the module, as well

as interactions between DHs and ACPs.

Bibliography

1.   Li, Y., Dodge, G. J., Fiers, W. D., Fecik, R. A., Smith, J. L., Aldrich, C. C., Functional characterization of a dehydratase domain from the pikromycin polyketide synthase. *Journal of the American Chemical Society* **2015,** *137* (22), 7003-7006.
2.   Berkhan, G., Hahn, F., A dehydratase domain in ambruticin biosynthesis displays additional activity as a pyran-forming cyclase. *Angewandte Chemie International Edition* **2014,** *53* (51), 14240-14244.
3.   Berkhan, G., Merten, C., Holec, C., Hahn, F., The interplay between a multifunctional dehydratase domain and a *C*-methyltransferase effects olefin shift in ambruticin biosynthesis. *Angewandte Chemie International Edition* **2016,** *55* (43), 13589-13592.
4.   Fiers, W. D., Dodge, G. J., Li, Y., Smith, J. L., Fecik, R. A., Aldrich, C. C., Tylosin polyketide synthase module 3: stereospecificity, stereoselectivity and steady-state kinetic analysis of β-processing domains via diffusible, synthetic substrates. *Chemical science* **2015,** *6* (8), 5027-5033.
5.   Fiers, W. D., Dodge, G. J., Sherman, D. H., Smith, J. L., Aldrich, C. C., Vinylogous dehydration by a polyketide dehydratase domain in curacin biosynthesis. *Journal of the American Chemical Society* **2016,** *138* (49), 16024-16036.
6.   Keatinge-Clay, A., Crystal structure of the erythromycin polyketide synthase dehydratase. *Journal of molecular biology* **2008,** *384* (4), 941-953.
7.   Worthington, A. S., Rivera, H., Torpey, J. W., Alexander, M. D., Burkart, M. D., Mechanism-based protein cross-linking probes to investigate carrier protein-mediated biosynthesis. *ACS chemical biology* **2006,** *1* (11), 687-691.
8.   Nguyen, C., Haushalter, R. W., Lee, D. J., Markwick, P. R. L., Bruegger, J., Caldara-Festin, G., Finzel, K., Jackson, D. R., Ishikawa, F., O'Dowd, B., McCammon, J. A., Opella, S. J., Tsai, S.-C., Burkart, M. D., Trapping the dynamic acyl carrier protein in fatty acid biosynthesis. *Nature* **2014,** *505* (7483), 427-431.
9.   Caffrey, P., Conserved amino acid residues correlating with ketoreductase stereospecificity in modular polyketide synthases. *ChemBioChem* **2003,** *4* (7), 654-657.

10.   Whicher, J. R., Dutta, S., Hansen, D. A., Hale, W. A., Chemler, J. A., Dosey, A. M., Narayan, A. R., Håkansson, K., Sherman, D. H., Smith, J. L., Structural rearrangements of a polyketide synthase module during its catalytic cycle. *Nature* **2014,** *510* (7506), 560.

11.   Chang, Z., Sitachitta, N., Rossi, J. V., Roberts, M. A., Flatt, P. M., Jia, J., Sherman, D. H., Gerwick, W. H., Biosynthetic pathway and gene cluster analysis of curacin A, an antitubulin natural product from the tropical marine cyanobacterium *Lyngbya majuscula*. *Journal of natural products* **2004,** *67* (8), 1356-1367.

12.   Akey, D. L., Razelun, J. R., Tehranisa, J., Sherman, D. H., Gerwick, W. H., Smith, J. L., Crystal structures of dehydratase domains from the curacin polyketide biosynthetic pathway. *Structure* **2010,** *18* (1), 94-105.

13.   Gerwick, W. H., Proteau, P. J., Nagle, D. G., Hamel, E., Blokhin, A., Slate, D. L., Structure of curacin A, a novel antimitotic, antiproliferative and brine shrimp toxic natural product from the marine cyanobacterium *Lyngbya majuscula*. *The Journal of organic chemistry* **1994,** *59* (6), 1243-1245.

14.   Yoo, H.-D., Gerwick, W. H., Curacins B and C, new antimitotic natural products from the marine cyanobacterium *Lyngbya majuscula*. *Journal of natural products* **1995,** *58* (12), 1961-1965.

15.   Dodge, G. J., Ronnow, D., Taylor, R. E., Smith, J. L., Molecular basis for olefin rearrangement in the gephyronic acid polyketide synthase. *Journal of the American Chemical Society* **2018**, In revision.

16.   Sung, K. H., Berkhan, G., Hollmann, T., Wagner, L., Blankenfeldt, W., Hahn, F., Insights into the dual activity of a bifunctional dehydratase-cyclase domain. *Angewandte Chemie International Edition* **2018,** *57* (1), 343-347.

17.   Taft, F., Brünjes, M., Knobloch, T., Floss, H. G., Kirschning, A., Timing of the $\Delta(10,12)$-$\Delta(11,13)$ double bond migration during ansamitocin biosynthesis in *Actinosynnema pretiosum*. *Journal of the American Chemical Society* **2009,** *131* (11), 3812-3813.

18.   Brock, D., Kass, L., Bloch, K., β-Hydroxydecanoyl thioester dehydrase II. Mode of action. *Journal of Biological Chemistry* **1967,** *242* (19), 4432-4440.

19.   Young, J., Stevens, D. C., Carmichael, R., Tan, J., Rachid, S., Boddy, C. N., Müller, R., Taylor, R. E., Elucidation of gephyronic acid biosynthetic pathway revealed unexpected SAM-dependent methylations. *Journal of Natural Products* **2013,** *76* (12), 2269-2276.

20.   Gay, D., You, Y.-O., Keatinge-Clay, A., Cane, D. E., Structure and stereospecificity of the dehydratase domain from the terminal module of the rifamycin polyketide synthase. *Biochemistry* **2013,** *52* (49), 8916-8928.

21.   Faille, A., Gavalda, S., Slama, N., Lherbet, C., Maveyraud, L., Guillet, V., Laval, F., Quémard, A., Mourey, L., Pedelacq, J.-D., Insights into substrate modification by dehydratases from type I polyketide synthases. *Journal of molecular biology* **2017,** *429* (10), 1554-1569.

22.   Maloney, F. P., Gerwick, L., Gerwick, W. H., Sherman, D. H., Smith, J. L., Anatomy of the β-branching enzyme of polyketide biosynthesis and its interaction with an acyl-ACP substrate. *Proceedings of the National Academy of Sciences* **2016,** *113* (37), 10316-10321.

23.   Leesong, M., Henderson, B. S., Gillig, J. R., Schwab, J. M., Smith, J. L., Structure of a dehydratase–isomerase from the bacterial pathway for biosynthesis of unsaturated fatty acids: two catalytic activities in one active site. *Structure* **1996,** *4* (3), 253-264.

24.   Herbst, D. A., Jakob, R. P., Zähringer, F., Maier, T., Mycocerosic acid synthase exemplifies the architecture of reducing polyketide synthases. *Nature* **2016,** *531* (7595), 533.

25.   Dutta, S., Whicher, J. R., Hansen, D. A., Hale, W. A., Chemler, J. A., Congdon, G. R., Narayan, A. R., Håkansson, K., Sherman, D. H., Smith, J. L., Structure of a modular polyketide synthase. *Nature* **2014,** *510* (7506), 512.

26.   Tarry, M. J., Haque, A. S., Bui, K. H., Schmeing, T. M., X-Ray crystallography and electron microscopy of cross-and multi-module nonribosomal peptide synthetase proteins reveal a flexible architecture. *Structure* **2017,** *25* (5), 783-793. e4.